Online ISSN：2186-490X
Print ISSN：1346-4272

地質調査研究報告

BULLETIN OF THE GEOLOGICAL SURVEY OF JAPAN

Vol. 76　No. 1/2　2025

産総研　地質調査総合センター

令和7年

地質調査研究報告

BULLETIN OF THE GEOLOGICAL SURVEY OF JAPAN

Vol. 76 No. 1/2 2025

表紙の写真

北上山地北部「門」地域の四季

左上：（春）穴目ヶ岳南斜面の新緑. 北上山地北部では 5 月に入っても時として積雪があり，新緑と新雪の珍しい組み合わせが見られることがある.

右上：（夏）折壁川上流域. 夏には樹木の葉に遮られ，沢沿いに届く日差しは少なくなる. 林床も植生に覆われて露頭の観察が困難になる.

左下：（秋）安家川上流域，坂本集落南西の山中の紅葉. 北上山地に広く分布するブナ林は，秋になると一面黄色に変化する.

右下：（冬）早坂峠南西，猫足又沢川. 太平洋寄りに位置する「門」地域では冬前半の積雪は少なめだが，特に標高の高い早坂高原などでは 11 月頃から積雪が始まる.

（写真と文：武藤　俊）

Cover Photograph

Four seasons in the Kado District

Upper left: (Spring) Fresh green leaves on the southern slope of Mt. Anamegadake. In the Kitakami Mountains, there can be snowfall as late as May, and a rare combination of young green leaves and fresh snow can be seen.

Upper right: (Summer) Upper reaches of the Orikabe River. In summer, leaves on the trees cut off a large part of sunlight to the stream. The forest floor is also covered by vegetation, making it difficult to observe outcrops.

Lower left: (Autumn) Autumn foliage in the mountains southwest of Sakamoto Settlement in the upper reaches of the Akka River. Beech forests that are widespread in the Kitakami Mountains produce a magnificent blanket of yellow in the autumn.

Lower right: (Winter) Nekosokomatazawa River, southwest of Hayasaka Pass. The Kado District is situated near the Pacific coast, where snow precipitation is relatively scarce in the first half of winter. However, in high altitudes like the Hayasaka Highlands, snow covers the ground from around November.

(Photograph and Caption by MUTO Shun)

Bulletin of the Geological Survey of Japan, vol. 76 (1/2), p. 1–29, 2025

Article

Carboniferous and Permian conodont fossils from bedded chert in Otori, Iwaizumi Town, Iwate Prefecture, with a review of previously reported conodonts from the North Kitakami Belt

MUTO Shun[1,*], TAKAHASHI Satoshi[2] and MURAYAMA Masafumi[3, 4]

MUTO Shun, TAKAHASHI Satoshi and MURAYAMA Masafumi (2025) Carboniferous and Permian conodont fossils from bedded chert in Otori, Iwaizumi Town, Iwate Prefecture, with a review of previously reported conodonts from the North Kitakami Belt. *Bulletin of the Geological Survey of Japan*, vol. 76 (1/2), p. 1–29, 9 figs and 1 table.

Abstract: Conodont biostratigraphy of pelagic deep-sea sequences in the Jurassic accretionary complex of Japan offers a globally correlative timescale for these rare sedimentary records. The northern Kitakami Mountains provide potential for conodont biostratigraphic research of the deep-sea sedimentary rocks, especially for the Paleozoic interval where zonal schemes remain incomplete. Herein, we report conodont fossils from a deep-sea section named the Otori section in Iwaizumi Town, Iwate Prefecture. Conodonts were visualized using microfocus X-ray computed tomography. We identified *Mesogondolella clarki*, *Mesogondolella* aff. *donbassica*, *Mesogondolella* cf. *bisselli*, *Mesogondolella* cf. *idahoensis*, *Jinogondolella* cf. *palmata*, *Jinogondolella postserrata*, *Sweetognathus iranicus*, *Jinogondolella altudaensis* and *Jinogondolella xuanhanensis*. These conodonts indicate the Moscovian (middle Pennsylvanian, Carboniferous) to the Capitanian (upper Guadalupian, Permian). We also compiled and reviewed previous reports of conodont occurrences in the northern Kitakami Mountains. While previous reports have recognized late Carboniferous to Triassic ages based on conodonts, a majority of the Permian ages are not attestable due to the lack of taxonomic descriptions and illustrations.

Keywords: Artinskian, Capitanian, Jurassic accretionary complex, Kado District, Kungurian, North Kitakami–Oshima Belt, Moscovian, Sakmarian, Wordian, X-ray micro-CT

1. Introduction

Conodont fossils played a major role in geological studies of the Jurassic accretionary complexes in Japan. Conodonts, along with radiolarians, provided biostratigraphic evidence that fragments of late Paleozoic and early Mesozoic material formed in the pelagic area of Panthalassa were accreted to the continental margin of proto-Japan during the Jurassic (Matsuda and Isozaki, 1991). Pelagic deep-sea strata in the accretionary complexes are valuable records of the abyssal plain that is now lost (Fig. 1A). Conodonts are used as age indicators in studies of palaeoenvironmental records preserved in the deep-sea strata (Isozaki, 1997; Takahashi *et al.*, 2009; Nishikane *et al.*, 2014; Muto *et al.*, 2020; Tomimatsu *et al.*, 2020; Muto, 2021).

Triassic conodont biostratigraphy of deep-sea sections has been intensely studied mainly in Southwest Japan (Isozaki and Matsuda, 1980; Yao *et al.*, 1980; Tanaka, 1980; Yamashita *et al.*, 2018; Muto *et al.*, 2019). Consequently, conodont biozonation is constructed for most of the Triassic. On the other hand, Paleozoic deep-sea sections are less studied (see Fig. 1B for the loction of study areas mentioned below). Yao *et al.* (2001) described two upper Permian sections corresponding to the upper Wuchiapingian and Changhsingian stages in Gifu and Shiga prefectures. Nishikane *et al.* (2011, 2014) studied the Guadalupian–Lopingian boundary in the Gifu study section of Yao *et al.* (2001). Kusunoki *et al.* (2004) studied a long-ranging section covering the uppermost Carboniferous and entire Permian in Kyoto Prefecture.

[1] AIST, Geological Survey of Japan, Research Institute of Geology and Geoinformation

[2] Department of Earth and Environmental Sciences, Nagoya University, Furo-cho, Chikusa-ku, Nagoya 464-8601, Japan

[3] Marine Core Research Institute, Kochi University, B200 Monobe, Nankoku, Kochi, Japan

[4] Department of Marine Resource Science, Faculty of Agriculture and Marine Science, Kochi University, B200 Monobe, Nankoku, Kochi, Japan

* Corresponding author: MUTO, S., AIST Tsukuba Central 7, 1-1-1 Higashi, Tsukuba, Ibaraki 305-8567, Japan. Email: s-muto@aist.go.jp

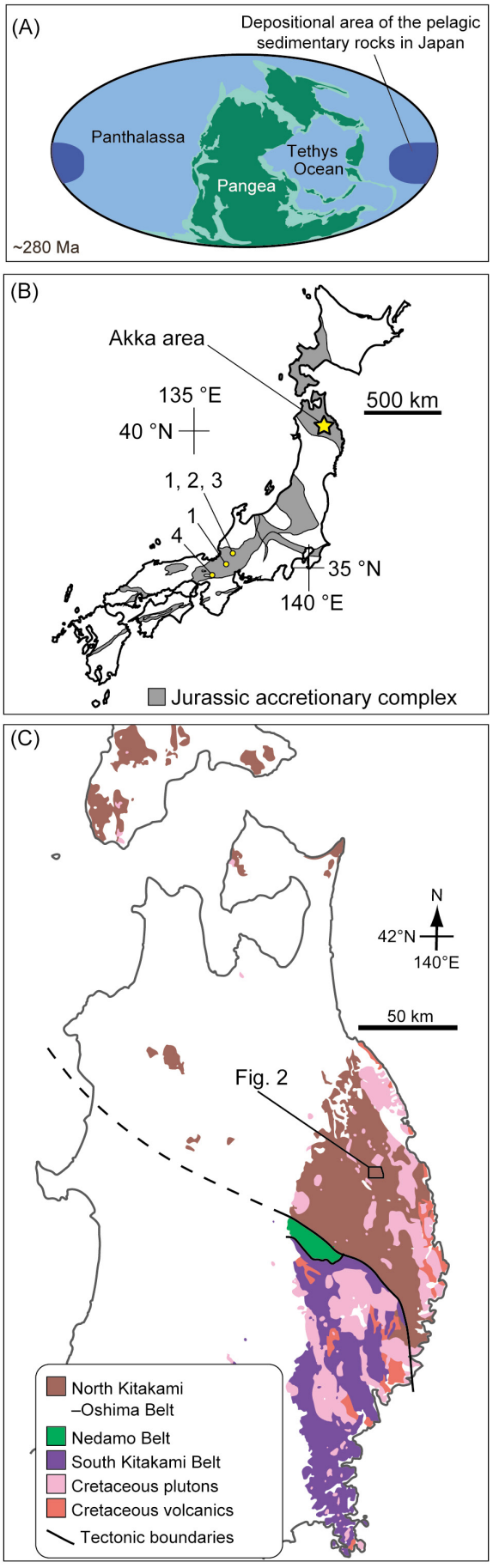

Yamakita *et al.* (2008) and Ehiro *et al.* (2008) drew attention to the Paleozoic deep-sea record in the northern Kitakami Mountains in Northeast Japan, in contrast to the above studies from Southwest Japan. These studies briefly reported on conodonts across the Carboniferous–Permian boundary in the Akka area in Iwate Prefecture, which includes the target area of the present study. Muto *et al.* (2023b) studied the boundary in detail and detected the successive appearance of globally useful zonal marker species. Thus, the northern Kitakami Mountains present a great potential for studies of conodont biostratigraphy of pelagic deep-sea sedimentary rocks.

In this study, we report Carboniferous and Permian conodonts from a section in the Akka area in the northern Kitakami Mountains, Northeast Japan, reported by Ehiro *et al.* (2008). The section is herein named the Otori section. The conodont occurrence of this study was introduced by Muto *et al.* (2022) in a conference, but illustrations of the specimens are published for the first time. This study also provides notes on previous reports of conodonts from the North Kitakami Belt, aiming to present an updated basis of conodont information in this region.

2. Geological outline

The Otori section is a pelagic deep-sea section in the upper reaches of the Akka River in Iwaizumi Town, Iwate Prefecture. Rocks distributed in this area belong to the Jurassic accretionary complex in the northeastern zone of the North Kitakami–Oshima Belt (e.g., Isozaki and Maruyama, 1991; Ehiro *et al.*, 2008; Fig. 1B, C). Based on surveys for the 1: 50,000 geological map of the Kado District for the Quadrangle Series of the Geological Survey of Japan, AIST, the Jurassic accretionary complex of the area is divided into three units with distinct lithofacies; the Otori, Seki and Takayashiki units in tectonically descending order (Takahashi *et al.*, 2016; Muto *et al.*, 2023a; Fig. 2). The Otori section belongs to the structurally lower part of the Otori Unit (the Okoshizawa Subunit) which is composed of stacked sheets of chert and siliceous mudstone (Muto *et al.*, 2023a; Fig. 2). The Otori Unit is composed of upper Carboniferous to Lower Jurassic pelagic deep-sea sedimentary rocks (mostly chert) (Toyohara *et al.*, 1980; Murai *et al.*, 1985; Ehiro *et al.*, 2008; Takahashi *et al.*, 2016; Muto *et al.*, 2023a, b, c) and

Fig. 1 (A) Palaeogeography of the late Carboniferous–middle Permian interval, represented by the Kungurian (by Laya *et al.*, 2013). (B) Distribution of the Jurassic accretionary complex in the Japanese Islands (after Isozaki *et al.*, 2010). The location of areas targeted in this study and previous studies are shown. 1: Yao *et al.* (2001). 2: Nishikane *et al.* (2011). 3: Nishikane *et al.* (2014). 4: Kusunoki *et al.* (2004). Akka area: Yamakita *et al.* (2008); Ehiro *et al.* (2008); Muto *et al.* (2023b); this study. (C) Geology of the basement rocks of northern the Tohoku Region (modified from Geological Survey of Japan, AIST, 2020).

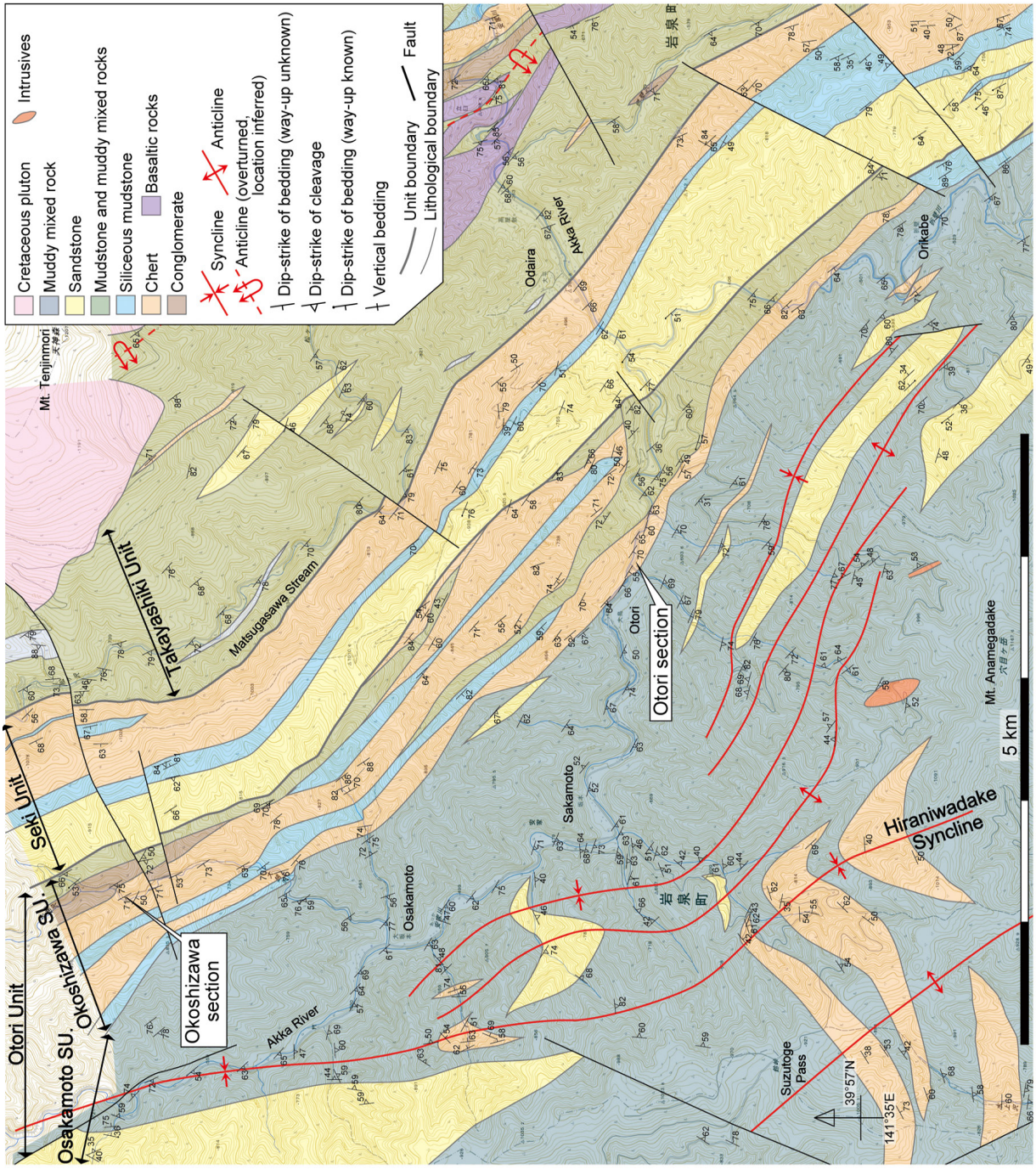

Fig. 2 The geology of the North Kitakami Belt in the upper reaches of the Akka River (updated from Muto *et al.*, 2023a). SU: subunit.

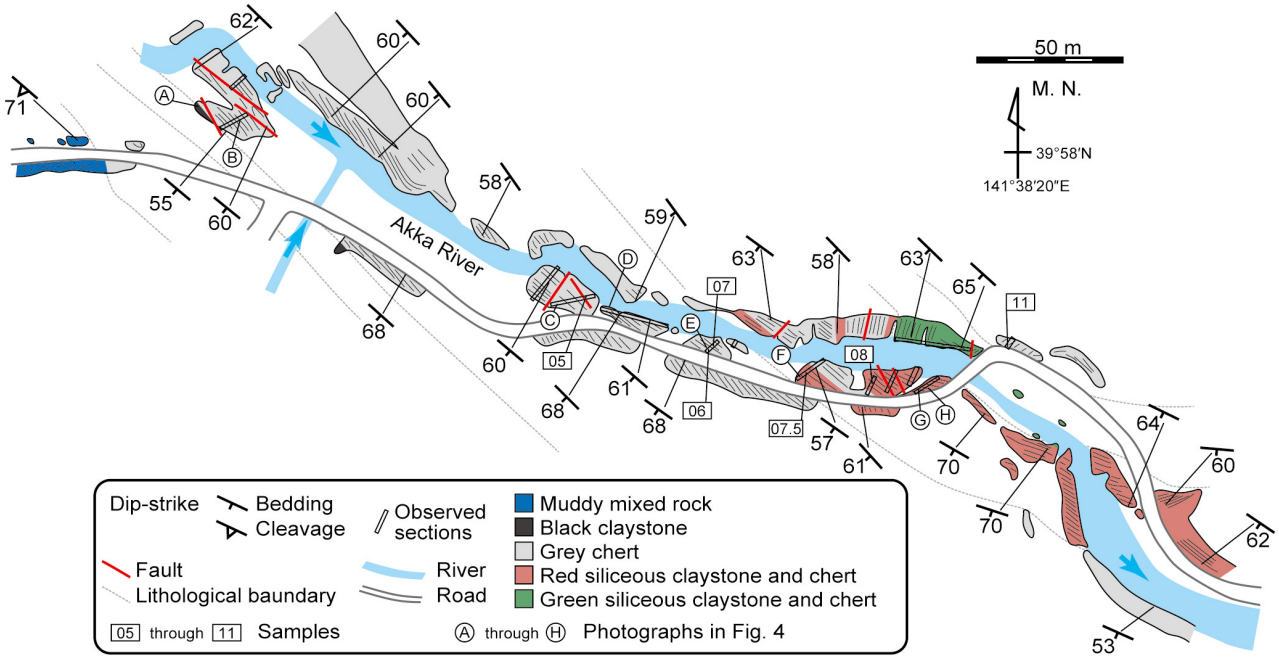

Fig. 3 Geological sketch map of the Otori section. M. N.: Magnetic north. Sample numbers correspond to the last two or three digits after 191213-.

Middle Jurassic hemipelagic to trench-fill sedimentary rocks (Suzuki *et al.*, 2007b; Ehiro *et al.*, 2008; Muto *et al.*, 2023a). Chert of the Otori Unit is accompanied by green and red siliceous claystone in the upper Carboniferous to lower Permian interval (Ehiro *et al.*, 2008; Muto *et al.*, 2023a, b) and black carbonaceous claystone and grey siliceous claystone at the Permian–Triassic boundary (Takahashi *et al.*, 2009; Muto *et al.*, 2023c).

The Otori section represents the Paleozoic portion of the pelagic deep-sea sedimentary rocks of the Otori Unit. The lithofacies is in ascending order grey bedded chert, green siliceous claystone, red siliceous claystone interbedded with reddish or greyish chert and grey bedded chert (Figs. 3–5). The total thickness is apparently ~90 m, but true stratigraphic thickness is unknown due to faults and folds. The green siliceous claystone is composed of 5–20 cm thick beds that are partly poorly defined. The interval of red siliceous claystone and reddish or greyish chert is composed of beds that are mostly 2–10 cm thick (Fig. 4F–H). The colour of the rocks have considerable lateral variation, changing between red to reddish purple or red to grey in the same bed. Single bed thickness and pattern of bedding in the grey bedded chert in the upper part of the Otori section show minor stratigraphic changes. The lower to middle part that include horizons yielding Guadalupian (middle Permian) conodonts have very thin clay partings mostly less than a few millimetres in thickness between individual chert beds (Fig. 4C–E). In this part, single bed thickness varies from 1–5 cm in thin-bedded parts (Fig. 4E) to around 20 cm in thick-bedded parts (Fig. 4C) and some intervals have poorly parted beds (Fig. 4D). In contrast, the upper part of the grey bedded chert tends to have thicker clay partings, and chert beds interbedded with 1–3 cm thick clayey beds that appear as yellowish bands on the outcrop surface are common (Fig. 4B). Single bed thickness is mostly 2–5 cm in the upper part of the grey bedded chert. At the top of the section is black carbonaceous claystone, which is lithostratigraphically correlated to the Permian–Triassic boundary (Fig. 4A).

3. Methods

Conodonts were found on cleaved surfaces of sampled rocks (Fig. 6) and scanned by an X-ray microscope using the method established by Muto *et al.* (2021b). Rock pieces containing well-preserved specimens

(→ p. 5)

Fig. 4 Outcrop photographs of the Otori section. (A) The Permian–Triassic boundary between grey bedded chert (below) and black carbonaceous claystone (above). The two lithofacies are in contact with a slip plane and the exact boundary may be lost. (B) Lopingian (?) grey bedded chert with thick clayey layers. (C) Guadalupian (?) grey thick bedded chert. (D) Guadalupian grey bedded chert. (E) Guadalupian grey bedded chert. (F) Cisuralian reddish grey siliceous claystone with a thick white chert interbed. (G) Cisuralian red and reddish purple red siliceous claystone with white chert interbeds. (H) Cisuralian greyish red siliceous claystone. Scale bars are 20 cm. The hammer in A and G are 30 cm long.


A
hammer
B
C
D
E
F
G
hammer
H

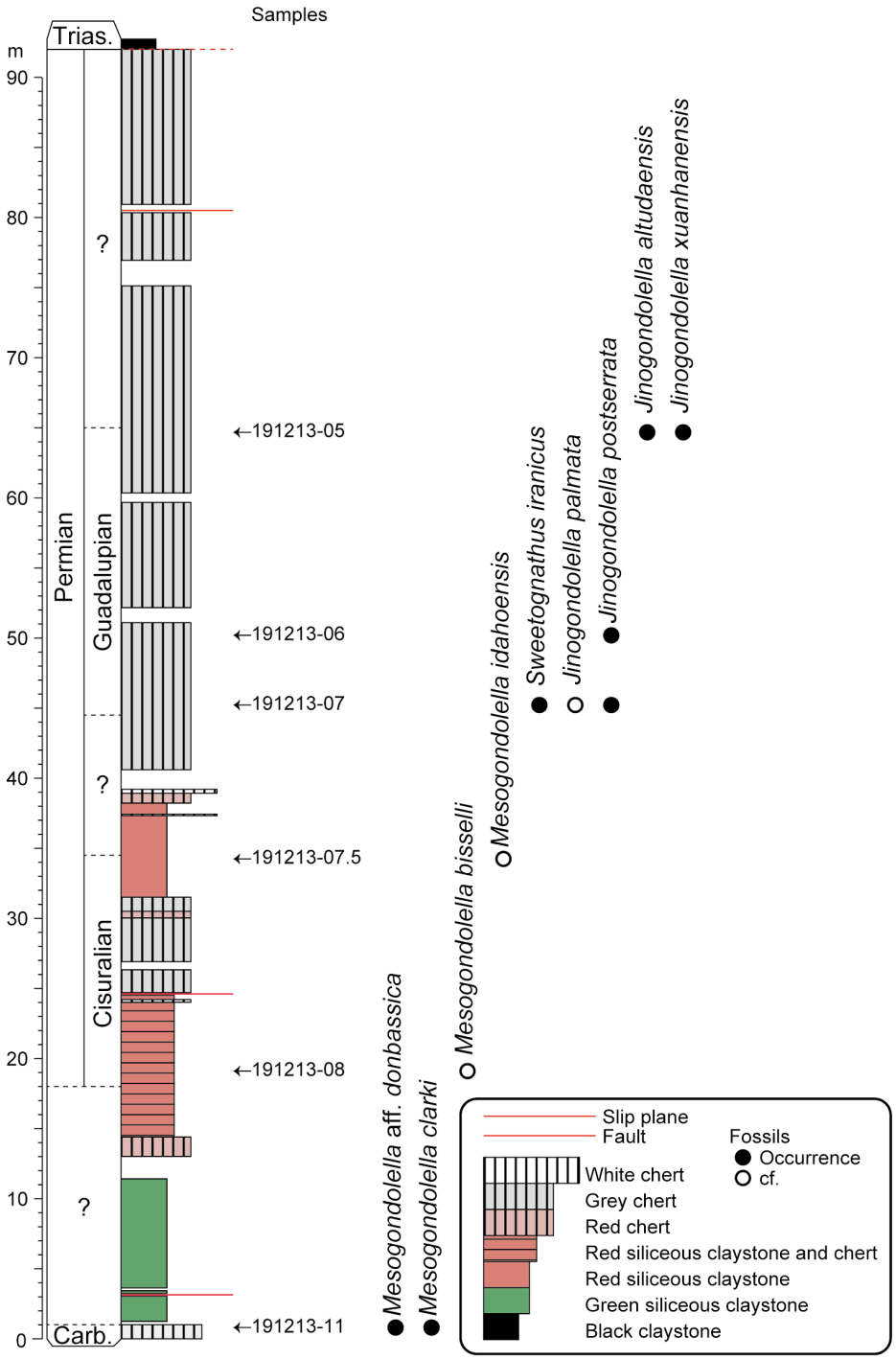

Fig. 5 Lithostratigraphy and conodont occurrence of the Otori section. Carb.: Carboniferous; Trias.: Triassic.

were selected and trimmed down to blocks of a few millimetres. The specimens on the rock pieces were enclosed in a "hedge" of concrete mortar to avoid effects of surface refraction of X-rays, glued onto the end of a pencil lead and scanned using a ZEISS Xradia 410 versa X-ray microscope equipped with a L8121-03 SEL X-ray source of Hamamatsu Photonics K.K. at the Marine Core Research Institute, Kochi University. Tomographic sections obtained by Xradia 410 versa were processed using Amira Software (Thermo Fisher Scientific). For details, see Muto *et al.* (2021b).

4. Conodont occurrence and age assignment of the Otori section

We obtained conodonts from six horizons in the Otori

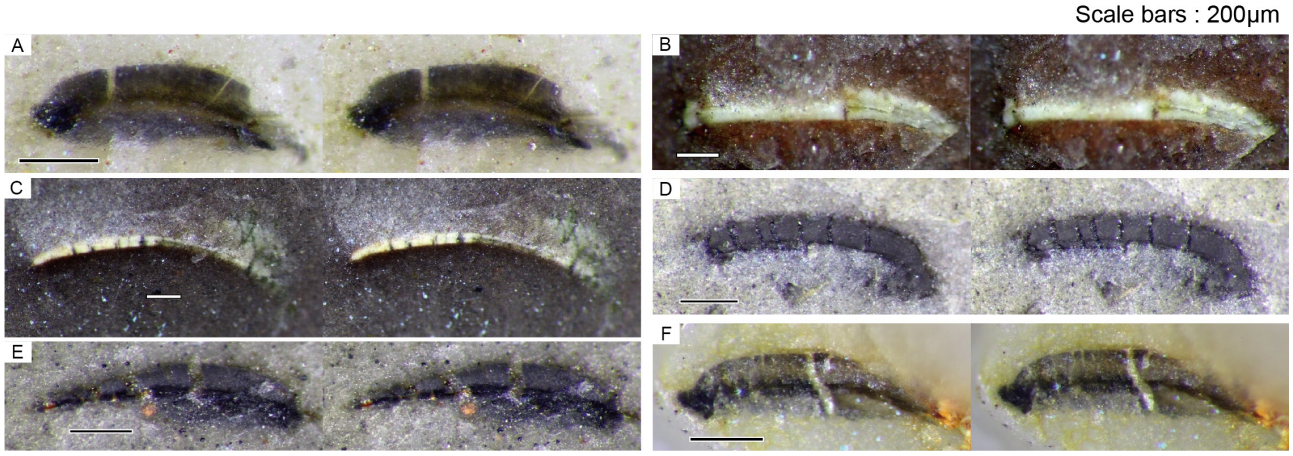

Fig. 6 Parallel-viewing stereoscopic photographs of representative conodont specimens from different rock types. (A) Grey chert, 191213-11, not in Fig. 7. (B) Red siliceous claystone, 191213-08, same specimen as Fig. 7S. (C) Red siliceous claystone, 191213-07.5, same specimen as Fig. 7R. (D) Grey chert, 191213-07, same specimen as Fig. 7N. (E) Grey chert, 191213-06, not in Fig. 7. (F) Grey chert, 191213-05, same specimen as Fig. 7G. Scale bars are 200 μm.

section (Figs. 5, 7). The basal part of the section (Sample 191213-11) yielded *Mesogondolella clarki* (Koike) and *Mesogondolella* aff. *donbassica* (Kossenko). The former has been shown from a similar horizon of the Otori section by Ehiro *et al.* (2008). *Mesogondolella clarki* is a widespread Moscovian (middle Pennsylvanian) species known from pelagic Panthalassa (Koike, 1967; Muto *et al.*, 2023b), the Donets Basin (Nemyrovska, 2011; 2017a) and South China (Wang and Qi, 2003; Qi *et al.*, 2014, 2016). *Mesogondolella donbassica* is known from the Moscovian of the Donets Basin (Nemyrovska *et al.*, 1999), Novaya Zemlya (Sobolev and Nakrem, 1996) and South China (Wang and Qi, 2003).

The lower part of the reddish siliceous claystone and chert interval (Sample 191213-08) yielded specimens comparable to *Mesogondolella bisselli* (Clark and Behnken). This species is known from the Sakmarian to Artinskian of pelagic Panthalassa (Igo, 1981; Igo and Hisada, 1986), South China (Wang and Wang, 1981), Novaya Zemlya (Sobolev and Nakrem, 1996), Urals (Chernykh, 2005) and western USA (Clark and Behnken, 1971; Behnken, 1975). The upper part of the reddish siliceous claystone and chert interval (Sample 191213-07.5) yielded specimens comparable to *Mesogondolella idahoensis* (Youngquist *et al.*, 1951). This species is an indicator of the Kungurian (late Cisuralian) and has a wide distribution occurring from Panthalassa (Igo, 1981; Muto *et al.*, 2021a), South China (Zhang *et al.*, 2010), Spitsbergen (Szaniawski and Malkowski, 1979) and western USA (e.g., Youngquist *et al.*, 1951; Behnken, 1975; Lambert *et al.*, 2007).

We obtained conodonts from two horizons in the lower part of the grey bedded chert. The lower horizon (Sample 191213-07) contained *Sweetognathus iranicus* Kozur *et al.*, *Jinogondolella* cf. *palmata* Nestell and Wardlaw and *Jinogondolella postserrata* (Behnken), while the higher horizon (Sample 191213-06) yielded *J. postserrata*. *Jinogondolella palmata* and *J. postserrata* respectively occur from the Wordian (middle Guadalupian) to lowermost Capitanian (upper Guadalupian) and the Capitanian in western USA (Wardlaw and Nestell, 2015) and South China (Sun *et al.*, 2017). *Sweetognathus iranicus* was originally reported from the Capitanian of Iran (Kozur *et al.*, 1975). It was later found from the Wordian of the Salt Range (Wardlaw and Mei, 1998) and the Kungurian of South China (Sun *et al.*, 2017).

The middle part of the grey bedded chert (Sample 191213-05) yielded *Jinogondolella altudaensis* (Kozur) and *Jinogondolella xuanhanensis* (Mei and Wardlaw in Mei *et al.*, 1994a). These species are known from Panthalassa (Nishikane *et al.*, 2011, 2014), western USA (e.g., Wardlaw, 2000; Wardlaw and Nestell, 2010; Lambert *et al.*, 2010) and South China (Mei *et al.*, 1994a, b; Sun *et al.*, 2017), and cooccur in the Capitanian.

Based on the above, the confirmed age of the Otori section spans from the Moscovian of the Pennsylvanian (late Carboniferous) to the Capitanian of the Guadalupian (middle Permian) (Fig. 5). No age diagnostic fossils have been found yet from the upper part of the grey bedded chert, but this part presumably includes Lopingian strata, based on its position below the Permian–Triassic boundary. Another deep-sea section in the Otori Unit, the Okoshizawa section (Fig. 2), has been studied for the Carboniferous–Permian boundary (Muto *et al.*, 2023b). While the two sections are composed of a similar set of lithologies, there are noticeable differences in lithostratigraphy. Red siliceous claystone is present in the basal Permian in both sections, but it does not extend up into the Artinskian in Okoshizawa, while it continues up to the Kungurian in Otori (Fig. 8). This degree of variation in apparent silica content in coeval beds is not known from other intervals of pelagic deep-sea sedimentary rocks

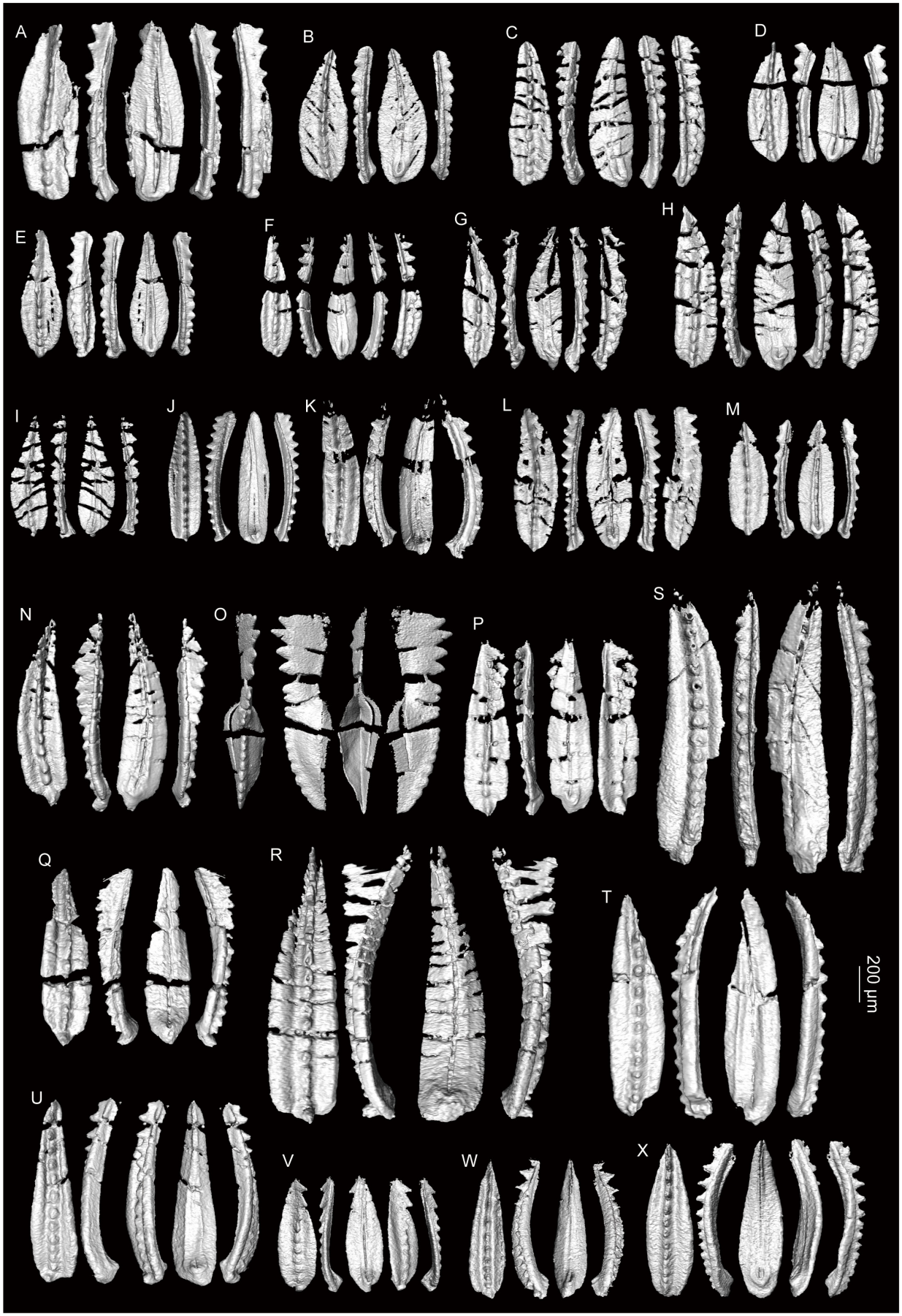
A
B
C
D
E
F
G
H
I
J
K
L
M
N
O
P
S
Q
R
T
200 µm
U
V
W
X

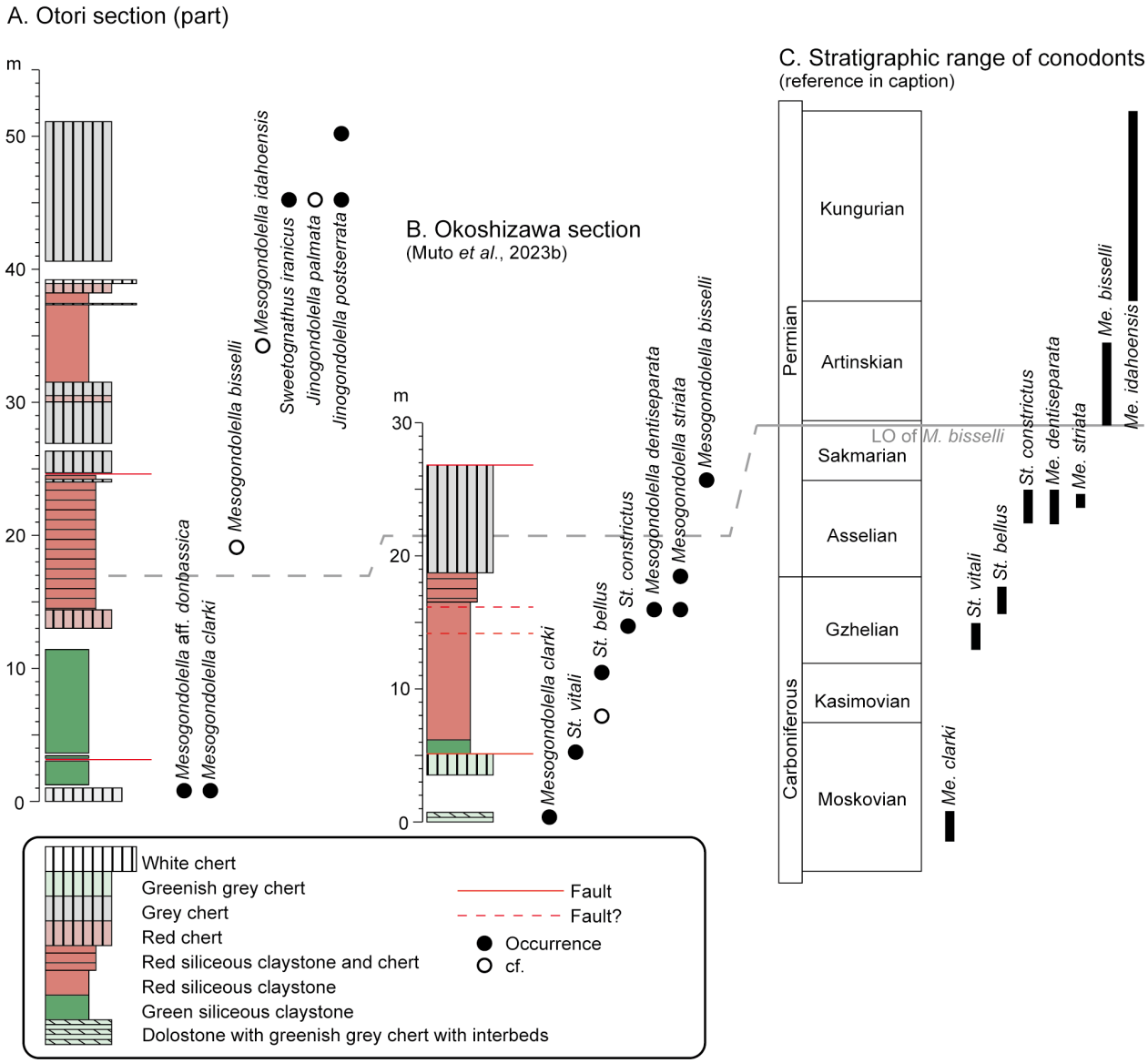

Fig. 8 Comparison of the lithostratigraphy and selected conodont occurrence of the Otori and Okoshizawa sections and correlation based on known stratigraphic range of conodonts. (A) Otori section (this study). (B) Okoshizawa section (Muto *et al.*, 2023b). (C) Range of conodonts (Henderson, 2018; Chernykh *et al.*, 2020; Ritter, 2020; Beauchamp *et al.*, 2022a, b). Only the Pennsylvanian to lower Guadalupian part of the Otori section is shown. The difference in lithofacies is easily noticed around the lowest occurrence (LO) of *M. bisselli*.

(←p. 8)

Fig. 7 Images of conodont specimens obtained by X-ray μCT. (A–E) *Jinogondolella altudaensis* (Kozur), 191213-05. (F, G) *Jinogondolella xuanhanensis* (Kozur), 191213-05. (H, I) *Jinogondolella*? sp., 191213-05. (J) *Jinogondolella postserrata* (Behnken), 191213-06. (K) *J.* cf. *postserrata* (Behnken), 191213-06. (L, M) *Jinogondolella*? sp., 191213-06. (N) *J. postserrata* (Behnken), 191213-07. (O) *Sweetognathus iranicus* Kozur *et al.*, 191213-07. (P) *Jinogondolella* cf. *palmata* Nestell and Wardlaw, 191213-07. (Q, R) *Mesogondolella* cf. *idahoensis* (Youngquist *et al.*), 191213-07.5. (S, T) *Mesogondolella* cf. *bisselli* Clark and Behnken, 191213-08. (U–W) *Mesogondolella clarki* (Koike), 191213-11. (X) *Mesogondolella* aff. *donbassica* (Kossenko). Scale bar is 200 μm.

in Japan. In addition, dolostone beds are present in the Moscovian of the Okoshizawa section, but not found in the Moscovian of the Otori section.

5. Notes on previously reported conodonts from the North Kitakami Belt

In the 1970s to 1980s, geologists investigated many localities of chert and limestone in the Jurassic accretionary complex of the North Kitakami Belt (the segment of the North Kitakami–Oshima Belt distributed in the Honshu Island). The occurrence of conodonts was highly significant, because the only age diagnostic fossils reported from the North Kitakami Belt till then were mostly fusulinids from limestone. Studies on conodonts eventually supported the introduction of plate tectonics to the region (Okami and Ehiro, 1988). Conodont fossils were of particular importance in the Kitakami Mountains, because metamorphism by Cretaceous plutons makes it mostly impossible to extract radiolarians from chert, leaving conodonts the only way of age assignment. Despite the significance, only a few works have presented illustrations of conodont fossils. In this section, we list previous reports of conodonts from the North Kitakami Belt (Table 1). Since conodont taxonomy has been significantly updated in the last few decades, some notes are made on the taxonomic aspect of the reports. Furthermore, we also aim to unravel the confusion caused by different works referring to the same locality without making it clear (shaded rows in Table 1).

5. 1. Carboniferous conodonts

Not many Carboniferous conodonts have been reported, and the majority comes from the Akka area of this study. Illustrations of specimens were scarce, but those from the Akka area are made available by Muto *et al.* (2023b) and this study. In addition to the Akka area, Murata *et al.* (1974) illustrated specimens that are undoubtedly of Carboniferous age including *Mesogondolella clarki* and *Idiognathodus* sp. (their *I. delicatus*). The oldest age confirmed by conodonts in the North Kitakami Belt is Moscovian: Toyohara *et al.* (1980) reported the occurrence of *Gondolella* sp. (their Loc. 36; Table 1), which would indicate the late Carboniferous, but no illustrations or descriptions were given.

5. 2. Permian conodonts

Permian conodonts have been reported from many localities in the North Kitakami Belt, but reliability is problematic in many of these reports. The term "Permian-type *Neogondolella*" was used in many localities with no clear definition and, in most cases, illustrations are not shown. The term apparently refers to Permian gondolellid genera currently placed under *Mesogondolella*, *Jinogondolella* and *Clarkina*, and it is true that they can be distinguished from Triassic gondolellids including the Middle Triassic *Neogondolella* (in the modern sense). However, without the statement of how "Permian-type *Neogondolella*" was distinguished, the age assignment cannot be accepted as decisive. Such cases are shown with brackets in our compilation list (Table 1). It should also be noted that classification of the aboral surface, which is probably the easiest way to differentiate between Carboniferous, Permian and Triassic gondolellids, is not applicable for early juveniles (Kozur, 1989). Since at least some of the figured specimens in previous works appear to be of early juvenile stages (Fig. 9A–D; Table 1), there is a significant degree of concern about the identification of these gondolellids. Of the previous reports of Permian conodonts, those including *Neostreptognathodus* can be regarded as reliable, since this genus only occurs in the Cisuralian, although the lack of illustrations of *Neostreptognathodus* is unhelpful. Also, those including *Anchignathodus* (*Hindeodus* in the present taxonomy) are generally reliable, since this taxon became extinct in the earliest Triassic. Ehiro *et al.* (2008) and Takahashi *et al.* (2016) illustrated "Permian-type *Neogondolella*" and stated that a wide platform characterizes this type. While the width of the platform is rather subjective as far as their illustrations show, terminal position of the loop (Fig. 10.1, 4 in Takahashi *et al.*, 2016), wide V-shaped attachment surface or low and discrete carina (Fig. 10.3 in Takahashi *et al.*, 2016), support placing at least some of their specimens in Permian taxa.

5. 3. Triassic conodonts

Triassic conodonts are the most abundantly reported conodonts in the North Kitakami Belt. Recognition of Triassic ages in the previous studies are based on identification of conodonts at the species level, unlike the case of the Permian. However, some of the species names reported therein need to be treated with caution, as detailed below.

Epigondolella abneptis (Huckriede) was recognized in many localities to indicate the Late Triassic. This species was chosen by Mosher (1968) as the type species of the genus *Epigondolella* that included Middle to Late Triassic conodonts with mostly denticulate platform margins, which are stratigraphically useful because of their distinct characters. However, *E. abneptis* was applied by many subsequent works to forms that would now be placed in different species or even different genera, partly due to the fact that Huckriede (1958) illustrated a wide range of forms from several ages when he erected this species (Moix *et al.*, 2007; Karádi, 2021). In the absence of clear illustrations in the works of the North Kitakami Belt, it is only possible to surmise that the occurrence of "*E. abneptis*" indicates the Middle or Upper Triassic. In fact, in the three cases where illustrations for "*E. abneptis*" were given, there are differences in morphological characters with the holotype of *E. abneptis* enough to conclude that they belong to a different species. The specimens in Pl. 3, fig. 1 of Murai *et al.* (1985) and Pl. 9 figs. 17–20 of Murata and Nagai (1972) have a rostro-caudally reduced

Table 1 List of reported conodont occurrences in the North Kitakami Belt with first citation in compilations (Suzuki *et al.* 2007a; Ehiro *et al.*, 2008; Uchino and Suzuki, 2020; this study), location in the division of 1: 50,000 Quadrangle Series, lithology of sample, presence or absence of figures, taxon name as in original reference, age indicated by the fossils and notes by the present authors. Numberings of bibliographic references follow Suzuki *et al.* (2007a), Ehiro *et al.* (2008) and Uchino and Suzuki (2020). Shadowed reports are citations of earlier reports that lacked referencing. Reports of conodonts with little biostratigraphic or taxonomic value, such as conodonts ranging across periods or elements belonging to many taxa of genus levels or higher are not listed here. In case of rarely used combination of genus and species names, currently used genus names are noted. When the age of the conodonts is mentioned in the original reference but is found to be questionable due to poor quality of the specimens, contradictory cooccurrence of taxa in modern biostratigraphic schemes or insufficient biostratigraphic constraints, the age is shown with a question mark.

	Reference	Locality	first citation	Quadrangle	Lithology	Fig.	taxon (as in original)	Period / Epoch	Stage	notes
6	Murata and Sugimoto (1971)		Suzuki *et al.* (2007a)	Rikuchu-Seki	limestone	no		Late Triassic	Norian?	*Ep. bidentata* fauna. Same occurrence reported in Sugimoto (1974)?
				Rikuchu-Seki	limestone	no		Late Triassic	Norian?	*Ep. abneptis* fauna; Same occurrence reported in Sugimoto (1974)?
17	Yoshida (1980)	Loc. 3	Suzuki *et al.* (2007a) Deleted in Ehiro *et al.* (2008) and Uchino and Suzuki (2020)	Kawai	chert	no	*Neogondolella bulgarica*	Middle Triassic	Anisian	
						no	*Pollognathus kochi*			Current genus *Cratognathodus* .
		Loc. 4		Kawai	chert	no	Permian-type *Neogondolella* sp.	Permian?		
		Loc. 5		Kawai	chert	no	*Neogondolella excelsa*? or *Neogondolella polygnathiformis*?	Middle? or Late? Triassic	Anisian to Carnian?	
		Loc. 6		Kawai	chert	no	?*Misikella hernsteini*	Late Triassic?	Norian or Rhaetian?	
18	Toyohara *et al.* (1980)	Loc. 1	Suzuki *et al.* (2007a)	Iwaizumi	chert	no	*Epigondolella bidentata*	Late Triassic	Norian or Rhaetian	
						no	*Misikella hernsteini*			
		Loc. 3	Suzuki *et al.* (2007a)	Rikuchu-Seki	limestone	no	*Epigondolella primitia*	Late Triassic	Carnian or Norian	
		Loc. 4	Suzuki *et al.* (2007a)	Rikuchu-Seki	limestone	no	?*Neogondolella navicula steinbergensis*	Late Triassic?	Norian?	
		Loc. 5	Suzuki *et al.* (2007a)	Rikuchu-Seki	limestone	no	*Epigondolella primitia*	Late Triassic	Carnian or Norian	
		Loc. 6	Suzuki *et al.* (2007a)	Rikuchu-Seki	limestone	no	*Epigondolella primitia*	Late Triassic	Carnian or Norian	
		Loc. 7	Suzuki *et al.* (2007a)	Rikuchu-Seki	chert	no	*Neogondolella* sp.	(Triassic)		
		Loc. 8	Suzuki *et al.* (2007a)	Rikuchu-Seki	chert	no	*Neogondolella polygnathiformis*	Late Triassic	Carnian	
		Loc. 11	Suzuki *et al.* (2007a)	Rikuchu-Seki	chert	no	*Neohindeodella aequiramosa*	Middle Triassic	Anisian	
		Loc. 12	Suzuki *et al.* (2007a)	Rikuchu-Seki	chert	no	*Neogondolella bulgarica*	Middle Triassic	Anisian	
						no	*Neohindeodella aequiramosa*			
		Loc. 14	Suzuki *et al.* (2007a)	Rikuchu-Seki	siliceous mudstone	no	*Neospathodus homeri*	Early Triassic		
		Loc. 16	This study	Kado	chert	no	Permian-type *Neogondolella* sp.	(Permian)		
		Loc. 17	This study	Kado	siliceous mudstone	no	*Neospathodus homeri*	Early Triassic		
		Loc. 19	Suzuki *et al.* (2007a)	Kado	chert	no	?*Neogondolella polygnathiformis*	Late Triassic?	Carnian?	
		Loc. 21	Suzuki *et al.* (2007a)	Kado	chert	no	?*Neogondolella polygnathiformis*	Late Triassic?	Carnian?	

to next page

Table 1 Continued.

	Reference	Locality	1st citation	Quadrangle	Lithology	Fig.	taxon (as in original)	Period / Epoch	Stage	notes
		Loc. 22	This study	Kado	chert	no	Permian-type *Neogondolella* sp.	(Permian)		
		Loc. 23	This study	Kado	chert	no	Permian-type *Neogondolella* sp.	(Permian)		
		Loc. 24	This study	Kado	chert	no	*Neogondolella* sp. (*constricta*-type)	Middle Triassic		
		Loc. 26	This study	Iwaizumi	chert	no	Permian-type *Neogondolella* sp.	early Permian		
						no	*Neostreptognathodus* sp.			
		Loc. 28	This study	Iwaizumi	Siliceous mudstone	no	*Neospathodus homeri*	Early Triassic	Olenekian	
						no	*Neohindeodella dropla*			
						no	*Neohindeodella benderi*			
		Loc. 30	Suzuki *et al.* (2007a)	Kado	chert	no	*Epigondolella bidentata*	Late Triassic	Norian	
						no	*Neogondolella navicula steinbergensis*			
		Loc. 31	Suzuki *et al*. (2007a)	Kado	chert	no	?*Neogondolella bulgarica*	Triassic	Anisian?	
						no	*Neohindeodella multihamata*			
						no	?*Pollognathus kochi*			Current genus *Cratognathodus*.
		Loc. 32	Suzuki *et al*. (2007a)	Kado	chert	no	?*Neogondolella bulgarica*	Triassic	Anisian	
						no	*Neohindeodella aequiramosa*			
						no	*Neohindeodella triassica*			
18	Toyohara *et al.* (1980) (continued)	loc. 33	Suzuki *et al*. (2007a)	Kado	chert	no	*Epigondolella abneptis*	Late Triassic	Norian	
						no	*Neogondolella navicula hallstattensis*			
						no	*Neohindeodella dropla*			
		Loc. 34	This study	Okawa	chert	no	Permian-type *Neogondolella* sp.	early? Permian		
						no	neostreptognathid			
						no	*Neohindeodella triassica*			Contradictory occurrence.
		Loc. 36	This study	Okawa	chert	no	*Gondolella* sp.	Carboniferous?		
						no	*Xaniognathus* sp.			
		Loc. 37	This study	Okawa	chert	no	Permian-type *Neogondolella* sp.	(Permian)		
		Loc. 38	This study	Okawa	chert	no	Permian-type *Neogondolella* sp.	Permian		
						no	*Anchignathodus* sp.			
						no	*Neohindeodella triassica*			Contradictory occurrence.
		Loc. 40	This study	Okawa	chert	no	*Neogondolella* cf. *rozenkrantzi*	late Permian		
		Loc. 41	Suzuki *et al*. (2007a)	Kado	chert	no	?*Neohindeodella aequiramosa*	Triassic?		
		Hirosaki P	Suzuki *et al*. (2007a)	Hirosaki?	chert	no	Not mentioned	Permian		
		Hirosaki ml?	Suzuki *et al*. (2007a)	Hirosaki?	chert	no	?*Neohindeodella multihamata*	Triassic?		Constitutes multielement apparatus with *C. kochi* (Koike, 1999)
	to next page	Natsudomari ab, Same as [47].	This study	Mutsukawauchi	limestone	no	*Epigondolella abneptis*	Late Triassic		

Table 1 Continued.

	Reference	Locality	First citation	Quadrangle	Lithology	Fig.	taxon (as in original)	Period / Epoch	Stage	notes
18	Toyohara *et al*. (1980) (continued)	Natsudomari bd, Same as [47].	This study	Mutsukawauchi	limestone	no	*Epigondolella bidentata*	Late Triassic		
		Shiriya E pr	Suzuki *et al.* (2007a)	Shiriyazaki	chert	no	*Epigondolella primitia*	Late Triassic	Carnian or Norian	
		Sw Yunokawa cn	This study	Mutsukawauchi	chert	no	*Neogondolella constricta*	Middle Triassic		
26	Ehiro *et al.* (2001)		Suzuki *et al*. (2007a)	Miyako	chert	no	*Cornudina breviramulis*	Triassic		Originally dated as the Anisian, Middle Triassic, but the species ranges up to the Norian.
31	Murai *et al.* (1985)	Loc. 7 Loc. 34 of [18]? (one mismatch)	Suzuki *et al.* (2007a)	Okawa	chert	no	*Neohindeodella triassica*	early Permian?		Contradictory cooccurrence.
						no	neostreptognathid			
		Loc. 8 Loc. 37 of [18]		Okawa	chert	no	Permian-type *Neogondolella* sp.	(Permian)		
		Loc. 9 Loc. 38 of [18]		Kado	chert	no	Permian-type *Neogondolella* sp.	Permian		
						no	*Anchignathodus* sp.			
						no	*Neohindeodella triassica*			Contradictory coocurrence.
		Loc. 10 Loc. 40 of [18]		Kado	chert	no	*Neogondolella* cf. *rosenkrantzi*	late Permian		
		Loc. 11		Kado	chert	no	*Neogondolella* cf. *carinata carinata*	late? Permian		Contradictory cooccurrence.
						yes	*Neogondolella* cf. *rosenkrantzi*			Figure not deciseve. (Aboral view only.)
						yes	*Anchignathodus minutus*			Figure not sharp.
		Loc. 12 Loc. 26 of [18]		Iwaizumi	chert	no	Permian-type *Neogondolella* sp.	early Permian		
						no	*Neostreptognathodus* sp.			
		Loc. 13 Loc. 28 of [18]		Iwaizumi	siliceous claystone	no	*Neospathodus homeri*	Early Triassic	Olenekian	
						no	*Neohindeodella benderi*			
						no	*Neohindeodella dropla*			
		Loc. 14 Loc. 6 of [18]		Kado	limestone	no	*Epigondolella primitius*	Late Triassic	Carnian or Norian	Misspelled.
						no	?*Epigondolella abneptis*			
		Loc. 15 Loc. 19 of [18]		Kado	chert	no	?*Neogondolella polygnathiformis*	Late Triassic?		
		Loc. 17 Loc. 21 of [18]		Kado	chert	no	?*Neogondolella polygnathiformis*	Late Triassic?		
		Loc. 18 Loc. 18 of [18]? Lithology mismatch.		Kado	chert	no	*Neogondolella* sp.	(Permian)		Age shown as "Permian" in text, but no indication as "Permian-type" for conodont occurrence.

to next page

Table 1 Continued.

	Reference	Locality	First citation	Quadrangle	Lithology	Fig.	taxon (as in original)	Period / Epoch	Stage	notes
		Loc. 19 Loc. 25 of [18].		Kado	chert	no	*Enantiognathus ziegleri*	Triassic?		Misspelled. Assigned to Middle Triassic but the species spans the entire Triassic.
						no	*Cypridodella muelleri*			Assigned to Middle Triassic but but the species spans the entire Triassic.
		Loc. 20		Kado	chert	yes	?*Epigondolella abneptis*	Triassic?		*E. abneptis* ? is "*E.* cf. *abneptis* " in Plate caption, probably *Mockina* .
						yes	*Neogondolella* sp.			Figure not sharp.
		Loc. 21		Kado	chert	yes	*Neogondolella* cf. *rosenkrantzi*			Unidentifiable juvenile. Age revised accordingly from "Permian" in original work.
		Loc. 22 Loc. 16 in [18].		Kado	chert	no	Permian-type *Neogondolella* sp.	Permian?		
		Loc. 23 Loc. 24 in [18]		Kado	chert	no	*Neogondolella* sp. (*constricta* -type)	Triassic?		
31	Murai *et al.* (1985) (continued)	Loc. 24	Suzuki *et al* . (2007a)	Rikuchu-Seki	chert	part	*Neogondolella jubata*	Early Triassic?		Contradictory cooccurrence. Figures not sharp.
						part	*Neogondolella* cf. *planata*			
						part	*Neogondolella* cf. *milleri*			
		Loc. 25		Kado	chert	no	*Neogondolella* cf. *rosenkrantzi*	late Permian		
						no	*Anchignathodus minutus*			
						no	*Ellisonia granada*			
						no	*Neospathodus arcucristus*			Current genus *Merrillina* .
		Loc. 26		Kado	chert	yes	*Neogondolella polygnathiformis*	Late Triassic	Carnian	Figure not sharp but probably *Paragondolella* sp.
						no	*Gondolella carpathica*			
		Loc. 27 Loc. 17 in [18]		Kado	siliceous claystone	no	*Neospathodus homeri*	Early Triassic		
						no	*Neohindeodella triassica*			
		Loc. 28 Loc. 22 in [18]		Kado	chert	no	Permian-type *Neogondolella* sp.	(Permian)		
		Loc. 29 Loc. 23 in [18]		Kado	chert	no	Permian-type *Neogondolella* sp.	(Permian)		
		Loc. 30		Kado	chert	no	Permian-type *Neogondolella* sp.	Permian		
						no	*Anchignathodus typicalis*			
		Loc. 31		Kado	chert	no	*Neogondolella balkanica*	Middle Triassic		Misspelled.
						no	*Neospathodus sp.*			Contradictory cooccurrence. *Nicoraella* sp.?
32	Murai *et al.* (1986)	Loc. 32	Suzuki *et al* . (2007a)	Kado	chert	no	*Neogondolella haslachensis*	Triassic?	Ladinian or Carnian?	Contradictory cooccurrence.
						no	*Neospathodus* cf. *newpassensis*			
		Loc. 33 Loc. 41 in [18]		Kado	chert	no	?*Neohindeodella aequiramosa*	Triassic?		
		Loc. 34 Loc. 31 in [18]		Kado	chert	no	?*Neogondolella bulgarica*	Triassic?		
						no	?*Pollognathus kochi*			Misspelled.

to next page

Table 1 Continued.

	Reference	Locality	First citation	Quadrangle	Lithology	Fig.	taxon (as in original)	Period / Epoch	Stage	notes
32	Murai *et al*. (1986) (continued)	Loc. 35 Loc. 32 in [18]? One mismatch.	Suzuki *et al*. (2007a)	Kado	chert	no	?*Neogondolella bulgarica*	Triassic?		
						no	*Neohindeodella triassica*			
		Loc. 36		Kado	chert	no	*Epigondolella mungoensis*	Middle or Late Triassic	Ladinian or Carnian	
						no	*Neospathodus* sp.			*Mosherella* ?
						no	*Gondolella mombergensis*			Contradictory cooccurrence. *N. mombergensis* is endemic to Europe.
		Loc. 37 Loc. 39 in [18]		Kado	chert	no	*Cypridodella muelleri*	Triassic?		
						no	*Neohindeodella suevica*			
		Loc. 38 Loc. 30 in [18]		Kado	chert	no	*Epigondolella bidentata*	Late Triassic	Norian	
						no	*Neogondolella navicula steinbergensis*			
		Loc. 39		Kado	chert	no	?*Neogondolella carinata carinata*	Middle or Late Triassic	Carnian?	Contradictory cooccurrence.
						no	*Neogondolella polygnathiformis*			
						no	*Neogondolella* cf. *reversa*			
						no	*Cratognathodus kochi*			
			Suzuki *et al*. (2007a)			no	*Gondolella haslachensis trammeri*			Contradictory cooccurrence. Misspelled.
		Loc. 40 Loc. 29 in [18]		Kado	chert	no	*Neohindeodella* sp.			
		Loc. 41		Kado	chert	no	*Neogondolella serrata postserrata*	middle Permian	Capitanian	
						no	*Anchignathodus minutus*			
		Loc. 42 Loc. 33 in [18]? One mismatch.		Okawa	chert	no	*Epigondolella abneptis*	Late Triassic	Norian	
						no	*Neogondolella navicula hallstattensis*			
		Loc. 43		Okawa	chert	no	*Neogondolella bulgarica*	Middle Triassic	Anisian	
		Loc. 44		Okawa	chert	no	*Neogondolella navicula navicula*	Late Triassic?		
34	Okami (1990)	OT-20	Suzuki *et al*. (2007a)	Otsuchi	chert	yes	*Neogondolella* cf. *navicula navicula*	(Triassic)		Unidentifiable juvenile.
		OT-4		Otsuchi	chert	yes	*Cornudina sp.*	(Triassic)		Unidentifiable ramiform.
						yes	*Neogondolella navicula navicula*			Unidentifiable juvenile.
		OT-5		Otsuchi	chert	yes	*Neogondolella* cf. *constricta*	(Late Triassic)		Unidentifiable juvenile.
						yes	*Neogondolella navicula hallstattensis*			Figure not sharp.
		OT-7		Otsuchi	chert	no	*Neogondolella* cf. *navicula navicula*	Late Triassic		
		OT-10-1		Otsuchi	chert	yes	*Neogondolella polygnathiformis*	Late Triassic		
						yes	*Neospathodus* sp.			Misidentified; basal cavity small and not upturned.
						no	*Neospathodus* cf. *newpassensis*			
		OT-10-2		Otsuchi	chert	yes	*Epigondolella* cf. *abneptis*	Late Triassic	Norian	*Mockina* sp. (Reduced platform in dorsal pat with upturned aboral margin).
						yes	*Epigondolella* sp.			Figure not sharp.

to next page

Table 1 Continued.

	Reference	Locality	First citation	Quadrangle	Lithology	Fig.	taxon (as in original)	Period / Epoch	Stage	notes
34	Okami (1990) (continued)	OT-17	Suzuki *et al*. (2007a)	Otsuchi	chert	no	*Neogondolella* cf. *polygnathiformis*	Late Triassic		
		OT-30		Otsuchi	chert	yes	*Neospathodus* cf. *spathi*	Early Triassic?		Misidentified; discrete denticles, low thick cusp. *Neospathodus cristagalli*?
		OT-32		Otsuchi	chert	yes	*Neogondolella* sp.	Middle or Late Triassic		Probably juvenile *Paragondolella* (high blade, dorsal platform development).
		O-2		Otsuchi	chert	no	*Cratognathodus kochi*	Late Triassic		
						no	*Neogondolella navicula*			
		O-8		Otsuchi	chert	yes	*Neogondolella* cf. *polygnathiformis*	Late Triassic		Image unclear. Broken?
		O-46		Otsuchi	chert	no	*Neogondolella jubata*	Middle Triassic?		
						no	*Neogondolella* cf. *regale*			
						no	*Neospathodus* cf. *spathi*			
						yes	*Neospathodus* sp.			Maybe *Chiosella* or *Paragondolella* (low blade and posterior brim of platform). Age revised accordingly.
		O-17		Otsuchi	chert	yes	*Neogondolella* sp.	Middle Triassic?		Figure not sharp.
						no	*Neospathodus triangularis*			Contradictory cooccurrence.
		O-19		Otsuchi	chert	no	*Cratognathodus kochi*	Middle Triassic		
						no	*Gondolella (Celsigondolella) watznaueri watznaueri*			
						no	*Neogondolella mombergensis*			*N. mombergensis* is endemic to the Germanic Basin.
		O-20		Otsuchi	chert	no	*Chirodella dindoides*	Triassic?		Contradictory cooccurrence.
						no	*Neospathodus dieneri*			
		O-21		Otsuchi	chert	no	*Neospathodus homeri*	Early or Middle Triassic		
						no	*Neospathodus timorensis*			
		O-48		Otsuchi	chert	no	*Neogondolella (Celsigondolella) watznaueri watznaueri*	Triassic		
						yes	*Neogondolella navicula navicula*			Figure not sharp.
35	Okami *et al*. (1993)	900914-1	Suzuki *et al*. (2007a)	Miyako	chert	no	*Neogondolella mombergensis*	(Triassic)		*N. mombergensis* is endemic to the Germanic Basin.
		900825-1		Miyako	chert	yes	*Anchignathodus typicalis*			Misspelled. *Hindeodus* sp.
		900825-7		Miyako	chert	yes	*Epigondolella abneptis*	Late Triassic	Norian?	*Epigondolella* sp.?
						yes	*Neogondolella polygnathiformis*			Long free blade: *Metapolygnathus*? Age interpreted based on revised identification.
						no	*Neogondoelalla* cf. *polygnathiformis*			
		900825-8		Miyako	chert	yes	*Neospathodus dieneri*	Early Triassic	Olenekian	*Neospathodus* ex gr. *waageni*, arcuate oral margin.
		900821-29		Miyako	chert	no	*Anchignathodus minutus*	Carboniferous or Permian?		Misspelled.
						no	*Diplognathodus* sp.			Misspelled.
		FRY-8		Miyako	chert	yes	*Neogondolella mombergensis*	Middle? Triassic		Misidentification (high middle carina); Triassic gondolellid. *N. mombergensis* is endemic to the Germanic Basin.
						no	*Neogondolella* cf. *mombergensis*			

to next page

Table 1 Continued.

	Reference	Locality	First citation	Quadrangle	Lithology	Fig.	taxon (as in original)	Period / Epoch	Stage	notes
		FRY-10		Miyako	chert	yes	*Epigondolella mungoensis*	Middle or Late Triassic	Ladinian or Carnian	Questionable (no free blade).
						no	*Gladigondolella* cf. *tethydis*			
						no	*Neogondolella foliata*			
		FRY-11		Miyako	chert	yes	*Neogondolella foliata*	Middle Triassic	Ladinian or Carnian	*Paragondolella tadpole* or *P. polygnathiformis* ? (free blade present)
						no	*Epigondolella mungoensis*			
		FRY-12		Miyako	chert	no	*Cratognathodus kochi*	Late Triassic	Carnian	
						no	*Epigondolella abneptis*			
						yes	*Neogondolella polygnathiformis*			Figure not sharp.
						no	*Neogondoelalla* cf. *polygnathiformis*			
						no	*Neospathodus newpassensis*			
		FRY-15		Miyako	chert	yes	*Neogondolella subcarinata*	late Permian	Changhsingian	Figure not sharp.
		KG-12		Miyako	chert	yes	*Antignathodus minutus*			Misspelled. *Hindeodus* sp.
		KGR-9-D		Miyako	chert	yes	*Neogondolella mombergensis*	Middle Triassic	Anisian	Misidentification (high middle carina); Triassic gondolellid.
						yes	*Neogondolella* cf. *bulgarica*			
		KGW-2		Miyako	chert	yes	*Neospathodus homeri*	Early Triassic	Olenekian	
						no	*Neohindeodella* cf. *triassica*			
35	Okami *et al.* (1993) (continued)	KGW-4	Suzuki *et al*. (2007a)	Miyako	chert	yes	*Neogondolella subcarinata*	late Permian	Changhsingian	Juvenile. Figure not sharp.
		KGW-5		Miyako	chert	no	*Neogondolella subcarinata*	late Permian	Changhsingian	
		KGW-8		Miyako	chert	no	*Neogondolella subcarinata*	late Permian	Changhsingian	
		KGW-11		Miyako	chert	yes	*Neospathodus homeri*	Middle Triassic?		*Nicoraella* sp? (narrow basal cavity, carminate); Age revised accordingly.
						no	*Neohindeodella dropla*			
		KGW-12		Miyako	chert	yes	*Anchignathodus minutus*	late Permian	Changhsingian	Misspelled.
						no	*Neogondolella subcarinata*			
		KGW-13		Miyako	chert	yes	*Neogondolella* cf. *carinata*	late Permian?		Contradictory cooccurrence.
						no	*Neogondolella subcarinata*			
		KGW-20		Miyako	chert	no	*Neogondolella polygnathiformis*	Late Triassic	Carnian	
						no	*Epigondolella abneptis*			
		MNM-4		Miyako	chert	yes	*Neogondolella subcarinata*	late Permian?		Figure not sharp.
						no	*Neogondolella* cf. *carinata*			Contradictory cooccurrence.
		MNM-7		Miyako	chert	yes	*Anchignathodus minutus*	Permian?		Misspelled. *Hindeodus* sp.
						no	*Anchignathodus* cf. *typicalis*			
						no	*Neogondolella* sp.			Probably Permian or Triassic gondolellid judging from other specimens.
		TMNM-10-1		Miyako	chert	no	*Neogondolella* cf. *carinata*	late? Permian		Judging from other cases of "*N. carinata*" occurrence, it is likely to refer to a Permian species.

to next page

Table 1 Continued.

	Reference	Locality	First citation	Quadrangle	Lithology	Fig.	taxon (as in original)	Period / Epoch	Stage	notes
35	Okami *et al*. (1993) (continued)	TMNM-10-2	Suzuki *et al*. (2007a)	Miyako	chert	yes	*Anchignathodus minutus*	early? Permian		Misspelled. *Hindeodus* sp.
						no	*Anchignathodus* cf. *minutus*			
						yes	*Neogondolella bisselli*			Juvenile, difficult to identify.
		TMNM-10-3		Miyako	chert	yes	*Diplognathodus* sp.	Carboniferous or Permian?		Figure not sharp. Very likely to be a misidentification.
		TMNM-14		Miyako	chert	no	*Neogondolella polygnathiformis*	Late Triassic		
		TYM-4		Miyako	chert	yes	*Neogondolella* cf. *navicula navicula*	Late Triassic		Juvenile, difficult to identify. TMNM-14 in figure caption.
						no	*Neospathodus newpassensis*			
38	Yoshida *et al*. (1987)	p. 14	Ehiro *et al*. (2008)	Rikuchu-Ono	chert	no	*Paragondolella polygnathiformis*	Late Triassic	Carnian	
		p. 17		Rikuchu-Seki	limestone	no	*Epigondolella abneptis*	Late Triassic	Norian	
		p. 18		Rikuchu-Seki	chert	no	*Epigondolella abneptis*	Late Triassic	Norian	
						no	*Epigondolella bidentata*			
		p. 19		Rikuchu-Seki	chert	no	*Epigondolella abneptis*	Late Triassic	Norian	
41	Takahashi *et al*. (2007) Illustrations published in Takahashi *et al*. (2009)	Pl. 1, fig. 1 (Takahashi *et al*., 2009)	Ehiro *et al*. (2008)	Rikuchu-Seki	chert	yes	Permian-type *Neogondolella* sp.	Permian		Narrowed ventral platform: *Clarkina*?; aboral view only.
		Pl. 1, fig. 2, 3 (Takahashi *et al*., 2009)		Rikuchu-Seki	siliceous claystone	yes	*Hindeodus parvus*	Early Triassic	Induan	
		Pl. 1, fig. 4 (Takahashi *et al*., 2009)		Rikuchu-Seki	siliceous claystone	yes	*Neospathodus cristagalli*	Early Triassic	Olenekian	
		Pl. 1, fig. 5 (Takahashi *et al*., 2009)		Rikuchu-Seki	siliceous claystone	yes	*Neospathodus waageni*	Early Triassic	Olenekian	
43	Yamakita *et al*. (2008)		Ehiro *et al*. (2008)	Rikuchu-Seki	chert	no	*Gondolella clarki*	late Carboniferous	Moscovian	Not mentioned whether fossils were found from one horizon or several different horizons.
						no	*Gondolella gymna*			
						no	*Idiognathodus delicatus*			
						no	*Idiognathoides sinuatus*			
						no	*Diplognathodus atetsuensis*			
						no	*Diplognathodus coloradoensis*			
				Rikuchu-Seki	tuffaceous chert	no	*Gondolella bella*	late Carboniferous	Gzhelian	Not mentioned whether fossils were found from one horizon or several different horizons.
						no	*Streptognathodus elongatus*			
				Rikuchu-Seki	tuffaceous chert	no	*Neogondolella bisselli*	early Permian	Sakmarian or Artinskian	Not mentioned whether fossils were found from one horizon or several different horizons. Sakmarian to Artinskian forms of *S. whitei* are now separated from *S. whitei* and placed in *S.* cf. *asymmetricus* (see Petryshen *et al*., 2020).
						no	*Sweetognathus* cf. *whitei*			

Table 1 Continued.

	Reference	Locality	First citation	Quadrangle	Lithology	Fig.	taxon (as in original)	Period / Epoch	Stage	notes
44	Yamakita *et al.* (2004)		Ehiro *et al.* (2008)	Miyako	chert	no	*Neogondolella bulgarica*	Middle Triassic	Anisian	
				Miyako	chert	no	*Neogondolella* cf. *excelsa*	Middle Triassic	Anisian or Ladinian	
				Miyako	chert	no	*Metapolygnathus polygnathiformis*	Late Triassic	Carnian	
				Miyako	chert	no	*Epigondolella* cf. *abneptis*	Late Triassic	Norian?	
				Miyako	chert	no	*Mockina* cf. *bidentata*	Late Triassic	Norian or Rhaetian	
45	Ehiro *et al.* (2008)	Fig.14.5, 14.6	Ehiro *et al.* (2008)	Kado	chert	yes	*Gondolella clarki*	late Carboniferous	Moscovian	Oral or aboral view only.
		Fig. 14.1, 14.2		Kado	chert (partly tuffaceous)	yes	*Mesogondolella* cf. *bisselli*	early Permian	Sakmarian–Artinskian?	Oral or aboral view only; Possibly other low-bladed *Mesogondolella*.
		Fig. 14.3, 14.4				yes	*Sweetognathus* cf. *whitei*			Rostro-caudal view only; *S.* cf. *asymmetricus* (see Petryshen *et al.*, 2020).
		Fig. 22.1–3		Rikuchu-Seki	chert	yes	*Neogondolella* sp.	Permian		Oral or aboral view only.
47	Murata and Nagai (1972)	Pl. 9 Fig. 21–24	Uchino and Suzuki (2020)	Asamushi	limestone	yes	*Epigondolella bidentata*	Late Triassic	Norian or Rhaetian	
		Pl. 9 Fig. 17–20			limestone	yes	*Epigondolella abneptis*	Late Triassic	Norian?	*Mockina* sp. (posterior carina).
49	Murata *et al.* (1974)		Uchino and Suzuki (2020)	Kodomari	chert, limestone	yes	*Gnathodus* cf. *roundyi*	Carboniferous	Moscovian	*Neognathodus roundyi* (current genus name) has narrower platform.
					chert, limestone	yes	*Gondolella clarki*	Carboniferous	Moscovian	Current genus *Mesogondolella*.
					chert, limestone	yes	*Idiognathodus delicatus*	Carboniferous	Moscovian	*I. delicatus* is often mistakenly used for other species.
					chert, limestone	yes	*Polygnathodella* cf. *convexa*	Carboniferous	Moscovian	Current genus *Idiognathoides*.
61	Takahashi *et al.* (2016)	F.L. 1	This study	Kado	chert	yes	*Epigondolella* sp.	Late Triassic	Norian	Probably *Epigondolella* or *Mockina.*
					chert	yes	*Metapolygnathus* cf. *polygnathiformis*	Late Triassic	Carnian	
		F.L. 2			chert	yes	Permian-type *Neogondolella* sp.	Permian		
					chert	yes	Permian-type *Neogondolella* sp.	Permian		
		F.L. 3			chert	yes	*Metapolygnathus* cf. *polygnathiformis*	Late Triassic	Carnian	Possibly *Metapolygnathus* sp.
		F.L. 5			chert	yes	*Metapolygnathus* cf. *polygnathiformis*	Late Triassic	Carnian	Possibly *Metapolygnathus* sp.
		F.L. 4			chert	yes	*Cratognathodus kochi*	Triassic		
		F.L. 8			chert	yes	Permian-type *Neogondolella* sp.	Permian		
62	Peyrotty *et al*. (2022)		This study	Shiriyazaki	limestone-chert alt.		*Epigondolella rigoi*	Late Triassic	Norian (lower)	
63	Muto *et al.* (2023a)		This study	Rikuchu-Seki	chert	yes	*Misikella longidentata*	Late Triassic	Carnian (lowermost)	
					chert	yes	*Paragondolella* cf. *inclinata*			
					chert	yes	*Paragondolella polygnathiformis*			
					chert	yes	*Sephardiella mungoensis*			
64	Muto *et al.* (2023b)		This study	Rikuchu-Seki	chert	yes	*Mesogondolella clarki*	late Carboniferous	Moscovian	
					chert	yes	*Idiognathodus sinuatus*			
					chert	yes	*Gondolella gymna*			

to next page

Table 1 Continued.

	Reference	Locality	First citation	Quadrangle	Lithology	Fig.	taxon (as in original)	Period / Epoch	Stage	notes
64	Muto *et al.* (2023b) continued.		This study	Rikuchu-Seki	chert	yes	*Streptognathodus vitali*	late Carboniferous	Gzhelian	
					chert	yes	*Streptognathodus* cf. *pauhuskaensis*			
					chert	yes	*Streptognathodus elongatus*			Also reported from same section in Muto *et al.* (2021b).
					chert	yes	*Streptognathodus ruzhencevi*			
					siliceous claystone	yes	*Streptognathodus* cf. *bellus*	late Carboniferous	Gzhelian	*S. bellus* reported from same section in Muto *et al.* (2021b).
					siliceous claystone	yes	*Gondolella postdenuda*			
					siliceous claystone	yes	*Streptognathodus constrictus*	early Permian	Asselian	
					siliceous claystone	yes	*Mesogondolella dentiseparata*			
					siliceous claystone	yes	*Mesogondolella belladontae*			
					siliceous claystone	yes	*Mesogondolella striata*			
					chert	yes	*Mesogondolella bisselli*	early Permian	Artinskian	
					chert	yes	*Mesogondolella* cf. *intermedia*			
					chert	yes	*Sweetognathus* cf. *asymmetricus*			
65	Muto *et al*. (2023c)		This study	Rikuchu-Seki	siliceous claystone	yes	*Ellisonia triassica*	Early Triassic	Olenekian	
					siliceous claystone	yes	*Distcretella* cf. *discreta*			
					siliceous claystone	yes	*Neospathodus dieneri*			
					siliceous claystone	yes	*Neospathodus cristagalli*			
					siliceous claystone	yes	*Neospathodus waageni eowaageni*			
					siliceous claystone	yes	*Neospathodus waageni*			
					siliceous claystone	yes	*Eurygnathodus costatus*			
					siliceous claystone	yes	*Guangxidella* cf. *bransoni*			
66	Ehiro (2008)	Fig. 4	This study	Kuzumaki	chert	yes	*Neogondolella foliata*	Middle Triassic	Ladinian	Age revised from original work.
67	Murai *et al.* (1983)	820827-85	This study	Miyako	chert	no		Late Triassic		
		K811007-44		Sotoyama	chert	no		Permian		
		81730-36		Sotoyama	chert	no		Permian		
		81730-39		Sotoyama	chert	no		Middle Triassic		
		81730-40		Sotoyama	chert	no		Middle Triassic		
		81802-05		Sotoyama	chert	no		Middle Triassic		

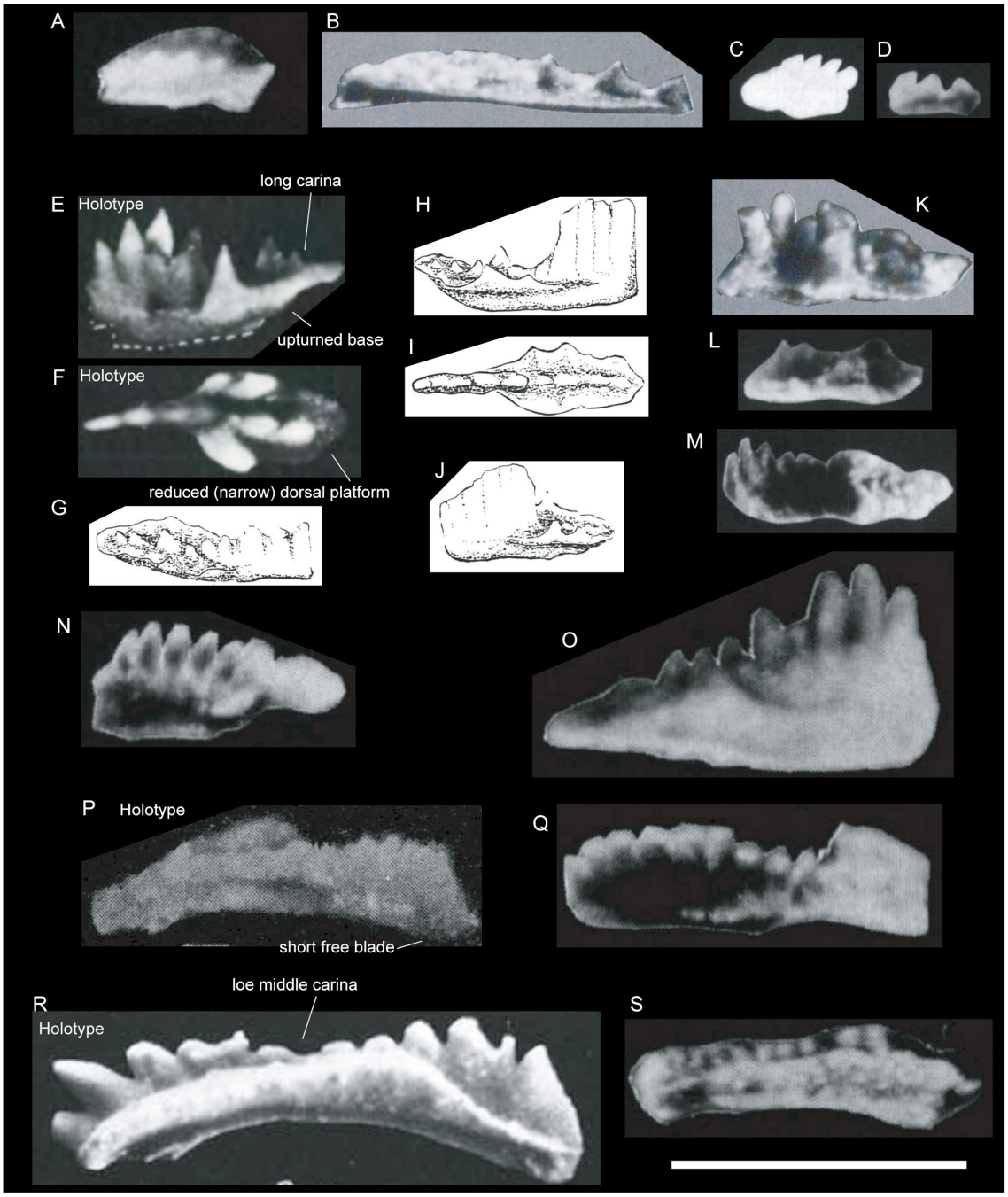

Fig. 9 Images of conodonts from previous studies compared to holotypes. Taxon names are maintained as in original paper. (A) *Neogondolella subcarinata*, Fig. 6.19 of Okami *et al.* (1993), KGW-4. (B) *Neogondolella* cf. *rosenkrantzi*, Pl. 3 Fig. 7 of Murai *et al.* (1985), Loc. 21. (C) *Neogondolella* cf. *constricta*, Fig. 8.6 of Okami (1990), OT-5. (D) *Neogondolella navicula navicula*, Fig. 8.20 of Okami (1990), OT-48. (E, F) Holotype of *Epigondolella postera*, the type species of *Mockina*, from Kozur and Mostler (1971). (E) Lateral view. (F) Oral view. (G–J) *Epigondolella abneptis* of Murata and Nagai (1972) Pl. 9. (G) Fig. 20. (H) Fig. 22. (I) Fig. 17. (J) Fig. 19. (K) *E.* cf. *abneptis* of Murai *et al.* (1985), Pl. 3 Fig. 1, Loc. 20. (L, M) *E.* cf. *abneptis* of Okami (1990), both from OT-10-2. (L) Fig. 8.11. (M) Fig. 8.12. (N, O) *E. abneptis* of Okami *et al.* (1993), both from 900825-7. (N) Fig. 6.9. (O) Fig. 6.10. (P) Holotype of *Gondolella polygnathiformis* from Budurov and Stefanov (1965). (Q) *Neogondolella polygnathiformis* of Okami *et al.* (1993) Fig. 6.18, 900825-7. (R) Holotype of *Gondolella mombergensis* from Tatge (1956). (S) *Neogondolella mombergensis* of Okami *et al.* (1993) Fig. 6.13, KGR-9-D. Scale bar is 500 μm.

and dorsally pointed platform with a carina extending to its end, which is seen in the late Norian genus *Mockina* (Fig. 9E–K). Specimens reported in Okami (1990) can also be placed in *Mockina* for the same reason (Fig. 9L, M). The two specimens in Figs. 6.9 and 6.10 in Okami *et al.* (1993) have respectively stepped and upturned aboral margins (Fig. 9N, O), while the holotype of *E. abneptis* has an arched one. Although this character in their Fig. 6.9 may be due to the immaturity of this specimen and not a taxonomic feature, the other figured specimen can certainly not be regarded as *E. abneptis*.

Epigondolella bidentata, now placed under the genus name *Mockina*, is another species that has been reported from many localities. This species is somewhat potentially problematic because early ontogenetic stages of Late Triassic conodonts with denticulate platforms can appear to be similar (e.g., Mazza and Martínez-Peréz, 2015), and many illustrated conodonts from the North Kitakami Belt are juveniles. On the other hand, at least some occurrences of true *M. bidentata* is confirmed from illustrated specimens (Murata and Nagai, 1972).

Epigondolella primitia, now placed under the genus *Metapolygnathus*, although debatably, have been used for forms now assigned to species of *Carnepigondolella* or *Metapolygnathus* (Mazza *et al.*, 2012; Karádi *et al.*, 2013). True *M. primitius* is considered to be endemic to North America (Mazza *et al.*, 2012). Due to the complete lack of illustrations, it is impossible to evaluate the specimens from the North Kitakami Belt, but it is probably safe to assume that they represent Carnian or Norian (Late Triassic) species.

There are other illustrated conodont specimens with identifications that need to be revised, apart from those mentioned above (refer to Table 1 for full list). In some cases, misidentification is evident, even in the rather poor image quality of the previous studies (Fig. 9P–S). Despite some problematic identifications, age assignment by Triassic conodonts in previous studies seem to be acceptable at the scales of epochs.

6. Conclusions

We investigated a pelagic deep-sea sequence composed of chert and siliceous claystone along the Akka River in Otori, Iwaizumi Town, Iwate Prefecture for conodont biostratigraphy. We identified *Mesogondolella clarki*, *Mesogondolella* aff. *donbasssica*, *Mesogondolella* cf. *bisselli*, *Mesogondolella* cf. *idahoensis*, *Jinogondolella* cf. *palmata*, *Jinogondolella postserrata*, *Sweetognathus iranicus*, *Jinogondolella altudaensis* and *Jinogondolella xuanhanensis* using microfocus X-ray computed tomography. These conodont species indicate the Moscovian of the Pennsylvanian to Capitanian of the Guadalupian for the sedimentary sequence. Comparing the Otori section with the Okoshizawa section, an earlier established pelagic deep-sea sequence in the same tectonostratigraphic unit, there are discrepancies in the stratigraphic distribution of red clayey lithologies. This type of lateral variation in pelagic deep-sea sedimentary rocks has rarely been reported.

We also compiled the reports of conodont occurrences from the North Kitakami Belt. Judging from the dates published, many of the previous reports are based on taxonomic concepts that are out-of-date, but the general lack of clear illustrations makes it impossible to evaluate most of the conodont occurrences. Permian ages of strata based on the occurrence of "Permian-type *Neogondolella*" are particularly problematic, and should be treated with great caution. Most of the species names of Triassic conodonts in the previous studies also do not comply with present taxonomic concepts, but age assignment based on these conodonts are generally acceptable at the epoch-level.

7. Taxonomic notes

(by Shun Muto)

This section is intended to provide objective reference for identification of conodonts and not a full systematic description.

Genus ***Jinogondolella*** Mei and Wardlaw, 1994

Type species ***Gondolella nankingensis*** Ching, 1960

Remarks: Generic distinction of Permian gondollelids is strictly defined by its multielement apparatus (Lambert *et al.*, 2007; Wardlaw and Nestell, 2010). In general, Cisuralian species and most Guadalupian and Lopingian cool-water species are placed in *Mesogondolella*, Guadalupian (mostly warm-water) species typically with serrated platform margins are placed in *Jinogondolella* and Lopingian warm-water species are placed in *Clarkina* (e.g., Henderson, 2018). *Jinogondolella* is the last erected of these three genera. Following this, part of the species included in *Mesogondolella* or *Clarkina* was assigned to *Jinogondolella* (e.g., Mei *et al.*, 1998; Wardlaw and Mei, 1998). While *Jinogondolella* P1 elements typically have serrations, although variably developed, on the ventral portion of the platform margins, our specimens are dominated by unserrated forms.

Jinogondolella altudaensis (Kozur)

(Fig. 7A–E)

1992 *Clarkina altudaensis* — Kozur, p. 103, 105–106, figs. 9–12, 14–17.

Remarks: This species is distinguished by a segminiplanate element with a platform that is biconvex in the dorsal part, rounded at the dorsal end and weakly biconcave in the ventral part due to increased narrowing around the ventral one fourth of the element. The carina is lowest at the middle and the cusp is small and indistinguishable.

Jinogondolella* cf. *palmata Nestell and Wardlaw

(Fig. 7P)

2010 *Jinogondolella palmata* — Nestell and Wardlaw, p. 188–192, pl. 1, figs. 1–26, pl. 2, figs. 1–10, pl. 3, figs. 1–9.

Remarks: This species is distinguished by a segminitpalante element with a broad platform and a carina that is fused in the middle and bears large denticles in the ventral part. Typical forms of this species are widest at the middle and has a cusp that is not distinct, but forms with a platform that is widest in the dorsal area and a distinguishably wide cusp, like the present specimen, are included in this species (e.g., Pl. 7 figs. 2, 6 in Wardlaw and Nestell, 2015).

Jinogondolella postserrata (Behnken)
(Fig. 7J, N)

Jinogondolella* cf. *postserrata (Behnken)
(Fig. 7K)

1975 *Neogondolella serrata postserrata* — Behnken, p. 307–308, pl. 2, figs. 28–36.

Remarks: This species is distinguished by a segminiplanate element with a narrow platform that has subparallel margins in the dorsal half, narrow but distinct furrows, erect cusp and denticles, and a carina that is lowest in the middle and forms a smooth arch in rostro-caudal view. Figure 7K is compared to this species because the cusp and ventral end of platform is partly not visible.

Jinogondolella xuanhanensis (Mei and Wardlaw)
(Fig. 7F, G)

1994a *Mesogonsolella xuanhanensis* — Mei and Wardlaw, p. 33, pl. 3, figs. 2–10, 14.

Remarks: This species is recognized by a segminiplanate element with a narrow platform tapering both ventrally and dorsally from near mid-point, a carina of partly fused denticles and a moderately large cusp.

Genus ***Mesogondolella*** Kozur 1989
Type species ***Gondolella bisselli*** Clark and Behnken, 1971

Remarks: Generally, *Mesogondolella* consists of all gondolellids in the Cisuralian and cold-water gondolellids in the Guadalupian to Lopingian. *Mesogondolella* species in the Pennsylvanian are somewhat problematic, since there is a gap in the stratigraphic record of this genus between the Moscovian and Asselian (Nemyrovska, 2017a; Chernykh, 2005; Muto *et al.*, 2023b). However, the Moscovian species are closer to the Permian *Mesogondolella* in their P1 element morphology compared with the coeval *Gondolella* and are placed in *Mesogondolella* for the time being.

Mesogondolella* cf. *bisselli (Clark and Behnken)
(Fig. 7S, T)

1971 *Gondolella bisselli* — Clark and Behnken, p. 429, pl. 1, figs. 12–14.

Remarks: This species is recognized by a long and narrow segminiplanate element with a low uniform carina and indistinct cusp at the rounded dorsal end.

Mesogondolella clarki (Koike)
(Fig. 7U–W)

1967 *Gondolella clarki* — Koike, p. 301–302, pl. 2, figs. 1–3, 6.

Remarks: This species is characterized by a low, discrete carina, biconvex platform and a cusp of moderate size, the base of which creates a posterior protrusion at the dorsal platform margin.

Mesogondolella* aff. *donbassica (Kossenko)
(Fig. 7X)

2016 *Mesogondolella donbassica* (Kossenko)— Qi *et al.*, fig. 7P.

Remarks: This species, distinguished by the wide, unornamented and round-ended platform and carina that ends short of the dorsal end, was first reported by Kossenko (1975) from the Donets Basin. The holotype has a fused ventral carina and a distinctive gap between the cusp and penultimate denticle. Our specimen has a platform and dorsal denticulation that is similar to *M. donbassica*, but it has more discrete denticles and no gap between the cusp and penultimate denticle, and is regarded as a separate species. Such a form has been reported from the Moscovian of South China (Qi *et al.*, 2016). The name of the author was spelled "Kosenko" in the English title of the original paper, but was spelled "Kossenko" in its systematic section and also in later works including an English paper summarizing the works of Ukranian conodont palaeontologists (Nemyrovska, 2017b).

Mesogondolella* cf. *idahoensis (Youngquist *et al.*)
(Fig. 7Q, R)

1951 *Gondolella idahoensis* — Youngquist, Hawley and Miller, p. 462, pl. 54, figs. 1–3, 14, 15.

Remarks: This species is distinguished by a segminiplanate element with a platform widest in the dorsal part, a squared dorsal margin in oral view, denticles lowering towards the cusp that is positioned at the dorsal end and dominantly higher and thicker than the other denticles. Specimens from near the type locality in Idaho including the holotype have a low ventral carina (Henderson and Mei, 2003, 2007), while forms with high and fused ventral carina are not uncommon elsewhere (Behnken, 1975; Lambert *et al.*, 2007; Zhang *et al.*, 2010). The present specimens from siliceous rocks deposited in pelagic deep Panthalassa belong to the latter type, as are previously recovered specimens from pelagic limestone deposited in Panthalassa (Igo, 1981; Muto *et al.*, 2021a).

Genus ***Sweetognathus*** Clark, 1972
Type species ***Spathognathodus whitei*** Rhodes, 1963

Sweetognathus iranicus Kozur *et al.*
(Fig. 7O)

1975 *Sweetognathus iranicus* — Kozur *et al.*, p. 9–10, pl. 4, figs. 1–10, pl. 5, fig. 1.

Remarks: This species is characterized by a carminiscaphate

element with a dorsal platform bearing a continuous carina of node-like denticles with pustular tops and a free blade about half the length of the platform. In our specimen, the free blade appears longer because the aboral part of the platform is broken off.

Acknowledgements: The authors are grateful to Masanori Ozeki for preparing some of the illustrations for this study. We thank Shinsuke Yagyu and Takuya Matsuzaki for performing μCT scans, Koji Seike for his support in the construction of 3D images using Amira Software, and Tsuyoshi Ito and Hideaki Nagamori for constructive reviews. This study was performed under the cooperative research program of Center for Advanced Marine Core Research (CMCR), Kochi University (Accept No. 22A048, 22B043, 23A025, 23B020).

References

Beauchamp, B., González, D. C., Henderson, C. M., Baranova, D. V., Wang, H. and Pelletier, E. (2022a) Late Pennsylvanian–Early Permian Tectonically Driven Stratigraphic Sequences and Carbonate Sedimentation Along Northern Margin of Sverdrup Basin (Otto Fiord Depression, Arctic Canada). *SEPM Special Publications*, **113**, 226–254. doi: 10.2110/sepmsp.113.12.

Beauchamp, B., Henderson, C. M., Dehari, E., von Bassenheim, D. W., Elliot, S. and González, D. C. (2022b) Carbonate Sedimentology and Conodont Biostratigraphy of Late Pennsylvanian–Early Permian Stratigraphic Sequences, Carlin Canyon, Nevada: New Insights Into the Tectonic and Oceanographic Significance of an Iconic Succession of the Basin and Range. *SEPM Special Publications*, **113**, 34–71. doi: 10.2110/sepmsp.113.14.

Behnken, F. H. (1975) Leonardian and Guadalupian (Permian) Conodont Biostratigraphy in Western and Southwestern United States. *Journal of Paleontology*, **49**, 284–315.

Budurov, K. and Stefanov, S. (1965) Gattung *Gondolella* aus der Trias Bulgariens. *Trudove Byrkhu Geologiyata na Bylgariya, Seriya Paleontologiya [Traveaux Géologiques de Bulagrie Série Paléontologie]*, **7**, 115–121. (in German)

Chernykh, V. V. (2005) *Zonal Method in Biostratigraphy, Zonal Conodont Scale of the Lower Permian in the Urals*. Institute of Geology and Geochemistry of RAN, Ekaterinburg, 217p. (in Russian)

Chernykh, V. V., Chuvashov, B. I., Shen, S. Z., Henderson, C. M., Yuan, D. X. and Stephenson, M. H. (2020) The Global Stratotype Section and Point (GSSP) for the base-Sakmarian Stage (Cisuralian, Lower Permian). *Episodes*, **43**, 961–979. doi: 10.18814/EPIIUGS/2020/020059.

Ching, Y. (1960) Conodonts from the Kufeng Suite (Formation) of Lungtan, Nanking. *Acta Palaeontologica Sinica*, **8**, 230–248.

Clark, D. L. (1972) Early Permian cirsis and its bearing on Permo–Triassic conodont taxonomy. *Geologica et Palaeontologica*, **1**, 147–158.

Clark, D. L. and Behnken, F. H. (1971) Conodonts and biostratigraphy of the Permian. *Memoir of the Geological Society of America*, **127**, 415–439. doi: 10.1130/MEM127-p415.

Ehiro, M. (2008) *Creation of the geologic cross section of the North Kitakami Belt of Northeast Japan: Towards the understanding of the late Mesozoic tectonics of the eastern margin of the Asian Continent*. Japan Society for the Promotion of Science, Tokyo, 16p. (in Japanese)*

Ehiro, M., Nogi, D., Mori, K., Kawashima, G., Suzuki, N. and Yoshihara, K. (2001) Discovery of scleractinian corals from the limestone conglomerate in the Kuzumaki-Kamaishi Belt, Northern Kitakami Massif, Northeast Japan and its significance. *The Journal of the Geological Society of Japan*, **107**, 531–534. doi: 10.5575/geosoc.107.531. (in Japanese with English abstract)

Ehiro, M., Yamakita, S., Takahashi, S. and Suzuki, N. (2008) Jurassic accretionary complexes of the North Kitakami Belt in the Akka-Kuji area. *The Journal of the Geological Society of Japan*, **114**, 121–139. (in Japanese)

Geological Survey of Japan, AIST (2020) Seamless digital geological map of Japan 1: 200,000. Geological Survey of Japan, AIST. https:// gbank.gsj.jp/seamless/v2full/ (Accessed: 2021-10-08)

Henderson, C. M. (2018) Permian conodont biostratigraphy. *Geological Society Special Publication*, **450**, 119–142. doi: 10.1144/SP450.9.

Henderson, C. M. and Mei, S. (2003) Stratigraphic versus environmental significance of Permian serrated conodonts around the Cisuralian–Guadalupian boundary: New evidence from Oman. *Palaeogeography, Palaeoclimatology, Palaeoecology*, **191**, 301–328. doi: 10.1016/S0031-0182(02)00669-7.

Henderson, C. M. and Mei, S. (2007) Geographical clines in Permian and lower Triassic gondolellids and its role in taxonomy. *Palaeoworld*, **16**, 190–201. doi: 10.1016/j.palwor.2007.05.014.

Huckriede, R. (1958) Die Conodonten der mediterranen Trias und ihr stratigraphischer Wert. *Paläontologische Zeitschrift*, **32**, 141–175. doi: 10.1007/BF02989028. (in German)

Igo, H. (1981) Permian conodont biostratigraphy of Japan. *Palaeontological Society of Japan, Special Papers*, **24**, 1–51.

Igo, H. and Hisada, K. (1986) Lower Permian conodonts from the Kawanori Formation of the southwestern Kanto Mountains, Tokyo. *Transactions and Proceedings of the Palaeontological Society of Japan. New series*, 516–527. doi: 10.14825/prpsj1951.1986.144_516.

Isozaki, Y. (1997) Permo-Triassic boundary superanoxia

and stratified superocean: Records from lost deep sea. *Science*, **276**, 235–238. doi: 10.1126/science.276.5310.235.

Isozaki, Y. and Maruyama, S. (1991) Studies on Orogeny based on Plate Tectonics in Japan and New Geotectonic Subdivision of the Japanese Islands. *Journal of Geography (Chigaku Zasshi),* **100**, 697–761. doi: 10.5026/jgeography.100.5_697.

Isozaki, Y. and Matsuda, T. (1980) Age of the Tamba Group along the Hozugawa 'Anticline', western hills of Kyoto, Southwest Japan. *Journal of Geosciences, Osaka City University*, **23**, 115–134.

Isozaki, Y., Maruyama, S., Aoki, K., Nakama, T., Miyashita, A. and Otoh, S. (2010) Geotectonic subdivision of the Japanese Islands revisited: categorization and definition of elements and boundaries of Pacific-type (Miyashiro-type) orogen—. C*higaku Zasshi (Jounal of Geography)*, **119**, 999–1053. doi: 10.5026/jgeography.119.235. (in Japanese with English abstract)

Karádi, V. (2021) Evolutionary trends of the genus Ancyrogondolella (Conodonta) and related taxa in the Norian (Late Triassic). *Journal of Earth Science*, **32**, 700–708. doi: 10.1007/s12583-020-1381-z.

Karádi, V., Kozur, H. W. and Görög, Á. (2013) Stratigraphically Important Lower Norian Conodonts From the Cs Vár Borehole (Csv-1), Hungary – Comparison With the Conodont Succession of the Norian Gssp Candidate Pizzo Mondello (Sicily, Italy). *New Mexico Museum of Natural History Bulletins*, **61**, 284–295.

Koike, T. (1967) A Carboniferous succession of conodont faunas from the Atetsu Limestone in southwest Japan (Studies of Asiatic conodonts, Part 4). *Tokyo Kyoiku Daigaku Science Reports, section C: Geology, Mineralogy, and Geography*, **92**, 279–318.

Koike, T. (1999) Apparatus of a Triassic conodont species Cratognathodus multihamatus (Huckriede). *Paleontological Research*, **3**, 234–248.

Kossenko, Z. A. (1975) New species of conodonts from deposits of the Moskovian Stage in the south-western part of the Donetz Basin (in Russian with English summary). *Geologicheskij Zhurnal*, **35**, 126–133.

Kozur, H. W. (1989) The taxonomy of the gondolellid conodonts in the Permian and Triassic. *1st international Senckenberg conference and 5th European conodont symposium (ECOS V); Contribution III, Papers on Ordovician to Triassic conodonts*, **117**, 409–469.

Kozur, H. W. (1992) Dzhulfian and early Changxingian (Late Permian) Tethyan conodonts from the Glass Mountains, West Texas. *Neues Jahrbuch für Geologie und Paläontologie. Abhandlungen*, **187**, 99–114.

Kozur, H. W. and Mostler, H. (1971) Probleme der Conodontenforschung in der Trias. *Geologisch - Palaeontologische Mitteilungen Innsbruck*, **1**, 1–19. (in German with English summary)

Kozur, H. W., Mostler, H. and Rahimi-Yazd, A. (1975) Beiträge zur Mikropaläontologie permotriadischer Schichtfolgen. Teil II: Neue Conodonten aus dem Oberperm und der basalen Trias von Nord-und Zentraliran. *Geologisch-Paläontologische Mitteilungen Innsbruck*, **5**, 1–23.

Kusunoki, T., Ohara, M. and Musashino, M. (2004) Carboniferous-Permian microbiostratigraphy in chert sequence from the southeastern part of the Tamba Belt, Shizugawa district, Uji City (Outline note). *Earth Science (Chikyu Kagaku)*, **58**, 37–54. (in Japanese with English abstract)

Lambert, L. L., Wardlaw, B. R. and Henderson, C. M. (2007) *Mesogondolella* and *Jinogondolella* (Conodonta): Multielement definition of the taxa that bracket the basal Guadalupian (Middle Permian Series) GSSP. *Palaeoworld*, **16**, 208–221. doi: 10.1016/j.palwor.2007.05.017.

Lambert, L. L., Bell, G. L., Fronimos, J. A., Wardlaw, B. R. and Yisa, M. O. (2010) Conodont biostratigraphy of a more complete Reef Trail member section near the type section, latest Guadalupian series type region. *Micropaleontology*, **56**, 233–253.

Laya, J. C., Tucker, M. E., GröCke, D. R. and Perez-Huerta, A. (2013) Carbon, oxygen and strontium isotopic composition of low-latitude permian carbonates (venezuelan andes): Climate proxies of tropical pangea. *Geological Society Special Publication*, **376**, 367–385. doi: 10.1144/SP376.10.

Matsuda, T. and Isozaki, Y. (1991) Well-documented travel history of Meoszoic pelagic chert in Japan: from remote ocean to subduction zone. *Tectonics*, **10**, 475–499.

Mazza, M. and Martínez-Peréz, C. (2015) Unravelling conodont (Conodonta) ontogenetic processes in the Late Triassic through growth series reconstructions and X-ray microtomography. *Bollottino della Societá Paleontologica Italiana*, **54**, 161–186. doi: 10.4435/BSPI.2015.10.

Mazza, M., Rigo, M. and Gullo, M. (2012) Taxonomy and biostratigraphic record of the Upper Triassic conodonts of the Pizzo Mondello section (western Sicily, Italy), GSSP candidate for the base of the Norian. *Rivista Italiana di Paleontologia e Stratigrafia*, **118**, 85–130.

Mei, S. and Wardlaw, B. R. (1994) *Jinogondolella*: A new genus of Permian gondolellids. *In Proceedings of the International Symposium on Permian Stratigraphy, Environments and Resources, Abstracts*. Guiyang, 20–21.

Mei, S., Jin, Y. and Wardlaw, B. R. (1994a) Succession of conodont zones from the Permian 'Kuhfeng' Formation, Xuanhan, Sichuan and its implication in global correlation. *Acta Palaeontologica Sinica*, **33**, 1–23. (in Chinese with English summary)

Mei, S., Jin, Y. and Wardlaw, B. R. (1994b) Zonation of conodonts from the Maokouan-Wuchianpingian boundary strata, South China. *Palaeoworld*, **4**, 225–233.

Mei, S., Jin, Y. and Wardlaw, B. R. (1998) Conodont succession of the Guadalupian-Lopingian boundary strata in Laibin of Guangxi, China and west Texas, USA. *Palaeoworld*, **9**, 53–76.

Moix, P., Stampfli, G. M. and Mostler, H. (2007) New paleontological, biostratigraphic and paleogeographic results From the Triassic of the Mersin Mélange, SE Turkey. *Natural History*, **41**, 282–311.

Mosher, L. C. (1968) Triassic conodonts from western North America and Europe and their correlation. *Journal of Paleontology*, **42**, 895–946.

Murai, T., Okami, K. and Kudo, H. (1983) *Report on Silica Stone Resources of Iwate Prefecture for the 1982 Fiscal Year*, The Commerce, Industry, and Labor Relations Division of Iwate Prefecture, Morioka, **43** p. (in Japanese, reference information translated by Suzuki *et al.*, 2007)

Murai, T., Okami, K. and Oishi, M. (1985) *Geology of the Pre-Cretaceous in Iwaizumi Town. Part 1*, p. 47. (in Japanese, reference information translated by Suzuki *et al.*, 2007)

Murai, T., Okami, K., Ehiro, M. and Oishi, M. (1986) *Geology of the Pre-Cretaceous in Iwaizumi Town. Part 2*. The Education Board of the Iwaizumi Town, Iwaizumi, p. 13. (in Japanese, reference information translated by Suzuki *et al.*, 2007)

Murata, M. and Nagai, T. (1972) Discovery of conodonts from Sekkenai, Hiranai-cho, Higashi-Tsugaru-gun, Aomori Prefecture, Japan. *Professor Jun-ichi Iwai Memorial Volume*, 709–717.

Murata, M. and Sugimoto, M. (1971) Late Triassic conodonts from the northern part of the Kitakami Massif, Northeast Japan. *The Journal of the Geological Society of Japan*, **77**, 393–394. doi: 10.5575/geosoc.77.393. (in Japanese)

Murata, M., Nagai, T. and Kawamura, S. (1974) Signification and occurrence of late Carboniferous conodont fossil from Cape Kodomari, Tsugaru Peninsula, Aomori Prefecture, Japan. *Aomori-Chigaku*, **26**, 3–5. (in Japanese)

Muto, S. (2021) Recurrent deposition of organic-rich sediments in Early Triassic pelagic Panthalassa and its relationship with global oceanic anoxia: New data from Kyoto, Southwest Japan. *Global and Planetary Change*, **197**, 103402. doi: 10.1016/j.gloplacha.2020.103402.

Muto, S., Takahashi, S., Yamakita, S., Soda, K. and Onoue, T. (2019) Conodont-based age calibration of the Middle Triassic Anisian radiolarian biozones in pelagic deep-sea bedded chert. *Bulletin of the Geological Survey of Japan*, **70**, 43–89. doi: 10.9795/bullgsj.70.43.

Muto, S., Takahashi, S., Yamakita, S. and Onoue, T. (2020) Scarcity of chert in upper Lower Triassic Panthalassic deep-sea successions of Japan records elevated clastic inputs rather than depressed biogenic silica burial flux following the end-Permian extinction. *Global and Planetary Change*, **195**, 103330. doi: 10.1016/j.gloplacha.2020.103330.

Muto, S., Okumura, Y. and Mizuhara, T. (2021a) Late Kungurian Conodonts of Pelagic Panthalassa from Seamount-Capping Limestone in Ogama, Kuzuu, Tochigi Prefecture, Japan. *Paleontological Research*, **25**, 105–119. doi: 10.2517/2020PR012.

Muto, S., Yagyu, S., Takahashi, S. and Murayama, M. (2021b) Identification of conodont fossils in pelagic deep-sea siliceous sedimentary rocks using laboratory-based X-ray computed microtomography. *Lethaia*, **54**, 687–699. doi: 10.1111/let.12432.

Muto, S., Takahashi, S. and Murayama, M. (2022) Cisuralian to Guadalupian (early to middle Permian) conodonts from a deep-sea siliceous succession in the Jurassic accretionary complex of Northeast Japan: implications on conodont biofacies of pelagic Panthalassa. *2022 Pander Society Fifth International Conodont Symposium (ICOS5) Program and Abstracts*, 38.

Muto, S., Ito, T. and Murayama, M. (2023a) Geology and accretionary age of the Otori Unit, North Kitakami Belt. *Bulletin of the Geological Survey of Japan*, **74**, 1–40.

Muto, S., Takahashi, S. and Murayama, M. (2023b) Conodont biostratigraphy of a Carboniferous–Permian boundary section in siliceous successions of pelagic Panthalassa revealed by X-ray computed microtomography. *Frontiers in Earth Science*, **11**, 1–19. doi: 10.3389/feart.2023.1162023.

Muto, S., Takahashi, S. and Yamakita, S. (2023c) Elevated sedimentation of clastic matter in pelagic Panthalassa during the early Olenekian. *Island Arc*, **32**, e12485.

Nemyrovska, T. I., Perret-Mirouse, M.-F. and Alekseev, A. S. (1999) On Moscovian (Late Carboniferous) conodonts of the Donets Basin, Ukraine. *Neues Jahrbuch für Geologie und Paläontologie. Abhandlungen*, **214**, 169–194.

Nemyrovska, T. I. (2011) Late Moscovian (Carboniferous) conodonts of the genus Swadelina from the Donets Basin, Ukraine. *Micropaleontology*, **57**, 491–505.

Nemyrovska, T. I. (2017a) Late Mississippian-Middle Pennsylvanian conodont zonation of Ukraine. *Stratigraphy*, **14**, 299–318. doi: 10.29041/strat.14.1-4.299-318.

Nemyrovska, T. I. (2017b) Paleozoic Conodont Studies in Ukraine. *Collection of Scientific Works of the Institute of Geological Sciences of the NAS of Ukraine*, **10**, 124–136. doi: 10.30836/igs.2522-9753.2017.142182.

Nestell, M. K. and Wardlaw, B. R. (2010) *Jinogondolella palmata*, a new Gondolellid conodont species from the Bell Canyon formation, middle Permian, West Texas. *Micropaleontology*, **56**, 185–194.

Nishikane, Y., Kaiho, K., Takahashi, S., Henderson, C. M., Suzuki, N. and Kanno, M. (2011) The Guadalupian-Lopingian boundary (Permian) in a pelagic sequence from Panthalassa recognized by

integrated conodont and radiolarian biostratigraphy. *Marine Micropaleontology*, **78**, 84–95. doi: 10.1016/j.marmicro.2010.10.002.

Nishikane, Y., Kaiho, K., Henderson, C. M., Takahashi, S. and Suzuki, N. (2014) Guadalupian-Lopingian conodont and carbon isotope stratigraphies of a deep chert sequence in Japan. *Palaeogeography, Palaeoclimatology, Palaeoecology*, **403**, 16–29. doi: 10.1016/j.palaeo.2014.02.033.

Okami, K. (1990) Depositional age and environment of bedded manganese deposits distributed in Otaniyama mine area, southeastern part of the northern Kitakami massif, Northeast Japan. *Mining Geology*, **40**, 257–268. doi: 10.11456/shigenchishitsu1951.40.257. (in Japanese with English abstract)

Okami, K. and Ehiro, M. (1988) Review and recent progress of studies on the Pre-Miyakoan sedimentary rocks of the Northern Kitakami Massif, Northeast Japan. *Earth Science (Chikyu Kagaku),* **42**, 187–201. (in Japanese with English abstract)

Okami, K., Koshiya, S., Tomokazu, S. and Araya, S. (1993) Stratigraphic study on the bedded manganese deposits distributed in the northern area of the Otaniyama mine, southeastern part of the Northern Kitakami Mountains, Northeast Japan. *Resource Geology*, **43**, 375–385. (in Japanese with English abstract)

Petryshen, W., Henderson, C. M., De Baets, K. and Jarochowska, E. (2020) Evidence of parallel evolution in the dental elements of *Sweetognathus* conodonts: *Sweetognathus* Evolutionary Mechanisms. *Proceedings of the Royal Society B: Biological Sciences*, **287**, 20201922. doi: 10.1098/rspb.2020.1922.

Peyrotty, G., Fucelli, A., Peybernes, C., Onoue, T., Ueda, H. and Martini, R. (2022) Sedimentology and biostratigraphy of the upper Triassic carbonates from the Shiriya cape, North Kitakami Belt, Japan. *Island Arc*, **31**, 1–19. doi: 10.1111/iar.12473.

Qi, Y., Hu, K., Wang, Q. and Lin, W. (2014) Carboniferous conodont biostratigraphy of the dianzishang section, Zhenning, Guizhou, South China. *Geological Magazine,* **151**, 311–327. doi: 0.1017/S0016756813000344.

Qi, Y. P., Lambert, L. L., Nemyrovska, T. I., Wang, X. D., Hu, K. Y. and Wang, Q. L. (2016) Late Bashkirian and early Moscovian conodonts from the Naqing section, Luodian, Guizhou, South China. *Palaeoworld*, **25**, 170–187. doi: 10.1016/j.palwor.2015.02.005.

Rhodes, F. H. T. (1963) Conodonts from the topmost Tensleep sandstone of the eastern Big Horn Mountains, Wyoming. *Journal of Paleontology*, **37**, 401–408.

Ritter, S. M. (2020) Improved conodont biostratigraphic constraint of the Carboniferous/Permian boundary in south-central New Mexico, USA. *Stratigraphy*, **17**, 39–56. doi: 10.29041/strat.17.1.39-56.

Sobolev, N. N. and Nakrem, H. A. (1996) Middle Carboniferous-Lower Permian conodonts of Novaya Zemlya. *Norsk Polarinstitut Skrifter*, **199**, 1–129.

Sugimoto, M. (1974) Stratigraphical study in the outer belt of the Kitakami Miassif, Northeast Japan. *Contributions from the Institute of Geology and Paleontology, Tohoku University*, **74**, 1–48. (in Japanese with English abstract)

Sun, Y. D., Liu, X. T., Yan, J. X., Li, B., Chen, B., Bond, D. P. G., Joachimski, M. M., Wignall, P. B., Wang, X. and Lai, X. L. (2017) Permian (Artinskian to Wuchapingian) conodont biostratigraphy in the Tieqiao section, Laibin area, South China. *Palaeogeography, Palaeoclimatology, Palaeoecology*, **465**, 42–63. doi: 10.1016/j.palaeo.2016.10.013.

Suzuki, N., Ehiro, M., Yoshihara, K., Kimura, Y., Kawashima, G., Yoshimoto, H. and Nogi, T. (2007a) Geology of the Kuzumaki-Kamaishi Subbelt of the North Kitakami Belt (a Jurassic accretionary complex), Northeast Japan: Case study of the Kawai-Yamada area, eastern Iwate Prefecture. *Bulletin of the Tohoku University Museum*, **6**, 103–174.

Suzuki, N., Yamakita, S., Takahashi, S. and Ehiro, M. (2007b) Middle Jurassic radiolarians from carbonate manganese nodules in the Otori Formation in the eastern part of the Kuzumaki-Kamaishi Subbelt, the North Kitakami Belt, Northeast Japan. *The Journal of the Geological Society of Japan*, **113**, 274–277. doi: 10.5575/geosoc.113.274. (in Japanese with English abstract)

Szaniawski, H. and Malkowski, K. (1979) Conodonts from the Kapp Starostin Formation (Permian) of Spitsbergen. *Acta Palaeontologica Polonica*, **24**.

Takahashi, S., Yamakita, Satoshi, Suzuki, N., Oba, M., Kakegawa, T., Kaiho, K. and Ehiro, M. (2007) A negative carbon isotope anomaly in deep-sea Permian/Triassic boundary of the North Kitakami Belt, Japan. *The 21st Century COE (Earth Science) International Symposium: Dynamic Earth: its origin and future, September 19, Sendai, Japan.*

Takahashi, S., Yamakita, S., Suzuki, N., Kaiho, K. and Ehiro, M. (2009) High organic carbon content and a decrease in radiolarians at the end of the Permian in a newly discovered continuous pelagic section: A coincidence? *Palaeogeography, Palaeoclimatology, Palaeoecology*, **271**, 1–12. doi: 10.1016/j.palaeo.2008.08.016.

Takahashi, S., Ehiro, M., Suzuki, N. and Yamakita, S. (2016) Subdivisional scheme of the North Kitakami Belt, Northeast Japan and its tectonostratigraphic correlation to the Oshima and South Chichibu belts: an examination of the Jurassic accretionary complex in the west Akka area. *Journal of the Geological Society of Japan*, **122**, 1–22. doi: 10.5575/geosoc.2015.0034. (in Japanese with English abstract)

Tanaka, K. (1980) Kanoashi Group, an olistostrome, in the Nichihara area, Shimane Prefecture. *Journal of the Geological Society of Japan*, **86**, 613–628. (in Japanese with English abstract)

Tatge, U. (1956) Conodonten aus dem germanischen Muschelkalk. *Paläontologische Zeitschrift*, **30**, 108–127. doi: 10.1007/BF03041777. (in German)

Tomimatsu, Y., Nozaki, T., Sato, H., Takaya, Y., Kimura, J.-I., Chang, Q., Naraoka, H., Rigo, M. and Onoue, T. (2020) Marine osmium isotope record during the Carnian "pluvial episode" (Late Triassic) in the pelagic Panthalassa Ocean. *Global and Planetary Change*, **197**, 103387. doi: 10.1016/j.gloplacha.2020.103387.

Toyohara, F., Uyesugi, K., Kimura, T., Ito, T., Murata, A. and Iwamatsu, A. (1980) Geosyncline in the northern Kitakami Massif and the Oshima Peninsula. *In*: Kimura, T. (ed.) *Report on the Multidiscipline Research Project A with 1979 Foundation of Grant-in-Aid for Scientific Research by the Education Ministry of Japan*, Tokyo Print Insatsu, Ltd., Tokyo, 27–36. (in Japanese)*

Uchino, T. and Suzuki, N. (2020) Late Jurassic radiolarians from mudstone near the U–Pb-dated sandstone of the North Kitakami Belt in the northeastern Shimokita Peninsula, Tohoku, Japan. *Bulletin of the Geological Survey of Japan*, **71**, 313–330. doi: 10.9795/bullgsj.71.313.

Wang, C. Y. and Wang, Z. H. (1981) Permian conodont biostratigraphy of China. *Special Paper of the Geological Society of America*, **187**, 227–236. doi: 10.1130/SPE187-p227.

Wang, Z. and Qi, Y. (2003) Upper Carboniferous (Pennsylvanian) conodonts from South Guizhou of China. *Rivista Italiana di Paleontologia e Stratigrafia*, **109**, 379–397.

Wardlaw, B. R. (2000) Guadalupian conodont biostratigraphy of the Glass and Del Norte Mountains. *In*: Wardlaw, B. R., Grant, R. E. and Rohr, D. M. (eds) *The Guadalupian Symposium Smithsonian Contribution to the Earth Sciences,* 2237–87.

Wardlaw, B. R. and Mei, S. (1998) A discussion of the early reported species of *Clarkina* (Permian Conodonta) and the possible origin of the genus. *Palaeoworld*, **9**, 33–52.

Wardlaw, B. R. and Mei, S. (1999) Redefined conodont biostratigraphy of the Permian and lowest Triassic of the Salt and Khizor Ranges, Pakistan. *In* Yin, H. and Tong, J. eds., *Proceedings of the International Conference on Pangea and the Paleozoic-Mesozoic Transition*. China University of Geosciences, Wuhan, 154–156.

Wardlaw, B. R. and Nestell, M. K. (2010) Latest middle Permian conodonts from the Apache mountains, West Texas. *Micropaleontology*, **56**, 149–184. doi: 10.47894/mpal.56.1.05.

Wardlaw, B. R. and Nestell, M. K. (2015) Conodont faunas from a complete basinal succession of the upper part of the Wordian (Middle Permian, Guadalupian, West Texas). *Micropaleontology*, **61**, 257–292.

Yamakita, S., Ehiro, M., Suzuki, N. and Kano, H. (2004) Conodonts from a chert–clastic sequence and its oceanic plate stratigraphy in southwestern part of the Northern Kitakami Belt. *Annual Meeting of the Geological Society of Japan, abstracts*, **172**. (in Japanese)

Yamakita, S., Ehiro, M., Takahashi, S. and Suzuki, N. (2008) Late Carboniferous and Early Permian conodonts from the Otori Formation in the North Kitakami Belt, Northeast Japan. *Abstracts with Programs The 2008 Annual Meeting The Palaeontological Society of Japan (July 4–6, Sendai, Miyagi),* **B07**, 34. (in Japanese)

Yamashita, D., Kato, H., Onoue, T. and Suzuki, N. (2018) Integrated Upper Triassic Conodont and Radiolarian Biostratigraphies of the Panthalassa Ocean. *Paleontological Research*, **22**, 167–197. doi: 10.2517/2017pr020.

Yao, A., Matsuda, T. and Isozaki, Y. (1980) Triassic and Jurassic radiolarians from the Inuyama area, central Japan. *Journal of Geosciences, Osaka City University*, **23**, 135–154.

Yao, J., Yao, A. and Kuwahara, K. (2001) Upper Permian biostratigraphic correlation between conodont and radiolarian zones in the Tamba-Mino Terrane, Southwest Japan. *Journal of Geosciences*, **44**, 97–119.

Yoshida, S. (1980) The geological relationship between the North Kitakami and South Kitakami belts. *In* Kimura, T. ed., *Report on the Multidiscipline Research Project A with 1979 Foundation of Grant-in-Aid for Scientific Research by the Education Ministry of Japan*. Tokyo Print Insatsu, Ltd., Tokyo, 9–26. (in Japanese)

Yoshida, T., Yoshii, M., Katada, M., Tanaka, K., Sakamoto, T. and Satoh, H. (1987) Geology of the Rikuchu-Ono district with Geological Sheet Map at 1: 50000, Geological Survey of Japan, 70 p. (in Japanese with English abstract)

Youngquist, W., Hawley, R. W., Miller, A. K., Journal, S. and May, N. (1951) Phosphoria Conodonts from Southeastern Idaho. *Sedimentary Geology*, **25**, 356–364.

Zhang, N., Henderson, C. M., Xia, W., Wang, G. and Shang, H. (2010) Conodonts and radiolarians through the Cisuralian-Guadalupian boundary from the Pingxiang and Dachongling sections, Guangxi region, South China. *Alcheringa*, **34**, 135–160. doi: 10.1080/03115510903523292.

*English translation from the original written in Japanese

Recieved February 13, 2024
Accepted November 6, 2024

岩手県岩泉町大鳥の層状チャートから産出した石炭紀・ペルム紀コノドント化石ならびに北部北上帯の既報コノドントのレビュー

武藤　俊・高橋　聡・村山　雅史

要　旨

ジュラ紀付加体中の遠洋域深海堆積岩層において，コノドント生層序は世界規模で対比可能な時間軸を与える．北部北上山地は，特にコノドント生層序区分が不完全な古生代の時代に関して研究を進展させうる層序記録を保持している．本報告では，岩手県岩泉町に位置する大鳥セクションと名付けた深海堆積岩セクションにおいて産出したコノドント化石を報告する．コノドント化石はマイクロフォーカスX線CTを用いた手法によって画像を取得した．同定された種は，*Mesogondolella clarki*, *Mesogondolella* aff. *donbassica*, *Mesogondolella* cf. *bisselli*，*Mesogondolella* cf. *idahoensis*, *Jinogondolella* cf. *palmata*，*Jinogondolella postserrata*，*Sweetognathus iranicus*，*Jinogondolella altudaensis*，*Jinogondolella xuanhanensis* である．これらのコノドントはモスコビアン期（ペンシルバニアン亜紀中期，石炭紀）からキャピタニアン期（グアダルピアン世後期，ペルム紀）の年代を示す．本研究ではさらに，先行研究による北部北上山地におけるコノドント産出報告をレビューした．先行研究でも石炭紀後期から三畳紀の時代がコノドント化石をもとに指示されているが，これらのうちペルム紀の年代の大部分は分類記載と画像が示されていないために検証できない．

難読･重要地名

Akka：安家，Okoshizawa：大越沢，Otori：大鳥

Bulletin of the Geological Survey of Japan, vol. 76 (1/2), p. 31–50, 2025

Article

Middle Jurassic radiolarians from manganese nodules obtained in the western part of the Kado District, northern Kitakami Mountains

MUTO Shun[1,*], ITO Tsuyoshi[1] and OZEKI Masanori[1, 2]

MUTO Shun, ITO Tsuyoshi and OZEKI Masanori (2025) Middle Jurassic radiolarians from manganese nodules obtained in the western part of the Kado District, northern Kitakami Mountains. *Bulletin of the Geological Survey of Japan*, vol. 76 (1/2), p. 31–50, 8 figs, 1 table and 5 plates.

Abstract: The accretionary history of the Jurassic accretionary complex of the North Kitakami Belt in Northeast Japan is obscured by the metamorphism of Cretaceous plutons that hinder extraction of radiolarian fossils. Some of the most successful cases of radiolarian extraction in this area treated manganese nodules. In this study, we obtained well-preserved radiolarians from three manganese nodules embedded in argillaceous rocks in the western part of the 1: 50,000 quadrangle series Kado District. The age of the radiolarian fossil assemblages is assigned to the early Bajocian and Aalenian to Bajocian (Middle Jurassic) for two samples from grey bedded mudstone and Bajocian (Middle Jurassic) for a sample from mudstone that possibly experienced tectonic mixing. The age of the assemblages approximates the accretionary age of the studied rocks. This is the first report of age diagnostic radiolarians from the western part of the Kado District.

Keywords: Aalenian, accretionary age, Bajocian, Jurassic accretionary complex, Nassellaria, North Kitakami–Oshima Belt, Otori Unit, Quadrangle Series, Toarcian

1. Introduction

The North Kitakami–Oshima Belt in Northeast Japan (e.g., Isozaki and Maruyama, 1991) mainly consists of an accretionary complex that was formed mostly during the Jurassic (Ehiro *et al.*, 2005; Kojima *et al.*, 2016). Works on radiolarian fossils and zircon dating clarified that the age of accretion, approximated by the age of trench-fill clastic rocks, was from the latest Triassic to Early Cretaceous, although the oldest accretionary complex may date back to the late Permian (Fig. 1B and references therein). The accretionary complex of the North Kitakami–Oshima Belt is much less studied in terms of accretionary history compared to its counterparts in Southwest Japan. One of the reasons is the difficulty in obtaining radiolarians due to metamorphism related to Cretaceous plutons that intrude the accretionary complex (Fig. 1B).

The best results of radiolarian investigation in the North Kitakami–Oshima Belt are arguably the works on manganese nodules (Mn-nodules) that are found in mudstone or siliceous mudstone (Yoshihara *et al.*, 2002; Suzuki and Ogane, 2004; Suzuki *et al.*, 2007a, b; Ehiro *et al.*, 2008; Muto *et al.*, 2023). Manganese nodules investigated in these works have yielded radiolarians with clearly observable external and internal test structures, even when radiolarians extracted from the surrounding argillaceous rocks are poorly preserved. However, Mn-nodules are relatively rare and not always easy to spot in the field, reflected in the few number of works.

The first author (Muto, S.) conducted surveys to produce the 1: 50,000 geological map of the Kado District for the Quadrangle Series of the Geological Survey of Japan, AIST. The district is located within the area of the North Kitakami Belt (the part of the North Kitakami–Oshima Belt distributed in Honshu). As part of this project, we investigated newly found Mn-nodules for radiolarians, in order to obtain further controls on the accretionary age of the surveyed strata. The Mn-nodules were found in the western part of the Kado District, in Iwaizumi Town and Kuzumaki Town in northeast Iwate Prefecture. This is the first time that age diagnostic radiolarians have been successfully extracted from rocks in this area.

2. Geological outline

The Kado District of the 1:50,000 Quadrangle Series is situated in the central area of the North Kitakami Belt and straddles the Omotogawa Fault (Omotogawa is the

[1] AIST, Geological Survey of Japan, Research Institute of Geology and Geoinformation
[2] Graduate School of Life and Environmental Sciences, University of Tsukuba, 1-1-1 Tennodai, Tsukuba, Ibaraki, 305-8572, Japan
* Corresponding author: MUTO, S., AIST Tsukuba Central 7, 1-1-1 Higashi, Tsukuba, Ibaraki 305-8567, Japan. Email: s-muto@aist.go.jp

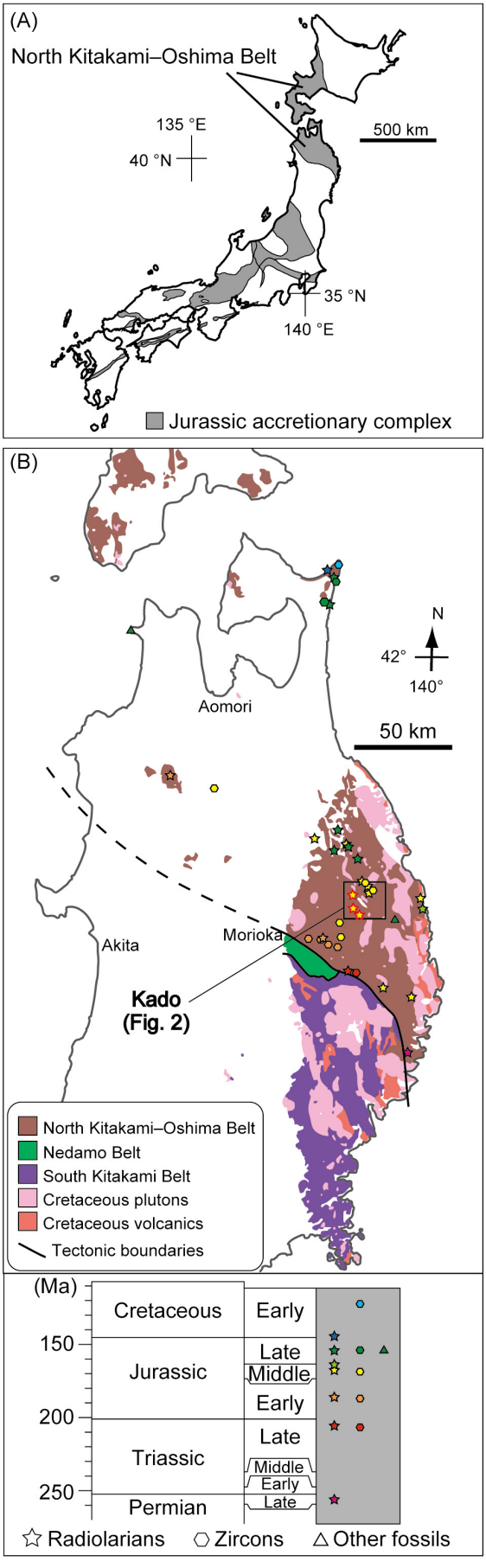

Japanese for the Omoto River) (Figs. 1B, 2). The area northeast of the Omotogawa Fault includes one of the better studied areas of the North Kitakami Belt. Sugimoto (1974) provided some of the first detailed geological maps and lithostratigraphic framework of the North Kitakami Belt in the Akka–Kuji area. Sugimoto (1980) extended the survey area to the Iwaizumi area. Following the wide acceptance of plate tectonics, the geology was revised based on the concept of accretionary complexes (Ehiro *et al.*, 2008; Takahashi *et al.*, 2016; Nakae *et al.*, 2021; Muto *et al.*, 2023), although fundamentals of the lithostratigraphic division by Sugimoto (1974, 1980) still stands. The more recent studies showed that the strata of the Akka–Kuji area comprise Middle to Late Jurassic accretionary complexes that generally trend NW–SE and become younger to the northeast. The age of the strata was determined by radiolarians (Nakae and Kamada, 2003; Suzuki *et al.*, 2007b; Ehiro *et al.*, 2008; Muto *et al.*, 2023) and detrital zircons (Muto *et al.*, 2023).

On the other hand, the area stretching from close to the Omotogawa Fault to the southwest part of the Kado district is less studied. Onuki (1969) proposed a rough stratigraphic division of this area. Yamaguchi (1981) published a geological map with more details in the eastern part of the map by Onuki (1969). Murai *et al.* (1985, 1986) extended the geological map by Sugimoto (1974, 1980) to the northwest part of Iwaizumi Town, updating the stratigraphic division by Onuki (1969). While these maps were informative about the general characteristics of lithofacies and geological structures in the area, these works lacked detailed traverse maps of main routes. These studies also did not obtain age data from clastic rocks that would constrain the time of accretion. Therefore, correlation of stratigraphic units or re-interpretation of the units as accretionary complexes are somewhat difficult. The first author (S. Muto) revised the stratigraphic division by the above works from the viewpoint of subduction–accretion, based on a geological field survey of the entire Kado District (Fig. 2). By this revision, most of the Jurassic accretionary complex mapped by Onuki (1969), Yamaguchi (1981) and Murai *et al.* (1985, 1986) is included in a tectonostratigraphic unit called the Otori Unit (sensu Muto *et al.*, 2023), except for strata that were already classified as other units by Takahashi *et al.* (2016) and Nakae *et al.* (2021). The strata of the Otori Unit are composed mainly of chert, mudstone and sandstone, which is in agreement to maps by previous workers.

Fig. 1 (A) Distribution of the Jurassic accretionary complex in Japan (after Isozaki *et al.*, 2010). (B) Geology of the basement rocks of the northern Tohoku Region (modified from Geological Survey of Japan, AIST, 2020). Age constraints for time of accretion are based on the compilation by Uchino and Suzuki (2020) and additional references in Muto *et al.* (2023). Data plots closed in red were obtained in this study.

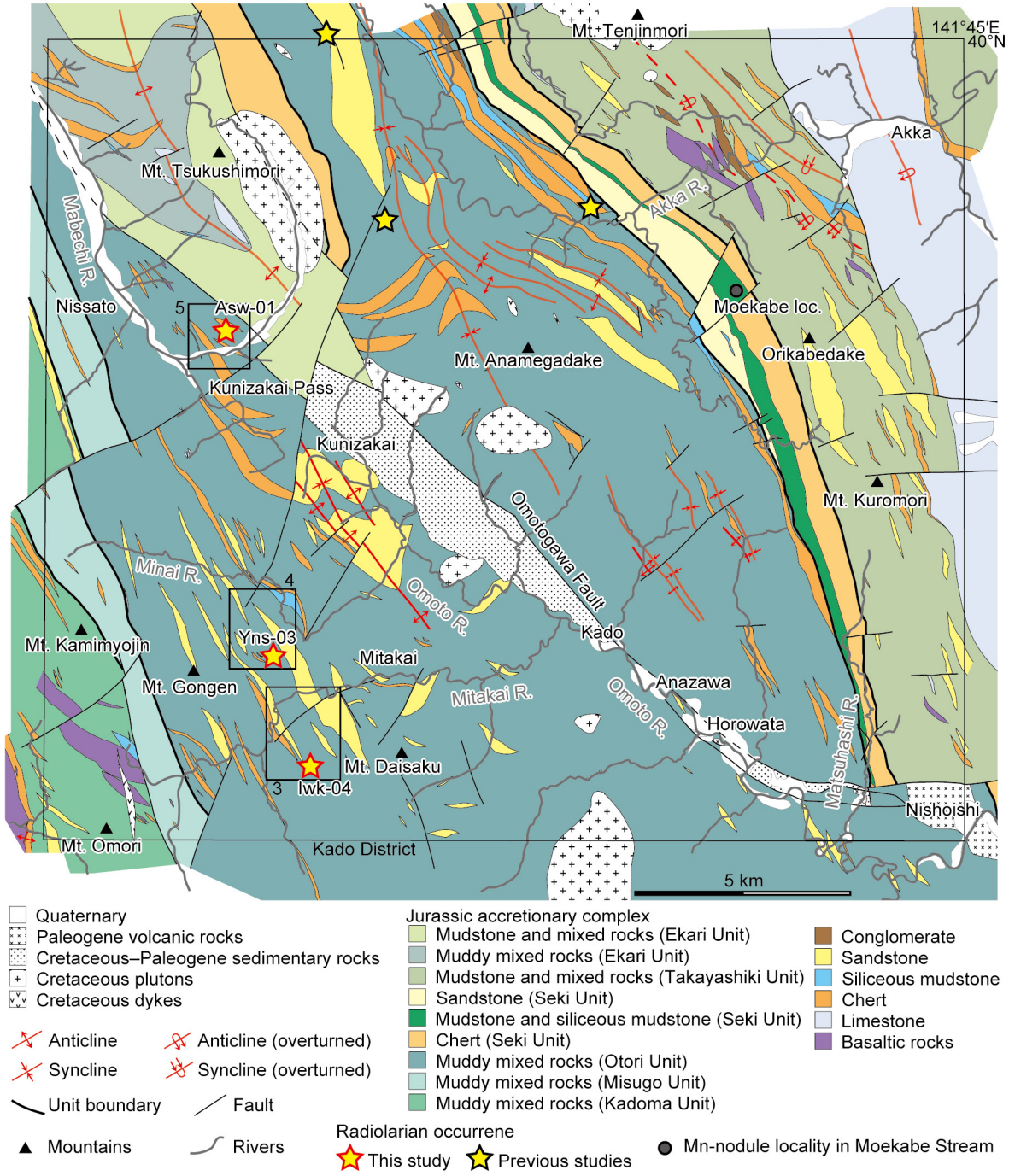

Fig. 2 Geological outline of the Kado District based on geological surveys conducted for the 1: 50,000 geological map of the "Kado" District for the Quadrangle Series of the Geological Survey of Japan, AIST by Muto, S. Locations of Figs. 3–5 are shown.

The samples investigated in this study were collected from the southwest part of the Otori Unit (Fig. 2). The accretionary age of the northeast part of the Otori Unit is the Middle Jurassic (Suzuki *et al.*, 2007b; Ehiro *et al.*, 2008; Muto *et al.*, 2023). To the southwest lie Middle Jurassic accretionary complexes belonging to another unit, the Kadoma Unit (Uchino and Komatsubara, 2024). Thus, strata of the studied area are expected to belong to a Middle Jurassic accretionary complex.

3. Materials and Methods

We investigated manganese nodule (Mn-nodule) samples from three localities for extraction of radiolarians

(Figs. 2–5).

Sample Iwk-04 was obtained from grey mudstone in a locality south of Mt. Iwakura in Gongen, Iwaizumi Town, along a small valley branching from the north bank of Orikabe Stream, a tributary of the Mitakai River (Figs. 2, 3). A major part of the lithofacies distributed around the locality are muddy mixed rocks with blocks of sandstone and chert (Fig. 6A). The muddy mixed rocks are accompanied by smaller amounts of sandstone, mudstone without blocks of other lithologies, siliceous mudstone and chert. Of these, grey bedded mudstone without exotic blocks (Fig. 6B) hosted Mn-nodules in the studied locality. The Mn-nodules are black and lenticular with their long axis parallel to the bedding and cleavage plain of the host mudstone. At the outcrop surface, the Mn-nodules tend to be preferentially eroded and appear as holes (Fig. 6C). The lack of exotic blocks of other lithologies in the grey mudstone that hosts the nodules imply that the Mn-nodules were not introduced by tectonic mixing.

Sample Yns-03 was obtained from grey mudstone exposed along Yunashigi Stream, a tributary of the Minai River in Minaikawa, Iwaizumi Town (Figs. 2, 4). The Yunashigi Stream locality is situated close to the lateral extension of the Mt. Iwakura locality (Fig. 2). The lithofacies distributed in the Yunashigi Stream locality is the same as that of the Mt. Iwakura locality, and is composed mostly of muddy mixed rocks with sandstone, mudstone, siliceous mudstone and chert (Fig. 4). The mode of occurrence of Mn-nodules is also same as that of the Mt. Iwakura locality (Fig. 6D).

Sample Asw-01 was obtained from dark brown weathered mudstone exposed to the north of Arasawaguchi in Ekari, Kuzumaki Town (Figs. 2, 5). Outcrops in this area are generally isolated and small, and in many cases the rocks are strongly weathered. Judging from the available outcrops, the lithofacies is composed of muddy mixed rocks with blocks of sandstone, siliceous mudstone and chert (Figs. 5, 6E), similar to the other two localities. The sample was collected from a very small outcrop of weathered mudstone (Fig. 6F). The mudstone contains no outstanding blocks of other lithologies, but is not distinguishable from mudstone matrix of mixed rocks in the area, which is usually black prior to strong weathering. Therefore, we consider that this sample was either originally contained in mudstone that later became the matrix of muddy mixed rocks, or was introduced into the present position from other lithologies, most likely grey mudstone or siliceous mudstone, which are the host of all other radiolarian-bearing Mn-nodules in the North Kitakami Belt.

In thin sections, all Mn-nodule samples are composed of metalliferous parts cemented by opaque minerals, most likely Mn-oxides, and silicified parts cemented with microcrystalline to cryptocrystalline quartz matrix (Figs. 7A–D). The metalliferous and silicified parts are amalgamated in a mosaic manner. This microfabric is quite different from Mn-nodules obtained from siliceous mudstone in the Jurassic accretionary complex in Southwest Japan (the Inuyama area; Nakada *et al.*, 2014). Radiolarian tests are present in both metalliferous (Fig. 7D) and silicified (Fig. 7B) parts, while preservation is better in the former. The grey mudstone that hosts the Mn-nodules in the Mt. Iwakura and Yunashigi Stream localities is composed of clay minerals and quartz grains in thin section (Fig. 7E). Coarse clastic grains of silt-size or greater are rare, indicating that these rocks represent clastic sedimentation close to the hemipelagic area.

A Mn-nodule sample was also collected near Moekabe Stream (Moebake loc. in Fig. 2), but this sample yielded no radiolarians, and will not be discussed further.

Manganese nodule samples were crushed into pieces a few centimetres across and treated with 36 % hydrochloric (HCl) acid for 24 h. The residues were rinsed and dried. Specimens were prepared into slides and photographed with an optical microscope with transmitted light, or mounted on metal stubs, coated with carbon and photographed by a scanning electron microscope (Hitachi SU3500) at the Geological Survey of Japan.

4. Radiolarian assemblage

The three samples Iwk-04, Yns-03 and Asw-01 yielded radiolarians with preservations well enough to observe internal and external test structures (Plate 1–5; Table 1). On the other hand, Our failed attempt on the sample from the Moekabe Stream shows that not all Mn-nodules are radiolarian-productive, as mentioned in Muto *et al.* (2023). Below, the age of the radiolarian assemblages is discussed based on stratigraphic ranges by Baumgartner *et al.* (1995) and O'Dogherty *et al.* (2009) (Fig. 8). The two samples from grey bedded mudstone that are lithostratigraphically well-controlled are explained first, followed by the sample from possibly mixed mudstone.

4. 1. Mt. Iwakura locality (Iwk-04)

Sample Iwk-04 had the poorest preservation of radiolarians among the three samples. This sample yielded *Eucyrtidiellum unumaense*, *Parahsuum*? *grande*, *Unuma* cf. *echinatus* and *Hexasaturnalis tetraspinus* (Plate 1, 5; Table 1). *Parahsuum*? *grande* is the characteristic species of the *Parahsuum*? *grande* Assemblage Zone of Hori (1990). According to stratigraphic ranges of radiolarians by Baumgartner *et al.* (1995), co-occurrence of *Eucyrtidiellum unumaense* and *Parahsuum*? *grande* is limited in the lower Bajocian, Middle Jurassic (Fig. 8A). The age of the sample is therefore estimated as early Bajocian (Fig. 8B). This is consistent with the occurrence

(→ p. 35)

Fig. 3 Geological traverse map of the Mt. Iwakura locality. Gongen, Iwaizumi Town. Base map produced from XYZ tiles provided by the Geospatial Information Authority of Japan.

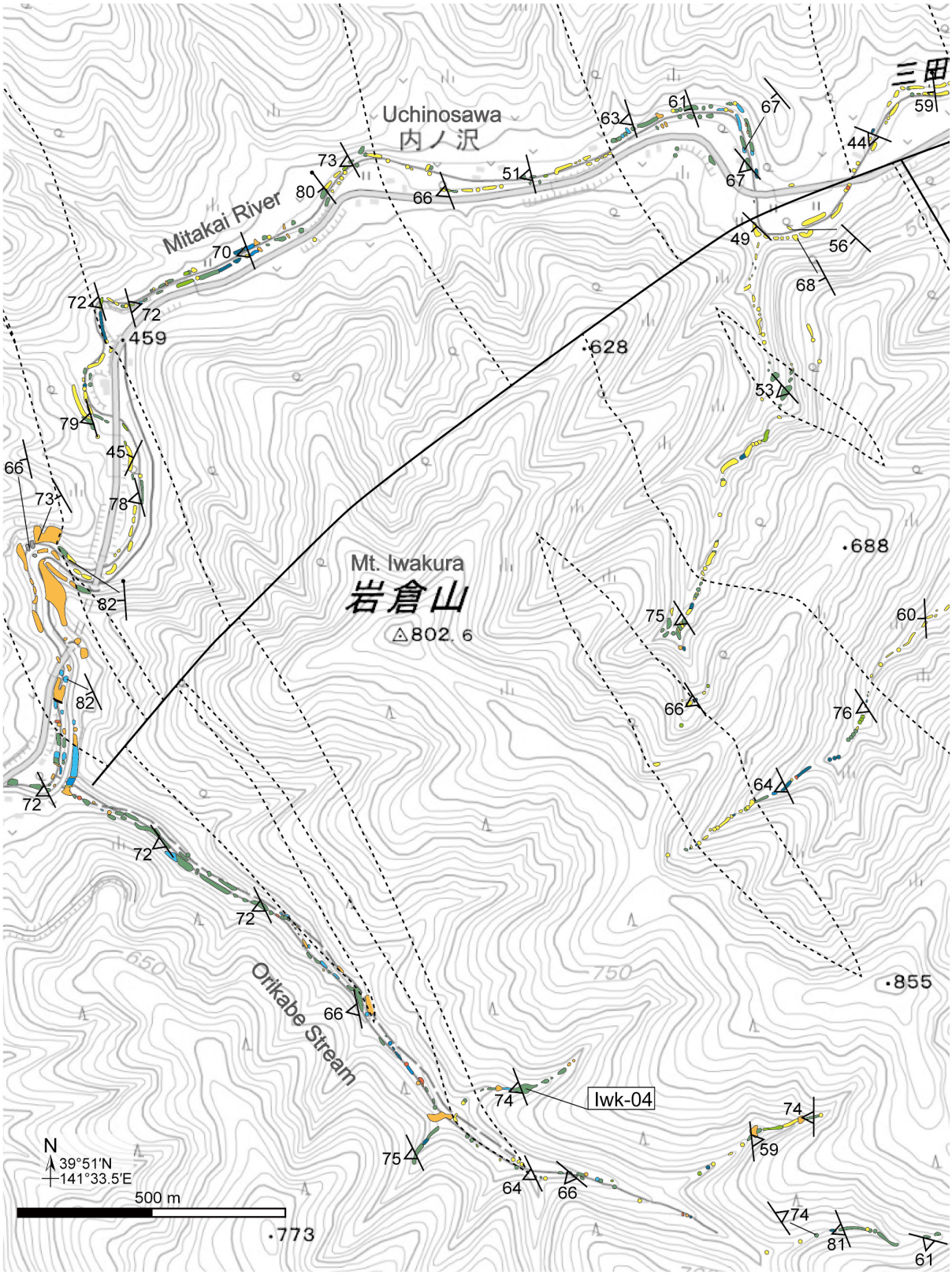
Uchinosawa
内ノ沢
Mitakai River
Mt. Iwakura
岩倉山
△802. 6
Orikabe Stream
Iwk-04
N
39°51′N
141°33.5′E
500 m
·459
·628
·688
·855
·773
三田
Intrusives (rhyolite, dacite and andesite)
Muddy mixed rock (including chert & basalt)
Muddy mixed rock (clastic rocks only)
Sandstone
Sandstone and mudstone
Mudstone
Siliceous/tuffaceous mudstone
Chert
Siliceous claystone
Black claystone
Lithological boundary
Fault
Dip-strike of bedding (way-up unknown)
Dip-strike of cleavage
Dip-strike of bedding (way-up known)
Vertical bedding

Fig. 4 Geological traverse map of the Yunashigi Stream locality. Minaikawa, Iwaizumi Town. Base map produced from XYZ tiles provided by the Geospatial Information Authority of Japan.

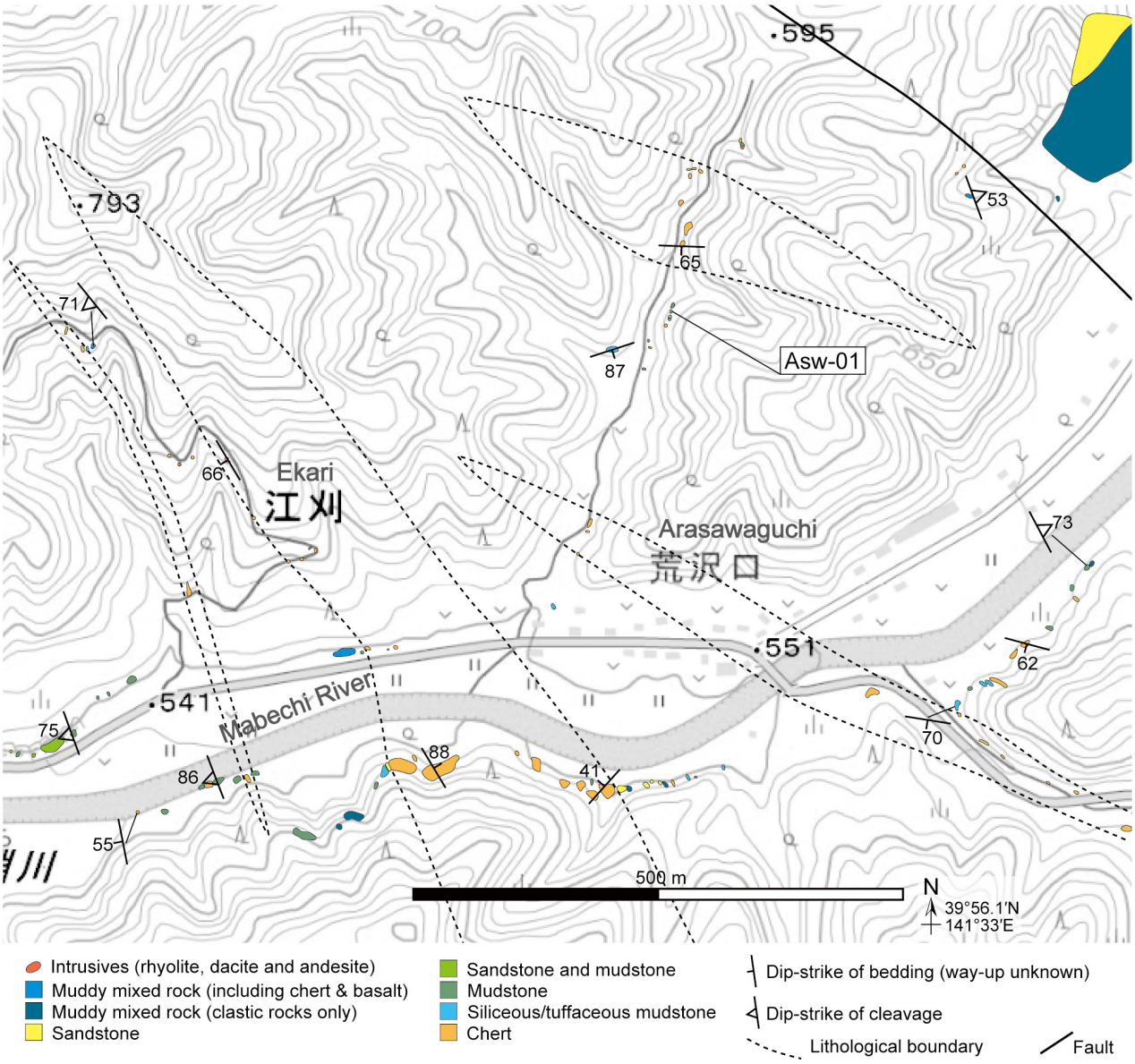

Fig. 5 Geological traverse map of the Arasawaguchi locality. Ekari, Kuzumaki Town. Base map produced from XYZ tiles provided by the Geospatial Information Authority of Japan.

ranges of *Unuma echinatus* and *Hexasaturnalis tetraspinus* (Fig. 8A), although the specimen of the former species from this sample is identified with confer. The occurrence of other specimens identified to the generic level from this sample (*Japonocapsa*, *Higumastra*, *Paronaella*, *Homeparonaella*, *Tritrabs* and *Xiphostylus*) is consistent with the estimated age according to occurrence ranges of Jurassic to Cretaceous radiolarian genera shown by O'Dogherty *et al.* (2009) (Fig. 8A).

4. 2. Yunashigi Stream locality (Yns-03)

Sample Yns-03 yielded *Napora nipponica*. This species occurs in the Aalenian to Bajocian (Baumgartner *et al.*, 1995) (Fig. 8A). Therefore, the age of this sample is within the Aalenian to Bajocian interval (Fig. 8B). This sample also yielded *Unuma* cf. *echinatus*, and the occurrence range of *Unuma echinatus* includes the Aalenian to Bajocian (Fig. 8A). The occurrence of other radiolarian genera from this sample (*Eucyrtidiellum*, *Hexasaturnalis*, *Higumastra*, *Paronaella* and *Tritrabs*) is consistent with this estimated age (Fig. 8A).

4. 3. Arasawaguchi locality (Asw-01)

Sample Asw-01 yielded most of the closed nassellarians obtained in this study. Among the stratigraphically important species, the occurrence range of *Unuma typicus* is restricted to the Bajocian (Baumgartner *et al.*, 1995) (Fig. 8A). Based on this occurrence range, the age of this sample is most probably the Bajocian (Fig. 8B). The occurrence of other species (*Japonocapsa fusiformis*,

Fig. 6 Photographs of outcrops of the Mn-nodules and surrounding lithofacies. (A) Mixed rock composed of muddy matrix and sandstone (Ss). Minai River. (B) Bedded grey mudstone. Same lithofacies as the host of Mn-nodule samples Iwk-04 and Yns-03. (C) Mn-nodule sample Iwk-04 (Mn), Mt. Iwakura locality. (D) Mn-nodule sample Yns-03 (Mn), Yunashigi Stream locality. (E) Mixed rock composed of muddy matrix, chert (Ch) and sandstone (Ss). (F) Mn-nodule sample Asw-01 (Mn), Arasawaguchi locality. The hammer in A, B, D and E is 30 cm long. The blue board in C and F is 20 cm wide.

Praewilliriedellum convexum, *Quarkus japonicus*, *Unuma echinatus* and *Eucyrtidiellum unumaense*) and genera (*Higumastra*, *Homoeoparonaella*, *Triactoma* and *Xiphostylus*) is consistent with the estimated age (Fig. 8A).

5. Accretionary age of the Otori Unit

This study obtained age constraints of clastic rocks in the southwest part of the Otori Unit for the first time. Previous data were obtained from the Akka area in the northeast part

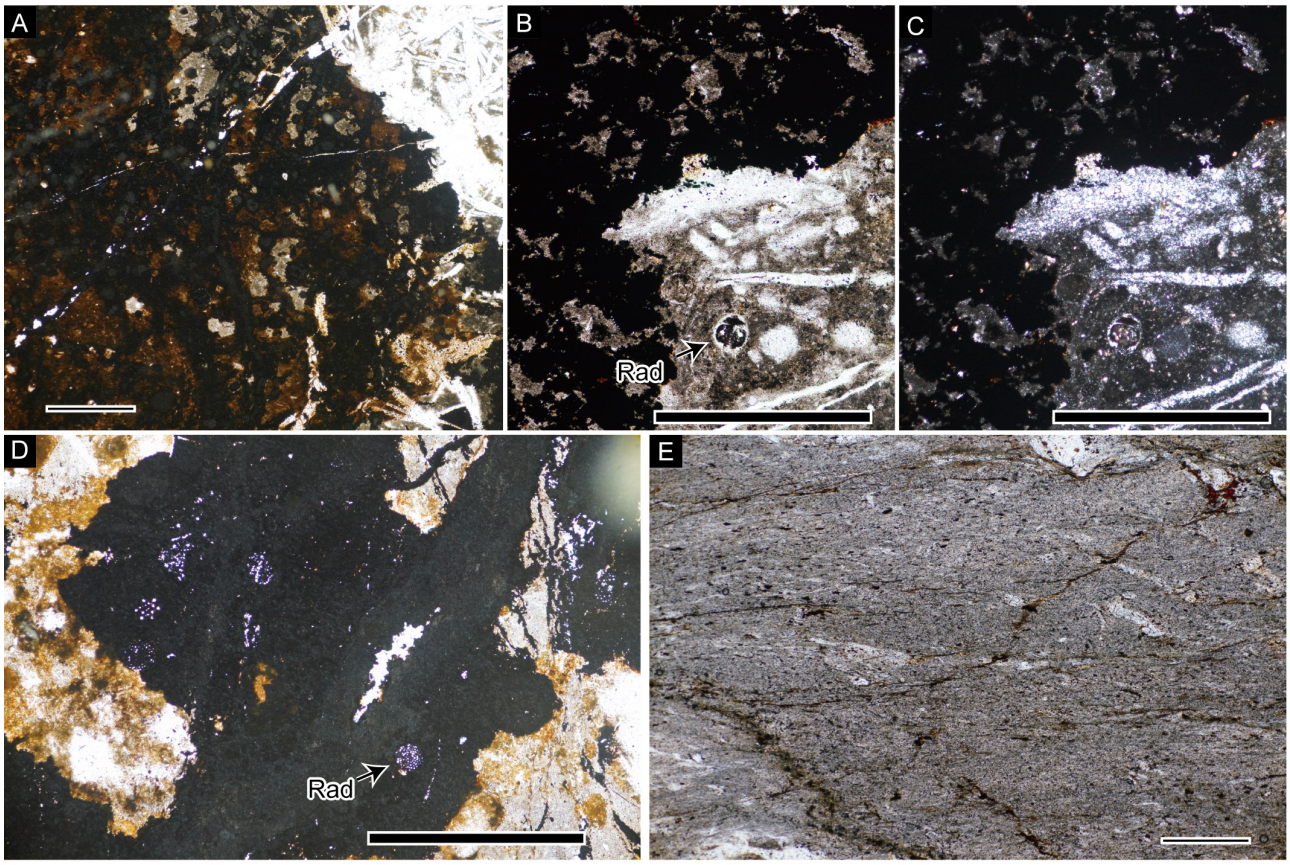

Fig. 7 Thin section micrographs of the Mn-nodules and host mudstone. All pictures except C were taken with transmitted plane-polarized light. C was taken with cross-polarized light. (A) Mn-nodule. Sample Asw-01. (B) Mn-nodule. Sample Asw-01. (C) Mn-nodule. Same field of view as B. (D) Mn-nodule. Sample Yns-03. (E) Mudstone hosting Mn-nodule sample Yns-03. Scale bars are 0.5 mm. Rad: radiolarian tests.

of the Otori Unit, where the unit was originally defined (Suzuki *et al.*, 2007b; Ehiro *et al.*, 2008; Muto *et al.*, 2023). These studies examined radiolarians from Mn-nodules in siliceous mudstone and identified radiolarians that indicate the Bajocian to early Bathonian (Suzuki *et al.*, 2007b; Ehiro *et al.*, 2008) or the Bathonian (Muto *et al.*, 2023). New U–Pb age of a tuff bed within mudstone is Bathonian at 166.69 ± 0.95 Ma, consistent with the above (Muto, 2025).

The three localities in this study are around 5–10 km away from the previously studied localities (Fig. 2). Radiolarians from samples Iwk-04 and Yns-03 indicate an Aalenian to Bajocian age for the lower part of trench-fill clastic sedimentary rocks. The original stratigraphic position of sample Asw-01 that yielded Bajocian radiolarians is not strictly known, and we propose two possibilities. The first possibility is that the nodule was contained in mudstone deposited in the trench area. The other possibility is that the nodule was introduced by tectonic mixing processes into mudstone from hemipelagic siliceous mudstone, which is the host of some Mn-nodules in the northeast part of the Otori Unit. In the former case, sample Asw-01 demonstrates that the age of fine trench-fill clastics in the southwest part of the Otori Unit is at least partly Bajocian. In the latter case, two accretionary complexes, an older one with Aalenian to Bajocian mudstone (bearing samples Iwk-04 and Yns-03) and a younger one with Bajocian siliceous mudstone (bearing Asw-01), coexists in an apparently similar structural position within the southwest part of the Otori Unit. At present, it is not possible to determine which of the two possibilities is true. Regardless, we can conclude that the depositional age of clastic rocks in the Otori Unit includes the Bajocian to Bathonian interval and also perhaps the Aalenian. Muto (2025) provides age constraints on the hemipelagic and trench-fill sedimentary rocks of the Otori Unit from zircon U–Pb dating of tuffs and sandstones. The obtained ages in the southwest part of the Otori Unit are 174–175 Ma (Toarcian to Aalenian) for tuffs from the hemipelagic–trench transitional area, 172 Ma (Aalenian) for a tuff within mudstone and 168 Ma (Bathonian) for sandstone (for details, see Muto, 2025). Thus, the zircon U–Pb ages and radiolarian ages in this study are consistent with the order of lithological succession expected from the conceptual oceanic plate stratigraphy. The combined data also implies a northeastward younging

Table 1 Occurrence list of radiolarians.

Sample id.	*Archaeohagiostrum* ? sp.	*Cryptocapsa* ? sp.	*Emiluvia* ? sp.	*Eucyrtidiellum unumaense* (Yao)	*Eucyrtidiellum* sp.	*Hexasaturnalis* sp.	*Higumastra* sp.	*Homoeparonaella elegans* (Pessagno)	*Homoeparonaella bronnimanni* (Pessagno)	*Homoeparonaella* sp.	*Hsuum* ? sp.	*Japonocapsa convexa* (Yao)	*Japonocapsa fusiformis* (Yao)	*Japonocapsa aff. mastoidea* (Yao)	*Japonocapsa mastoidea* (Yao)	*Japonocapsa cf. parvipora* (Tan Sin Hok) *sensu* Yao (1979)	*Japonocapsa yaoi* (Kozur)	*Japonocapsa?* sp.	*Napora nipponica* Takemura	*Napora* sp.	*Napora* ? sp.	*Pantanellium* sp.	*Paronaella mulleri* Pessagno	*Parvicingula* ? sp.	*Perispyridium* ? sp.	*Protunuma japonica* Ichikawa and Yao	*Sethocapsa* sp.	*Spongotripus* ? sp	*Staurolonche* ? sp.	*Striatojaponocapsa plicarum* (Yao)	*Stylosphaera* ? sp.	*Triactoma* sp.	*Unuma echinatus* Ichikawa and Yao	*Parahsuum* ? sp.	*Xiphostylus gasquetensis* Pessagno and Yang in Pessagno *et al*	*Xiphostylus simuosus* Pessagno and Yang in Pessagno *et al.*
Iwk-04			+	+	+		+	+	+		+							+					+					+					+			+
Yns-03			+		+	+	+		+										+	+			+	+	+			+	+	+						
Asw-01	+	+	+	+			+	+		+		+	+	+	+	+	+				+	+			+	+	+	+			+	+	+	+	+	+	

trend of the age of accretion within the Otori Unit.

6. Conclusions

Radiolarians were obtained from Mn-nodules embedded in mudstone within the Jurassic accretionary complex of the North Kitakami Belt in the western part of the Kado District, northeast Iwate Prefecture. We investigated three samples from the Otori Unit: samples Iwk-04 and Yns-03 from grey bedded mudstone in the southwestern area of the unit and sample Asw-01 from weathered mudstone. Surface and internal test structure was well observed despite the widespread metamorphism by Cretaceous plutons. Radiolarians indicate the early Bajocian for Iwk-04, Aalenian to Bajocian for Yns-03 and Bajocian for Asw-01. The radiolarians provide the first approximation of accretionary age in the area. The new age data on accretionary age indicates the wide distribution of Middle Jurassic accretionary units.

7. Palaeontological notes

(by Tsuyoshi Ito)

The taxonomic classification in this chapter mainly employs the scheme of O'Dogherty *et al.* (2009, 2017). The specimens identified at the species level are described here.

Order **NASSELLARIA** Ehrenberg, 1875
Family **HSUUIDAE** Pessagno and Whalen, 1982
Genus ***Parahsuum*** Yao, 1982
Type species *Parahsuum simplum* Yao, 1982

Parahsuum*? *grande Hori and Yao, 1988
Plate 1, fig. 7
Remarks: The specimen has an elongate conical test composed of more than 11 segments. Continuous longitudinal costae are present on the surface. In the distal part, some circumferential ridges and discontinuous costae are observed. The characteristics are the same as those of *Parahsuum*? *grande* described by Hori and Yao (1988).

Family **WILLIRIEDELLIDAE** Dumitrica, 1970
Genus ***Hemicryptocapsa*** Tan, 1927
Type species *Hemicryptocapsa capita* Tan, 1927

Hemicryptocapsa yaoi (Kozur, 1984)
Plate 2, fig. 1; Plate 3, figs. 5, 8, 9; Plate 5, fig. 11
Remarks: The specimens have a spherical three-segmented test with a truncate-conical cephalis, a conical or oval upper half and a spherical lower half. The surface of the test is ornamented with large hexagonal frames with narrow ridges and small pores in each frame. The characteristics are the same as those of *Praezhamoidellum yaoi* described by Kozur (1984). This species was later included into *Hemicryptocapsa* Tan, 1927 by O'Dogherty *et al.* (2017).

Hemicryptocapsa*? cf. *parvipora (Tan, 1927) sensu Yao (1979)
Plate 3, fig. 6
Remarks: The specimens have a three-segmented test with a conical or oval upper half and spherical lower half. The pores on the surface of the test are sparse, small and circular. They are the same as *Tricolocapsa* cf. *parvipora* described by Yao (1979) in the characteristics of the test. This species was included by Kozur (1984) in a newly erected genus *Praezhamoidellum*. However, O'Dogherty *et al.* (2009, 2017) later considered that *Praezhamoidellum* is a junior synonym of *Hemicryptocapsa* Tan, 1927. Because they did not mention the attribution of *T.* cf. *parvipora* sensu Yao (1979), we tentatively assign the

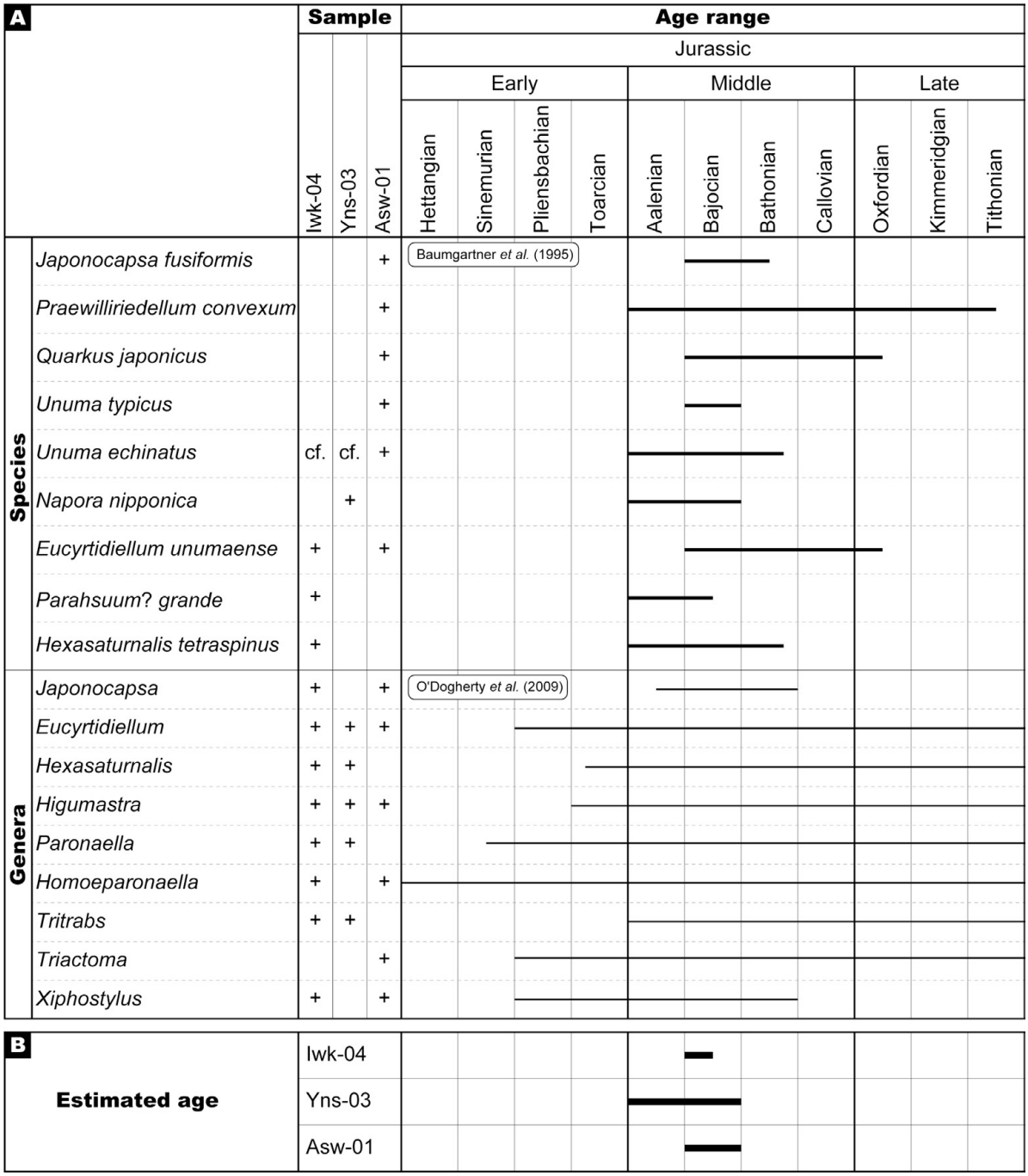

Fig. 8 (A) Stratigraphic range of important radiolarian species and genera. (B) Estimated age of the radiolarian assemblages obtained in this study.

specimens to *Hemicryptocapsa* with a question mark.

Family **DIACANTHOCAPSIDAE** O'Dogherty, 1994
Subfamily **JAPONOCAPSINAE** Kozur, 1984
Genus ***Japonocapsa*** Kozur, 1984
Type species *Tricolocapsa*? *fusiformis* Yao, 1979

Japonocapsa fusiformis (Yao, 1979)
Plate 3, figs. 10–12

Remarks: The specimens have a fusiform four-segmented test. A dish-like fourth segment was recognized. The characteristics are the same as those of *J. fusiformis* (Yao, 1979).

Genus ***Yaocapsa*** Kozur, 1984
Type species *Cyrtocapsa mastoidea* Yao, 1979

Yaocapsa* aff. *mastoidea (Yao, 1979)
Plate 3, figs. 13, 14

Remarks: The test of the specimens has a large basket-like fourth segment. In outline, it closely resembles *Yaocapsa mastoidea*; however, the species has a five-segmented test in the original description by Yao (1979). Our specimens seem to have a four-segmented test; therefore, these specimens were identified as a separate species.

Family **EUCYRTIDIELLIDAE** Takemura, 1986
Genus ***Eucyrtidiellum*** Baumgartner, 1984
Type species *Eucyrtidium*? *unumaensis* Yao, 1979

Eucyrtidiellum unumaense (Yao, 1979)
Plate 1, figs. 5, 6; Plate 3, fig. 18
Remarks: The specimens have a test composed of a small cephalis with an apical horn and a truncate-conical thorax. The characteristics are same as those of *Eucyrtidiellum unumaense* (Yao, 1979), although features such as surface microstructure and the fourth segment are partly or entirely lost.

Family **UNUMIDAE** Kozur, 1984
Genus ***Unuma*** Ichikawa and Yao, 1976
Type species *Unuma typicus* Ichikawa and Yao, 1976

Unuma typicus Ichikawa and Yao, 1976
Plate 3, fig. 15
Remarks: The specimen has a spindle-shaped multi-segmented test. Longitudinal plicae without spines were recognized on the surface. These characteristics are the same as those of *U. typicus* Ichikawa and Yao, 1976.

Unuma echinatus Ichikawa and Yao, 1976
Plate 3, fig. 16
Remarks: The specimen has a spindle-shaped multi-segmented test. Longitudinal plicae and some stout radial spines from the plicae were recognized on the surface. These characteristics are the same as those of *U. echinatus* Ichikawa and Yao, 1976.

Family Unnamed pro **STICHOCAPSIDAE** Haeckel, 1881
Genus ***Praewilliriedellum*** Kozur, 1984
Type species *Praewilliriedellum cephalospinosum* Kozur, 1984

Praewilliriedellum convexum (Yao, 1979)
Plate 3, figs. 1, 2
Remarks: The specimens have a four-segmented test with a conical upper half and spherical lower half. The pores on the surface of the test are small and circular. The specimens are identical to *Praewilliriedellum convexum* in these test characteristics (Yao, 1979).

Genus ***Quarkus*** Pessagno, Blome and Hull, 1993
Type species *Quarkus madstonensis* Pessagno, Blome and Hull, 1993

Quarkus japonicus (Yao, 1979)
Plate 3, figs. 4
Remarks: The specimen has a four-segmented test with a conical upper half and flattened-spherical lower half. The pores on the surface of the test are small, circular and arranged sparsely. These characteristics are the same as those of *Quarkus japonicus* (Yao, 1979).

Family **ULTRANAPORIDAE** Pessagno 1977b
Genus ***Napora*** Pessagno 1977a
Type species *Napora bukryi* Pessagno 1977a

Napora nipponica Takemura, 1986
Plate 2, fig. 4; Plate 5, fig. 7
Remarks: The specimens have a small cephalis with straight apical horn, hemispherical thorax and three feet. Circular pores on the cephalis are arranged transversely and the feet are curved convexly. These characteristics are the same as those of *Napora nipponica* Takemura, 1986.

Order **SPUMELLARIA** Ehrenberg, 1875
Family **SPONGURIDAE** Haeckel, 1862
Subfamily **HEXASATURNALINAE** Kozur and Mostler, 1983
Genus ***Hexasaturnalis*** Kozur and Mostler, 1983
Type species *Spongosaturnalis*? *hexagonus* Yao, 1972

Hexasaturnalis tetraspinus (Yao, 1972)
Plate 5, fig. 3
Remarks: The specimen seems to have a hexagonal ring with four short strong spines, although the ring is partially broken. These characteristics are the same as those of *Hexasaturnalis tetraspinus* (Yao, 1972).

Acknowledgements: We are grateful to the members of the Geological Sample Preparation Group of the Geoinformation Service Center, GSJ for preparing thin sections for this study. We thank Satoshi Nakae for numerous review comments that helped improve the manuscript, editor Tomonori Naya for handling the manuscript and Rie S. Hori for sharing her knowledge on radiolarian assemblages.

References

Baumgartner, P. O. (1984) A Middle Jurassic–Early Cretaceous low latitude radiolarian zonation based on unitary associations and age of Tethyan radiolarites. *Eclogae geologicae Helvetiae*, **77**, 729–841.

Baumgartner, P. O., O'Dogherty, L., Goričan, S., Dumitrica-Jud, R., Dumitrica, P., Pillevuit, A., Urquhart, E., Matsuoka, A., Danelian, T., Bartolini, A., Carter, E. S., De Wever, P., Kito, N., Marcucci, M. and Steiger, T. (1995) Radiolarian catalogue and systematics of Middle Jurassic to Early Cretaceous Tethyan genera and species. *Mémoires de Géologie (Lausanne)*, **23**, 37–685.

Dumitrica, P. (1970) Cryptocephalic and cryptothoracic

Nassellaria in some Mesozoic deposits of Romania. *Revue Roumaine de Géologie, Géophysique et Géographie (série Géologie)*, **14**, 45–124.

Ehiro, M., Kawamura, M. and Kawamura, T. (2005) 1.1 Summary and Tectonostratigraphic divisions. *In* The Publishing Committee of the Geology of Japan ed., *The Geology of Japan. The Supplement*. Kyoritsu Publishing Co. Ltd, Tokyo, 49–50. (in Japanese)

Ehiro, M., Yamakita, S., Takahashi, S. and Suzuki, N. (2008) Jurassic accretionary complexes of the North Kitakami Belt in the Akka-Kuji area (in Japanese). *The Journal of the Geological Society of Japan*, **114**, 121–139.

Ehrenberg, C. G. (1875) *Fortsetzung der mikrogeologischen Studien als Gesammt-Uebersichtder mikroskopischen Palaontologie gleichartig analysirter Gebirgsarten der Erde, mit specieller Rucksicht auf den Polycystinen-Mergel von Barbados*. Abhandlungen der königlichen preussichen Akademie der Wissenschaften zu Berlin, 1–225.

Geological Survey of Japan, AIST (2020) Seamless digital geological map of Japan 1: 200,000. Geological Survey of Japan, AIST. https:// gbank.gsj.jp/seamless/ v2full/ (Accessed: 2021-10-08)

Haeckel, E. (1862) Die Radiolarien (Rhizopoda Radiaria). Eine Monographie, Reimer, Berlin, 572p.

Haeckel, E. (1881) Entwurf eines Radiolarien-Systems auf Grund von Studien der Challenger-Radiolarien. Jenaische Zeitschrift für Naturwissenschaft, **15**, 418–472.

Hori, R. (1990) Lower Jurassic radiolarian zones of SW Japan. *Transactions and Proceedings of the Palaeontological Society of Japan, New Series*, no. 159, 562–586.

Hori, R. and Yao, A. (1988) *Parahsuum* (Radiolaria) from the Lower Jurassic of the Inuyama area, central Japan. *Journal of Geosciences, Osaka City University*, **31**, 47–61.

Ichikawa, K. and Yao, A. (1976) Two new genera of Mesozoic cyrtoid radiolarians from Japan. *In* Takayanagi, Y. and Saito, T., eds. *Progress in Micropaleontology, Special Publication*, Micropaleontology Press, The American Museum of Natural History, New York, 110–117.

Isozaki, Y. and Maruyama, S. (1991) Studies on Orogeny based on Plate Tectonics in Japan and New Geotectonic Subdivision of the Japanese Islands. *Journal of Geography (Chigaku Zasshi),* **100**, 697–761. doi: 10.5026/jgeography.100.5_697.

Isozaki, Y., Maruyama, S., Aoki, K., Nakama, T., Miyashita, A. and Otoh, S. (2010) Geotectonic subdivision of the Japanese Islands revisited: categorization and definition of elements and boundaries of Pacific-type (Miyashiro-type) orogen. *Chigaku Zasshi (Jounal of Geography)*, **119**, 999–1053, doi:10.5026/ jgeography.119.235. (in Japanese with English abstract)

Kojima, S., Hayasaka, Y., Hiroi, Y., Matsuoka, A., Sano, H., Sugamori, Y., Suzuki, N., Takemura, S., Tsujimori, T. and Uchino, T. (2016) 2b Pre-Cretaceous accretionary complexes. *In*: Moreno, T., Wallis, S., Kojima, T. and Gibbons, W. (eds) *The Geology of Japan*, 61–100.

Kozur, H. (1984) New radiolarian taxa from the Triassic and Jurassic. *Geologisch Paläontologische Mitteilungen Innsbruck*, **13**, 49–88.

Kozur, H. and Mostler, H. (1983) The polyphyletic origin and the classification of the Mesozoic saturnalids (Radiolaria). *Geologisch Paläontologische Mitteilungen Innsbruck*, **13**, 1–47.

Murai, T., Okami, K. and Oishi, M. (1985) *Geology of the Pre-Cretaceous in Iwaizumi Town. Part 1*. The Education Board of the Iwaizumi Town, Iwaizumi, 1–47. (in Japanese, reference information translated by Suzuki *et al.*, 2007)

Murai, T., Okami, K., Ehiro, M. and Oishi, M. (1986) *Geology of the Pre-Cretaceous in Iwaizumi Town. Part 2*. The Education Board of the Iwaizumi Town, Iwaizumi 1–43. (in Japanese, reference information translated by Suzuki *et al.*, 2007)

Muto, S. (2025) Accretionary age of the Jurassic accretionary complex of the North Kitakami Belt: new data from zircon geochronology in the Kado District. *Bulletin of the Geological Survey of Japan*, **76**, 49–98.

Muto, S., Ito, T. and Murayama, M. (2023) Geology and accretionary age of the Otori Unit, North Kitakami Belt. *Bulletin of the Geological Survey of Japan*, **74**, 1–40.

Nakada, R., Shirai, T., Takahashi, S., Suzuki, N., Ogawa, K. and Takahashi, Y. (2014) A geochemical constraint on the formation process of a manganese carbonate nodule in the siliceous mudstone of the Jurassic accretionary complex in the Mino Belt, Japan. *Journal of Asian Earth Sciences*, **96**, 59–68. doi: 10.1016/j. jseaes.2014.08.032.

Nakae, S. and Kamada, K. (2003) Late Jurassic radiolarians from the Rikuchu-Seki district in the North Kitakami Belt, Northeast Japan. *The Journal of the Geological Society of Japan*, **109**, 722–725. (in Japanese with English abstract)

Nakae, S., Kamada, K., Kubo, K. and Kudo, T. (2021) *Geology of the Rikuchu Seki District*. Quadrangle Series, 1:50,000, Geological Survey of Japan, AIST. (in Japanese with English abstract)

O'Dogherty, L. (1994) Biochronology and paleontology of mid-Cretaceous radiolarians from Northern Apennines (Italy) and Betic Cordillera (Spain). *Mémoires de Géologie (Lausanne)*, **21**, 1–415.

O'Dogherty, L., Carter, E. S., Dumitrica, P., Goričan, Š., De Wever, P., Bandini, A. N., Baumgartner, P. O. and Matsuoka, A. (2009) Catalogue of Mesozoic radiolarian genera. Part 2: Jurassic–Cretaceous. *Geodiversitas*, **31**, 271–356.

O'Dogherty, L., Goričan, Š. and Gawlick, H.-J. (2017)

Middle and Late Jurassic radiolarians from the Neotethys suture in the Eastern Alps. *Journal of Paleontology*, **91**, 25–72.

Onuki, Y. (1969) Geology of the Kitakami Massif, Northeast Japan. *Tohoku University, Institute of Geology and Paleontology Contributions*, **69**, 1–239.

Pessagno, E. A. (1977a) Upper Jurassic Radiolaria and radiolarian biostratigraphy of the California Coast Ranges. *Micropaleontology*, **23**, 56–113.

Pessagno, E. A. (1977b) Lower Cretaceous radiolarian biostratigraphy of the Great Valley Sequence and Franciscan Complex, California Coast Ranges. *Contribution Cushman Foundation for foraminiferal Research, special Publication*, **15**, 1–87.

Pessagno, E. A. and Whalen, P. (1982) Lower and Middle Jurassic Radiolaria (multicyrtid Nassellariina) from California, east-central Oregon and the Queen Charlotte Islands, B. C. *Micropaleontology*, **28**, 111–169.

Pessagno, E. A., Blome, C. D. and Hull, D. M. (1993) Radiolaria. *In* Pessagno, E. A., Blome, C. D., Hull, D. M. and Six, W. M., eds., *Jurassic Radiolaria from the Josephine ophiolite and overlying strata, Smith River subterrane (Klamath Mountains), northwestern California and southwestern Oregon: Micropaleontology*, **39**, 93–166.

Sugimoto, M. (1974) Stratigraphical study in the outer belt of the Kitakami Miassif, Northeast Japan. *Tohoku University, Institute of Geology and Paleontology Contributions*, **74**, 1–48. (in Japanese with English abstract)

Sugimoto, M. (1980) Geological structure of the Akka-Iwaizumi District, Northern Kitakami Massif, Northeast Japan (Preliminary report). *In: Report on the Multidiscipline Research Project A with 1979 Foundation of Grant-in-Aid for Scientific Research by the Education Ministry of Japan*, Tokyo Print Insatsu, Ltd., Tokyo 37–44. (in Japanese)*

Suzuki, N. and Ogane, K. (2004) Paleoceanographic affinities of radiolarian faunas in late Aalenian time (Middle Jurassic) recorded in the Jurassic accretionary complex of Japan. *Journal of Asian Earth Sciences*, **23**, 343–357. doi: 10.1016/S1367-9120(03)00113-5.

Suzuki, N., Ehiro, M., Yoshihara, K., Kimura, Y., Kawashima, G., Yoshimoto, H. and Nogi, T. (2007a) Geology of the Kuzumaki-Kamaishi Subbelt of the North Kitakami Belt (a Jurassic accretionary complex), Northeast Japan: Case study of the Kawai-Yamada area, eastern Iwate Prefecture. *Bulletin of the Tohoku University Museum*, **6**, 103–174.

Suzuki, N., Yamakita, S., Takahashi, S. and Ehiro, M. (2007b) Middle Jurassic radiolarians from carbonate manganese nodules in the Otori Formation in the eastern part of the Kuzumaki-Kamaishi Subbelt, the North Kitakami Belt, Northeast Japan. *The Journal of the Geological Society of Japan*, **113**, 274–277. doi: 10.5575/geosoc.113.274. (in Japanese with English abstract)

Takahashi, S., Ehiro, M., Suzuki, N. and Yamakita, S. (2016) Subdivisional scheme of the North Kitakami Belt, Northeast Japan and its tectonostratigraphic correlation to the Oshima and South Chichibu belts: an examination of the Jurassic accretionary complex in the west Akka area. *The Journal of the Geological Society of Japan*, **122**. 1–22, doi:10.5575/geosoc.2015.0034. (in Japanese with English abstract)

Takemura, A. (1986) Classification of Jurassic Nassellarians (Radiolaria). *Palaeontographica Abteilung A: Palaozoologie-Stratigraphie*, no. 195, 29–74.

Tan, S. H. (1927) Over de samenstelling en het onstaan van krijt- en mergel-gesteenten van de Molukken. *Jaarboek van het mijnwezen in Nederlandsch Oost-Indië*, jaargang 55, 1926, verhandelingen, 3rd gedeelte, 5–165.

Uchino, T. and Komatsubara, T. (2024) *Geology of the Sotoyama District*. Quadrangle Series, 1:50,000, Geological Survey of Japan, AIST, 131p. (in Japanese with English abstract)

Uchino, T. and Suzuki, N. (2020) Late Jurassic radiolarians from mudstone near the U–Pb-dated sandstone of the North Kitakami Belt in the northeastern Shimokita Peninsula, Tohoku, Japan. *Bulletin of the Geological Survey of Japan*, **71**, 313–330. doi:10.9795/bullgsj.71.313.

Yamaguchi, Y. (1981) Geological structure of the eastern part of the North Kitakami Mountains, Japan—with special reference to structural subdivision. *Tohoku University, Institute of Geology and Paleontology Contributions*, **83**, 1–19.

Yao, A. (1972) Radiolarian fauna from the Mino Belt in the northern part of the Inuyama Area, central Japan, Part I: Spongosaturnalids. *Journal of Geosciences, Osaka City University*, **15**, 21–65.

Yao, A. (1979) Radiolarian fauna from the Mino belt in the northern part of the Inuyama Area, central Japan, Part II: Nassellaria 1. *Journal of Geosciences, Osaka City University*, **22**, 21–72.

Yao, A. (1982) Middle Triassic to Early Jurassic radiolarians from the Inuyama area, central Japan. *Journal of Geosciences, Osaka City University*, **25**, 53–70.

Yoshihara, K., Suzuki, N. and Ehiro, M. (2002) Middle Jurassic radiolarian-bearing manganese nodules from the Kuzumaki-Kamaishi Belt in the Northern Kitakami Massif and its significance. *The Journal of the Geological Society of Japan*, **108**, 536–539. (in Japanese with English abstract)

*English translation from the original written in Japanese

Recieved February 13, 2024
Accepted November 6, 2024

北上山地北部「門」地域西部から産出したマンガンノジュールから得られたジュラ紀中期放散虫化石

武藤　俊・伊藤　剛・大関　仁智

要　旨

東北日本の北部北上帯ジュラ紀付加体においては，白亜紀深成岩類の接触変成作用により放散虫化石の分離が困難であるため，付加体形成史の解明が妨げられている．本地域で放散虫化石の分離に成功した研究例には，マンガンノジュールを扱ったものがある．本研究では，5 万分の 1 地質図幅「門（かど）」地域西部の 3 地点にて泥質岩中に胚胎されるマンガンノジュールを採取し，これらから保存良好な放散虫化石を抽出した．得られた放散虫化石群集の年代は，灰色層状泥岩から採取した 2 試料についてはそれぞれ前期バッジョシアン期とアーレニアン期からバッジョシアン期（いずれも中期ジュラ紀）と，構造的混在化を受けた可能性がある泥岩から採取した 1 試料についてはバッジョシアン期（中期ジュラ紀）と推定した．これらの年代は検討した層準の付加時期を近似できる．「門」地域西部からの年代指標となる放散虫化石の報告は，本研究が初めてである．

難読･重要地名

Arasawaguchi：荒沢口，Gongen：権現，Mt. Iwakura：岩倉山，
Yunashigi Stream：ユナシギ沢，Minai River：見内川，Orikabe Stream：オリカベ沢

Plate 1

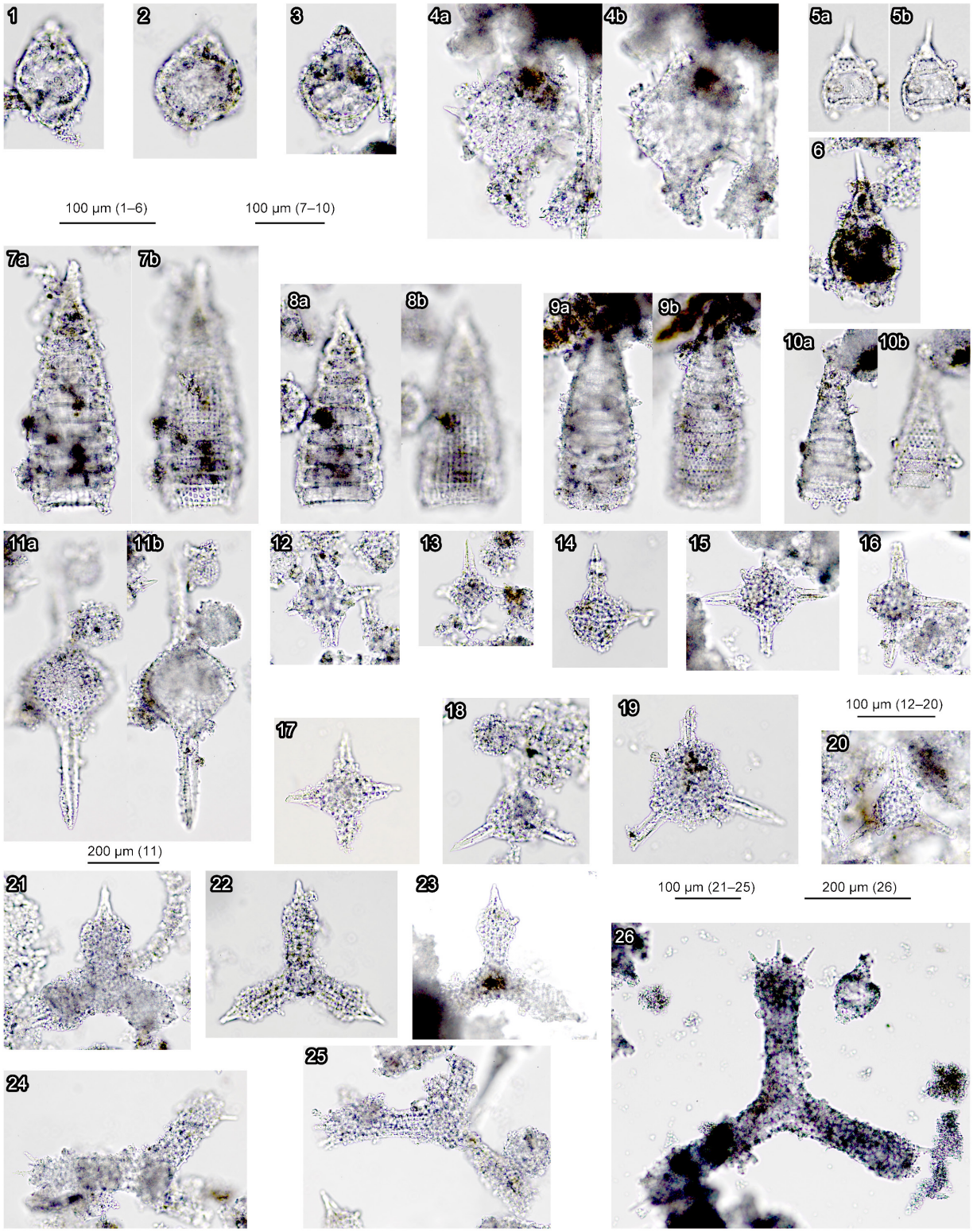

Plate 1 Middle Jurassic radiolarians from sample Iwk-04. 1, 3: *Japonocapsa* sp.; 2: Diacanthocapsidae? gen. et sp. indet.; 4: *Unuma* cf. *echinatus* Ichikawa and Yao, 1976; 5, 6: *Eucyrtidiellum unumaense* (Yao, 1979); 7: *Parahsuum*? *grande* Hori and Yao, 1988; 8: *Parahsuum*? sp.; 9, 10: *Praeparvicingula*? sp.; 11: *Xiphostylus* sp.; 12–16: *Emiluvia*? sp.; 17: *Higumastra* sp.; 18–20: *Acaeoniotylopsis*? sp.; 21: *Paronaella* sp.; 22, 23: *Homoeoparonaella* sp.; 24: *Tritrabs*? sp.; 24–26: *Tritrabs* sp.

Plate 2

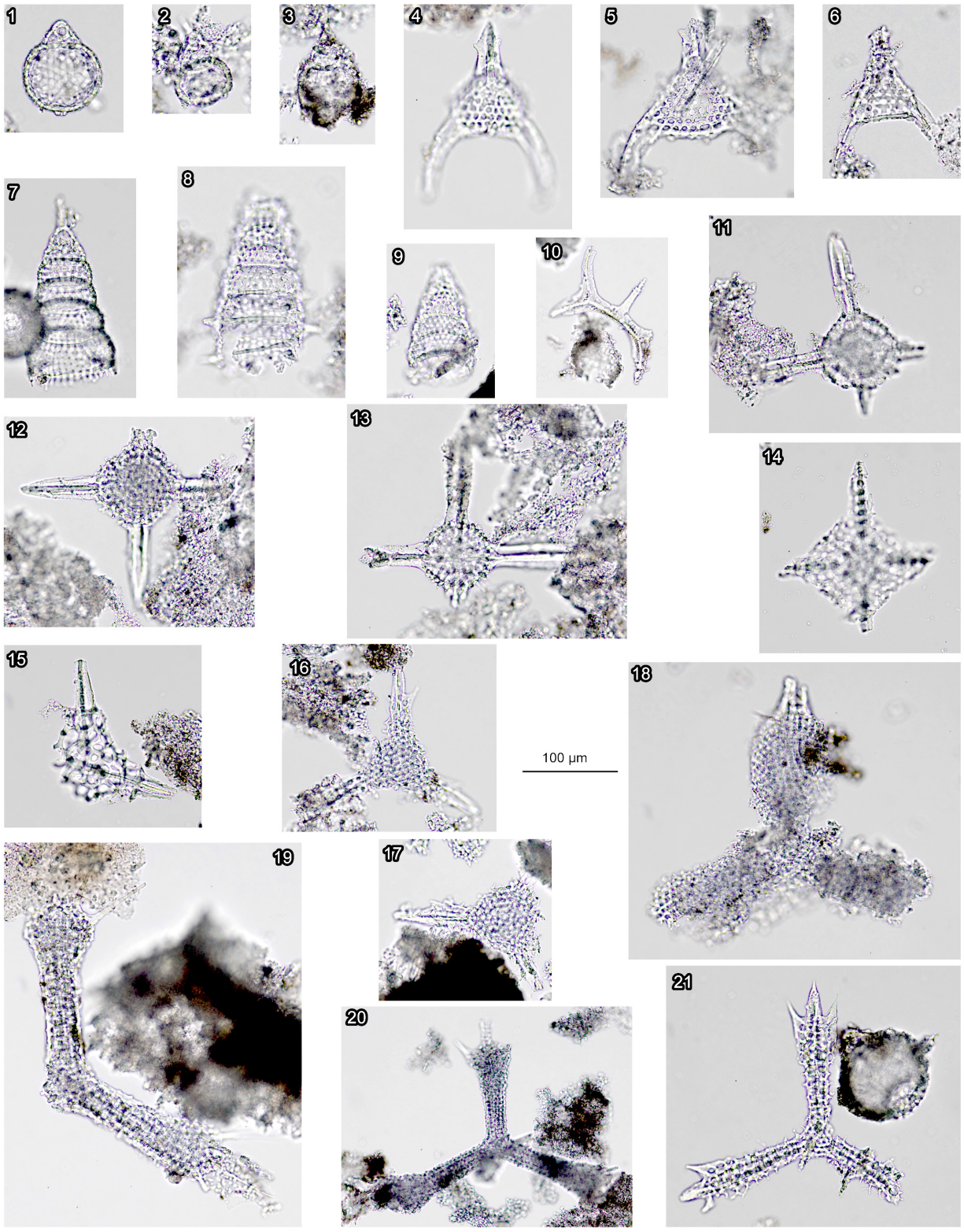

Plate 2 Middle Jurassic radiolarians from sample Yns-03. 1: *Hemicryptocapsa yaoi* (Kozur, 1984); 2, 3: *Eucyrtidiellum* sp.; 4: *Napora nipponica* Takemura, 1986; 5, 6: *Napora* sp.; 7–9: *Stichomitra*? sp.; 10: *Hexasaturnalis* sp.; 11: *Staurolonche*? sp.; 12, 13: *Higumastra*? sp.; 14: *Higumastra* sp.; 15: *Perispyridium*? sp.; 16, 17: *Cryptostephanidium*? sp.; 18: *Paronaella* sp.; 19-21: *Tritrabs* sp.

Plate 3

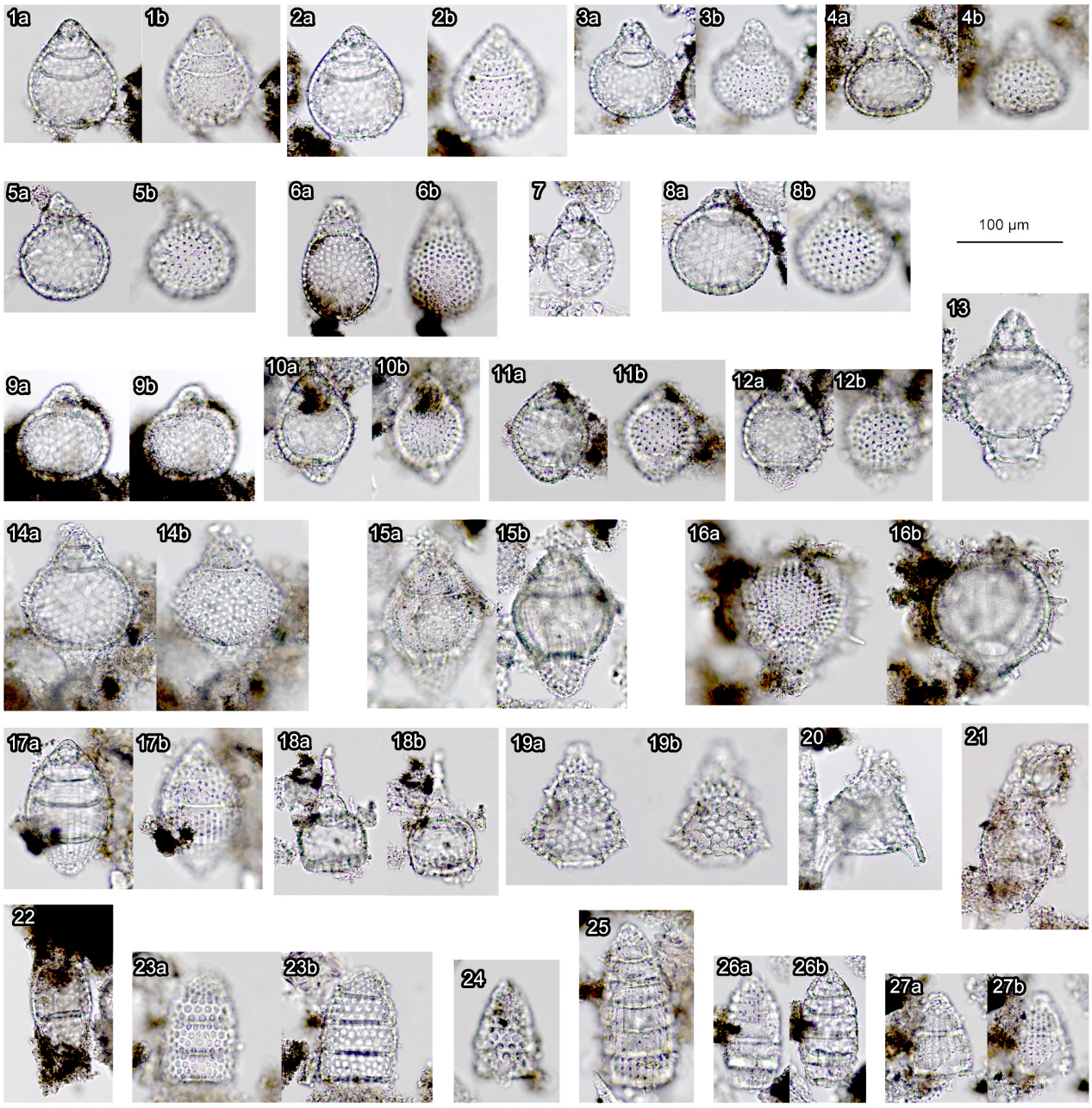

Plate 3 Middle Jurassic radiolarians (Nassellaria) from sample Asw-01. 1, 2: *Praewilliriedellum convexum* (Yao, 1979); 3, 7: *Praewilliriedellum*? sp.; 4: *Quarkus japonicus* (Yao, 1979); 5, 8, 9: *Hemicryptocapsa yaoi* (Kozur, 1984); 6: *Hemicryptocapsa*? cf. *parvipora* (Tan, 1927) sensu Yao (1979); 10–12: *Japonocapsa fusiformis* (Yao, 1979); 13, 14: *Yaocapsa* aff. *mastoidea* (Yao, 1979); 15: *Unuma typicus* Ichikawa and Yao, 1976; 16: *Unuma echinatus* Ichikawa and Yao, 1976; 17: *Helvetocapsa*? sp.; 18: *Eucyrtidiellum unumaense* (Yao, 1979), 19: *Eucyrtidiellum* sp.; 20: *Farcus*? sp.; 21, 22: Closed nassellarian; 23: *Mizukidella*? sp.; 24: *Takemuraella*? sp.; 25–27: *Archaeodictyomitra*? sp.

Plate 4

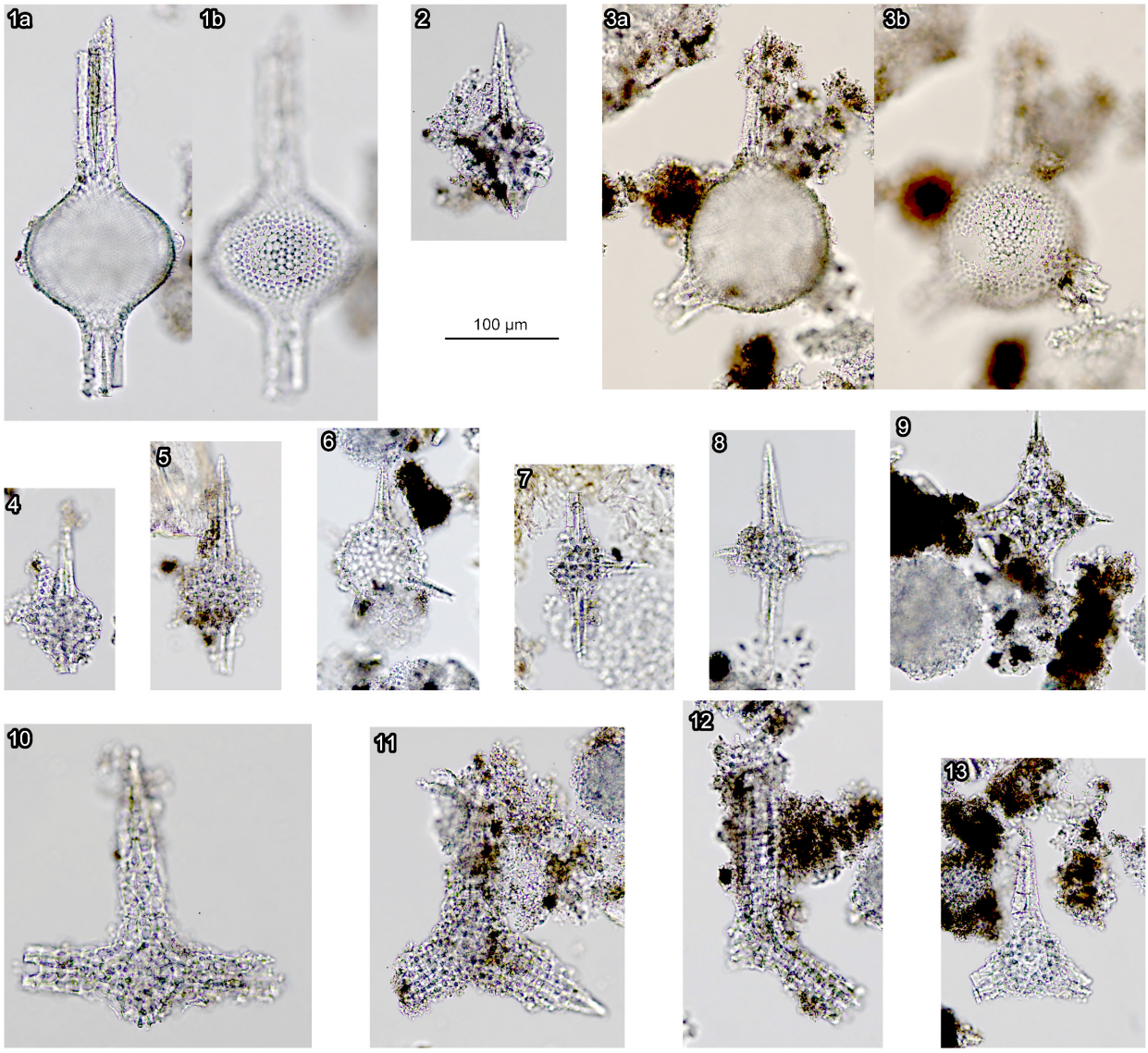

Plate 4 Middle Jurassic radiolarians (Spumellaria) from sample Asw-01. 1: *Xiphostylus* sp.; 2: *Pantanellium*? sp.; 3: *Triactoma* sp.; 4, 5: *Stylosphaera*? sp.; 6–8: *Emiluvia*? sp.; 9: *Higumastra* sp.; 10: *Archaeohagiostrum*? sp.; 11, 12: *Homoeoparonaella* sp.; 13: *Perispyridium*? sp.

Plate 5

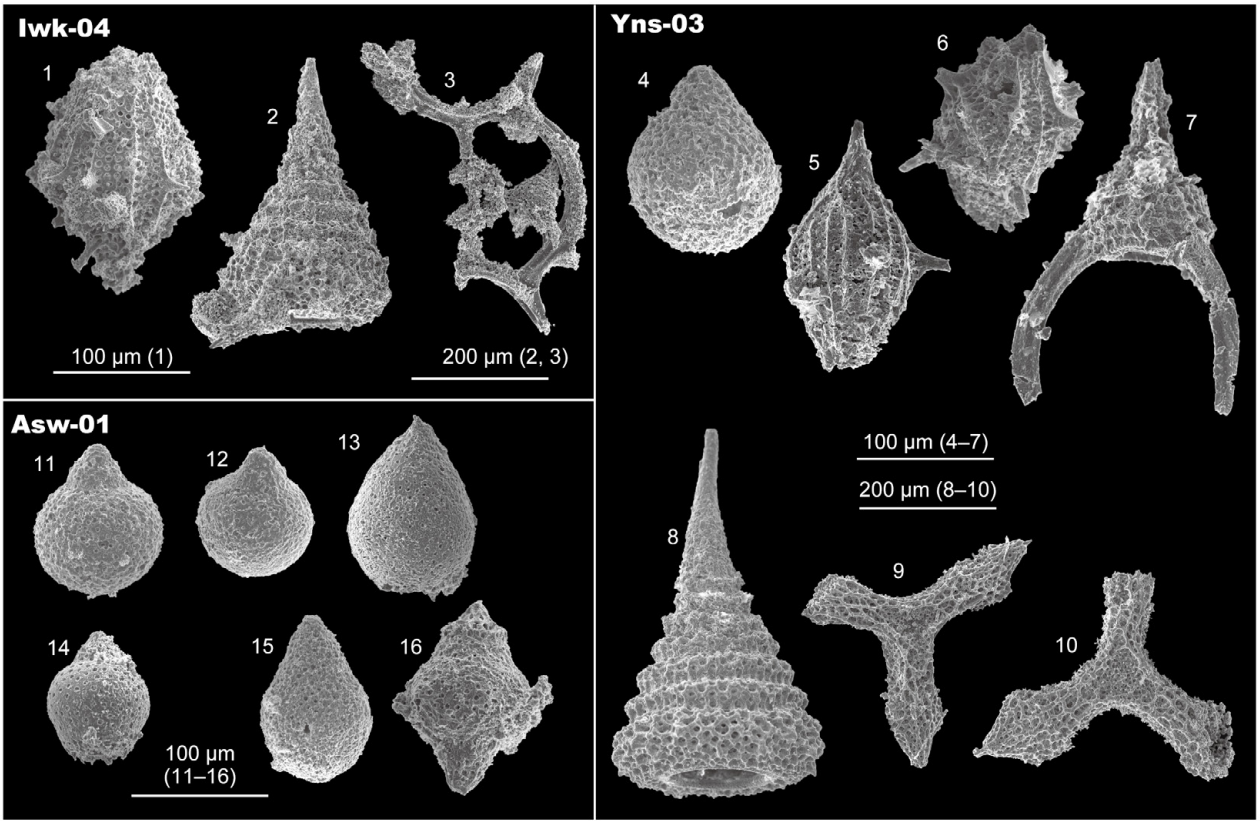

Plate 5 Middle Jurassic radiolarians (Spumellaria) from sample Iwk-04, Yns-03 and Asw-01. 1, 5, 6: *Unuma* cf. *echinatus* Ichikawa and Yao, 1976; 2, 8: *Palinandromeda*? sp.; 3: *Hexasaturnalis tetraspinus* (Yao, 1972); 4: *Praewilliriedellum*? sp.; 7: *Napora nipponica* Takemura, 1986; 9, 10: *Paronaella* sp.; 11: *Hemicryptocapsa yaoi* (Kozur, 1984); 12–15: Diacanthocapsidae? gen. et sp. indet.; 16: *Quarticella*? sp.

Bulletin of the Geological Survey of Japan, vol. 76 (1/2), p. 51–100, 2025

Article

Accretionary age of the Jurassic accretionary complex of the North Kitakami Belt: new data from zircon geochronology in the Kado District

MUTO Shun[1,*]

MUTO Shun (2025) Accretionary age of the Jurassic accretionary complex of the North Kitakami Belt: new data from zircon geochronology in the Kado District. *Bulletin of the Geological Survey of Japan*, vol. 76 (1/2), p. 51–100, 21 figs and 13 appendices.

Abstract: The study on the accretionary history of the Jurassic accretionary complex of the North Kitakami Belt in Northeast Japan has been hampered by the scarcity of reports on radiolarians due to metamorphism of Cretaceous plutons. Recently, zircon geochronology is being employed to elucidate the age of accretion from strata that yield rare or no microfossils. This study reports zircon U–Pb ages from igneous zircons in tuff and detrital zircons in sandstone from the 1: 50,000 Kado District in northeast Iwate Prefecture. Based on compilation of available data, the accretionary complex distributed in the main part of the northern Kitakami Mountains is classified mainly into the following seven tectonostratigraphic units: The Kadoma Unit of Rhaetian to Middle or early Late Jurassic age, the Misugo Unit of undetermined age, the Aalenian to Bathonian Otori Unit, the Bathonian to Kimmeridgian Seki Unit the Oxfordian to Kimmeridgian Takayashiki Unit, the Kayamori Unit of undetermined age and the Kimmeridgian Ekari Unit. The former six units are structurally stacked up in this order. The exact structural position of the Ekari Unit is not clear, but it is correlated to the Takayashiki Unit or a lower and younger unit, in terms of age. The new data in this study provided constraints on the accretionary age of the Ekari, Takayashiki, Seki, Otori and Kadoma units, although detrital zircons from sandstone were not always useful. The Ekari Unit lies in fault contact between older units, meaning that the faults have vertical displacements. Such faults and kilometre-scale folds interrupt the general oceanward younging trend of the accretionary complex of the North Kitakami Belt. Zircons in tuffs have not widely been used to estimate accretionary ages, but this study shows that they can be powerful tools, especially when microfossils are difficult to obtain.

Keywords: accretionary age, detrital zircon, Quadrangle Series, sandstone, tuff, U–Pb age

1. Introduction

The North Kitakami–Oshima Belt in Northeast Japan is defined by the distribution of mainly Jurassic accretionary complexes (Ehiro *et al.*, 2005; Kojima *et al.*, 2016; Fig. 1A). In characterization of accretionary complexes, the time of accretion at the subduction zone plays a key role (e.g., Matsuoka *et al.* 1998; Nakae, 2000) and is estimated based on the age of trench-fill clastic rocks at the top of the oceanic plate stratigraphy. Herein, I refer to this age as the trench-arrival age (TAA), since the trench-fill clastic rocks are deposited when the oceanic plate arrives at the trench area. This terminology aims to distinguish the depositional age of the clastic rocks from the timing of actual accretion, which takes place when the subducting plate submerges beneath the overriding plate. Based on radiolarian fossils and zircon dating, the TAA of the North Kitakami Belt–Oshima Belt is mostly within the Jurassic, but the oldest part is late Triassic or even late Permian, and the youngest part is Early Cretaceous (Fig. 1B). Compilation of available data (Suzuki *et al.*, 2007a; Ehiro *et al.*, 2008; Uchino and Suzuki, 2020) indicate a general younging of TAA from the southwest to northeast (landward to oceanward) (Fig. 1B). On the other hand, age data on TAA is limited in the North Kitakami–Oshima Belt compared to coeval accretionary complexes in Southwest Japan, due to the poor occurrence of radiolarians as a result of contact metamorphism of Cretaceous plutons. Recent development of zircon U–Pb chronology provided the potential to obtain age data from clastic rocks from which extraction of identifiable radiolarians is almost hopeless (e.g., Ueda *et al.*, 2018; Uchino, 2019; Muto *et al.*, 2023; Osaka *et al.*, 2023). However, U–Pb dating of zircons are mostly conducted on detrital zircons in

[1] AIST, Geological Survey of Japan, Research Institute of Geology and Geoinformation

* Corresponding author: MUTO, S., AIST Tsukuba Central 7, 1-1-1 Higashi, Tsukuba, Ibaraki 305-8567, Japan. Email: s-muto@aist.go.jp

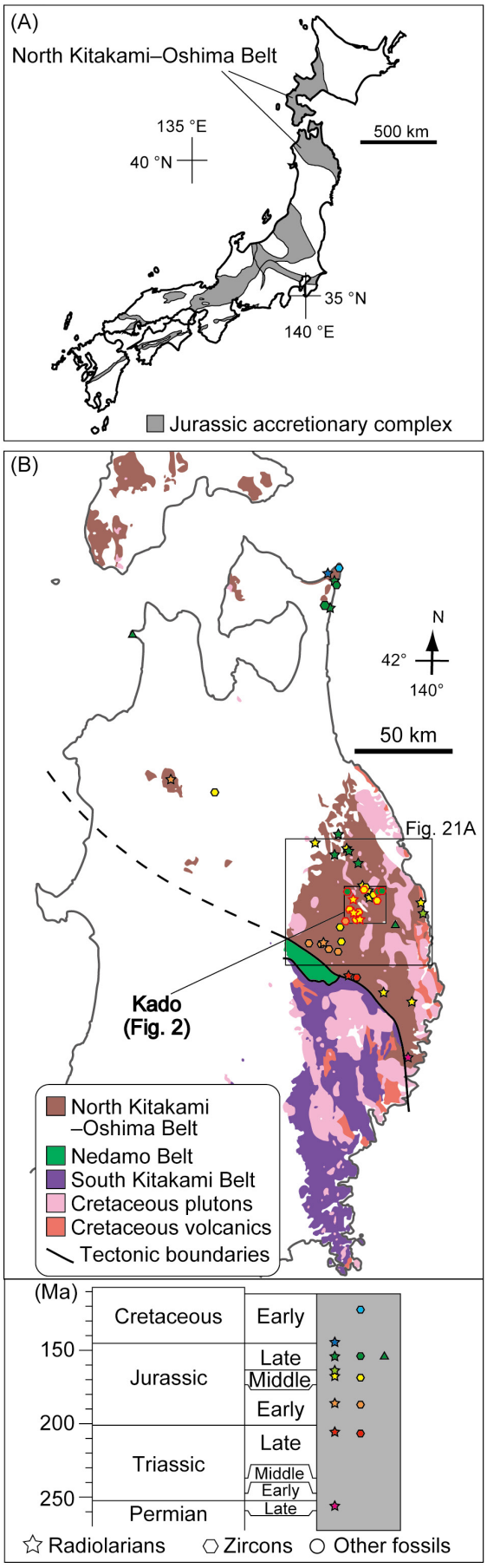

Fig. 1 (A) Distribution of the Jurassic accretionary complex in Japan (after Isozaki *et al.*, 2010). (B) Geology of the basement rocks of the northern Tohoku Region (modified from Geological Survey of Japan, AIST, 2020). Age constraints for time of accretion are based on the compilation by Uchino and Suzuki (2020), this study and additional references in Muto *et al.* (2023). Data plots closed in red were obtained in this study and Muto *et al.* (2025).

sandstones. It is known that young detrital zircons are usually only a small portion of the entire population, and the age of the youngest population may appear older than the depositional age by tens of millions of years, at least in the North Kitakami–Oshima Belt (Uchino, 2021; Muto *et al.*, 2023). Thus, it is important to obtain data from tuffs that will point to the depositional age of the strata.

The present author has worked on the production the 1: 50,000 geological map of the Kado District for the Quadrangle Series of the Geological Survey of Japan, AIST, which is located within the area of the North Kitakami Belt (the segment of the North Kitakami–Oshima Belt distributed in Honshu). As part of this project, tuffs and sandstones were investigated for U–Pb zircon geochronology. The age data from the tuffs provide depositional ages of clastic rocks that were previously poorly dated or not dated at all. Sandstones were investigated to compare the age of the youngest cluster in detrital zircons to that of tuffs from a nearby horizon. New data are compiled with previous studies to present the present understanding of the accretionary history and geological structure of the North Kitakami Belt.

2. Geological outline

The Kado District of the 1: 50,000 Quadrangle Series is situated in the central area of the North Kitakami Belt. The Jurassic accretionary complex in this district can generally be divided into two areas with respect to the quality and quantity of available geological data. The northeast part, including the area around the Akka River, was the target of detailed geological studies by Sugimoto (1974, 1980). Although researchers at that time were not aware that the studied strata were formed through accretionary processes, more recent studies adopting the concept of accretionary complexes (Takahashi *et al.*, 2016; Nakae *et al.*, 2021) proved the distribution of lithofacies and geological structures illustrated by Sugimoto (1974, 1980) to be mostly correct. The tectonostratigraphic division of Jurassic accretionary complexes in this area has been slightly different between researchers (see Muto *et al.*, 2023). In this study, we distinguish the Takayashiki, Seki and Otori units in tectonically ascending order, based on data obtained during the production of the 1: 50,000 geological map of the Kado District by the present author (Fig. 2). The division basically follows Nakae *et al.* (2021), while the Kassenba and Seki complexes are

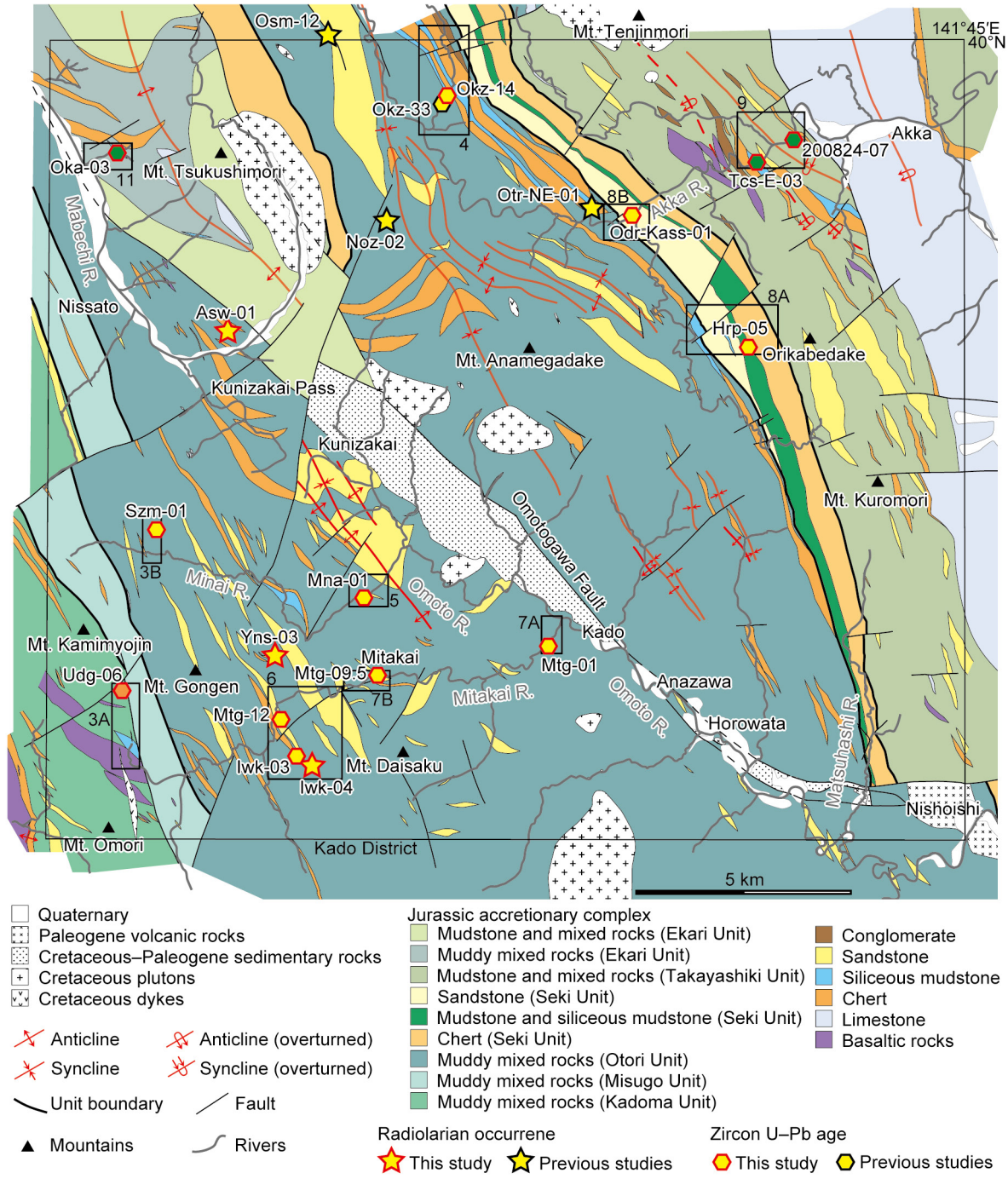

Fig. 2 Geological outline of the Kado District based on geological surveys conducted for the 1: 50,000 geological map of the Kado District for the Quadrangle Series of the Geological Survey of Japan, AIST by Muto, S. Areas of traverse maps (Figs. 3–9, 11) are shown with black boxes. The prefix "Fig." for these boxes are omitted. For legends to colours of the age data plots, see Fig. 1B.

united into the Seki Unit as in Takahashi *et al.* (2016) ("complex" in Nakae *et al.* (2021) is equivalent to "unit" in this paper). This area is one of the best studied areas in the North Kitakami Belt.

The southwest part of the Kado District, consisting of a large part of the catchment area of the Omoto River and the catchment area of the Mabechi River, is less well studied. In this area, partly overlapping geological maps were published by Onuki (1969), Yamaguchi (1981) and Murai *et al.* (1985, 1986). These studies date before the acceptance of subduction–accretion processes by scientists working on the North Kitakami Belt. Due to the lack of detailed traverse maps of type localities or any age data from clastic rocks, it is difficult to re-

interpret the published maps as accretionary complexes or to establish precise correlation between different units recognized therein. Based on geological surveys for the Kado District obtained by the present author, most of the Jurassic accretionary complex in the southwest part of the district not classified by the detailed maps of Sugimoto (1974, 1980) is included in the Otori Unit (Fig. 2). The exception is the Ekari Unit in the northwest corner of the district, and the Misugo and Kadoma units in the southwest corner (Fig. 2). The Ekari and Misugo units are newly recognized units and will be detailed in the outcoming 1:50,000 map of the Kado District. The Ekari Unit is mainly composed of broken facies of mudstone with sandstone layers, alternating mudstone and sandstone and muddy mixed rocks. It is bounded by faults between the Seki Unit to the east and the Otori Unit to the west (Fig. 2). The Misugo Unit is composed of muddy mixed rocks and characterized by intercalations of light green claystone within mudstone. The Kadoma Unit was defined by Kawamura *et al.* (2013) and corresponds to the Nakatsugawa Unit of Uchino (2019). The distribution of this unit continues from the southwest edge of the Kado District to the southwest boundary of the North Kitakami Belt, where it is in contact with the Nedamo Belt.

In the revised tectonostratigraphic division, the Jurassic accretionary complex in the Kado District is divided into the Takayashiki, Seki, Otori, Misugo, Kadoma and Ekari units. The first five units are stacked in this tectonically ascending order, while the strict position of the Ekari Unit is not determined. Based mainly on radiolarian occurrences, the Seki Unit accreted during the Bathonian of the Middle Jurassic to the Kimmeridgean of the Late Jurassic (Nakae and Kamada, 2003; Nakae, 2016), and the northeastern part of the Otori Unit accreted around the Bathonian (Suzuki *et al.*, 2007b; Ehiro *et al.*, 2008; Muto *et al.*, 2023). The Takayashiki Unit was considered to be accreted during the Oxfordian based on an ammonoid-bearing float (Suzuki *et al.* 2007a), but this sample needs to be viewed with great caution (see Chapter 5).

The samples investigated in this study cover all the tectonostratigraphic units in the Kado District except the Misugo Unit, from which suitable samples were not obtained. Tuff samples were obtained from tuff layers with a sedimentary contact in clastic or hemipelagic rocks, or from bedded tuffs, rather than tuff blocks in mixed rocks. Sandstone samples were mostly taken from medium grained bedded sandstones. Details on the sampling horizons are explained in the following text and figures (Figs. 3–11).

3. Methods

The author investigated eight tuff samples and five sandstone samples. Samples were observed in thin section to check for the presence of zircons. Zircon separation and U–Pb dating were conducted by Kyoto Fission-Track Co. Ltd. Zircon U–Pb dating was conducted at the Hirata-Lab. of the University of Tokyo by laser ablation inductively coupled plasma mass spectrometry (LA-ICP-MS). The LA part was CARBIDE (LIGHT CONVERSION) and the ICP-MS part was New Plasma Ⅱ (Nu instruments). Ablation pit size was 10 μm, energy density was 3.2 J/cm^2, and pulse repetition rate was 10 Hz. Laser ablation was conducted on polished sections of zircons embedded in PFA Teflon sheets. Analyses were performed after one-shot cleaning. The details of the analysis are described in Iizuka and Hirata (2004) and Hirata *et al.* (2005). Primary standard was the Plešovice zircon with a ^{238}U–^{206}Pb age of 337.13 ± 0.37 Ma (Sláma *et al.*, 2008). Secondary standard was the standard zircon 91500 with a ^{238}U–^{206}Pb age of 1062.4 ± 0.4 Ma (Wiedenbeck *et al.*, 1995) and zircon OD-3 with a ^{238}U–^{206}Pb age of 33.04 ± 0.10 Ma (Iwano *et al.*, 2013). U–Pb age data with ^{238}U–^{206}Pb age/^{235}U–^{207}Pb age ratio between 90 % and 110 % were regarded as concordant age data (Tokiwa *et al.*, 2019). For tuffs, the zircon population with a maximum number of grains where all the grains fall within the 95 % confidence interval of the weighted average of the population within 2σ errors were considered to indicate the age of eruption. For sandstones the weighted mean age of the youngest two or more grains (YC1σ; Dickinson and Gehrels, 2009) was considered for estimation of accretionary age.

4. Zircon U–Pb geochronology

4. 1. Kadoma Unit

One tuff sample from the Kadoma Unit was investigated in this study. No sandstone samples were investigated.

The analyzed sample (Udg-06) was obtained in a small tributary of Udouge Stream in the uppermost reaches of the Mitakai River in northwest Iwaizumi Town (Fig. 3A). The lithofacies of the Kadoma Unit around the locality is composed of muddy mixed rocks with blocks of basaltic rocks, siliceous and tuffaceous mudstone and chert, in this order of abundance. These rocks of the Jurassic accretionary complex are intruded by dyke rocks, notably porphyric tonalite up to 30 m thick. Sample Udg-06 is a grey tuff bed in black mudstone. The tuff bed has a sharp contact at the base and grades upwards into mudstone (Fig. 12A). The tuff part of the sampled horizon is composed of fine sand- to silt-sized grains supported in a matrix of microcrystalline to cryptocrystalline quartz and white mica (Fig. 14A–C). The grains are mostly quartz including shards with low roundness and sphericity with smaller amounts of plagioclase, opaque minerals and zircons (Fig. 14B, C). Part of the quartzose and micaceous matrix appear to be pseudomorphs of felsic grains. The sedimentary contact between tuff and mudstone is confirmed in thin section as well (Fig. 14A). Only the tuff part of the sample was processed for zircon extraction. Thirty zircon grains were analyzed for U–Pb dating, all of which yielded concordant U–Pb ages (Fig. 18A; Table A1). The age of the grains cluster around 200 Ma, and twenty-eight of the cluster are accepted as grains indicating the age of

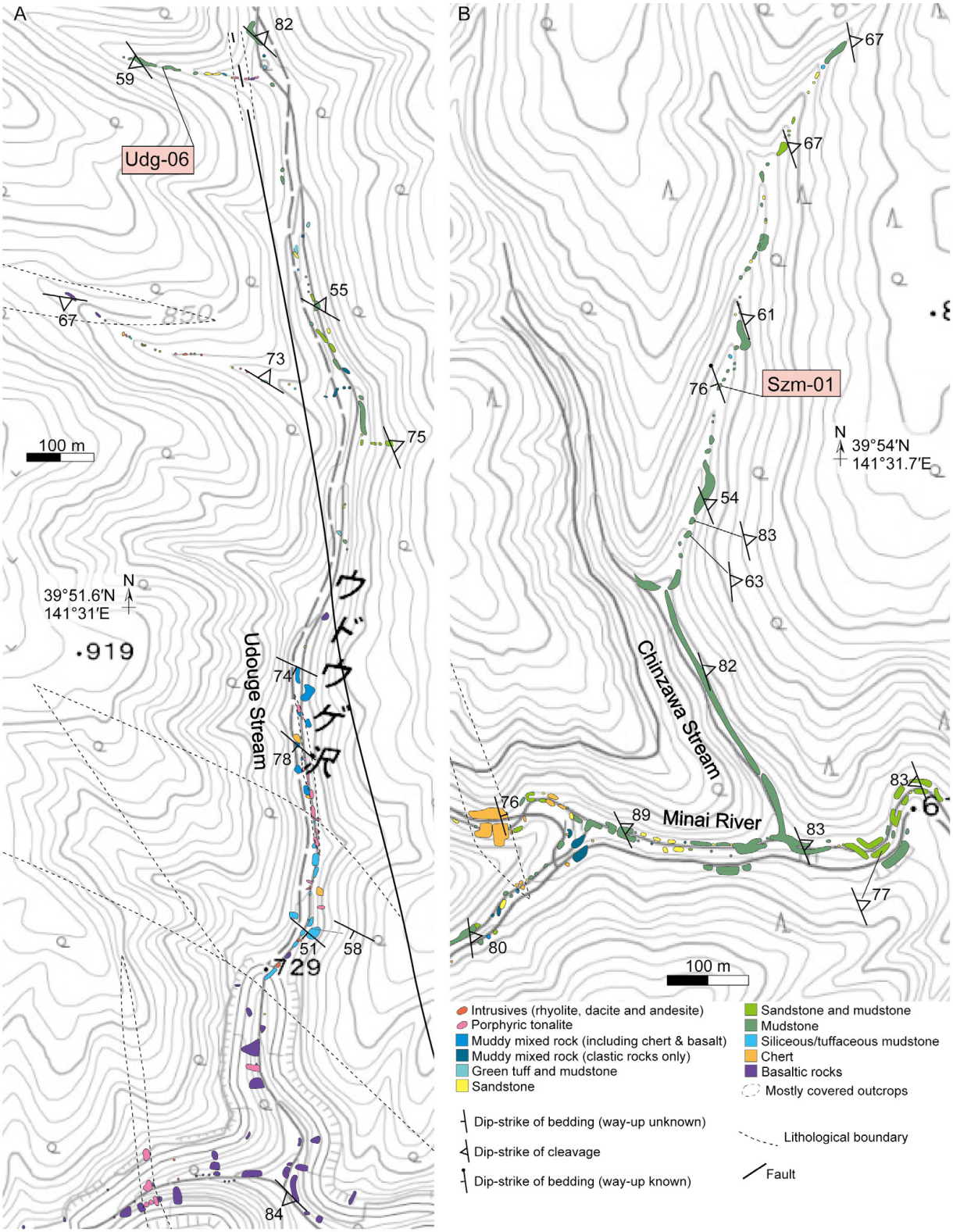

Fig. 3 Geological traverse maps of (A) Chinzawa Stream (sampling locality of Szm-01) and (B) Udouge Stream (sampling locality of Udg-06), both in Kamatsuta-Gongen, Iwaizumi Town. Base map produced from XYZ tiles provided by the Geospatial Information Authority of Japan.

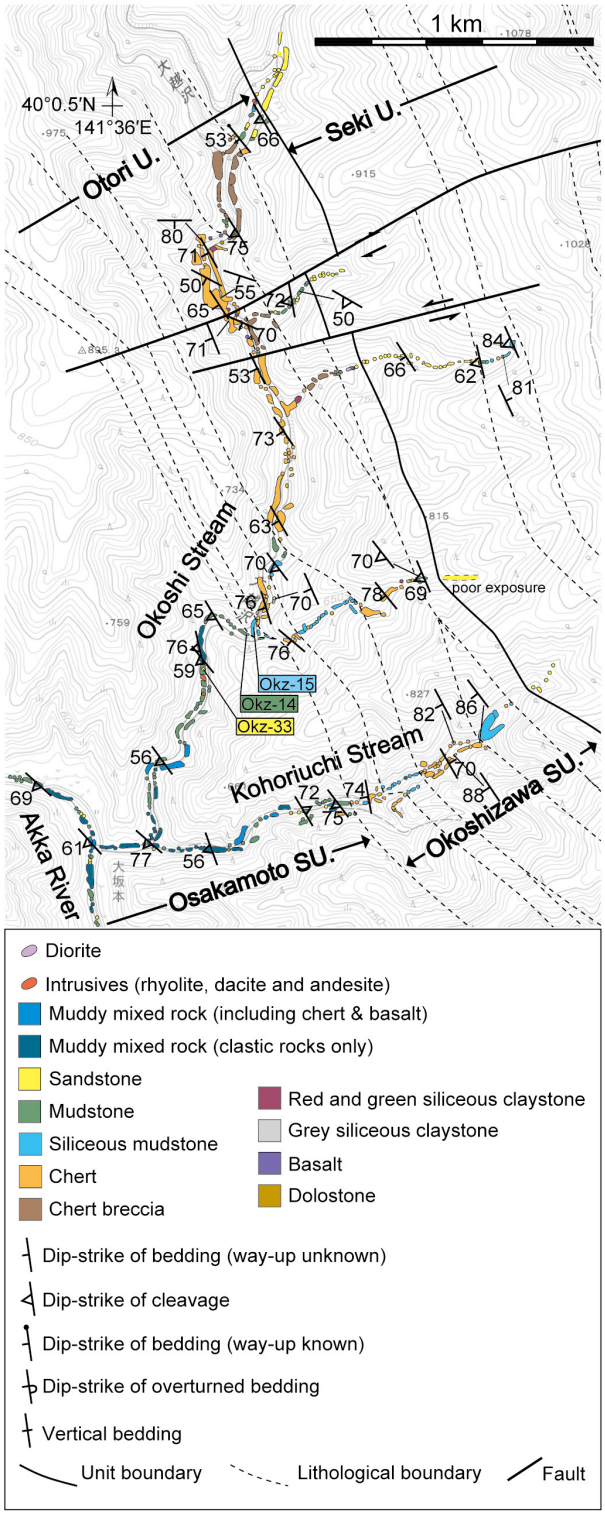

Fig. 4 Geological traverse map of Okoshi Stream, Akka, Iwaizumi Town (sampling locality of Okz-14). Modified from Muto *et al.* (2023). Localities of samples Okz-14 and -33 in Muto *et al.* (2023) are also shown. Base map produced from XYZ tiles provided by the Geospatial Information Authority of Japan.

eruption, resulting in a weighted average of 203.1 ± 1.2 Ma (Fig. 20).

4. 2. Otori Unit

Four tuff samples and three sandstone samples were analyzed in this study. From the northeast part of the Otori Unit, which is relatively well-studied and has been included in the Otori Unit by previous studies, one tuff sample (Okz-14) was analyzed. In this area, detrital zircons from sandstone blocks have been analyzed by Muto *et al.* (2023). The southwest part of the Otori Unit is much less studied and is combined into this unit for the first time. From this part of the unit, three tuff samples (Mna-01, Iwk-03, Szm-01) and three sandstone samples (Mtg-01, Mtg-09.5, Mtg-12) were analyzed.

4. 2. 1 Tuff (Okz-14, Mna-01, Iwk-03, Szm-01)

Sample Okz-14 was obtained from the northeast part of the Otori Unit in Okoshi Stream, a tributary of the Akka River in north Iwaizumi Town (Fig. 4). The rocks distributed around the locality are coherent chert–siliceous mudstone sequences and mixed facies of mudstone, chert and sandstone. Muto *et al.* (2023) named the former as the Okoshizawa Subunit and the latter as the Osakamoto Subunit. Muto *et al.* (2023) also reported radiolarians from siliceous mudstone and detrital zircons from sandstone along the same route. Sample Okz-14 was obtained from a white tuff bed in black mudstone that overlies a coherent chert–siliceous mudstone sequence (Figs. 4, 12B). In thin section, this sample is composed of quartz grains with low sphericity supported in a matrix composed of microcrystalline to cryptocystalline quartz and white micas (Fig. 15A, B). Part of the matrix appears to be pseudomorphs of felsic grains. Zircons and opaque minerals are present as accessory minerals. The tuff bed is in contact with radiolarian-bearing mudstone with a sedimentary boundary (Fig. 15A, B). Thirty zircon grains from sample Okz-14 were analyzed for U–Pb dating, all of which yielded concordant U–Pb ages (Fig. 18B; Table A2). All grains are accepted as grains indicating the age of eruption, resulting in a weighted average of 166.69 ± 0.95 Ma (Fig. 20).

Sample Mna-01 was obtained from the southwest part of the Otori Unit along the Minai River, a tributary of the Omoto River in northwest Iwaizumi Town (Fig. 5). The lithofacies around the locality is composed mainly of muddy mixed rocks, sandstone and bedded coherent mudstone. The latter two are considered to be blocks within muddy mixed rocks on scales of kilometres. Sample Mna-01 was collected from bedded tuffaceous mudstone within an outcrop composed mostly of mudstone (Figs. 5, 12C). In thin section, this sample is composed of mostly silt-sized grains and a matrix composed of microcrystalline to cryptocystalline quartz and clay minerals (Fig. 14D, E). The grains are largely quartz, but also include lithic fragments and plagioclase. Some of the quartz grains are shards that are angular and have low-sphericity.

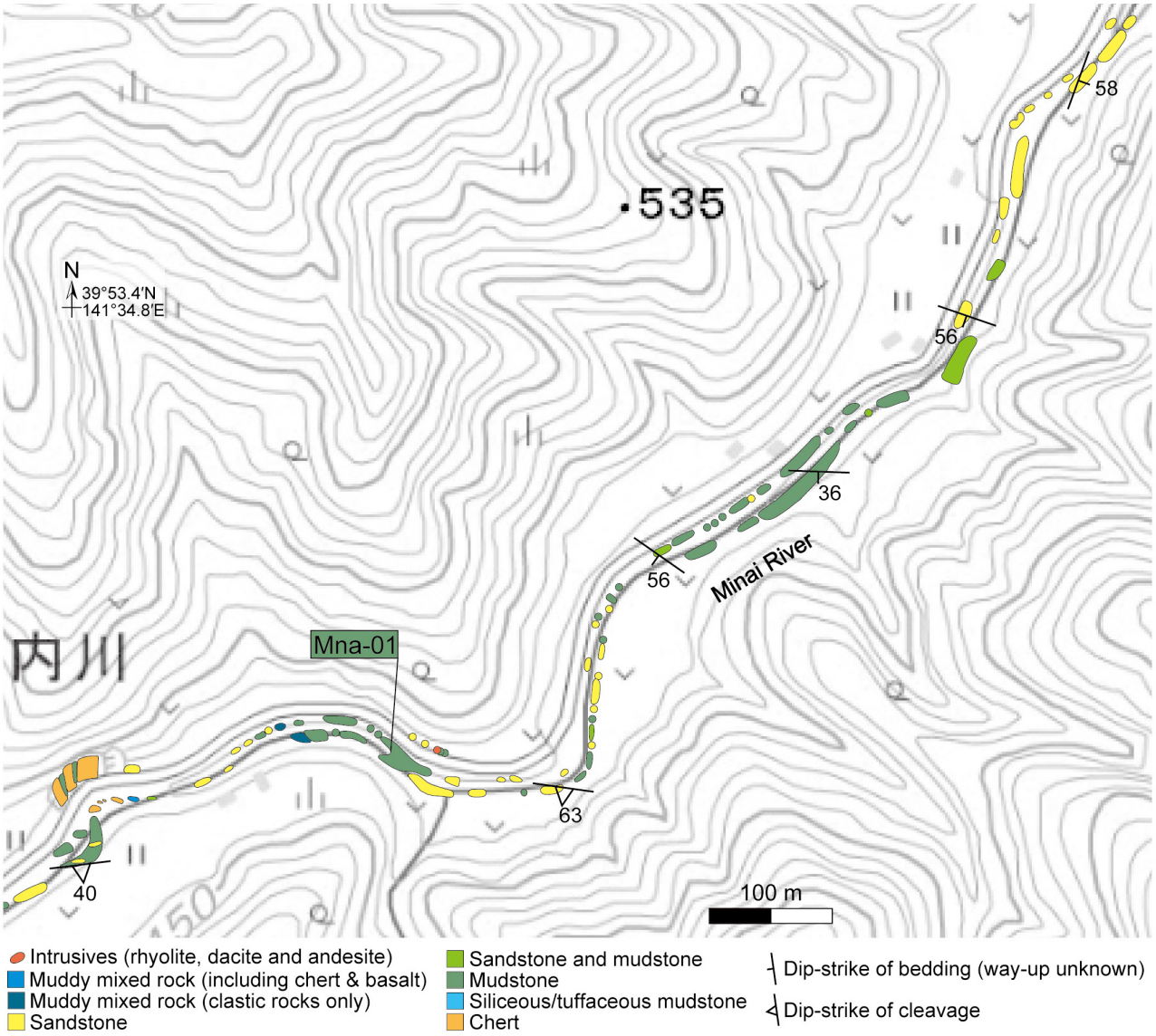

Fig. 5 Geological traverse map around Minaikawa, Kado, Iwaizumi Town (sampling locality of Mna-01). Base map produced from XYZ tiles provided by the Geospatial Information Authority of Japan.

Radiolarian tests and zircons are present as accessory components. The association of components imply that this sample was deposited as a mixture of volcanic tuff, detrital grains and radiolarian skeletons in the hemipelagic to trench area. Thirty zircon grains from sample Mna-01 were analyzed for U–Pb dating, all of which yielded concordant U–Pb ages (Fig. 18C; Table A3). Two has an age of ~1800 Ma and the age of all other grains are around 175 Ma (Fig. 18C). Twenty-five of the young zircons are accepted as grains indicating the age of eruption, resulting in a weighted average of 174.46 ± 0.93 Ma (Fig. 20).

Sample Iwk-03 was obtained from the southwest part of the Otori Unit in a locality south of Mt. Iwakura along Orikabe Stream, a tributary of the Mitakai River in northwest Iwaizumi Town (Fig. 6). The lithofacies around the locality is composed mainly of muddy mixed rocks, sandstone, chert and bedded coherent mudstone. The latter three are blocks within muddy mixed rocks on scales of kilometres. Sample Iwk-03 was collected from pale yellow bedded tuff, which is a minor lithological component in the area (Figs. 6, 12D). A radiolarian-yielding Mn-nodule sample was obtained close to sample Iwk-03 (Fig. 6) (Iwk-04; Muto *et al.*, 2025). The position of the sampled pale yellow tuff in the oceanic plate stratigraphy is not immediately obvious. However, this pale yellow tuff is closely associated with siliceous mudstone and mudstone in this route, implying that it can be roughly correlated to a position near the boundary between hemipelagic siliceous mudstone and trench-fill mudstone. In thin section, this sample is composed of two parts. The first part is composed mainly of quartz and lithic grains with clayey and siliceous matrix, and the second

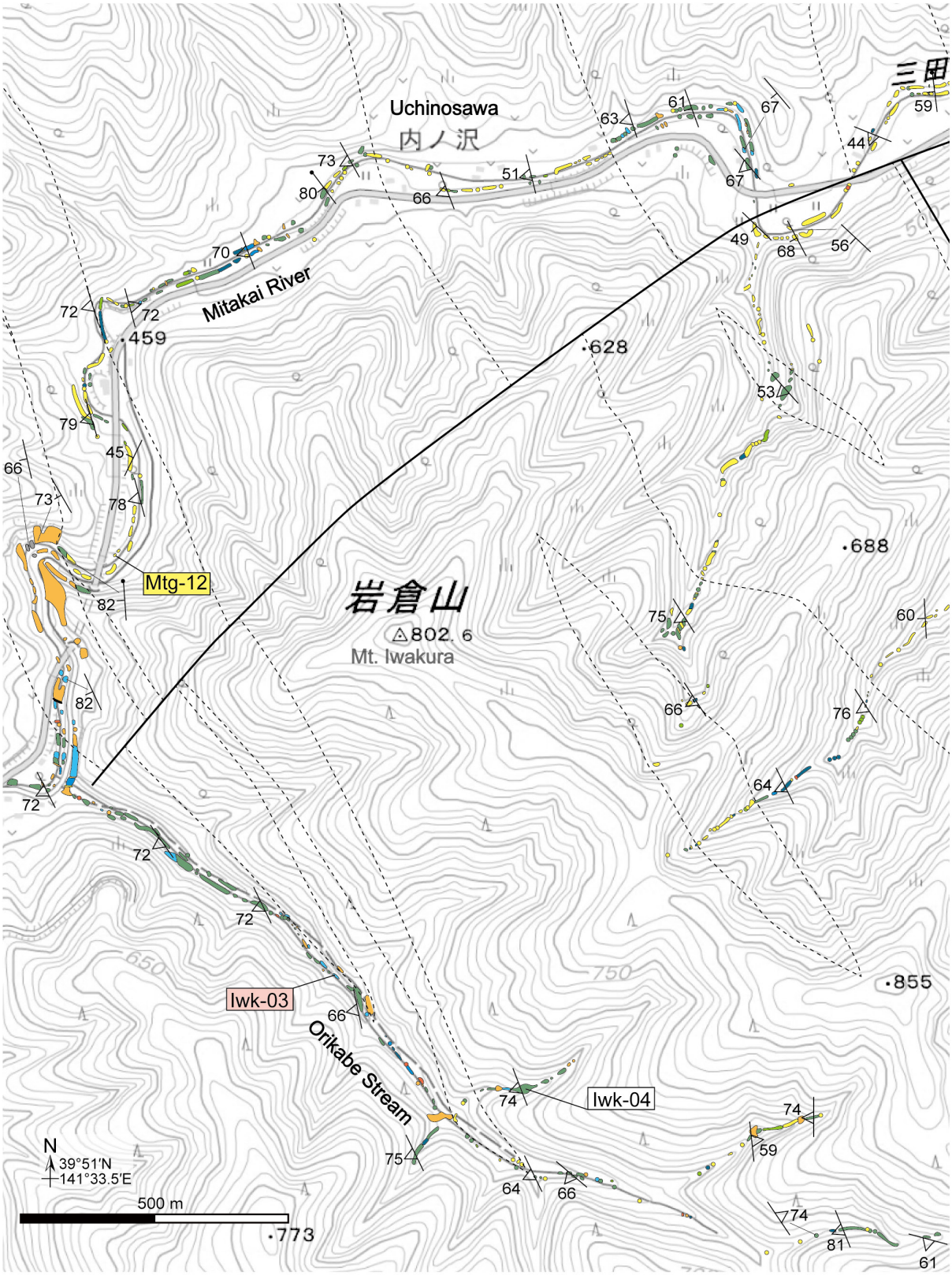
Uchinosawa
内ノ沢
三田
Mitakai River
岩倉山
△802.6
Mt. Iwakura
Mtg-12
Iwk-03
Iwk-04
Orikabe Stream
·459
·628
·688
·855
·773
650
750
N
39°51′N
141°33.5′E
500 m
Intrusives (rhyolite, dacite and andesite)
Muddy mixed rock (including chert & basalt)
Muddy mixed rock (clastic rocks only)
Sandstone
Sandstone and mudstone
Mudstone
Siliceous/tuffaceous mudstone
Chert
Siliceous claystone
Black claystone
Lithological boundary
Fault
Dip-strike of bedding (way-up unknown)
Dip-strike of cleavage
Dip-strike of bedding (way-up known)
Vertical bedding

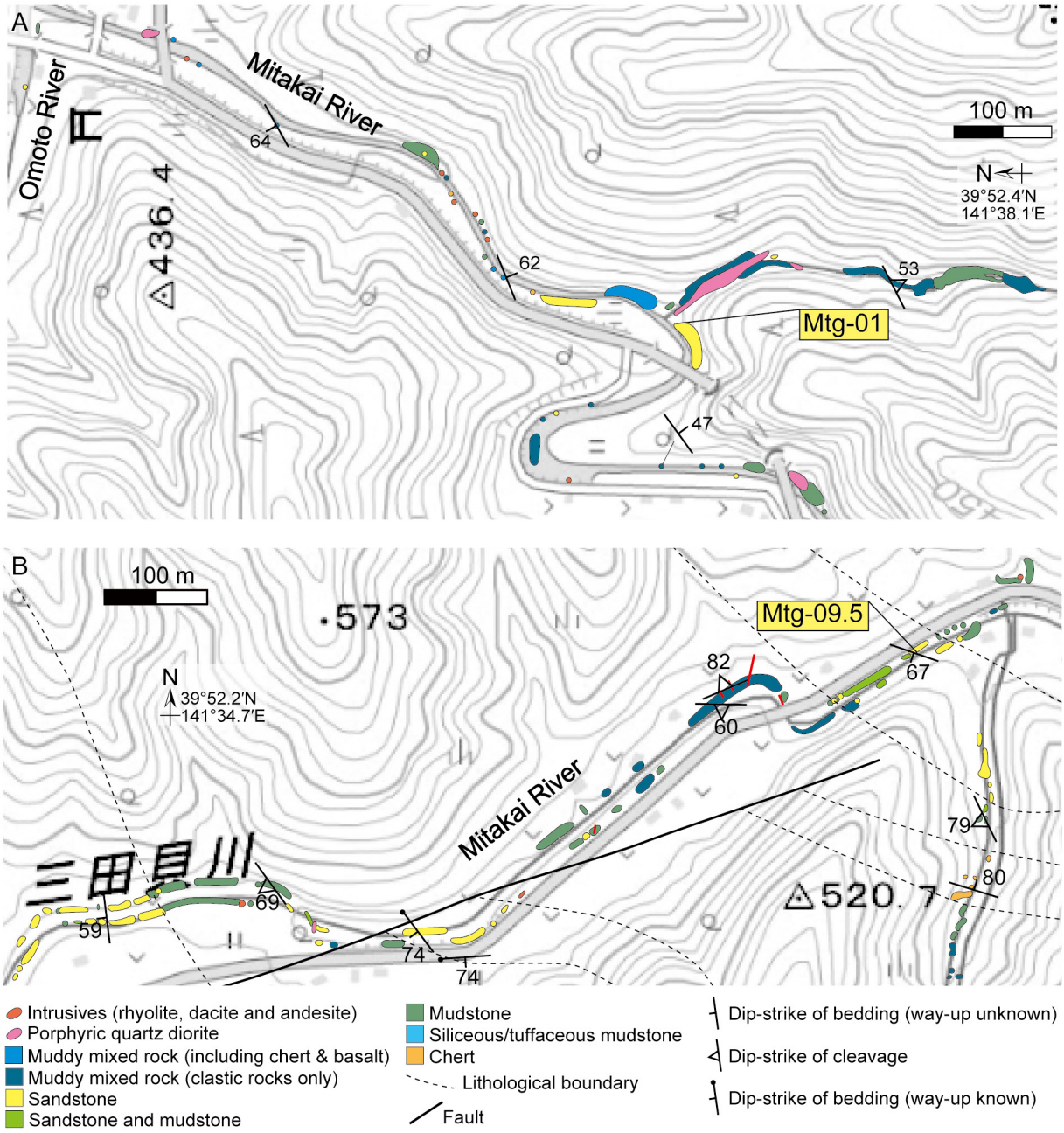

Fig. 7 Geological traverse maps of the Mitakai River around (A) the junction with the Omoto River (sampling locality of Mtg-01) and (B) Mitakai (sampling locality of Mtg-09.5), both in Kado, Iwaizumi Town. Base map produced from XYZ tiles provided by the Geospatial Information Authority of Japan.

(← p. 58)

Fig. 6 Geological traverse map around Mt. Iwakura, Kamatsuta-Gongen, Iwaizumi Town (sampling locality of Iwk-03 and Mtg-12). Sample locality of Muto *et al.* (2025) is also shown. Base map produced from XYZ tiles provided by the Geospatial Information Authority of Japan.

part is composed mainly of quartz grains supported in a matrix of microcrystalline and cryptocrystalline quartz and white mica (Fig. 14F, G). Comparing this with other samples of known stratigraphic position, it is supported that this lithofacies belongs to the hemipelagic interval of the oceanic plate stratigraphy, probably in its upper part. Thirty zircon grains from sample Iwk-03 were analyzed for U–Pb dating, all of which yielded concordant U–Pb ages (Fig. 18D; Table A4). The age of two of them is ~220

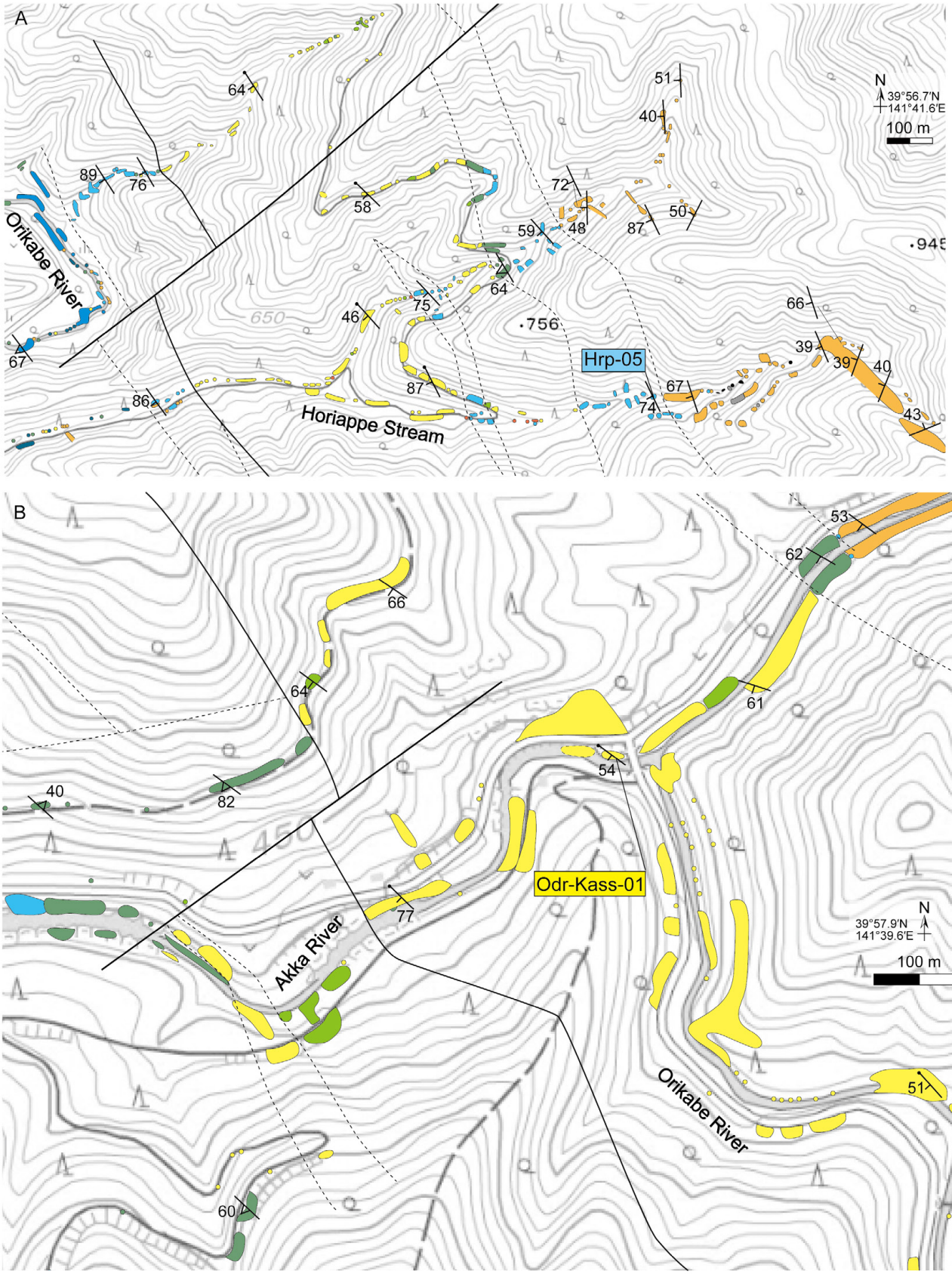
A
N
39°56.7'N
141°41.6'E
100 m
Orikabe River
Horiappe Stream
Hrp-05
650
·756
·945
B
N
39°57.9'N
141°39.6'E
100 m
Akka River
Orikabe River
Odr-Kass-01
Intrusives (rhyolite, dacite and andesite)
Muddy mixed rock (including chert & basalt)
Muddy mixed rock (clastic rocks only)
Sandstone
Sandstone and mudstone
Mudstone
Siliceous/tuffaceous mudstone
Chert
Siliceous claystone
Black claystone
Mostly covered outcrops
Lithological boundary
Unit boundary
Fault
Dip-strike of bedding (way-up unknown)
Dip-strike of cleavage
Dip-strike of bedding (way-up known)

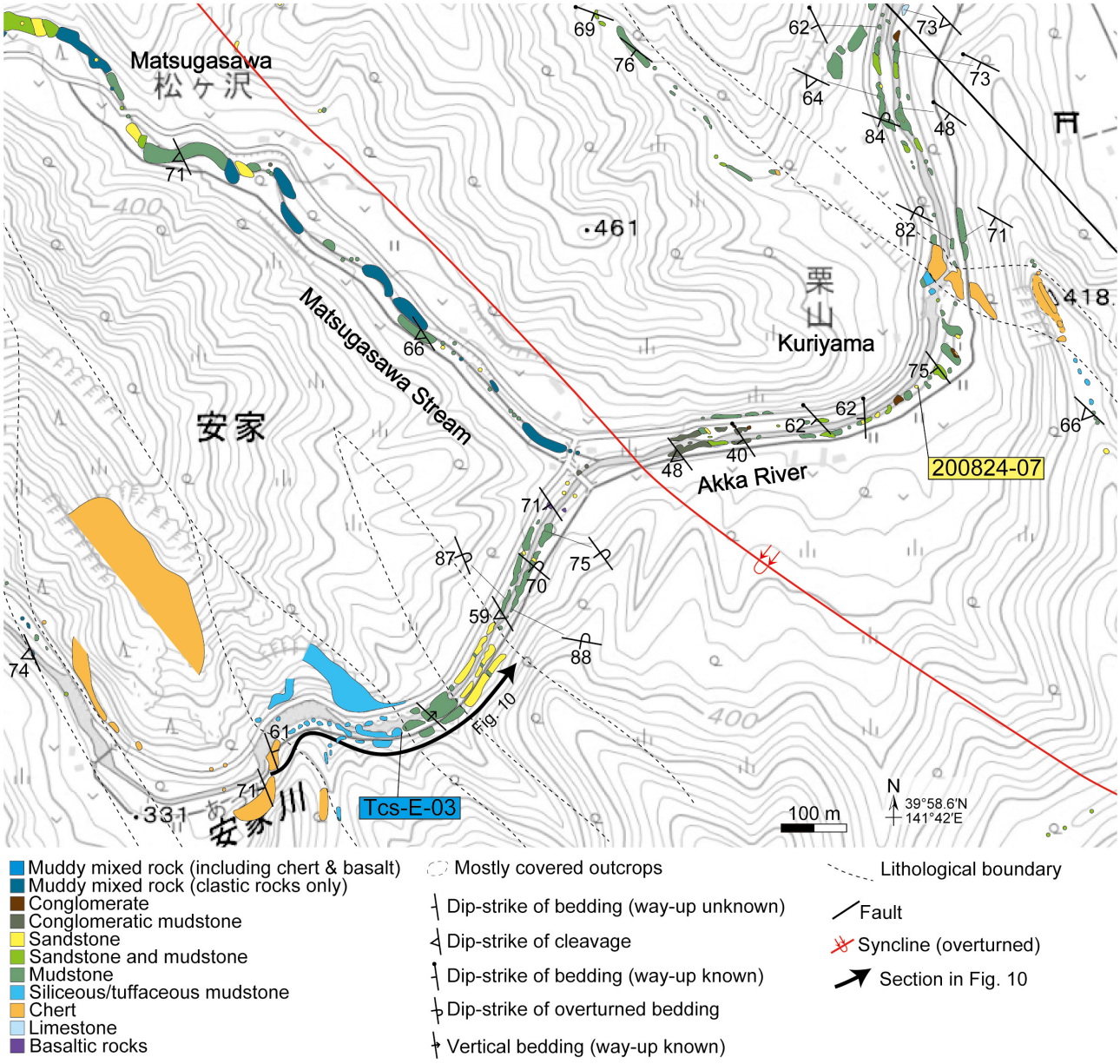

Fig. 9 Geological traverse map around Kuriyama, Akka, Iwaizumi Town (sampling locality of Tcs-E-03 and 200824-07). The route along which Fig. 10 was measured is shown. Base map produced from XYZ tiles provided by the Geospatial Information Authority of Japan.

(← p. 60)

Fig. 8 Geological traverse maps of (A) Horiappe Stream (sampling locality of Hrp-05) and (B) the junction of the Akka and Orikabe Rivers (sampling locality of Odr-Kass-01), both in Akka, Iwaizumi Town. Base map produced from XYZ tiles provided by the Geospatial Information Authority of Japan. Note that the exposures in the northeast edge of (B) have been altered due to construction.

Ma and the age of all other grains cluster around 175 Ma (Fig. 18D). All grains in this cluster is accepted as grains indicating the age of eruption, resulting in a weighted average of 174.87 ± 0.78 Ma (Fig. 20).

Sample Szm-01 was obtained from the southwest part of the Otori Unit along Chinzawa Stream, a tributary of the Minai River in northwest Iwaizumi Town (Fig. 3B). The lithofacies around the locality is composed mainly of mudstone with smaller amounts of sandstone and chert as blocks in matrix. Sample Szm-01 was collected from a horizon of mudstone with abundant tuff layers within an outcrop composed mostly of mudstone (Fig. 3B). In thin section, this sample is composed of mostly silt-sized

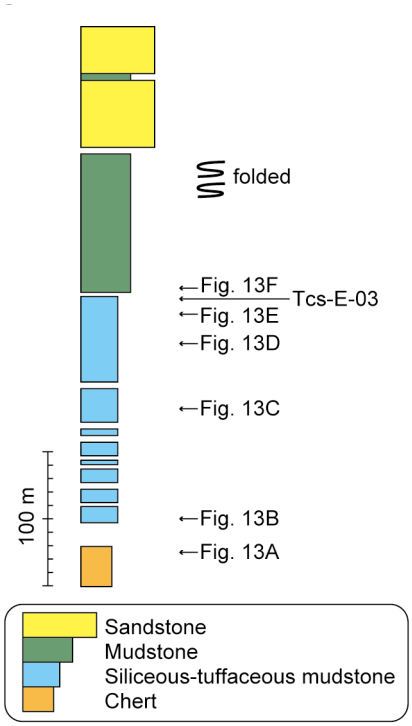

Fig. 10 Apparent stratigraphic column of the chert–clastic sequence at the sampling locality of Tcs-E-03.

grains of quartz, opaque minerals, apatite, plagioclase and zircon, in this general order of abundance (Fig. 14H–K). These grains are supported in a matrix composed of microcrystalline to cryptocystalline quartz and white mica. Part of the quartzose and micaceous matrix appear to be pseudomorphs of felsic grains. The tuff layers have a sharp sedimentary base and grades upwards into mudstone (Fig. 14H). The tuff-poor parts in the sample were too thin to be trimmed and were thus included in zircon extraction. Thirty zircon grains from sample Szm-01 were analyzed for U–Pb dating, of which twenty-nine yielded concordant U–Pb ages (Fig. 18E; Table A5). Despite tuff-poor parts being included in the sample processing, all grains are accepted as grains indicating the age of eruption, resulting in a weighted average of 171.9 ± 1.6 Ma (Fig. 20).

4. 2. 2 Sandstone (Mtg-01, Mtg-09. 5, Mtg-12)

Sample Mtg-01 was obtained along the Mitakai River near its junction with the Omoto River in northwest Iwaizumi Town (Fig. 7A). The lithofacies around this locality is composed mainly of mixed mudstone and sandstone with irregular boundaries and poorly developed cleavage. These rocks of the Jurassic accretionary complex are intruded by many dyke rocks, most of which are andesites or porphyric quartz diorites. Sample Mtg-01 was obtained from a massive sandstone outcrop surrounded

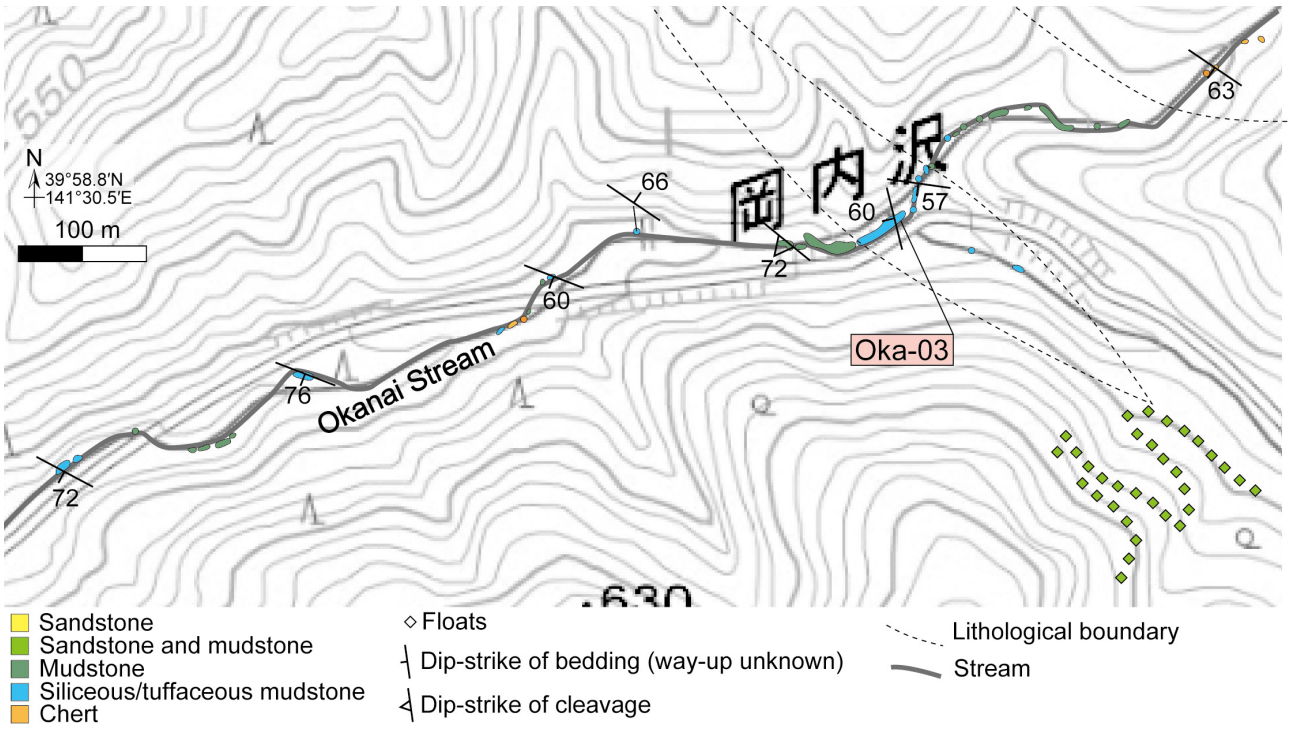

Fig. 11 Geological traverse map of Okanai Stream, Ekari, Kuzumaki Town (sampling locality of Oka-03). Base map produced from XYZ tiles provided by the Geospatial Information Authority of Japan. The actual flow of the stream is different from that on the base map and is indicated in dark grey.

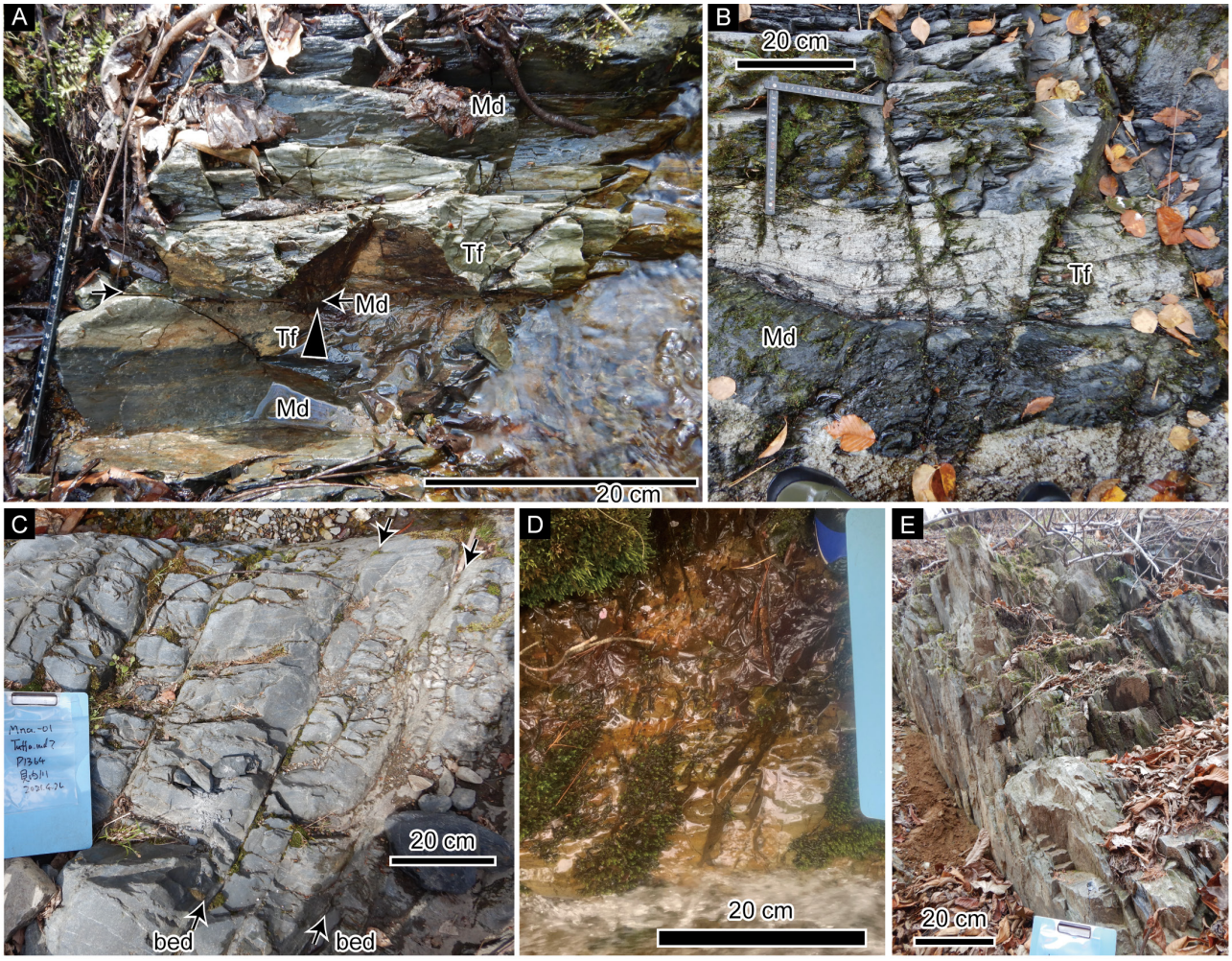

Fig. 12 Outcrop photographs of analyzed tuffs and associated lithologies. (A) Tuff bed in mudstone (sample Udg-06). Black triangle indicates grading of tuff into mudstone. (B) Tuff bed in mudstone (sample Okz-14). (C) Tuffaceous mudstone (sample Mna-01). Bedding planes are indicated by arrows labeled as "bed". (D) Bedded pale yellow tuff (sample Iwk-03). (E) Tuff in siliceous mudstone (sample Hrp-05).

by mixed rocks of mudstone and sandstone (Fig. 7A). This sample consists mainly of medium grains of quartz, plagioclase and lithic fragments and also contains accessory components such as zircons (Fig. 17A). Sixty zircon grains were analyzed for U–Pb dating, all of which yielded concordant U–Pb ages (Fig. 19F; Table A6). The majority of grains fall within the Permian, accompanied by grains of Carboniferous through Cambrian and pre-Cambrian age (Fig. 19D, E). The YC1σ age is calculated from eleven grains and has a weighted average of 254.1 ± 1.5 Ma (Fig. 19E).

Sample Mtg-09.5 was obtained along the Mitakai River, west of Mitakai Settlement in northwest Iwaizumi Town (Fig. 7B). The lithofacies around this locality is composed mainly of sandstone partly interbedded with mudstone, mudstone, mixed facies of mudstone and sandstone, and chert. Sandstone and chert are tectonic blocks in mixed facies at the scale of kilometres. Sample Mtg-09.5 was obtained from an outcrop of bedded sandstone with mudstone interbeds (Figs. 16A). This sample consists mainly of medium grains of quartz, plagioclase and lithic fragments. Sixty-two zircon grains were analyzed for U–Pb dating, all of which yielded concordant U–Pb ages (Fig. 19I; Table A10). The majority of grains fall within the late Permian to Jurassic, accompanied by grains of Cambrian and pre-Cambrian age (Fig. 19G, H). The late Cenozoic grains seem to consist of several clusters with populations around 170 Ma, 190 Ma, 220 Ma and 260 Ma (Fig. 19H). The YC1σ age is calculated from fifteen grains, the largest number of grains in a youngest cluster of detrital zircons in this study, and has a weighted average of 168.1 ± 1.0 Ma (Fig. 20).

Sample Mtg-12 was obtained along the Mitakai River west of Mt. Iwakura in northwest Iwaizumi Town (Fig. 6). This locality is close to the locality of the tuff sample Iwk-03, and the lithofacies around this locality is explained in the previous text. Sample Mtg-12 was obtained from an outcrop of bedded sandstone with black mudstone

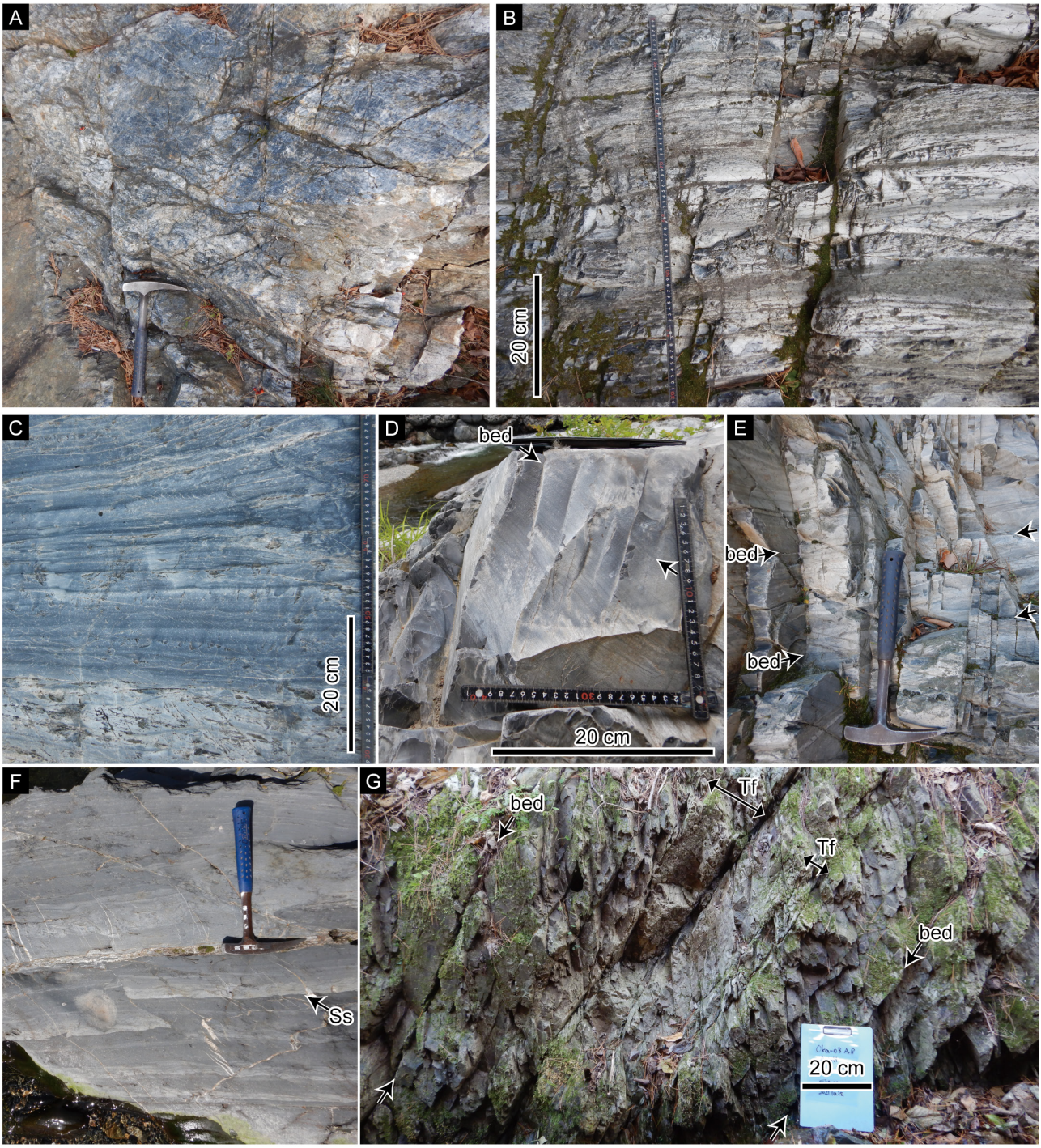

Fig. 13 Outcrop photographs of analyzed tuffs and associated lithologies. (A) Chert below sample Tcs-E-03. (B) Siliceous mudstone below sample Tcs-E-03. (C) Tuffaceous mudstone below sample Tcs-E-03. Intermediate lithofacies between B and D. (D, E) Tuff. Same lithology as sample Tcs-E-03. (F) Black mudstone with sandstone layers (Ss) above sample Tcs-E-03. (G) Siliceous mudstone with tuff beds (Oka-03). Bedding planes are indicated by arrows labeled as "bed". See Fig. 10 for location of A–F. The hammer is 33 cm long.

(→ p. 65)

Fig. 14 Thin section micrographs of analyzed tuffs. Figures C, E, G and K were taken with cross-polarized light and all others with transmitted plane-polarized light. (A–C) Tuff sample Udg-06, same field of view for B and C. (D, E) Tuffaceous mudstone sample Mna-01, same field of view. (F, G) Tuff sample Iwk-03, same field of view. (H–K) Tuff sample Szm-01, same field of view for G and H. Ap: apatite; LiTf: lithic tuff; Md: mudstone part; Pl: plagioclase; QV: quartz vein; Qz: quartz; Rad: radiolarian tests; Tf: tuff part; Zrn: zircon. Scale bars are 0.5 mm.

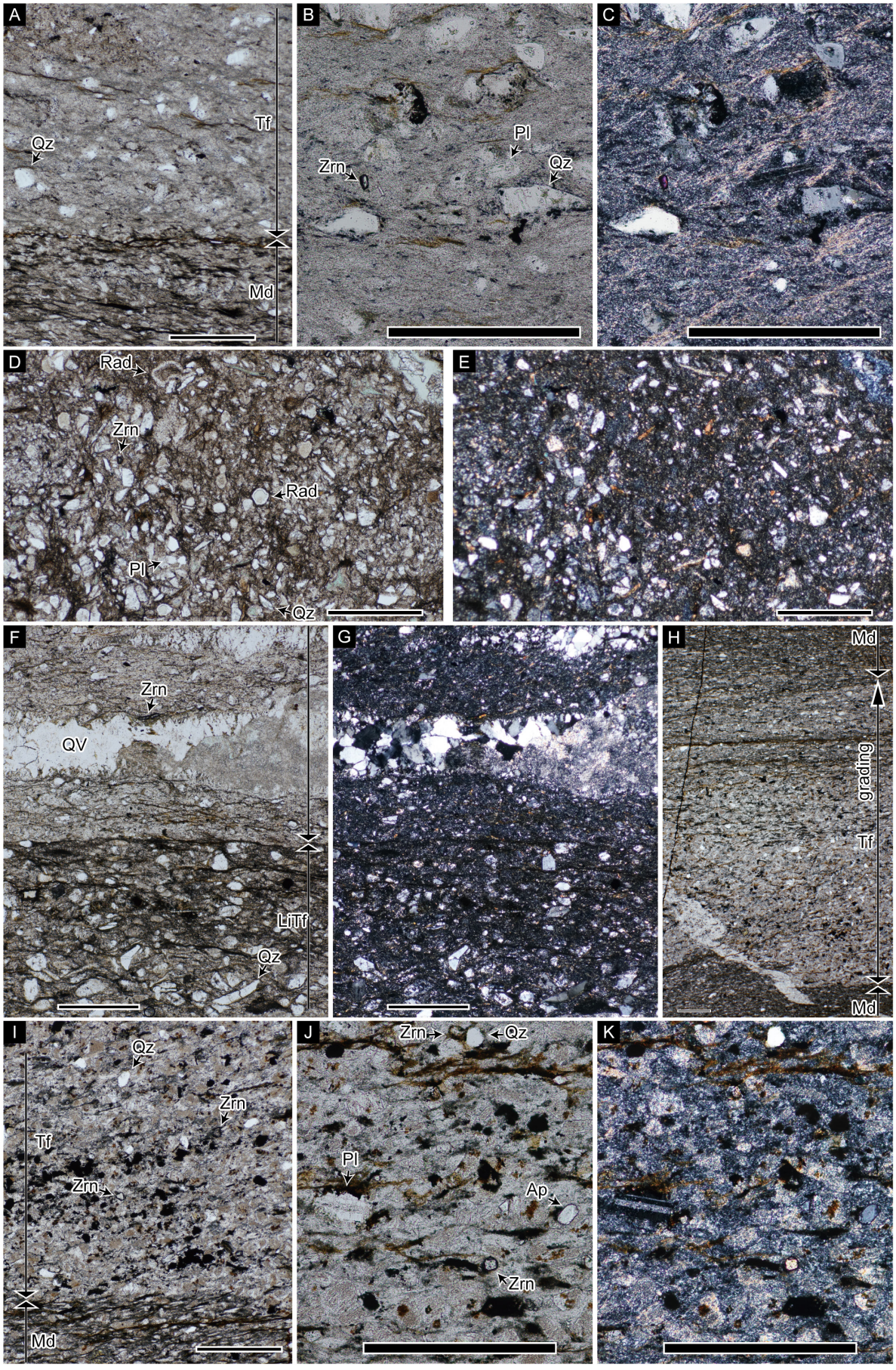
A
Tf
Qz
Md
B
Pl
Zrn
Qz
C
D
Rad
Zrn
Rad
Pl
Qz
E
F
Zrn
QV
LiTf
Qz
G
H
Md
grading
Tf
Md
I
Qz
Zrn
Tf
Zrn
Md
J
Zrn
Qz
Pl
Ap
Zrn
K

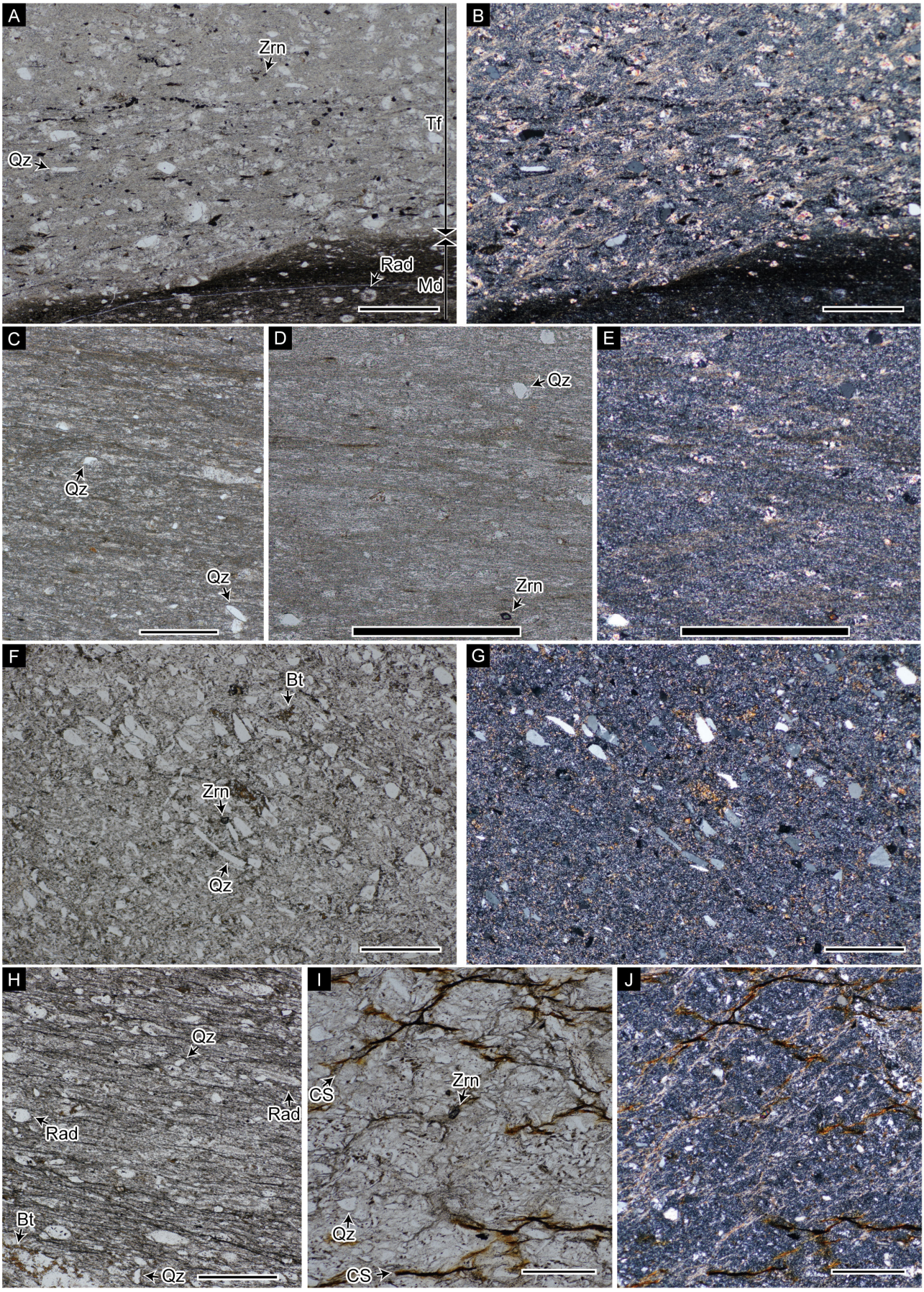
A
Zrn
Tf
Qz
Rad
Md
B
C
Qz
Qz
D
Qz
Zrn
E
F
Bt
Zrn
Qz
G
H
Qz
Rad
Rad
Bt
Qz
I
CS
Zrn
Qz
CS
J

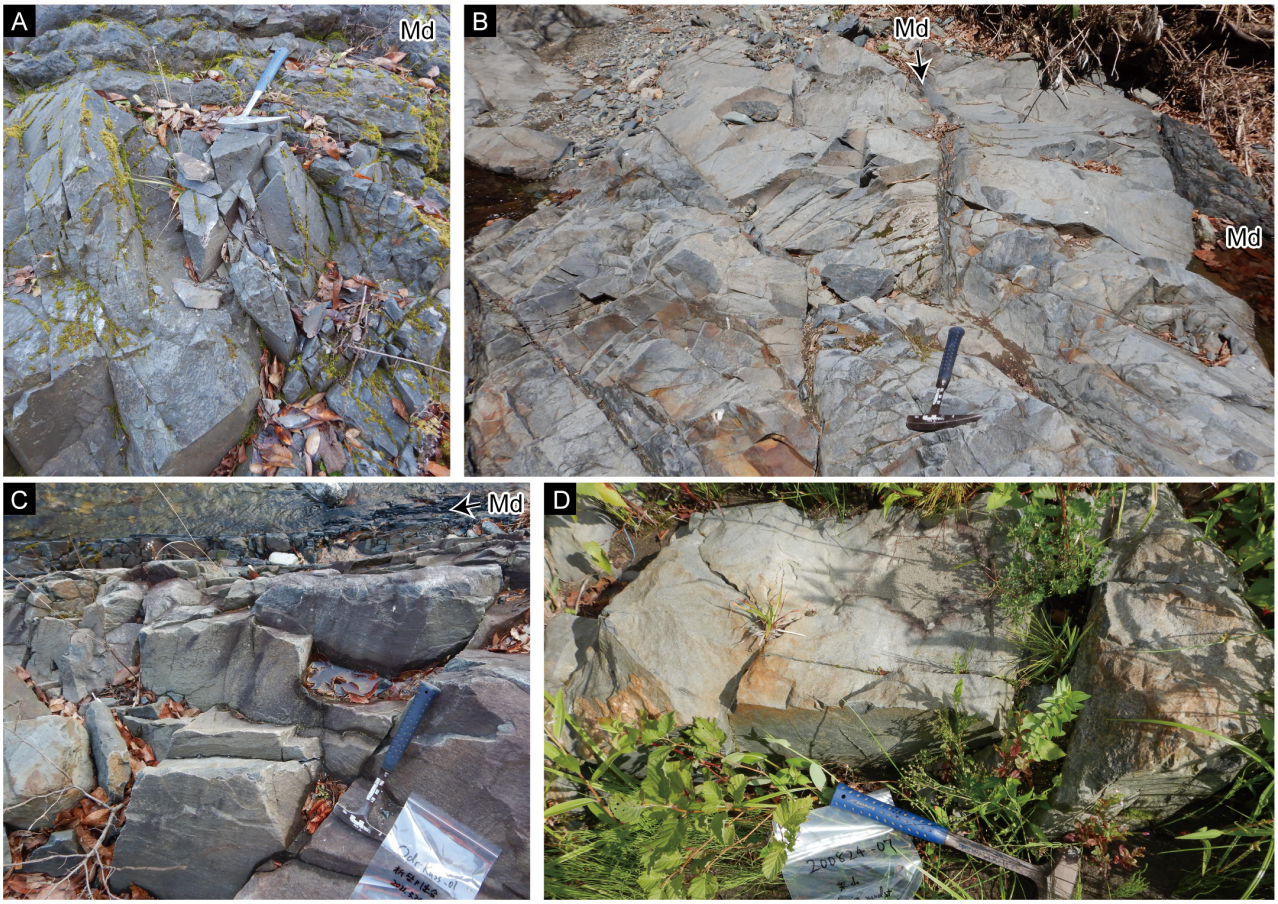

Fig. 16 Outcrop photographs of analyzed sandstones. (A) Sample Mtg-09.5. (B) Sample Mtg-12. Md: mudstone beds. (C) Sample Odr-Kass-01. (D) Sample 200824-07. The pick hammer in A–C is 33 cm long and the crack hammer in D is 40 cm long.

interbeds (Figs. 6, 16B). This sample consists mainly of grains of quartz, plagioclase and lithic fragments and also contains accessory components such as zircons (Fig. 17B). A large part of the grains is of medium size, but the sample is somewhat poorly sorted. Sixty zircon grains were analyzed for U–Pb dating, all of which yielded concordant U–Pb ages (Fig. 19L; Table A8). The majority of grains fall within the Permian to Jurassic, accompanied by grains of older Paleozoic and pre-Cambrian age (Fig. 19J, K). The late Cenozoic grains seem to consist of several populations, with peaks around 170–180, 190, 220 and 260 Ma (Fig. 19K). The YC1σ age is calculated from only two grains that belong to the youngest of these peaks and has a weighted average of 172 ± 27 Ma (Fig. 20).

(← p. 66)

Fig. 15 Thin section micrographs of analyzed tuffs. Figures B, E, G and J were taken with cross-polarized light and all others with transmitted plane-polarized light. (A, B) Tuff sample Okz-14, same field of view. (C, D, E) Tuff sample Hrp-05, same field of view for D and E. (F, G) Tuff sample Tcs-E-03, same field of view. (H) Siliceous mudstone below sample Tcs-E-03 (Fig. 13B). (I, J) Tuff sample Oka-03, same field of view. Bt: biotite; CS: clay seams; Md: mudstone part; Qz: quartz; Rad: radiolarian tests; Tf: tuff part; Zrn: zircon. Scale bars are 0.5 mm.

4. 3. Seki Unit

4. 3. 1 Tuff (Hrp-05)

This sample was obtained from the Horiappe Stream, a tributary of the Orikabe River in northeast Iwaizumi Town (Fig. 8A). The sample comes from a chert–clastic sequence composed mainly of bedded chert, grey siliceous mudstone and bedded sandstone in ascending order, which characterizes the Seki Unit (Fig. 8A). Grey siliceous mudstone is associated with grey mudstone which contains only minor amounts of radiolarian tests. However, the two rock types are usually not easily distinguished in the field, so both are included in one lithofacies as grey siliceous mudstone. Black to dark grey mudstone is partly present at the top of the grey siliceous mudstone. The analyzed sample is a grey tuff obtained from the lower part of the grey siliceous mudstone (Figs. 8A, 12E. It is composed of fine-grained white micas and microcrystalline to cryptocrystalline quartz matrix and contains minor amounts of quartz grains and

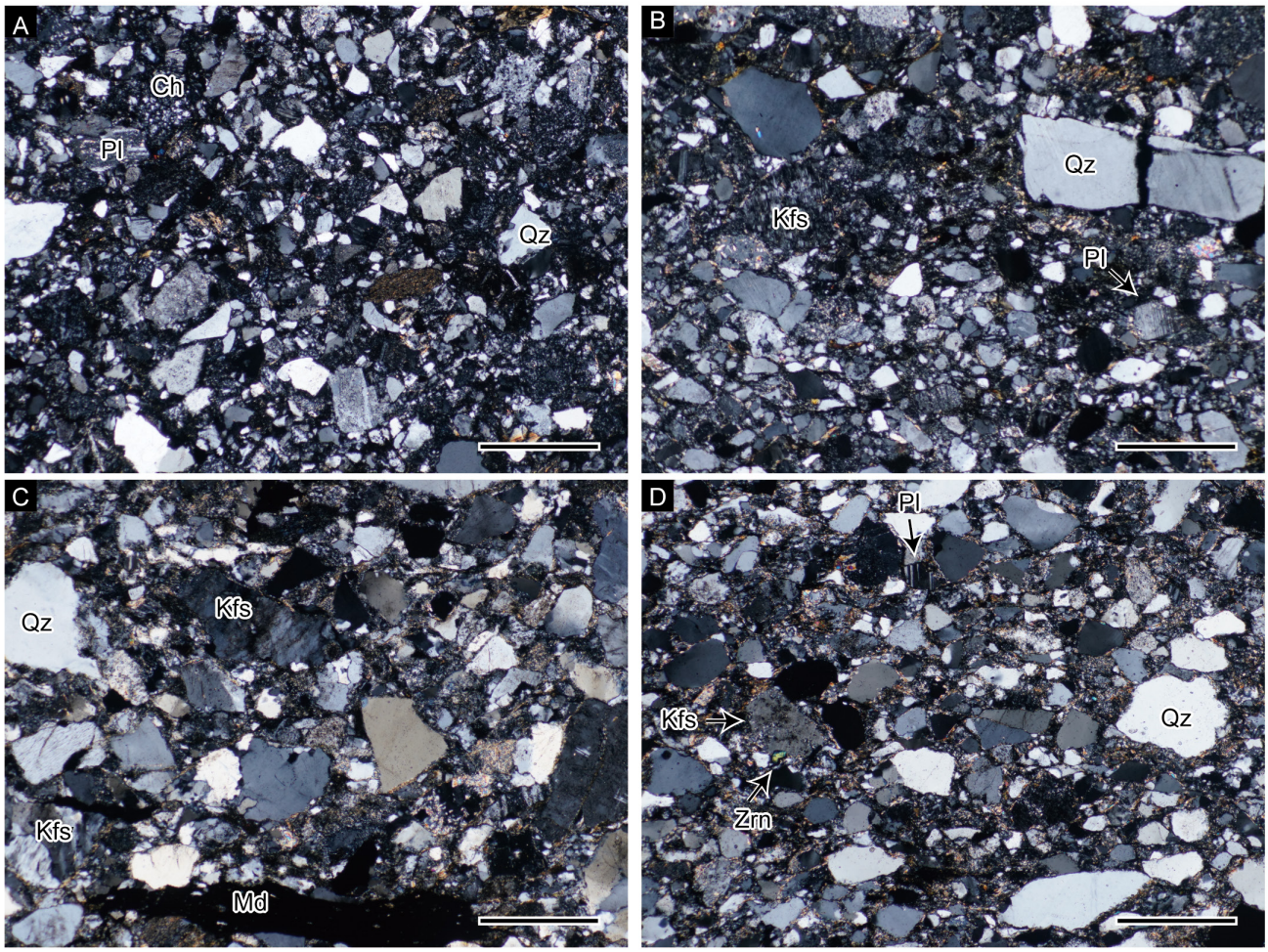

Fig. 17 Thin section micrographs of analyzed sandstones. All photographs were taken with cross-polarized light. (A) Sample Mtg-01. (B) Sample Mtg-12. (C) Sample Odr-Kass-01. (D) Sample 200824-07. Ch: chert fragment; Kfs: K-feldspar; Md: mudstone fragment; Pl: plagioclase; Qz: quartz; Zrn: zircon. Scale bars are 0.5 mm.

small zircons (Fig. 15C–E). Thirty zircon grains were analyzed for U–Pb dating, all of which yielded concordant U–Pb ages (Fig. 18F; Table A9). Most ages are gathered around 165 Ma, while six grains are distinctly younger (Fig. 18F). The young ages were obtained from zircons that were cracked during laser ablation. Twenty-two of the cluster are accepted as grains indicating the age of eruption, resulting in a weighted average of 167.4 ± 1.1 Ma (Fig. 20).

4. 3. 2 Sandstone (Odr-Kass-01)

This sample was collected at the junction of the Orikabe and Akka rivers in northeast Iwaizumi Town (Fig. 8B). The chert–clastic sequence of the Seki Unit, much like that in Horiappe Stream mentioned above but lacking the grey siliceous mudstone, is exposed around this locality. The sample was taken from an outcrop of bedded, normal-grading sandstone with intercalated black mudstone, (Figs. 8B, 16C). This sample consists mainly of medium grains of quartz, K-feldspars, plagioclase and lithic fragments and also contains accessory components such as zircons (Fig. 17C). Lithic fragments include mudstone clasts, which are easily observed also at the outcrop. Sixty-four zircon grains were analyzed for U–Pb dating, of which sixty-two yielded concordant U–Pb ages (Fig. 19O; Table A10). The zircon age spectra show that the majority of grains have Triassic to Jurassic ages, while a small number of Permian, Devonian and pre-Cambrian zircons are present (Fig. 19M, N). The Triassic to Jurassic grains seems to consist of several clusters, with peaks around 180, 190 and 220 Ma (Fig. 19N). The YC1σ age is calculated from only three grains that sit outside these main peaks and has

(→ p. 69)

Fig. 18 Concordia diagrams of zircon ages from tuffs. (A) Udg-06, Kadoma Unit. Red ellipses are concordant ages and black dashed ellipses are discordant ages. (B) Okz-14, Otori Unit. (C) Mna-01, Otori Unit. (D) Iwk-03, Otori Unit. (E) Szm-01, Otori Unit. (F) Hrp-05, Seki Unit. (G) Tcs-E-03, Takayashiki Unit. (H) Oka-03, Ekari Unit. Figures were produced by Isoplot/Ex 4.15 (Ludwig, 2012).

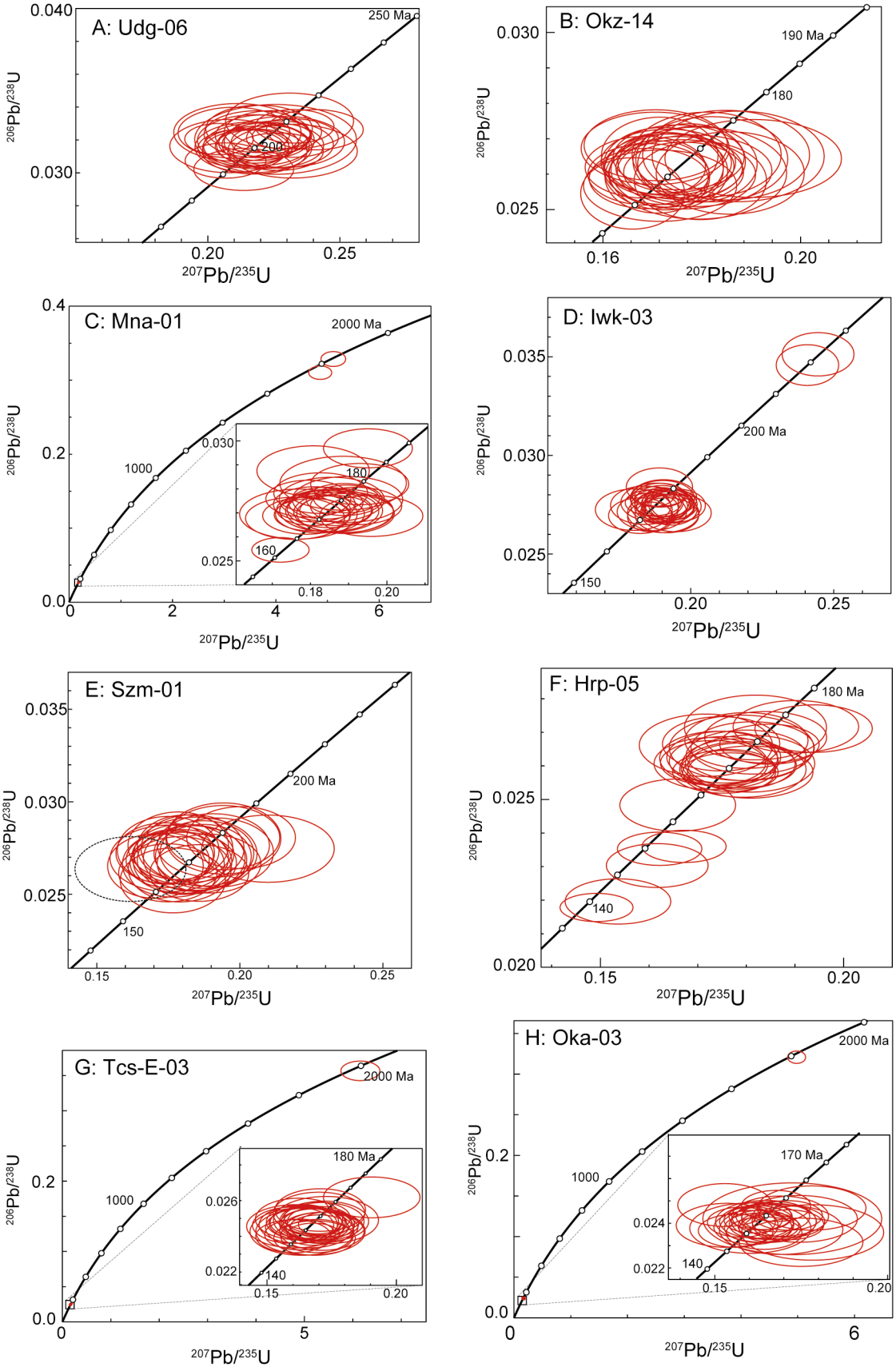
A: Udg-06
250 Ma
200
0.040
0.030
0.20
0.25
$^{206}Pb/^{238}U$
$^{207}Pb/^{235}U$
B: Okz-14
190 Ma
180
0.030
0.025
0.16
0.20
C: Mna-01
2000 Ma
1000
0.030
0.025
180
160
0.18
0.20
0.4
0.2
0.0
0
2
4
6
D: Iwk-03
200 Ma
150
0.035
0.030
0.025
E: Szm-01
200 Ma
150
0.15
F: Hrp-05
180 Ma
140
0.020
G: Tcs-E-03
180 Ma
0.026
0.022
140
5
H: Oka-03
170 Ma
0.024
0.022

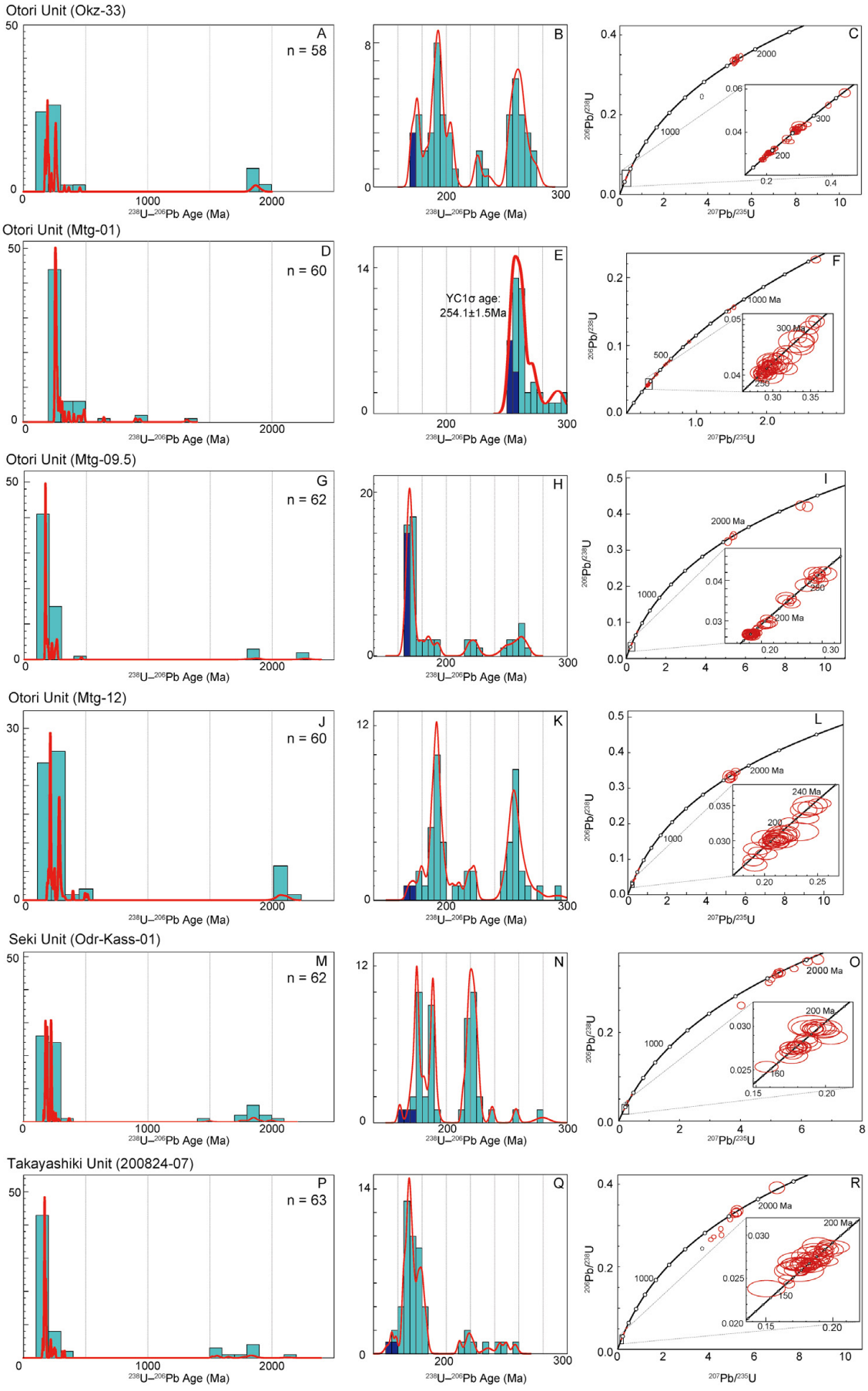
Otori Unit (Okz-33)
A
n = 58
B
C
Otori Unit (Mtg-01)
D
n = 60
E
YC1σ age:
254.1±1.5Ma
F
Otori Unit (Mtg-09.5)
G
n = 62
H
I
Otori Unit (Mtg-12)
J
n = 60
K
L
Seki Unit (Odr-Kass-01)
M
n = 62
N
O
Takayashiki Unit (200824-07)
P
n = 63
Q
R
238U–206Pb Age (Ma)
207Pb/235U
206Pb/238U

a weighted average of 171.4 ± 2.2 Ma (Fig. 20).

4. 4. Takayashiki Unit

Samples from the Takayashiki Unit was obtained from outcrops along the Akka River near Kuriyama Settlement, Iwaizumi Town, Iwate Prefecture (Fig. 9). This route is the type locality of the Takayashiki Unit. Chert, siliceous mudstone, bedded tuff, mudstone, sandstone, conglomerate and muddy mixed rocks are the main lithofacies distributed in the area and forms a tight syncline (Fig. 9). The lithofacies is generally a broken facies on scales of kilometres, and therefore strata on the two limbs of folds may not be exact equivalents, also suggested by some differences in lithofacies. On scales of hundreds of metres or less, characters such as chert–clastic sequences and sedimentary structures indicate coherent facies.

4. 4. 1 Tuff (Tcs-E-03)

This sample is a dark brownish grey tuff from a chert–clastic sequence (Fig. 9). The chert–clastic sequence is composed in ascending order of bedded chert, siliceous mudstone, tuff, mudstone and sandstone (Figs. 10, 13A–F). The general coarsening upward and layers with graded bedding (Fig. 13F), flame structures or burrows mainly in mudstone indicate a coherent facies, although folds of metre-scale or smaller are present. Siliceous mudstone and tuff in this sequence is not easily distinguished from each other in the field. They are both bedded, either dark grey to pale grey depending on the condition of the outcrop surface, hard and have conchoidal fractures similar to chert (Fig. 13B–E). End members can be clearly distinguished in thin section: siliceous mudstone contains abundant radiolarian tests (Fig. 15H), while tuff contains abundant angular mineral fragments in microcrystalline quartz matrix (Fig. 15F, G). On the other hand, there are intermediate varieties making it even harder to draw a line between siliceous mudstone and tuff in the field. Contact metamorphism probably by subsurface plutons, represented by the formation of biotite (Fig. 15F–H) may also be contributing to the difficulty. Due to the above, siliceous mudstone, tuff and intermediate lithofacies (tuffaceous mudstone) are here not distinguished in classification of lithofacies in the field.

The investigated sample was obtained from the top of the siliceous mudstone–tuff sequence and is overlain by mudstone with sandstone and tuff layers (Fig. 10). In thin section, it is composed of angular, poorly sorted quartz grains supported in a matrix of microcrystalline quartz, white mica and biotite (Fig. 15F, G). The form of many quartz grains are thin and sharp shards. Part of the quartzose and micaceous matrix appears to be pseudomorphs of felsic grains. Thirty zircon grains were analyzed for U–Pb dating, all of which yielded concordant U–Pb ages (Fig. 18G; Table A11). One grain has an age of ~2000 Ma and the age of all other grains cluster around 156 Ma (Fig. 18G). Twenty-eight of the cluster are accepted as grains indicating the age of eruption, resulting in a weighted average of 156.39 ± 0.92 Ma (Fig. 20).

4. 4. 2 Sandstone (200824-07)

This sample was collected from an outcrop of bedded sandstone within mudstone, broken alternation of sandstone and mudstone, and conglomerate (Figs. 9, 16D). This lithofacies composed of mudstone and coarse clastic rocks is situated above a sequence of chert, siliceous mudstone and mudstone to the north. Thus, the sample comes from the clastic part of a chert–clastic sequence. This sample consists mainly of medium grains of quartz, K-feldspars, plagioclase and lithic fragments and also contains accessory components such as zircons (Fig. 17D). Sixty-four zircon grains were analyzed for U–Pb dating, of which sixty-three yielded concordant U–Pb ages (Fig. 19R; Table A12). The majority of the grains fall within the Jurassic, accompanied by grains of Triassic, Permian, Carboniferous and pre-Cambrian age (Fig. 19P, Q). The Jurassic grains seems to consist of at least three populations, centred around 150, 170 and 180 Ma (Fig. 19Q). The YC1σ age is calculated from only two grains and has a weighted average of 154 ± 17 Ma (Fig. 20).

4. 5. Ekari Unit

One tuff sample from the Ekari Unit was investigated in this study. No sandstone samples were investigated.

The analyzed sample (Oka-03) was obtained in Okanai Stream, a tributaty of the Mabechi River in Ekari, southeast Kuzumaki Town, Iwate Prefecture (Fig. 11). The lithofacies around the locality is composed of mudstone, siliceous and tuffaceous mudstone, chert and broken facies of mudstone and sandstone, although exposures are limited. Sample Oka-03 was collected from a white tuff bed intercalated in bedded grey siliceous mudstone (Fig. 13G). The sample is composed of silt-sized quartz including shards with low roundness and sphericity supported in a matrix of microcrystalline to cryptocrystalline quartz and white mica (Fig. 15I, J). Part of the quartzose and micaceous matrix appear to be

(← p. 70)

Fig. 19 (A, B, D, E, G, H, J, K, M, N, P, Q) Probability density plot of concordant zircon ages from sandstone. (A, D, G, J, M, P) All grains. (B, E, H, K, N, Q) Late Phanerozoic grains. (C, F, I, L, O, R) Concordia diagrams of zircon ages from sandstone. Red ellipses are concordant ages and black dashed ellipses are discordant ages. (A–C) Okz-33, Otori Unit. (D–F) Mtg-01, Otori Unit. (G–I) Mtg-09.5, Otori Unit. (J–L) Mtg-12, Otori Unit. (M–O) Odr-Kass-01, Seki Unit. (P–R) 200824-07, Takayashiki Unit. The youngest cluster determined by overlaps of 1σ error (YC1σ) is shown with deep blue in the histograms of young grains. Red lines indicate relative probability. Figures were produced by Isoplot/Ex 4.15 (Ludwig, 2012). Data for sample Okz-33 are reillustrated from Muto *et al.* (2023).

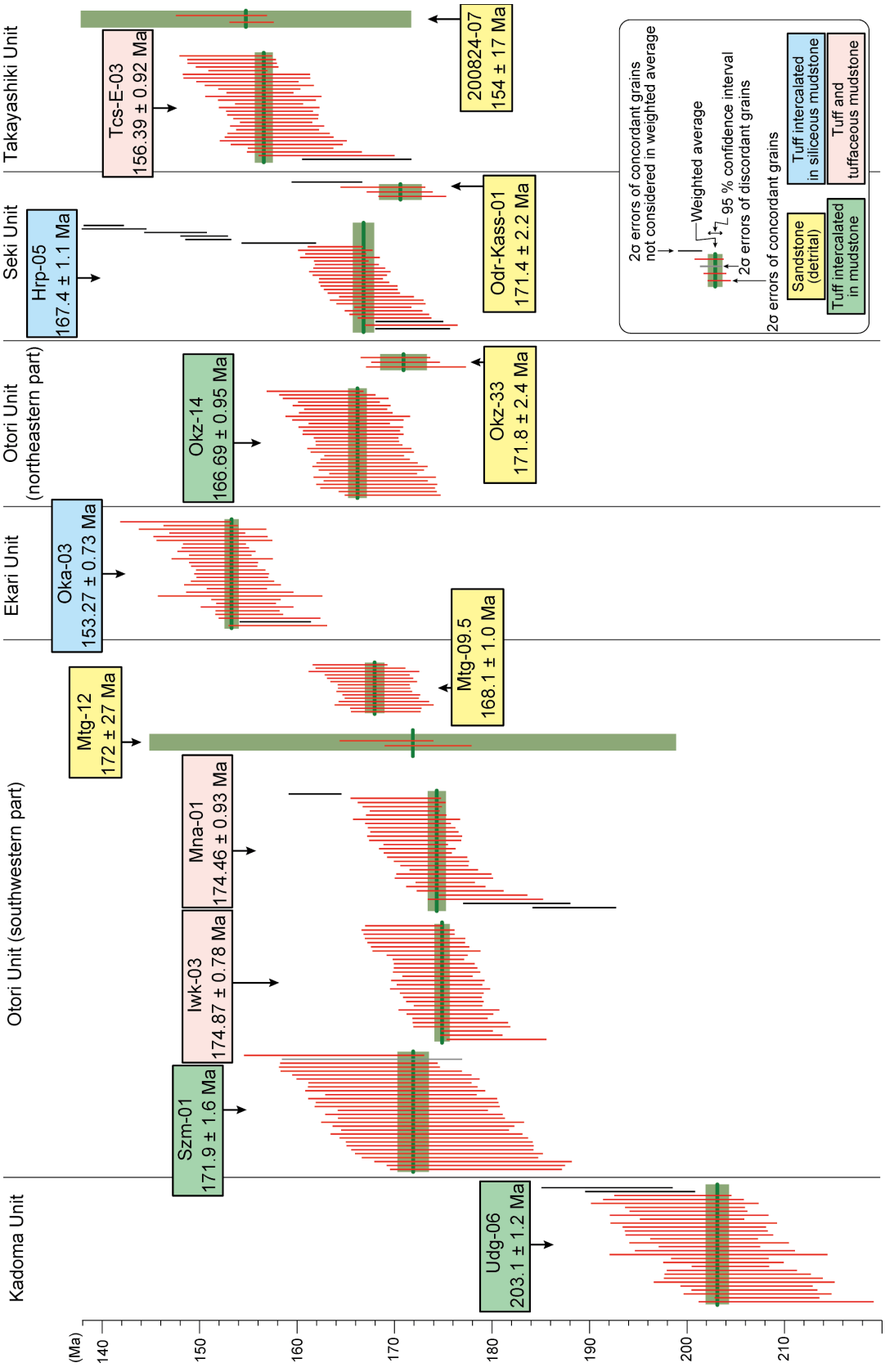

Fig. 20 Weighted average of zircons from tuffs and youngest clusters in sandstones. Samples are arranged in general order of geographic distribution. Figures were produced by Isoplot/Ex 4.15 (Ludwig, 2012). MSWD (mean square weighted deviation) for each sample is Oka-03: 1.08; Tcs-E-03: 0.86; 200824-07: 1.4; Hrp-05: 2.0; Odr-Kass-01: 0.59; Okz-14: 0.50; Mna-01: 1.2; Iwk-03: 1.00; Szm-01: 0.63; Okz-33: 0.24; Mtg-09.5: 0.27; Mtg-12: 1.7; Udg-06: 0.79. Data for sample Okz-33 are reillustrated from Muto *et al.* (2023).

pseudomorphs of felsic grains. Biotite of metamorphic origin are present, especially around clayey seams. Thirty zircon grains were analyzed for U–Pb dating, all of which yielded concordant U–Pb ages (Fig. 18H; Table A13). One has an age of ~1800 Ma and the age of all other grains cluster around 155 Ma (Fig. 18H). Twenty-eight of the cluster are accepted as grains indicating the age of eruption, resulting in a weighted average of 153.27 ± 0.73 Ma (Fig. 20).

5. Trench-arrival age of the Jurassic accretionary complex in the North Kitakami Belt

The geochronological data in this study and radiolarians from Mn-nodules reported in this issue (Muto *et al.*, 2025) provide new information on the tectonostratigraphic division of the Jurassic accretionary complex of the North Kitakami Belt. Here, I compile data that can constrain the trench-arrival age (TAA) from the main part of the northern Kitakami Mountains (Fig. 21). The compilation covers nine tectonostratigraphic units. More information is available for the seven units distributed around the Kado District, owing to the larger number of studies that conform to the concept of plate tectonics. These are the Kayamori, Takayashiki, Seki, Otori, Misugo and Kadoma units that structurally overlie one another in this order, and the Ekari Unit. Two other units in the eastern part, the Magisawa and Akashika units, are based on coherent formations defined by Sugimoto (1974) and Minoura and Tsushima (1984). They were adopted as accretionary tectonostratigraphic units in more recent works, but studies of their characters as accretionary complexes are very few. In this chapter, I will first discuss units with new data in this study and compare them with previous age data. Following this, I will give an overview on the trend of TAA across the North Kitakami Belt in the main part of the northern Kitakami Mountains.

5. 1. Tectonostratigraphic units with new data in this study

The TAA of the Kadoma Unit has been estimated in the Sotoyama and Hayachine San districts to the southwest of the Kado District (Matsuoka, 1988; Kawamura *et al.*, 2013; Uchino, 2017; Uchino, 2019; Osaka *et al.*, 2023). These studies showed that the Kadoma Unit has a TAA from the Early Jurassic or possibly late Late Triassic to the late Middle Jurassic with a younging trend towards the northeast (oceanward) direction (Fig. 21). On the other hand, the present study identified a tuff bed in mudstone that has a Rhaetian (end-Triassic) age from the northeast margin of the Kadoma Unit (Figs. 20, 21). While the confirmation of a latest Triassic TAA is in accordance with previous data, the occurrence of the oldest accretionary units in the northeast margin is unexpected. This implies that the internal structure of the Kadoma Unit is not a simple one in which younger accretionary complexes are progressively stacked towards the present oceanward direction.

The TAA of the northeast part of the Otori Unit was constrained from radiolarians from Mn-nodules in siliceous mudstone that indicate the Bajocian to Bathonian (Suzuki *et al.*, 2007b; Ehiro *et al.*, 2008; Muto *et al.*, 2023). The tuff sample Okz-14 from mudstone has a Bathonian age compatible with the radiolarian age (Fig. 21B). In contrast, the detrital zircons analyzed by Muto *et al.* (2023) has a YC1σ age ~5 Myr older (Fig. 20). Muto *et al.* (2023) suggested that the YC1σ age may be close to the depositional age. However, since sandstone is expected to be younger than siliceous mudstone in the concept of oceanic plate stratigraphy, the YC1σ age of sandstone probably does not record its depositional age. In the case of this particular sample, even the youngest single zircon is probably older than the depositional age (Fig. 20).

The TAA of the southwest part of the Otori Unit is constrained by three tuff samples of late Toarcian to Aalenian age and the sandstone sample Mtg-09.5 with a Bathonian YC1σ age (Fig. 21B). The YC1σ age of sample Mtg-09.5 is consistent with data from tuffs, and hence is likely close to its depositional age. In addition, this sample has a youngest cluster consisting of fifteen grains (~25 % of total grains), much more than in other sandstone samples. The YC1σ age of the sandstone sample Mtg-12 is not in direct contradiction with these data, but will not be considered further for TAA because of its large uncertainty. The sandstone sample Mtg-01 yielded a latest Permian YC1σ age, which is calculated from the young portion of a prominent Permian population (Fig. 19D). This age is unlikely to represent TAA considering other data from the Otori Unit. Notably, this sample is unique in containing Mesoproterozoic and Neoproterozoic grains (Fig. 19). Perhaps sample Mtg-01 has a very small portion of grains from Mesozoic provenances, so that Mesozoic grains were undetected, while in other samples, Mesoproterozoic and Neoproterozoic grains were undetected due to dilution from Mesozoic provenances.

The position of the tuffs from the southwest part of the Otori Unit in the oceanic plate stratigraphy is the upper part of the hemipelagic siliceous mudstone interval for Iwk-03, siliceous mudstone to mudstone interval for Mna-01 and the mudstone interval for sample Szm-01. The U–Pb age of these samples, that of the sandstone sample Mtg-09.5, and the age of mudstone indicated by radiolarians from Mn-nodules (Muto *et al.*, 2025) is completely consistent with the stratigraphic order assumed from the lithology of the samples (Fig. 21B). Two Mn-nodules from grey bedded mudstone that contains mostly clay-sized detrital grains and only rare silt-sized ones (Fig. 7E of Muto *et al.*, 2025) yielded Aalenian to Bajocian radiolarians (Muto *et al.*, 2025). This lithology is likely to represent the lower portion of trench-fill clastic rocks. This interval corresponds to or is close to where tuff samples Iwk-03 and Mna-01 are derived from, which is in accordance with the late Toarcian to early Aalenian U–Pb age of the tuffs (Fig. 21B). The mudstone hosting sample Szm-01 and sandstone represented by sample Mtg-09.5 are from successively higher horizons, in good agreement with the respective Aalenian and Bajocian

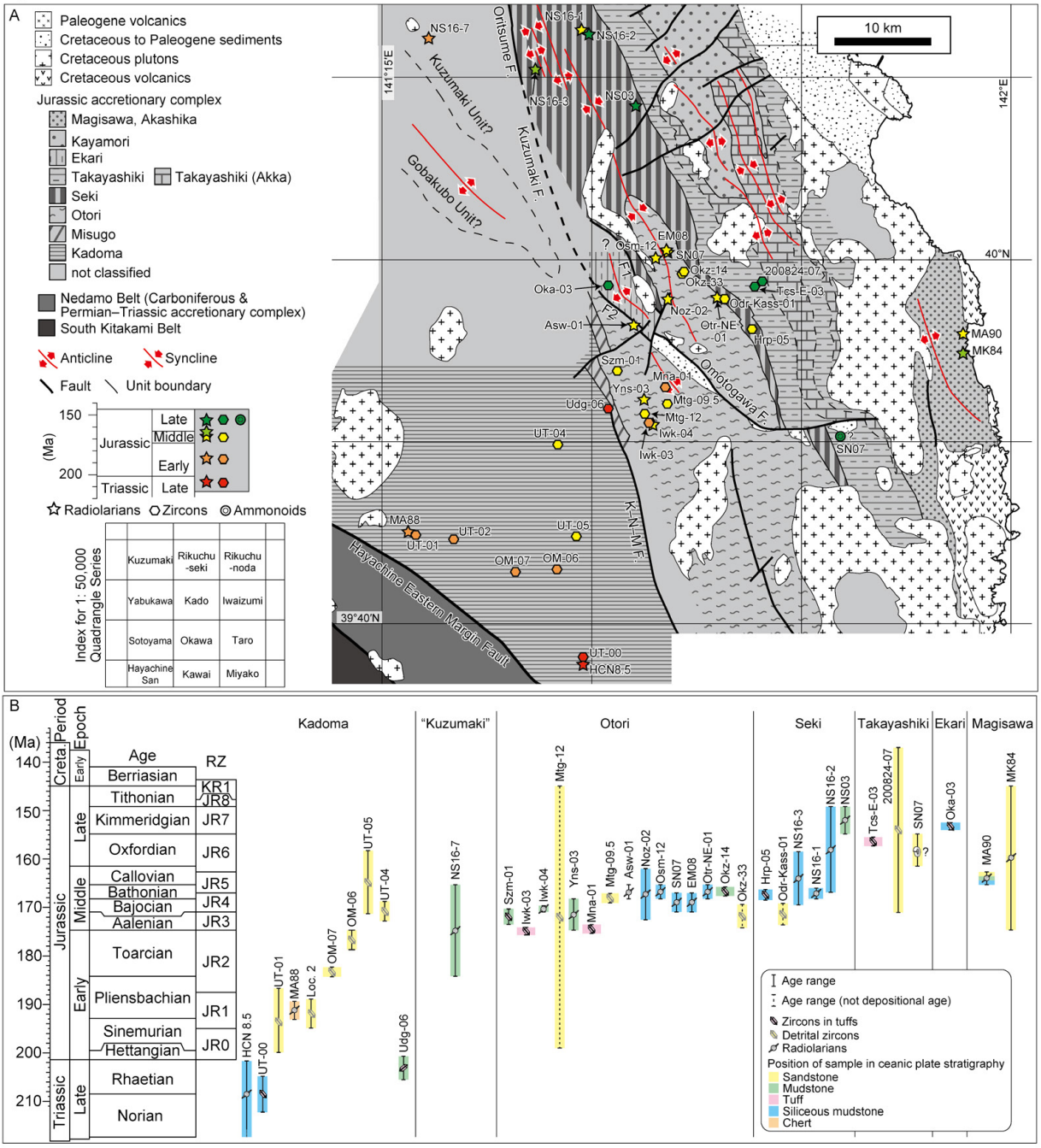

Fig. 21 (A) Constraints on the accretionary age of the North Kitakami Belt plotted on a simplified geological map of the main part of the North Kitakami Belt. Vertical and horizontal lines show the border grid of the 1: 50,000 quadrangle maps. As a useful key horizon, the palaeo-seamount comprising the Akka Limestone and its basement mafic rocks is differentiated from the rest of the Takayashiki Unit and shown as "Takayashiki (Akka)". The Kuzumaki and Gobakubo units (based respectively on Nakae *et al.*, 2021 and Ehiro *et al.*, 2008) are not well studied and hence not officially classified here. The Misugo Unit is only recognized in the Kado District, but may extend further. K–N–M F.: Kamatsuta–Natsuya–Michimata Fault. (B) Data in figure A shown with uncertainties and position of sample in the oceanic plate stratigraphy against the international chronostratigraphy (2023 version; Cohen *et al.*, 2013; updated). HCN8.5: Fig. 8.5 of Kawamura *et al.* (2013); UT-00: Uchino *et al.* (2017) (Loc. 0 of Osaka *et al.*, 2023); UT-01, 02, 04: Uchino (2019) (Locs. 1, 2 and 4 respectively therein); UT-05: Uchino (2021) (Loc. 5 therein, Loc. 3 in Osaka *et al.*, 2023, close to but not the same as Loc. 3 of Uchino, 2019); MA88: Matsuoka (1988); MA90; Matsuoka and Oji (1990); EM08: Ehiro *et al.* (2008); MK84; Minoura and Tsushima (1984); NS16: Nakae (2016), following number indicates locality number therein; NS03: Nakae and Kamada (2003); OM-06, OM-07: Osaka *et al.* (2023); SN07: Suzuki *et al.* (2007b); Okz-33: Muto *et al.* (2023); Iwk-04, Yns-03, Asw-01: Muto *et al.* (2025). RZ: radiolarian biozone.

or Bathonian ages (Fig. 21B). A Mn-nodule sample from mudstone that has possibly experienced tectonic mixing (Asw-01) yielded late Bajocian radiolarians, and is regarded to indicate the age of either mudstone or siliceous mudstone (Muto *et al.*, 2025). The former case seems more favourable considering that the structural position of this locality is apparently close to samples Mna-01 and Mtg-09.5 that indicate trench-fill clastic deposition during the Bajocian. However, a decisive conclusion is suspended, partly because geological structures around the locality of sample Asw-01 is somewhat complex. Regardless, it is safe to conclude that the southwest part of the Otori Unit consists of an oceanic plate that moved into the hemipelagic zone in the late Toarcian to Aalenian and passed into the trench during the Aalenian to Bathonian.

Based on the above, the entire Otori Unit, despite its wide distribution, has a TAA within a short window between the Aalenian to Bathonian. There appears to be a slight younging trend of TAA within the Otori unit towards the structurally lower part (Fig. 21), implying that imbricate structures during accretion is preserved in the unit. Further data constraining the entire span of depositional age of hemipelagic to trench-fill sedimentary rocks in different parts of the Otori Unit are desired in order to confirm this trend.

The TAA of the Seki Unit was constrained from siliceous mudstone that has a range from the Bathonian to Kimmeridgian and mudstone of Kimmeridgian age (Nakae and Kamada, 2003; Nakae, 2016). The tuff sample Hrp-05 from siliceous mudstone is Bathonian, consistent with the above (Fig. 21). On the other hand, the YC1σ age of detrital zircons from sandstone is ~4 Myr older (Fig. 20). As in the case of sample Okz-33 of the Otori Unit, the YC1σ age of sandstone probably does not record its depositional age. In contrast, the youngest single zircon in the sandstone sample (161.5 ± 3.3 Ma) is younger than the age of the tuff sample and may be close to the depositional age of the sandstone (Fig. 20). In sum, the TAA of this unit has a range from the Bathonian to Kimmeridgian.

The Takayashiki Unit was estimated to have an Oxfordian TAA based on an ammonoid bearing float (Suzuki *et al.*, 2007a). New data in this study indicate that the tuff between the hemipelagic and trench-fill strata was deposited in the late Oxfordian and the sandstone around the early Kimmeridgian or younger, although uncertainties are large (Figs. 20, 21). While the new data do not contradict with the previous age by the ammonoid bearing float, the ammonoid occurrence needs to be treated with great caution. Firstly, the origin of the float is quite obscure. Not only is the sample a float, but the description of the collected site is not consistent between authors. Onuki (1956) wrote that the specimen was collected in a stream southeast of the Iwaizumi Electric Powerplant, which is to the west of the junction of the Soiri and Omoto rivers (p.139 therein), but Suzuki *et al.* (2007), incorporating personal communications, stated that the float was collected to the east of the said junction (p.166 therein). Secondly, detailed surveys of the Takayashiki Unit have never reported the occurrence of macrofossil-bearing sandstones (Sugimoto, 1974, 1980; Takahashi *et al.*, 2016; Nakae *et al.*, 2021). Due to the above, I consider that the present zircon data are the only robust age constraints for the TAA.

The TAA of the Ekari Unit is constrained by the tuff from siliceous mudstone that has a Kimmeridgian age. This unit must have arrived at the trench shortly following this time, around the end of the Jurassic. This age is much younger than the accretionary age of the Otori Unit that is distributed next to the Ekari Unit with fault contacts. In fact, it is even younger than known hemipelagic or clastic rocks of the Takayashiki Unit, which is the youngest accretionary complex in the study area. Because younger accretionary complexes are accreted tectonically below older ones, the present juxtaposition of Ekari Unit to the Otori Unit can be attributed to vertical displacement by the bounding faults (F1 and F2 in Fig. 21A), although deformation structures showing the sense of displacement have not been found. This is the first time that an accretionary complex correlative to the Takayashiki Unit or younger units has been identified west of the boundary between the Takayashiki and Seki units. The lithofacies of the Ekari Unit has shared characteristics with the Takayashiki Unit such as the wide distribution of mudstone with broken beds of sandstone. However, there are also distinct differences, such as the abundance of conglomerate and basaltic rocks that is only widely distributed in the Takayashiki Unit. Therefore, the two are treated as separate units in the present study.

5. 2. Trends of trench-arrival age in the North Kitakami Belt

From compilation of available data, it is confirmed that a large part of the North Kitakami Belt in the northern Kitakami Mountains is composed of accretionary units that generally become older towards the southwest in terms of TAA (Fig. 21A). The TAA of adjacent units appears to be separated by very short gaps or even overlapping. For example, the age of mudstone in the Seki and Takayashiki units overlaps around the Kimmeridgian and the age of siliceous mudstone in the Seki and Otori units overlap in the Bathonian (Fig. 21). In addition, the TAA of the Otori and Kadoma units probably overlaps around the Aalenian to Bathonian, even though the Misugo Unit lies between them. Accordingly, the boundary of tectonostratigraphic units cannot simply be explained as temporal gaps in the formation of accretionary prisms. Rather, the boundaries are related to sudden changes in the lithology of accretionary complexes and/or post-accretion juxtaposition of accretionary complexes with different lithologies.

The general structure of tectonostratigraphic units being stacked in the NE–SW direction is interrupted by structures of smaller scales, mostly due to kilometre-scale folds and faults (Fig. 21A). These include sets of synclines and anticlines in the Kado District and to its north, many of which have been previously recognized (e.g., Sugimoto, 1974). In addition, this study identified faults with vertical

displacements that caused the Ekari Unit to be uplifted from its original structurally lower position ("F1" and "F2" in Fig. 21A). The F1 fault was regarded as an extension of the Kuzumaki Tectonic Line/Fault (Sugimoto, 1974; Onuki, 1981), but this is not followed here because the nature of these faults are quite different. The F2 fault was shown by Onuki (1969) as the Kunizakaitoge Fault. Of the F1 and F2 faults, the latter with the larger displacement is tentatively regarded as an extension of the Oritsume Fault, which is an active fault, and the Kuzumaki Fault sensu Nakae (2018) and Nakae *et al.* (2021) (Fig. 21A). The Oritsume and Kuzumaki faults cut between the Seki Unit and the "Kuzumaki Unit" (see next paragraph for notes on this unit) and the Oritsume Fault is the segment that was reactivated in the late Neogene. If the assumption that the F2, Kuzumaki and Oritsume faults are connected is correct, this fault is a major geological structure cutting more than 30 km through the North Kitakami Belt. Faults with vertical displacements like the F1 and F2 faults have not received much attention in the past, but they may be important in understanding the geological structure of the North Kitakami Belt. New data of the eastern margin of the Kadoma Unit revealed a significant reversal in the trend of TAA in the unit (Fig. 21). This may be due to folds or faults similar to those explained above. In fact, the sampled locality is very close to the Kamatsuta–Natsuya–Michimata Fault, which cuts the eastern margin of the Kadoma Unit in the area (Fig. 21A). However, currently available information on geological structure is not sufficient to clarify why the TAA of the northeastern margin of the Kadoma Unit is so old.

The area to the east and northwest of the Kado District is poorly studied in terms of the tectonic history of accretionary complexes. Below is a brief summary of the current status. In the eastern area near the Pacific coast, the Magisawa and Akashika units can be recognized from lithostratigraphic formations established originally by Sugimoto (1974). Sugimoto originally defined another formation, the Koshimeguri Formation, above the Magisawa Formation, but the two were combined by Minoura and Tsushima (1984), which was followed by Ehiro *et al.* (2008). The Magisawa and Akashika units cannot yet confidently be correlated to accretionary units further inland and are maintained as distinct units herein. The Magisawa Unit yielded Middle Jurassic radiolarians from siliceous mudstone and alternating mudstone and sandstone (Matsuoka and Oji, 1990) and Middle or Late Jurassic radiolarians from mudstone intercalated in bedded sandstone (Minoura and Tsushima, 1984). This, along with the lithofacies of the Magisawa Unit which is characterized by coherent sequences of chert, siliceous mudstone, mudstone and sandstone, suggest that the unit may correspond to the Seki Unit. On the other hand, the structurally lower Akashika Unit contains limestone and greenstone, and therefore may correspond to the Takayashiki Unit. However, proof of this correlation awaits additional data from the Magisawa and Akashika units. In the area northwest of the Kado District, the Kuzumaki and Gobakubo formations were recognized before the acceptance of plate tectonics by researchers (Iwai *et al.*, 1964). These formations have been translated to tectonostratigraphic units of accretionary complexes (Ehiro *et al.*, 2008; Nakae *et al.*, 2021), but the poor description of the original definition makes it very difficult to correlate these units with more well-established accretionary units. The "Kuzumaki Unit" may be equivalent to the Otori Unit, based on TAA and structural position (Fig. 21). In the absence of clear definitions, these two units are not formally distinguished in the present compilation.

Data on TAA have been obtained in the southeastern part of the North Kitakami Belt outside the area of compilation in the present study (Yoshihara *et al.*, 2002; Suzuki and Ogane, 2004; Suzuki *et al.*, 2007a). Correlation of this area with the compilation in the present study is difficult, due to apparent discontinuity in the geological structure and lack of data in the area that lies between. Hence, the southwest part of the North Kitakami Belt will not be dealt with in this study.

6. Detrital zircon age as an indicator for trench-arrival age

Detrital zircon analysis of sandstone is often used as a means to constrain the age of fossil-barren strata, in concrete, coarse clastic rocks and metamorphosed rocks (e.g., Shimura *et al.* 2017; Uchino, 2019). In the Jurassic, Cretaceous and early Paleogene accretionary complexes of Southwest Japan in the Kii Peninsula and Shikoku, youngest clusters of detrital zircons of sandstone are generally in accordance with ages based on radiolarians and tuffs (Shimura *et al.*, 2019; Tokiwa *et al.*, 2019, 2021; Hara *et al.*, 2017, 2020). In these cases, the age of the youngest cluster of detrital zircons are likely to be close to the depositional age of the sandstone. In the case of the accretionary units around the Kado District, most sandstone samples did not yield depositional ages or had large uncertainties due to the small number of grains in the youngest cluster. In particular, parts of the Seki and Otori units formed in the Bajocian to Bathonian yielded YC1σ ages of ~170 Ma, in three out of four cases (Fig. 21B). This suggests the dominance of ~170 Ma detrital zircons and the scarcity of younger zircons in the subduction zone of the North Kitakami Belt during the Bajocian to Bathonian. In the present study, the only detrital zircon age regarded to be close to the depositional age is that of sample Mtg-09.5 of the Otori unit. This sample is outstanding in that the youngest cluster consists of ~25 % of all grains, whereas the percentage is generally less than 10 % in the North Kitakami Belt (Uchino, 2019, 2021; Muto *et al.*, 2023, Osaka *et al.*, 2023; this study).

It is noteworthy that the number of grains measured for each sample in this study (~60) is smaller than that in previous studies which at least partly obtained detrital zircon ages compatible with radiolarian-based depositional ages (Shimura *et al.*, 2019; Tokiwa *et al.*, 2019, 2021; Hara *et al.*, 2020). In theory, 60 grains would

suffice to detect a population that constitutes 5 % of the entire population by 95 % (Dodson *et al.*, 1988). Based on the same theoretical calculation (e.g., Johnstone *et al.*, 2019; updated), in order to obtain at least three grains by a probability of 95 %, which would generally give a YC1σ age with small enough errors for meaningful discussion, the youngest population needs to be more than 10 % of the entire population. The necessary number of grains to detect one or any given number of the youngest population depends on the relative abundance of the youngest population. Therefore, there can be no universal criteria for the number of grains to analyze to obtain depositional ages (Sharman and Malkowski, 2020). In reality, even in active trenches, where zircons with ages close to the sedimentary age are relatively abundant, the proportion of zircons within 10 Myr of the depositional age can be less than 1 % (Clift *et al.*, 2013). This will require analysis of 630 grains in order to capture 3 grains from the youngest population (Johnstone *et al.* 2019; updated). On the other hand, analysis of 60 grains have yielded YC1σ ages compatible with microfossil age in some ancient sediments (e.g., Hara *et al.*, 2017). In the case of the Middle Jurassic units of the North Kitakami Belt, the situation is closer to the former case.

7. Summary

Tuffs and sandstones from the Kado District of the 1: 50,000 Quadrangle Series were analyzed for U–Pb dating in order to better understand the division and accretionary history of the North Kitakami Belt. The new data provide constraints for the trench-arrival age (TAA) of the Jurassic accretionary complex in the Kado District. Based on compilation of new data and previous data, the following points were clarified.

(1) The main tectonostratigraphic units and their TAA in the northern Kitakami Mountains are in structurally ascending order, the Kayamori Unit of undetermined age, the Oxfordian to Kimmeridgian Takayashiki Unit, the Bathonian to Kimmeridgean Seki Unit, the Aalenian to Bathonian Otori Unit, the Misugo Unit of undetermined age and the Rhaetian to Middle or early Late Jurassic Kadoma Unit.

(2) In addition to the above, the Kimmeridgian Ekari Unit, equivalent to the Takayashiki Unit or a structurally lower unit, was recognized.

(3) These units are distributed with a general younging polarity to the northeast, but the polarity is interrupted by folds and faults with vertical displacements. Some folds and faults that contribute to these interruptions are probably not yet recognized.

(4) Accretionary complexes in the east, northwest and southeast part of the northern Kitakami Mountains remain poorly correlated.

(5) Zircons in tuffs in hemipelagic and trench-fill sediments are useful material in constraining TAA, while detrital zircons in sandstone are generally less reliable, particularly in the Middle Jurassic of the North Kitakami Belt.

Acknowledgements: The authors thank Hideki Iwano and Tohru Danhara of Kyoto Fission-Track Co. Ltd. for extraction and analysis of detrital zircons. The author is grateful to the members of the Geological Sample Preparation Group of the Geoinformation Service Center, GSJ for preparing thin sections for this study. Sincere gratitude is offered to Yusuke Shimura and Tadashi Maruyama who provided fruitful comments that benefited the manuscript.

References

Clift, P. D., Carter, A., Nicholson, U. and Masago, H. (2013) Zircon and apatite thermochronology of the Nankai Trough accretionary prism and trench, Japan: Sediment transport in an active and collisional margin setting. *Tectonics*, **32**, 377–395. doi: 10.1002/tect.20033.

Cohen, K.M., Finney, S.C., Gibbard, P.L. and Fan, J.-X. (2013; updated) The ICS International Chronostratigraphic Chart. *Episodes*, **36**, 199–204.

Dickinson, W. R. and Gehrels, G. E. (2009) Use of U–Pb ages of detrital zircons to infer maximum depositional ages of strata: A test against a Colorado Plateau Mesozoic database. *Earth and Planetary Science Letters*, **288**, 115–125. doi: 10.1016/j.epsl.2009.09.013.

Dodson, M. H., Compston, W., Williams, I. S. and Wilson, J. F. (1988) A search for ancient detrital zircons in Zimbabwean sediments. *Journal of the Geological Society, London*, **145**, 977–983. doi: 10.1144/gsjgs.145.6.0977.

Ehiro, M., Kawamura, M. and Kawamura, T. (2005) 1.1 Summary and Tectonostratigraphic divisions. *In* The Publishing Committee of the Geology of Japan, ed., *The Geology of Japan*. *The Supplement*. Kyoritsu Pub. Co. Ltd., Tokyo. 49–50. (in Japanese)

Ehiro, M., Yamakita, S., Takahashi, S. and Suzuki, N. (2008) Jurassic accretionary complexes of the North Kitakami Belt in the Akka-Kuji area. *The Journal of the Geological Society of Japan*, **114**, 121–139. (in Japanese)

Hara, H., Nakamura, Y., Hara, K., Kurihara, T., Mori, H., Iwano, H., Danhara, T., Sakata, S. and Hirata, T. (2017) Detrital zircon multi-chronology, provenance, and low-grade metamorphism of the Cretaceous Shimanto accretionary complex, eastern Shikoku, Southwest Japan: Tectonic evolution in response to igneous activity within a subduction zone. *Island Arc*, **26**, 1–24. doi: 10.1111/iar.12218.

Hara, H., Ueki, T. and Hara, K. (2020) *Geology of the Umaji District*. Quadrangle Series, 1:50,000, Geological Survey of Japan, AIST. (in Japanese with Engish abstract)

Hirata, T., Iizuka, T. and Orihashi, Y. (2005) Reduction of mercury background on ICP-mass spectrometry for in situ U–Pb age determinations of zircon samples. *Journal of Analytical Atomic Spectrometry*, **20**, 696–701. doi: 10.1039/b504153h.

Iizuka, T. and Hirata, T. (2004) Simultaneous determinations of U-Pb age and REE abundances for zircons using ArF excimer laser ablation-ICPMS. *Geochemical Journal,* **38**, 229–241. doi: 10.2343/geochemj.38.229.

Isozaki, Y., Maruyama, S., Aoki, K., Nakama, T., Miyashita, A. and Otoh, S. (2010) Geotectonic subdivision of the Japanese Islands revisited: categorization and definition of elements and boundaries of Pacific-type (Miyashiro-type) orogen. *Chigaku Zasshi (Jounal of Geography)*, **119**, 999–1053. doi: 10.5026/jgeography.119.235. (in Japanese with English abstract)

Iwai, J., Murata, M., Hase, H. and Omura, K. (1964) Paleozoic strata of the northern Kitakami Mountains around Kuzumaki. *Journal of the Geological Society of Japan*, **70**, 382–383. (in Japanese, title translated)

Iwano, H., Orihashi, Y., Hirata, T., Ogasawara, M., Danhara, T., Horie, K., Hasebe, N., Sueoka, S., Tamura, A., Hayasaka, Y., Katsube, A., Ito, H., Tani, K., Kimura, J. I., Chang, Q., Kouchi, Y., Haruta, Y. and Yamamoto, K. (2013) An inter-laboratory evaluation of OD-3 zircon for use as a secondary U-Pb dating standard. *Island Arc*, **22**, 382–394. doi: 10.1111/iar.12038.

Johnstone, S. A., Schwartz, T. M. and Holm-Denoma, C. S. (2019; updated) A stratigraphic approach to inferring depositional ages from detrital geochronology data. *Frontiers in Earth Science*, **7**, 1–19. doi: 10.3389/feart.2019.00057.

Kawamura, T., Uchino, T., Kawamura, M., Yoshida, K., Nakagawa, M. and Nagata, H. (2013) *Geology of the Hayachinesan District.* Quadrangle Series, 1:50,000, Geological Survey of Japan, AIST. (in Japanese with English abstract)

Kojima, S., Hayasaka, Y., Hiroi, Y., Matsuoka, A., Sano, H., Sugamori, Y., Suzuki, N., Takemura, S., Tsujimori, T. and Uchino, T. (2016) 2b Pre-Cretaceous accretionary complexes. *In* Moreno, T., Wallis, S., Kojima, T. and Gibbons, W. eds., *The Geology of Japan*. Geological Society of London, London, 61–100.

Matsuoka, A. (1988) Discovery of Early Jurassic radiolarians from the North Kitakami Belt (s. s.), northeast Japan. *Earth Science (Chikyu Kagaku)*, **42**, 104–106. (in Japanese)

Matsuoka, A. and Oji, T. (1990) Middle Jurassic radiolarian fossils from the Magisawa Formation in the Taro Belt, North Kitakami Mountains. *The Journal of the Geological Society of Japan*, **96**, 239–241. (in Japanese)

Matsuoka, A., Yamakita, S., Sakakibara, M. and Hisada, K. (1998) Unit division for the Chichibu Composite Belt from a view point of accretionary tectonics and geology of western Shikoku, Japan. *The Journal of the Geological Society of Japan*, **104**, 634–653. (in Japanese with English abstract)

Minoura, K. and Tsushima, M. (1984) Geology of the Omoto district in the eastern margin of the North Kitakami Massif. *Science reports of the Hirosaki University*, **31**, 93–107. (in Japanese with English abstract)

Murai, T., Okami, K. and Oishi, M. (1985) *Geology of the Pre-Cretaceous in Iwaizumi Town. Part 1*. The Education Board of the Iwaizumi Town, Iwaizumi. (*in Japanese, reference information translated by Suzuki et al., 2007*)

Murai, T., Okami, K., Ehiro, M. and Oishi, M. (1986) *Geology of the Pre-Cretaceous in Iwaizumi Town. Part 2*. The Education Board of the Iwaizumi Town, Iwaizumi. (*in Japanese, reference information translated by Suzuki et al., 2007*)

Muto, S., Ito, T. and Murayama, M. (2023) Geology and accretionary age of the Otori Unit, North Kitakami Belt. *Bulletin of the Geological Survey of Japan*, **74**, 1–40.

Muto, S., Ito, T. and Ozeki, M. (2025) Middle Jurassic radiolarians from manganese nodules from the western part of the Kado District, northern Kitakami Mountains. *Bulletin of the Geological Survey of Japan*, **76**, 29–48.

Nakae, S. (2000) Regional correlation of the Jurassic accretionary complex in the Inner Zone of Southwest Japan. *The Memoirs of the Geological Society of Japan*, **55**, 73–98. (in Japanese with English abstract)

Nakae, S. (2016) Jurassic radiolarians from the Ichinohe–Kunohe area (Iwate Prefecture) in the North Kitakami Belt, Japan. *Bulletin of the Geological Survey of Japan*, **67**, 81–100. doi: 10.9795/bullgsj.67.81.

Nakae, S. (2018) *Geology of the Ichinohe Disrict*, 3, Jurassic of the North Kitakami Belt. Quadrangle Series, 1:50,000, Geological Survey of Japan, AIST, 102–119. (in Japanese)

Nakae, S. and Kamada, K. (2003) Late Jurassic radiolarians from the Rikuchu-Seki district in the North Kitakami Belt, Northeast Japan. *The Journal of the Geological Society of Japan*, **109**, 722–725. (in Japanese with English abstract)

Nakae, S., Kamada, K., Kubo, K. and Kudo, T. (2021) *Geology of the Rikuchu Seki District*. Quadrangle Series, 1:50,000, Geological Survey of Japan, AIST. (in Japanese with English abstract)

Onuki, Y. (1956) Geology of the Kitakami Mountains. *In* IwatePrefecture ed., *Explanatory Notes on the Geology of Iwate Prefecture. Part 2*. Iwate Prefecture, Morioka, 1–189. (in Japanese)

Onuki, Y. (1969) Geology of the Kitakami Massif, Northeast Japan. *Contributions from the Institute of Geology and Paleontology, Tohoku University*, **69**, 1–239. (in Japanese with English abstract)

Onuki, Y. (1981) Part 1. The Kitakami Mountains (in Japanese). *In* Hase Chishitsu Chosa Jimusho ed., *Explanation of the Geological Map of the Kitakami River Area, Kitakami Mountains, at the Scale of 1: 20,000*. Hase Chishitsu Chosa Jimusho, Sendai, 3–223.

Osaka, M., Aoki, S., Uchino, T. and Fukuyama, M. (2023) Constraint on the spatial distribution of the Early and Middle Jurassic units within the Nakatsugawa Complex of the North Kitakami Belt by detrital zircon U – Pb dating. *Bulletin of the Geological Survey of Japan*, **74**, 155–166.

Sharman, G. R. and Malkowski, M. A. (2020) Needles in a haystack: Detrital zircon U–Pb ages and the maximum depositional age of modern global sediment. *Earth-Science Reviews*, **203**, 103109. doi: 10.1016/j.earscirev.2020.103109.

Shimura, Y., Tokiwa, T., Takeuchi, M. and Yamamoto, K. (2017) Geology and detrital zircon U-Pb age of the Cretaceous Mugitani Formation in the Shimanto Belt, central Kii Peninsula, Southwest Japan. *The Journal of the Geological Society of Japan*, **123**, 925–937. doi: 10.5575/geosoc.2017.0032.

Shimura, Y., Tokiwa, T., Takeuchi, M., Mori, H. and Yamamoto, K. (2019) Lithological, structural, and chronological relationships between the Sanbagawa Metamorphic Complex and the Cretaceous Shimanto Accretionary Complex on the central Kii Peninsula, SW Japan. *Island Arc*, **28**, 1–19. doi: 10.1111/iar.12325.

Sláma, J., Košler, J., Condon, D. J., Crowley, J. L., Gerdes, A., Hanchar, J. M., Horstwood, M. S. A., Morris, G. A., Nasdala, L., Norberg, N., Schaltegger, U., Schoene, B., Tubrett, M. N. and Whitehouse, M. J. (2008) Plešovice zircon - A new natural reference material for U-Pb and Hf isotopic microanalysis. *Chemical Geology*, **249**, 1–35. doi: 10.1016/j.chemgeo.2007.11.005.

Sugimoto, M. (1980) Geological structure of the Akka-Iwaizumi District, Northern Kitakami Massif, Northeast Japan (Preliminary report). *In Report on the Multidiscipline Research Project A with 1979 Foundation of Grant-in-Aid for Scientific Research by the Education Ministry of Japan*. Tokyo Print Insatsu, Ltd., Tokyo, 37–44. (in Japanese)

Sugimoto, M. (1974) Stratigraphical study in the outer belt of the Kitakami Miassif, Northeast Japan. *Contributions from the Institute of Geology and Paleontology, Tohoku University*, **74**, 1–48. (in Japanese with English abstract)

Suzuki, N. and Ogane, K. (2004) Paleoceanographic affinities of radiolarian faunas in late Aalenian time (Middle Jurassic) recorded in the Jurassic accretionary complex of Japan. J*ournal of Asian Earth Sciences*, **23**, 343–357. doi: 10.1016/S1367-9120(03)00113-5.

Suzuki, N., Ehiro, M., Yoshihara, K., Kimura, Y., Kawashima, G., Yoshimoto, H. and Nogi, T. (2007a) Geology of the Kuzumaki-Kamaishi Subbelt of the North Kitakami Belt (a Jurassic accretionary complex), Northeast Japan: Case study of the Kawai-Yamada area, eastern Iwate Prefecture. *Bulletin of the Tohoku University Museum*, **6**, 103–174.

Suzuki, N., Yamakita, S., Takahashi, S. and Ehiro, M. (2007b) Middle Jurassic radiolarians from carbonate manganese nodules in the Otori Formation in the eastern part of the Kuzumaki-Kamaishi Subbelt, the North Kitakami Belt, Northeast Japan. *The Journal of the Geological Society of Japan*, **113**, 274–277. doi: 10.5575/geosoc.113.274. (in Japanese with English abstract)

Takahashi, S., Ehiro, M., Suzuki, N. and Yamakita, S. (2016) Subdivisional scheme of the North Kitakami Belt, Northeast Japan and its tectonostratigraphic correlation to the Oshima and South Chichibu belts: an examination of the Jurassic accretionary complex in the west Akka area. *Journal of the Geological Society of Japan*, **122**, 1–22. doi: 10.5575/geosoc.2015.0034. (in Japanese with English abstract)

Tokiwa, T., Shimura, Y., Takeuchi, M., Shimosato, S., Yamamoto, K. and Mori, H. (2019) Provenance of trench-fill deposits of the Jurassic Chichibu accretionary complex, Southwest Japan. *Journal of Asian Earth Sciences*, **184**, 103970. doi: 10.1016/j.jseaes.2019.103970.

Tokiwa, T., Shimura, Y., Takeuchi, M. and Mori, H. (2021) Use of detrital zircon U–Pb ages to assess the timing of deposition of Cretaceous trench-fill deposits in the active continental arc along the East Asian margin. *Journal of Asian Earth Sciences*, **207**. doi: 10.1016/j.jseaes.2020.104657.

Uchino, T. (2017) Late Triassic U-Pb-zircon age from tuffaceous mudstone in the Kadoma Complex, North Kitakami Belt, Northeast Japan. *The Journal of the Geological Society of Japan*, **123**, 977–982. doi: 10.5575/geosoc.2017.0024. (in Japanese with English abstract)

Uchino, T. (2019) Detrital zircon U–Pb ages of sandstone within the Jurassic accretionary complex in the North Kitakami Belt of the Sotoyama District, Iwate Prefecture. *Bulletin of the Geological Survey of Japan*, **70**, 357–372. (in Japanese with English abstract)

Uchino, T. (2021) Middle Jurassic zircon age from sandstone within the accretionary complex in the North Kitakami Belt, Kamatsuda area in Iwaizumi Town, Iwate Prefecture, Northeast Japan: Verifying the age of the accretionary complex containing the Okawa Sample. *Bulletin of the Geological Survey of Japan*, **72**, 99–107. (in Japanese with English abstract)

Uchino, T. and Suzuki, N. (2020) Late Jurassic radiolarians from mudstone near the U–Pb-dated sandstone of the North Kitakami Belt in the northeastern Shimokita Peninsula, Tohoku, Japan. *Bulletin of the Geological Survey of Japan*, **71**, 313–330. doi: 10.9795/bullgsj.71.313.

Ueda, H., Kimura, S., Saito, T., Takano, Y., Iizuka, N. and

Orihashi, Y. (2018) Material recycling in a sediment-starved trench recorded in the Early Cretaceous Shiriya accretionary complex, Northeast Japan. *Island Arc*, **27**, 1–20. doi: 10.1111/iar.12272.

Wiedenbeck, M., Alle, P., Corfu, F. y, Griffin, W. L., Meier, M., Oberli, F. v, Quadt, A. von, Roddick, J. C. and Spiegel, W. (1995) Three natural zircon standards for U-Th-Pb, Lu-Hf, trace element and REE analyses. *Geostandards newsletter*, **19**, 1–23.

Yamaguchi, Y. (1981) Geological structure of the eastern part of the North Kitakami Mountains, Japan—with special reference to structural subdivision. *Contributions from the Institute of Geology and Paleontology, Tohoku University*, **83**, 1–19. (in Japanese with English abstract)

Yoshihara, K., Suzuki, N. and Ehiro, M. (2002) Middle Jurassic radiolarian-bearing manganese nodules from the Kuzumaki-Kamaishi Belt in the Northern Kitakami Massif and its significance (in Japanese with English abstract). *Journal of the Geological Society of Japan*, **108**, 536–539.

Recieved February 13, 2024
Accepted November 29, 2024

北部北上帯ジュラ紀付加体の付加年代：「門」地域からの新たなジルコン地質年代学データ

武藤　俊

要　旨

東北日本北部北上帯ジュラ紀付加体では，白亜紀深成岩類の変成作用に起因して放散虫の報告が少なく，付加体の形成時期の検討にはジルコン年代学が用いられてきている．本研究では，5 万分の 1 地質図幅「門」地域のジュラ紀付加体中の砂岩中の砕屑性ジルコンと凝灰岩中の火成ジルコンの U–Pb 年代を報告する．先行研究と合わせて，北上山地北部に分布する主なジュラ紀付加体の構造層序ユニットとその砕屑岩の年代は下記の通りである：レーティアン期から中期ジュラ紀または後期ジュラ紀前期の門馬ユニット，付加年代未詳の三巣子ユニット，アーレニアン期からバトニアン期の大鳥ユニット，バトニアン期からキンメリッジアン期の関ユニット，オックスフォーディアン期からキンメリッジアン期の高屋敷ユニット，付加年代未詳の茅森ユニット，キンメリッジアン期直後の江刈ユニット．これらのうち前者の 6 ユニットはこの順に構造的に累重している．江刈ユニットの厳密な構造的位置は確かではないが，年代からは高屋敷ユニットまたはより下位に対比され，垂直変位を持つ断層によってより古いユニットの間に再配置したと判断される．このような断層やキロメートルオーダーの褶曲構造によって，北部北上帯の付加体に見られる大局的な海洋側への若化極性は乱されている．

難読･重要地名

Akka：安家，Chinzawa Stream：沈沢，Ekari：江刈，Kayamori：茅森，Misugo：三巣子，Kadoma：門馬，Minai River：見内川，Mitakai：三田貝，Okanai Stream：岡内沢，Omotogawa：小本川，Orikabe Stream：オリカベ沢，Otori：大鳥

Appendix

Table A1 Zircon U–Pb isotopic data for sample Udg-06 obtained by quadrupole inductively coupled plasma mass spectrometry.

No.	Isotopic ratios						U-Pb age (Ma)				U (ppm)	Th (ppm)
	$^{207}Pb/^{206}Pb$	Error 2σ	$^{206}Pb/^{238}U$	Error 2σ	$^{207}Pb/^{235}U$	Error 2σ	$^{206}Pb/^{238}U$	Error 2σ	$^{207}Pb/^{235}U$	Error 2σ		
1	0.0472	0.0040	0.0325	0.0014	0.2112	0.0197	205.9	± 9.3	194.6	± 19.8	136	80
2	0.0511	0.0052	0.0320	0.0017	0.2257	0.0250	203.3	± 11.2	206.6	± 25.1	89	15
3	0.0534	0.0029	0.0326	0.0010	0.2406	0.0150	207.0	± 6.4	218.9	± 15.1	316	202
4	0.0517	0.0036	0.0317	0.0012	0.2265	0.0172	201.3	± 7.6	207.3	± 17.3	205	95
5	0.0462	0.0021	0.0321	0.0008	0.2043	0.0106	203.4	± 5.0	188.7	± 10.7	586	429
6	0.0524	0.0028	0.0321	0.0010	0.2320	0.0142	203.8	± 6.2	211.9	± 14.3	339	208
7	0.0501	0.0030	0.0325	0.0011	0.2247	0.0150	206.2	± 6.8	205.8	± 15.2	278	167
8	0.0508	0.0023	0.0319	0.0008	0.2233	0.0118	202.4	± 5.2	204.7	± 11.9	517	353
9	0.0493	0.0027	0.0315	0.0009	0.2144	0.0134	200.2	± 6.0	197.3	± 13.5	344	228
10	0.0512	0.0034	0.0317	0.0011	0.2236	0.0166	201.0	± 7.3	204.9	± 16.7	220	131
11	0.0500	0.0025	0.0318	0.0009	0.2192	0.0124	201.8	± 5.5	201.3	± 12.5	440	275
12	0.0537	0.0042	0.0313	0.0013	0.2321	0.0201	198.8	± 8.6	211.9	± 20.2	150	57
13	0.0499	0.0038	0.0316	0.0013	0.2173	0.0181	200.3	± 8.1	199.6	± 18.2	172	65
14	0.0487	0.0026	0.0308	0.0009	0.2067	0.0125	195.3	± 5.6	190.8	± 12.6	384	258
15	0.0490	0.0028	0.0315	0.0010	0.2128	0.0135	199.9	± 6.1	195.9	± 13.7	330	149
16	0.0490	0.0033	0.0324	0.0012	0.2187	0.0164	205.3	± 7.5	200.8	± 16.5	217	119
17	0.0495	0.0037	0.0320	0.0013	0.2182	0.0181	202.9	± 8.2	200.4	± 18.2	174	69
18	0.0504	0.0034	0.0313	0.0011	0.2178	0.0162	198.7	± 7.2	200.0	± 16.3	222	111
19	0.0500	0.0034	0.0316	0.0011	0.2184	0.0164	200.8	± 7.3	200.6	± 16.5	218	124
20	0.0505	0.0039	0.0331	0.0014	0.2310	0.0198	210.2	± 9.0	211.0	± 19.9	153	80
21	0.0499	0.0024	0.0316	0.0008	0.2175	0.0120	200.6	± 5.3	199.8	± 12.1	471	307
22	0.0477	0.0039	0.0316	0.0013	0.2082	0.0184	200.7	± 8.5	192.0	± 18.5	155	63
23	0.0469	0.0035	0.0324	0.0013	0.2099	0.0173	205.8	± 8.1	193.5	± 17.4	181	90
24	0.0521	0.0038	0.0319	0.0013	0.2290	0.0186	202.3	± 8.2	209.4	± 18.7	174	86
25	0.0512	0.0034	0.0302	0.0010	0.2136	0.0154	191.9	± 6.7	196.6	± 15.6	242	110
26	0.0496	0.0030	0.0323	0.0010	0.2209	0.0147	204.7	± 6.7	202.6	± 14.9	285	161
27	0.0514	0.0023	0.0328	0.0008	0.2328	0.0122	208.2	± 5.4	212.5	± 12.3	511	364
28	0.0525	0.0029	0.0313	0.0009	0.2267	0.0139	198.6	± 6.0	207.5	± 14.0	343	131
29	0.0487	0.0033	0.0327	0.0012	0.2194	0.0165	207.3	± 7.6	201.4	± 16.6	216	134
30	0.0513	0.0017	0.0322	0.0006	0.2281	0.0092	204.5	± 4.0	208.6	± 9.3	1234	972

Standards are the same as in Table A8

Table A2 Zircon U–Pb isotopic data for sample Okz-14 obtained by quadrupole inductively coupled plasma mass spectrometry.

No.	Isotopic ratios						U-Pb age (Ma)				U (ppm)	Th (ppm)
	$^{207}Pb/^{206}Pb$	Error 2σ	$^{207}Pb/^{235}U$	Error 2σ	$^{206}Pb/^{238}U$	Error 2σ	$^{206}Pb/^{238}U$	Error 2σ	$^{207}Pb/^{235}U$	Error 2σ		
1	0.0499	0.0025	0.1790	0.0107	0.0260	0.0008	165.4 ±	5.1	167.2 ±	10.8	504	207
2	0.0488	0.0021	0.1784	0.0095	0.0265	0.0007	168.5 ±	4.8	166.7 ±	9.6	735	314
3	0.0488	0.0021	0.1768	0.0094	0.0262	0.0007	166.9 ±	4.8	165.3 ±	9.5	749	635
4	0.0486	0.0022	0.1766	0.0097	0.0263	0.0008	167.6 ±	4.9	165.1 ±	9.8	652	276
5	0.0494	0.0020	0.1785	0.0092	0.0262	0.0007	166.6 ±	4.7	166.8 ±	9.3	839	692
6	0.0473	0.0024	0.1743	0.0107	0.0267	0.0008	170.1 ±	5.4	163.1 ±	10.8	467	388
7	0.0525	0.0030	0.1916	0.0128	0.0264	0.0009	168.3 ±	5.8	178.0 ±	12.9	341	346
8	0.0471	0.0023	0.1744	0.0104	0.0268	0.0008	170.6 ±	5.3	163.2 ±	10.5	516	293
9	0.0499	0.0018	0.1793	0.0087	0.0261	0.0007	165.8 ±	4.5	167.5 ±	8.8	1059	306
10	0.0477	0.0019	0.1725	0.0087	0.0262	0.0007	166.7 ±	4.6	161.6 ±	8.8	917	603
11	0.0489	0.0017	0.1777	0.0082	0.0263	0.0007	167.5 ±	4.4	166.1 ±	8.3	1317	729
12	0.0503	0.0026	0.1812	0.0112	0.0261	0.0008	166.1 ±	5.3	169.1 ±	11.3	446	213
13	0.0494	0.0027	0.1751	0.0111	0.0257	0.0008	163.4 ±	5.3	163.9 ±	11.2	427	336
14	0.0485	0.0019	0.1731	0.0086	0.0259	0.0007	164.7 ±	4.5	162.1 ±	8.7	976	576
15	0.0483	0.0019	0.1731	0.0088	0.0260	0.0007	165.4 ±	4.6	162.1 ±	8.9	903	476
16	0.0478	0.0016	0.1751	0.0084	0.0265	0.0009	168.7 ±	5.7	163.8 ±	8.5	962	447
17	0.0489	0.0018	0.1762	0.0089	0.0261	0.0009	166.0 ±	5.7	164.8 ±	9.0	789	660
18	0.0506	0.0024	0.1843	0.0110	0.0264	0.0010	168.1 ±	6.3	171.7 ±	11.1	447	397
19	0.0506	0.0030	0.1819	0.0128	0.0260	0.0011	165.7 ±	6.8	169.7 ±	12.9	285	240
20	0.0496	0.0015	0.1803	0.0081	0.0264	0.0009	167.8 ±	5.6	168.3 ±	8.2	1241	730
21	0.0489	0.0015	0.1764	0.0081	0.0261	0.0009	166.2 ±	5.5	165.0 ±	8.2	1155	910
22	0.0488	0.0014	0.1746	0.0076	0.0259	0.0008	165.0 ±	5.4	163.4 ±	7.7	1547	1300
23	0.0510	0.0027	0.1868	0.0121	0.0265	0.0010	168.9 ±	6.6	173.9 ±	12.2	351	347
24	0.0485	0.0018	0.1757	0.0087	0.0262	0.0009	166.9 ±	5.7	164.4 ±	8.8	862	267
25	0.0501	0.0017	0.1817	0.0086	0.0263	0.0009	167.3 ±	5.7	169.6 ±	8.7	981	394
26	0.0517	0.0028	0.1890	0.0124	0.0265	0.0010	168.6 ±	6.7	175.7 ±	12.6	330	161
27	0.0501	0.0024	0.1834	0.0108	0.0266	0.0010	168.9 ±	6.3	171.0 ±	10.9	468	371
28	0.0522	0.0024	0.1876	0.0107	0.0260	0.0009	165.7 ±	6.1	174.5 ±	10.8	502	238
29	0.0512	0.0020	0.1823	0.0096	0.0258	0.0009	164.3 ±	5.8	170.0 ±	9.7	676	560
30	0.0485	0.0014	0.1703	0.0075	0.0255	0.0008	162.1 ±	5.3	159.7 ±	7.6	1441	827
Standards												
91500epo 4-1	0.0762	0.0032	1.9001	0.1263	0.1808	0.0091	1071.3 ±	58.3	1081.1 ±	120.8	78	26
91500epo 4-2	0.0754	0.0031	1.9344	0.1258	0.1860	0.0091	1099.6 ±	58.6	1093.1 ±	120.3	82	31
91500epo 4-3	0.0748	0.0031	1.9631	0.1297	0.1901	0.0095	1121.9 ±	61.1	1102.9 ±	123.8	78	38
91500epo 4-4	0.0734	0.0030	1.8238	0.1175	0.1802	0.0087	1068.1 ±	55.7	1054.0 ±	112.8	86	31
91500epo 4-5	0.0708	0.0029	1.7801	0.1152	0.1823	0.0088	1079.5 ±	56.3	1038.2 ±	110.7	86	33
GJ1 4-1	0.0596	0.0020	0.7859	0.0367	0.0956	0.0027	588.6 ±	17.6	588.8 ±	36.6	391	24
GJ1 4-2	0.0601	0.0019	0.8070	0.0371	0.0973	0.0028	598.6 ±	17.7	600.8 ±	37.0	411	28
GJ1 4-3	0.0608	0.0019	0.8188	0.0375	0.0976	0.0028	600.3 ±	17.7	607.4 ±	37.4	415	25
GJ1 4-4	0.0600	0.0019	0.7888	0.0364	0.0953	0.0027	587.0 ±	17.3	590.5 ±	36.3	413	21
GJ1 4-5	0.0593	0.0019	0.7988	0.0371	0.0976	0.0028	600.4 ±	17.9	596.2 ±	37.0	396	27
OD-3 4-1	0.0487	0.0041	0.0346	0.0030	0.0052	0.0002	33.1 ±	1.0	34.6 ±	3.1	799	1123
OD-3 4-2	0.0447	0.0037	0.0315	0.0027	0.0051	0.0002	32.9 ±	1.0	31.5 ±	2.7	920	1294
OD-3 4-3	0.0487	0.0038	0.0346	0.0028	0.0051	0.0002	33.1 ±	1.0	34.5 ±	2.9	947	1349
OD-3 4-4	0.0454	0.0041	0.0324	0.0030	0.0052	0.0002	33.2 ±	1.1	32.4 ±	3.0	749	804
OD-3 4-5	0.0430	0.0037	0.0308	0.0027	0.0052	0.0002	33.3 ±	1.0	30.8 ±	2.8	872	1093

Table A3 Zircon U–Pb isotopic data for sample Mna-01 obtained by quadrupole inductively coupled plasma mass spectrometry.

No.	Isotopic ratios						U-Pb age (Ma)				U (ppm)	Th (ppm)
	$^{207}Pb/^{206}Pb$	Error 2σ	$^{207}Pb/^{235}U$	Error 2σ	$^{206}Pb/^{238}U$	Error 2σ	$^{206}Pb/^{238}U$	Error 2σ	$^{207}Pb/^{235}U$	Error 2σ		
1	0.0456	0.0028	0.1807	0.0120	0.0288	0.0009	182.7 ±	5.5	168.7 ±	12.1	186	66
2	0.0496	0.0025	0.1929	0.0105	0.0282	0.0007	179.3 ±	4.5	179.1 ±	10.6	305	204
3	0.0476	0.0021	0.1950	0.0095	0.0297	0.0007	188.6 ±	4.3	180.9 ±	9.6	427	263
4	0.0487	0.0019	0.1840	0.0079	0.0274	0.0005	174.3 ±	3.5	171.5 ±	8.0	712	213
5	0.0491	0.0023	0.1825	0.0095	0.0269	0.0006	171.4 ±	4.1	170.2 ±	9.6	365	191
6	0.0476	0.0024	0.1827	0.0100	0.0278	0.0007	176.9 ±	4.5	170.4 ±	10.1	310	234
7	0.0490	0.0015	0.1722	0.0061	0.0255	0.0004	162.1 ±	2.7	161.3 ±	6.2	2202	1220
8	0.0496	0.0027	0.1854	0.0110	0.0271	0.0007	172.3 ±	4.7	172.7 ±	11.1	245	184
9	0.0484	0.0032	0.1886	0.0135	0.0282	0.0009	179.5 ±	5.9	175.4 ±	13.6	148	87
10	0.0488	0.0027	0.1856	0.0112	0.0276	0.0008	175.3 ±	4.9	172.8 ±	11.3	233	144
11	0.0497	0.0019	0.1888	0.0081	0.0276	0.0005	175.2 ±	3.5	175.6 ±	8.2	704	224
12	0.0483	0.0019	0.1808	0.0079	0.0271	0.0005	172.6 ±	3.5	168.7 ±	8.0	687	347
13	0.0508	0.0026	0.1892	0.0104	0.0270	0.0007	171.6 ±	4.4	175.9 ±	10.5	297	131
14	0.0499	0.0029	0.1897	0.0118	0.0276	0.0008	175.3 ±	5.0	176.4 ±	11.9	212	137
15	0.0486	0.0020	0.1805	0.0082	0.0269	0.0006	171.2 ±	3.6	168.5 ±	8.3	594	342
16	0.0495	0.0021	0.1851	0.0091	0.0271	0.0006	172.5 ±	3.9	172.5 ±	9.2	454	240
17	0.1136	0.0029	4.8587	0.1820	0.3101	0.0074	1741.4 ±	47.6	1795.1 ±	169.8	280	73
18	0.0510	0.0023	0.1919	0.0098	0.0273	0.0006	173.5 ±	4.1	178.3 ±	9.9	395	233
19	0.1127	0.0029	5.1118	0.1953	0.3286	0.0082	1831.7 ±	52.6	1838.1 ±	181.1	245	202
20	0.0528	0.0027	0.1959	0.0110	0.0269	0.0007	170.9 ±	4.5	181.7 ±	11.2	285	138
21	0.0480	0.0020	0.1810	0.0088	0.0274	0.0006	174.0 ±	3.9	168.9 ±	8.9	493	222
22	0.0482	0.0022	0.1789	0.0093	0.0269	0.0006	171.0 ±	4.1	167.1 ±	9.4	392	239
23	0.0476	0.0031	0.1768	0.0126	0.0270	0.0009	171.4 ±	5.5	165.3 ±	12.7	168	91
24	0.0502	0.0028	0.1876	0.0115	0.0271	0.0008	172.2 ±	4.9	174.6 ±	11.6	233	154
25	0.0499	0.0017	0.1866	0.0077	0.0271	0.0005	172.4 ±	3.3	173.7 ±	7.8	924	588
26	0.0471	0.0021	0.1795	0.0091	0.0276	0.0006	175.4 ±	4.1	167.6 ±	9.2	426	188
27	0.0476	0.0026	0.1760	0.0106	0.0268	0.0007	170.3 ±	4.6	164.6 ±	10.7	259	103
28	0.0495	0.0025	0.1849	0.0106	0.0271	0.0007	172.2 ±	4.5	172.3 ±	10.7	286	140
29	0.0498	0.0015	0.1895	0.0070	0.0276	0.0005	175.4 ±	3.0	176.2 ±	7.1	1656	665
30	0.0506	0.0026	0.1887	0.0107	0.0270	0.0007	172.0 ±	4.5	175.5 ±	10.8	293	200
Standards												
91500 tef 1-1	0.0758	0.0032	1.9032	0.0853	0.1819	0.0073	1077.3 ±	47.2	1082.2 ±	83.2	102	30
91500 tef 1-2	0.0728	0.0030	1.7870	0.0792	0.1780	0.0071	1055.9 ±	45.4	1040.7 ±	77.4	108	36
91500 tef 1-3	0.0766	0.0031	1.9128	0.0825	0.1811	0.0071	1072.9 ±	45.5	1085.6 ±	80.5	114	38
91500 tef 1-4	0.0751	0.0031	1.8754	0.0821	0.1809	0.0072	1072.0 ±	45.9	1072.4 ±	80.1	110	37
91500 tef 1-5	0.0766	0.0031	1.9165	0.0820	0.1814	0.0071	1074.7 ±	45.3	1086.8 ±	80.0	116	34
91500 tef 1-6	0.0759	0.0025	1.8875	0.0921	0.1802	0.0061	1067.8 ±	39.3	1076.7 ±	89.4	109	34
91500 tef 1-7	0.0738	0.0025	1.8124	0.0887	0.1780	0.0060	1056.3 ±	38.8	1049.9 ±	86.3	109	35
GJ1 1-1	0.0604	0.0024	0.8149	0.0278	0.0978	0.0030	601.6 ±	19.4	605.2 ±	27.9	374	20
GJ1 1-2	0.0607	0.0023	0.8258	0.0276	0.0986	0.0030	606.3 ±	19.3	611.3 ±	27.7	406	24
GJ1 1-3	0.0602	0.0023	0.8130	0.0270	0.0979	0.0030	602.0 ±	19.1	604.1 ±	27.1	420	23
GJ1 1-4	0.0613	0.0024	0.8303	0.0275	0.0982	0.0030	603.9 ±	19.1	613.8 ±	27.5	422	24
GJ1 1-5	0.0610	0.0024	0.8083	0.0270	0.0960	0.0029	591.1 ±	18.8	601.5 ±	27.1	410	22
GJ1 1-6	0.0593	0.0018	0.7893	0.0310	0.0965	0.0021	594.1 ±	13.5	590.8 ±	31.0	410	23
GJ1 1-7	0.0596	0.0018	0.7950	0.0314	0.0967	0.0021	595.2 ±	13.7	594.0 ±	31.4	393	24
OD3 1-1	0.0488	0.0044	0.0346	0.0030	0.0051	0.0002	33.1 ±	1.2	34.6 ±	3.0	431	506

Table A3 Continued.

No.	Isotopic ratios						U-Pb age (Ma)				U (ppm)	Th (ppm)
	$^{207}Pb/^{206}Pb$	Error 2σ	$^{207}Pb/^{235}U$	Error 2σ	$^{206}Pb/^{238}U$	Error 2σ	$^{206}Pb/^{238}U$	Error 2σ	$^{207}Pb/^{235}U$	Error 2σ		
OD3 1-2	0.0466	0.0037	0.0336	0.0025	0.0052	0.0002	33.6 ±	1.1	33.5 ±	2.5	610	819
OD3 1-3	0.0442	0.0035	0.0320	0.0024	0.0052	0.0002	33.8 ±	1.1	32.0 ±	2.4	621	762
OD3 1-4	0.0440	0.0035	0.0318	0.0024	0.0052	0.0002	33.7 ±	1.1	31.8 ±	2.4	650	719
OD3 1-5	0.0515	0.0039	0.0370	0.0026	0.0052	0.0002	33.5 ±	1.1	36.9 ±	2.6	631	825

Table A4 Zircon U–Pb isotopic data for sample Iwk-03 obtained by quadrupole inductively coupled plasma mass spectrometry.

No.	Isotopic ratios						U-Pb age (Ma)				U (ppm)	Th (ppm)
	$^{207}Pb/^{206}Pb$	Error 2σ	$^{207}Pb/^{235}U$	Error 2σ	$^{206}Pb/^{238}U$	Error 2σ	$^{206}Pb/^{238}U$	Error 2σ	$^{207}Pb/^{235}U$	Error 2σ		
1	0.0490	0.0017	0.1893	0.0072	0.0280	0.0005	177.9 ±	3.2	176.0 ±	7.3	481	160
2	0.0491	0.0019	0.1869	0.0080	0.0276	0.0005	175.5 ±	3.5	174.0 ±	8.1	353	199
3	0.0485	0.0014	0.1869	0.0059	0.0279	0.0004	177.5 ±	2.6	173.9 ±	6.0	888	304
4	0.0521	0.0023	0.1948	0.0101	0.0271	0.0008	172.3 ±	5.0	180.7 ±	10.2	273	208
5	0.0514	0.0015	0.1932	0.0074	0.0273	0.0006	173.4 ±	4.2	179.4 ±	7.5	763	379
6	0.0496	0.0021	0.1905	0.0095	0.0278	0.0008	176.9 ±	5.0	177.0 ±	9.6	313	268
7	0.0505	0.0017	0.2445	0.0103	0.0351	0.0009	222.5 ±	5.8	222.1 ±	10.4	438	369
8	0.0490	0.0021	0.1823	0.0090	0.0269	0.0007	171.4 ±	4.8	170.1 ±	9.1	331	284
9	0.0479	0.0026	0.1801	0.0110	0.0272	0.0009	173.3 ±	5.5	168.1 ±	11.1	193	125
10	0.0505	0.0012	0.1918	0.0065	0.0275	0.0006	175.2 ±	4.0	178.2 ±	6.6	1321	1385
11	0.0493	0.0023	0.1879	0.0101	0.0276	0.0008	175.6 ±	5.2	174.8 ±	10.2	259	224
12	0.0511	0.0018	0.1935	0.0083	0.0274	0.0007	174.3 ±	4.5	179.6 ±	8.4	490	450
13	0.0503	0.0020	0.1902	0.0091	0.0274	0.0007	174.5 ±	4.8	176.8 ±	9.2	351	326
14	0.0502	0.0016	0.1897	0.0076	0.0274	0.0007	174.2 ±	4.3	176.3 ±	7.7	646	234
15	0.0515	0.0017	0.1952	0.0081	0.0275	0.0007	174.6 ±	4.4	181.1 ±	8.2	558	382
16	0.0506	0.0016	0.1920	0.0076	0.0275	0.0007	174.9 ±	4.3	178.3 ±	7.7	650	572
17	0.0498	0.0023	0.1864	0.0099	0.0271	0.0008	172.6 ±	5.0	173.6 ±	10.0	268	183
18	0.0515	0.0020	0.1917	0.0091	0.0270	0.0007	171.5 ±	4.7	178.1 ±	9.2	361	377
19	0.0498	0.0019	0.1899	0.0078	0.0276	0.0007	175.7 ±	4.4	176.5 ±	7.9	344	266
20	0.0511	0.0016	0.1942	0.0066	0.0275	0.0006	175.0 ±	4.0	180.2 ±	6.7	526	563
21	0.0505	0.0017	0.2408	0.0089	0.0346	0.0008	219.1 ±	5.4	219.1 ±	9.0	357	183
22	0.0509	0.0017	0.1924	0.0070	0.0274	0.0006	174.1 ±	4.1	178.6 ±	7.1	450	258
23	0.0501	0.0016	0.1859	0.0065	0.0269	0.0006	171.0 ±	4.0	173.1 ±	6.6	512	427
24	0.0485	0.0024	0.1839	0.0098	0.0275	0.0008	174.7 ±	5.1	171.4 ±	9.9	199	139
25	0.0503	0.0012	0.1893	0.0052	0.0273	0.0006	173.5 ±	3.7	176.0 ±	5.3	932	293
26	0.0483	0.0023	0.1891	0.0095	0.0284	0.0008	180.5 ±	5.1	175.8 ±	9.6	221	206
27	0.0496	0.0022	0.1902	0.0091	0.0278	0.0008	176.8 ±	4.9	176.8 ±	9.2	243	139
28	0.0510	0.0026	0.1904	0.0102	0.0271	0.0008	172.1 ±	5.1	177.0 ±	10.3	188	126
29	0.0499	0.0014	0.1903	0.0058	0.0276	0.0006	175.7 ±	3.8	176.8 ±	5.9	710	287
30	0.0494	0.0011	0.1871	0.0049	0.0274	0.0006	174.4 ±	3.6	174.1 ±	4.9	1112	622
Standards												
91500 1-1	0.0760	0.0021	1.9221	0.0777	0.1832	0.0056	1084.6 ±	35.78	1088.8 ±	76.01	96	38
91500 1-2	0.0759	0.0021	1.8588	0.0749	0.1774	0.0053	1052.8 ±	34.36	1066.6 ±	73.38	98	40
91500 1-3	0.0748	0.0021	1.8806	0.0771	0.1823	0.0056	1079.5 ±	36.08	1074.3 ±	75.44	94	38
91500 1-4	0.0749	0.0021	1.8907	0.0786	0.1829	0.0057	1083.0 ±	36.80	1077.8 ±	76.79	90	36
91500 1-5	0.0750	0.0021	1.8259	0.0760	0.1765	0.0055	1048.0 ±	35.43	1054.8 ±	74.39	91	36
91500 2-1	0.0759	0.0021	1.8773	0.0817	0.1794	0.0068	1063.6 ±	43.94	1073.1 ±	79.78	72	28
GJ 1-1	0.0632	0.0014	0.8602	0.0249	0.0987	0.0017	606.9 ±	11.13	630.2 ±	25.01	405	25
GJ 1-2	0.0627	0.0015	0.8524	0.0255	0.0985	0.0018	605.5 ±	11.53	626.0 ±	25.53	362	23
GJ 1-3	0.0622	0.0014	0.8325	0.0243	0.0970	0.0017	596.8 ±	10.97	615.0 ±	24.38	401	25
GJ 1-4	0.0628	0.0015	0.8461	0.0248	0.0976	0.0017	600.3 ±	11.14	622.5 ±	24.88	391	24
GJ 1-5	0.0618	0.0014	0.8375	0.0248	0.0983	0.0018	604.2 ±	11.34	617.8 ±	24.88	378	24
GJ 2-1	0.0616	0.0012	0.8347	0.0216	0.0982	0.0023	603.9 ±	14.73	616.2 ±	21.73	382	24
GJ 2-2	0.0615	0.0012	0.8259	0.0215	0.0973	0.0023	598.6 ±	14.63	611.3 ±	21.64	377	24

Table A5 Zircon U–Pb isotopic data for sample Szm-01 obtained by quadrupole inductively coupled plasma mass spectrometry. Shadowed data indicate discordant age data.

No.	Isotopic ratios						U-Pb age (Ma)				U (ppm)	Th (ppm)
	$^{207}Pb/^{206}Pb$	Error 2σ	$^{206}Pb/^{238}U$	Error 2σ	$^{207}Pb/^{235}U$	Error 2σ	$^{206}Pb/^{238}U$	Error 2σ	$^{207}Pb/^{235}U$	Error 2σ		
1	0.0484	0.0036	0.0275	0.0015	0.1835	0.0147	174.7	± 9.6	171.1	± 14.8	255	247
2	0.0499	0.0035	0.0272	0.0014	0.1874	0.0143	173.0	± 9.3	174.4	± 14.4	291	664
3	0.0497	0.0039	0.0257	0.0014	0.1766	0.0150	163.9	± 9.2	165.1	± 15.1	224	182
4	0.0476	0.0033	0.0275	0.0014	0.1809	0.0136	175.0	± 9.3	168.8	± 13.7	308	363
5	0.0503	0.0039	0.0280	0.0016	0.1943	0.0164	178.1	± 10.1	180.3	± 16.6	210	155
6	0.0481	0.0037	0.0266	0.0015	0.1768	0.0145	169.4	± 9.4	165.3	± 14.7	244	250
7	0.0492	0.0044	0.0272	0.0016	0.1845	0.0176	172.9	± 10.4	171.9	± 17.7	161	119
8	0.0494	0.0039	0.0269	0.0015	0.1833	0.0156	170.9	± 9.7	170.9	± 15.7	215	215
9	0.0466	0.0035	0.0265	0.0014	0.1705	0.0137	168.8	± 9.2	159.9	± 13.8	272	251
10	0.0492	0.0038	0.0263	0.0014	0.1790	0.0147	167.7	± 9.3	167.2	± 14.8	244	209
11	0.0488	0.0035	0.0267	0.0014	0.1800	0.0141	170.1	± 9.2	168.1	± 14.2	279	211
12	0.0502	0.0034	0.0270	0.0014	0.1873	0.0137	172.0	± 9.1	174.3	± 13.8	329	385
13	0.0495	0.0036	0.0269	0.0015	0.1841	0.0145	171.3	± 9.3	171.6	± 14.6	266	229
14	0.0510	0.0040	0.0273	0.0015	0.1919	0.0162	173.3	± 9.8	178.3	± 16.3	213	182
15	0.0468	0.0035	0.0276	0.0015	0.1785	0.0144	175.6	± 9.6	166.7	± 14.5	259	163
16	0.0463	0.0036	0.0274	0.0015	0.1750	0.0145	174.1	± 9.7	163.7	± 14.6	241	155
17	0.0515	0.0036	0.0267	0.0013	0.1892	0.0148	169.6	± 8.4	176.0	± 14.9	308	130
18	0.0463	0.0033	0.0272	0.0013	0.1739	0.0141	173.2	± 8.6	162.8	± 14.2	296	338
19	0.0472	0.0028	0.0268	0.0012	0.1748	0.0119	170.7	± 7.7	163.6	± 12.0	555	681
20	0.0481	0.0034	0.0272	0.0013	0.1804	0.0144	172.8	± 8.5	168.4	± 14.5	303	320
21	0.0518	0.0035	0.0281	0.0014	0.2005	0.0155	178.4	± 8.8	185.5	± 15.6	304	297
22	0.0502	0.0037	0.0281	0.0014	0.1942	0.0162	178.4	± 9.1	180.2	± 16.3	248	154
23	0.0445	0.0040	0.0264	0.0014	0.1618	0.0158	167.7	± 9.2	152.3	± 16.0	181	128
24	0.0515	0.0034	0.0261	0.0013	0.1859	0.0141	166.4	± 8.1	173.1	± 14.2	344	274
25	0.0554	0.0045	0.0275	0.0015	0.2099	0.0189	174.6	± 9.6	193.4	± 19.0	183	102
26	0.0500	0.0037	0.0276	0.0014	0.1908	0.0160	175.7	± 9.0	177.3	± 16.1	245	517
27	0.0473	0.0027	0.0270	0.0012	0.1765	0.0116	171.9	± 7.7	165.1	± 11.7	629	581
28	0.0489	0.0037	0.0267	0.0013	0.1803	0.0152	169.9	± 8.7	168.3	± 15.3	253	172
29	0.0484	0.0035	0.0262	0.0013	0.1749	0.0140	166.5	± 8.2	163.6	± 14.2	301	294
30	0.0472	0.0041	0.0269	0.0015	0.1753	0.0169	171.4	± 9.5	164.0	± 17.0	176	146
Standards												
91500 1-1	0.0748	0.0043	0.1776	0.0099	1.8315	0.1734	1053.8	± 63.4	1056.8	± 162.3	98	41
91500 1-2	0.0763	0.0044	0.1817	0.0105	1.9107	0.1836	1076.0	± 67.1	1084.8	± 171.1	89	40
91500 1-3	0.0746	0.0042	0.1789	0.0098	1.8412	0.1726	1061.2	± 62.7	1060.3	± 161.7	104	43
91500 1-4	0.0748	0.0043	0.1794	0.0100	1.8507	0.1752	1063.6	± 64.1	1063.7	± 163.9	98	43
91500 1-5	0.0721	0.0041	0.1866	0.0104	1.8549	0.1756	1102.7	± 66.7	1065.2	± 164.3	97	46
91500 3-1	0.0745	0.0039	0.1719	0.0107	1.7669	0.1349	1022.4	± 68.5	1033.4	± 128.5	85	32
91500 3-2	0.0758	0.0040	0.1755	0.0109	1.8345	0.1389	1042.2	± 69.6	1057.9	± 132.0	86	31
91500 5-1	0.0773	0.0044	0.1847	0.0108	1.9708	0.1574	1092.4	± 69.3	1105.6	± 148.4	79	32
91500 5-2	0.0773	0.0043	0.1756	0.0098	1.8734	0.1450	1042.7	± 63.0	1071.7	± 137.5	90	31
91500 5-3	0.0736	0.0042	0.1779	0.0102	1.8057	0.1429	1055.5	± 65.4	1047.5	± 135.7	84	34
91500 5-4	0.0724	0.0041	0.1853	0.0107	1.8520	0.1471	1095.9	± 68.5	1064.1	± 139.3	82	31
91500 5-5	0.0766	0.0043	0.1849	0.0107	1.9538	0.1547	1093.5	± 68.5	1099.8	± 146.1	82	31
GJ1 1-1	0.0594	0.0031	0.0928	0.0036	0.7607	0.0636	572.2	± 23.2	574.4	± 62.6	401	29
GJ1 1-2	0.0609	0.0032	0.0952	0.0037	0.7996	0.0667	586.2	± 23.8	596.6	± 65.5	405	22
GJ1 1-3	0.0581	0.0031	0.0974	0.0038	0.7799	0.0653	598.9	± 24.4	585.4	± 64.2	393	25

Table A5 Continued.

No.	Isotopic ratios						U-Pb age (Ma)				U (ppm)	Th (ppm)
	$^{207}Pb/^{206}Pb$	Error 2σ	$^{206}Pb/^{238}U$	Error 2σ	$^{207}Pb/^{235}U$	Error 2σ	$^{206}Pb/^{238}U$	Error 2σ	$^{207}Pb/^{235}U$	Error 2σ		
GJ1 1-4	0.0606	0.0032	0.0981	0.0038	0.8199	0.0685	603.0	± 24.6	608.0	± 67.2	394	28
GJ1 1-5	0.0594	0.0031	0.0986	0.0038	0.8081	0.0674	606.4	± 24.6	601.4	± 66.2	404	28
Gj1 3-1	0.0586	0.0027	0.0950	0.0044	0.7679	0.0463	585.3	± 28.3	578.5	± 45.9	351	20
Gj1 3-2	0.0615	0.0029	0.0965	0.0045	0.8195	0.0491	594.1	± 28.7	607.8	± 48.7	352	17
GJ1 5-1	0.0613	0.0031	0.0954	0.0037	0.8073	0.0512	587.6	± 24.0	601.0	± 50.7	345	13
GJ1 5-2	0.0595	0.0030	0.0999	0.0039	0.8196	0.0520	613.8	± 25.2	607.8	± 51.5	339	11
GJ1 5-3	0.0604	0.0031	0.0976	0.0038	0.8133	0.0515	600.6	± 24.5	604.3	± 50.9	349	20
GJ1 5-4	0.0618	0.0031	0.0976	0.0038	0.8317	0.0521	600.2	± 24.3	614.6	± 51.6	369	20
GJ1 5-5	0.0608	0.0031	0.0957	0.0037	0.8029	0.0506	588.9	± 23.9	598.5	± 50.2	359	13
OD-3 1-1	0.0437	0.0050	0.0052	0.0002	0.0315	0.0041	33.6	± 1.5	31.5	± 4.1	574	745
OD-3 1-2	0.0472	0.0052	0.0052	0.0002	0.0339	0.0043	33.5	± 1.5	33.8	± 4.3	588	751
OD-3 1-3	0.0483	0.0060	0.0050	0.0002	0.0331	0.0045	31.9	± 1.5	33.0	± 4.6	460	572
OD-3 1-4	0.0406	0.0041	0.0051	0.0002	0.0287	0.0034	33.0	± 1.3	28.7	± 3.4	853	1138
OD-3 1-5	0.0442	0.0045	0.0050	0.0002	0.0304	0.0036	32.1	± 1.3	30.4	± 3.6	800	1096
OD-3 3-1	0.0440	0.0044	0.0050	0.0002	0.0305	0.0032	32.3	± 1.6	30.5	± 3.2	723	904
OD-3 3-2	0.0466	0.0044	0.0051	0.0002	0.0330	0.0033	33.0	± 1.6	32.9	± 3.3	771	943
OD-3 5-1	0.0491	0.0047	0.0051	0.0002	0.0343	0.0034	32.6	± 1.3	34.3	± 3.4	813	993
OD-3 5-2	0.0484	0.0047	0.0051	0.0002	0.0342	0.0034	32.9	± 1.3	34.1	± 3.5	786	995
OD-3 5-3	0.0511	0.0047	0.0052	0.0002	0.0366	0.0035	33.4	± 1.3	36.5	± 3.6	821	995
OD-3 5-4	0.0466	0.0045	0.0051	0.0002	0.0328	0.0033	32.8	± 1.3	32.8	± 3.3	829	1021
OD-3 5-5	0.0489	0.0046	0.0052	0.0002	0.0351	0.0034	33.5	± 1.3	35.1	± 3.5	839	1027

Table A6 Zircon U–Pb isotopic data for sample Mtg-01 obtained by quadrupole inductively coupled plasma mass spectrometry.

No.	Isotopic ratios						U-Pb age (Ma)				U (ppm)	Th (ppm)
	$^{207}Pb/^{206}Pb$	Error 2σ	$^{207}Pb/^{235}U$	Error 2σ	$^{206}Pb/^{238}U$	Error 2σ	$^{206}Pb/^{238}U$	Error 2σ	$^{207}Pb/^{235}U$	Error 2σ		
1	0.0520	0.0013	0.2959	0.0086	0.0412	0.0009	260.4 ±	5.9	263.2 ±	8.7	167	139
2	0.0542	0.0019	0.3379	0.0137	0.0452	0.0013	285.0 ±	8.2	295.6 ±	13.8	73	85
3	0.0513	0.0010	0.2876	0.0064	0.0406	0.0008	256.6 ±	5.1	256.6 ±	6.5	332	173
4	0.0539	0.0011	0.4351	0.0110	0.0585	0.0013	366.7 ±	8.2	366.8 ±	11.1	180	86
5	0.0520	0.0009	0.3365	0.0070	0.0469	0.0009	295.7 ±	5.9	294.6 ±	7.1	349	316
6	0.0511	0.0016	0.2945	0.0108	0.0418	0.0011	263.7 ±	6.9	262.1 ±	10.9	100	87
7	0.0518	0.0010	0.3535	0.0081	0.0494	0.0010	310.9 ±	6.4	307.3 ±	8.2	266	339
8	0.0514	0.0008	0.3052	0.0053	0.0430	0.0008	271.6 ±	5.0	270.4 ±	5.3	668	517
9	0.0554	0.0009	0.5420	0.0111	0.0709	0.0014	441.4 ±	9.1	439.7 ±	11.2	274	195
10	0.0517	0.0013	0.2943	0.0082	0.0413	0.0009	260.7 ±	5.8	261.9 ±	8.3	187	350
11	0.0517	0.0011	0.2898	0.0070	0.0407	0.0008	256.9 ±	5.3	258.4 ±	7.0	271	201
12	0.0512	0.0007	0.2864	0.0045	0.0406	0.0007	256.3 ±	4.6	255.7 ±	4.6	998	270
13	0.0526	0.0012	0.2982	0.0076	0.0411	0.0009	259.6 ±	5.5	265.0 ±	7.7	230	155
14	0.0531	0.0022	0.3193	0.0151	0.0436	0.0014	275.2 ±	8.8	281.3 ±	15.3	54	16
15	0.0516	0.0011	0.2877	0.0073	0.0404	0.0008	255.2 ±	5.4	256.7 ±	7.4	238	200
16	0.0712	0.0007	1.5346	0.0217	0.1563	0.0028	936.2 ±	18.1	944.4 ±	21.8	636	261
17	0.0571	0.0008	0.6211	0.0103	0.0788	0.0015	489.0 ±	9.4	490.6 ±	10.4	483	135
18	0.0534	0.0021	0.4250	0.0204	0.0577	0.0019	361.4 ±	12.4	359.6 ±	20.5	43	36
19	0.0528	0.0013	0.3029	0.0086	0.0416	0.0009	262.5 ±	5.9	268.6 ±	8.7	173	240
20	0.0542	0.0013	0.3087	0.0086	0.0413	0.0009	260.9 ±	5.9	273.2 ±	8.7	179	97
21	0.0542	0.0011	0.3450	0.0084	0.0461	0.0010	290.6 ±	6.2	301.0 ±	8.5	233	223
22	0.0534	0.0012	0.2964	0.0074	0.0402	0.0008	254.3 ±	5.4	263.6 ±	7.5	243	162
23	0.0572	0.0007	0.6063	0.0091	0.0768	0.0014	477.2 ±	8.8	481.2 ±	9.2	734	159
24	0.0526	0.0021	0.3402	0.0160	0.0469	0.0015	295.3 ±	9.5	297.4 ±	16.1	53	49
25	0.0525	0.0013	0.2888	0.0080	0.0398	0.0009	251.9 ±	5.6	257.7 ±	8.1	191	121
26	0.0541	0.0021	0.2982	0.0131	0.0399	0.0012	252.4 ±	7.5	265.0 ±	13.2	66	37
27	0.0519	0.0009	0.3135	0.0063	0.0438	0.0008	276.3 ±	5.4	276.9 ±	6.4	406	417
28	0.0508	0.0010	0.2828	0.0067	0.0403	0.0008	254.8 ±	5.2	252.9 ±	6.8	287	205
29	0.0514	0.0010	0.2945	0.0063	0.0415	0.0008	262.1 ±	5.2	262.1 ±	6.4	364	378
30	0.0514	0.0008	0.2819	0.0050	0.0398	0.0007	251.3 ±	4.6	252.1 ±	5.0	670	460
31	0.0534	0.0006	0.3887	0.0080	0.0528	0.0008	331.6 ±	5.3	333.4 ±	8.1	661	402
32	0.0518	0.0010	0.2872	0.0074	0.0402	0.0007	254.2 ±	4.6	256.4 ±	7.5	308	258
33	0.0865	0.0008	2.7042	0.0573	0.2265	0.0041	1316.3 ±	26.3	1329.6 ±	56.6	238	109
34	0.0515	0.0025	0.3001	0.0173	0.0422	0.0014	266.7 ±	9.2	266.5 ±	17.5	39	27
35	0.0580	0.0008	0.6320	0.0147	0.0789	0.0014	489.8 ±	9.0	497.3 ±	14.8	278	148
36	0.0518	0.0013	0.2921	0.0096	0.0409	0.0009	258.4 ±	5.5	260.2 ±	9.7	151	129
37	0.0513	0.0011	0.2957	0.0082	0.0418	0.0008	263.7 ±	5.0	263.0 ±	8.3	239	107
38	0.0515	0.0010	0.2916	0.0079	0.0411	0.0007	259.4 ±	4.8	259.9 ±	8.0	263	190
39	0.0538	0.0007	0.4823	0.0106	0.0650	0.0011	405.8 ±	7.0	399.6 ±	10.7	407	159
40	0.0565	0.0010	0.5696	0.0148	0.0731	0.0014	454.6 ±	9.0	457.7 ±	14.9	195	95
41	0.0504	0.0012	0.2907	0.0090	0.0418	0.0008	263.8 ±	5.4	259.1 ±	9.1	177	94
42	0.0513	0.0009	0.2951	0.0075	0.0417	0.0007	263.3 ±	4.7	262.6 ±	7.6	326	358
43	0.0521	0.0011	0.3484	0.0102	0.0485	0.0010	305.3 ±	6.2	303.5 ±	10.3	183	72
44	0.0510	0.0008	0.2825	0.0066	0.0402	0.0007	253.8 ±	4.2	252.7 ±	6.6	470	253
45	0.0513	0.0019	0.2858	0.0127	0.0404	0.0011	255.3 ±	6.9	255.3 ±	12.8	72	85
46	0.0701	0.0006	1.4559	0.0273	0.1505	0.0023	903.8 ±	15.0	912.3 ±	27.3	665	247
47	0.0515	0.0009	0.2902	0.0074	0.0409	0.0007	258.2 ±	4.6	258.7 ±	7.5	327	356

Table A6 Continued.

No.	Isotopic ratios						U-Pb age (Ma)				U (ppm)	Th (ppm)
	$^{207}Pb/^{206}Pb$	Error 2σ	$^{207}Pb/^{235}U$	Error 2σ	$^{206}Pb/^{238}U$	Error 2σ	$^{206}Pb/^{238}U$	Error 2σ	$^{207}Pb/^{235}U$	Error 2σ		
48	0.0526	0.0016	0.3026	0.0112	0.0417	0.0010	263.4	± 6.2	268.4	± 11.3	107	82
49	0.0521	0.0025	0.3307	0.0188	0.0460	0.0016	289.7	± 10.2	290.1	± 19.0	37	26
50	0.0514	0.0011	0.3043	0.0085	0.0429	0.0008	270.8	± 5.2	269.8	± 8.6	231	194
51	0.0514	0.0007	0.2871	0.0064	0.0405	0.0006	255.7	± 4.2	256.3	± 6.5	555	348
52	0.0526	0.0014	0.3131	0.0106	0.0432	0.0009	272.4	± 6.0	276.6	± 10.7	133	186
53	0.0523	0.0008	0.3580	0.0085	0.0496	0.0008	311.9	± 5.5	310.7	± 8.6	356	189
54	0.0507	0.0010	0.2874	0.0080	0.0411	0.0008	259.4	± 4.9	256.5	± 8.1	244	92
55	0.0529	0.0024	0.3060	0.0165	0.0419	0.0013	264.6	± 8.7	271.0	± 16.6	44	48
56	0.0512	0.0013	0.2855	0.0090	0.0404	0.0008	255.5	± 5.3	255.0	± 9.1	172	48
57	0.0523	0.0010	0.3014	0.0081	0.0417	0.0008	263.6	± 4.9	267.5	± 8.2	265	125
58	0.0503	0.0011	0.2966	0.0085	0.0427	0.0008	269.9	± 5.2	263.7	± 8.6	221	169
59	0.0565	0.0013	0.3206	0.0099	0.0411	0.0008	259.8	± 5.4	282.3	± 10.0	167	100
60	0.0613	0.0007	0.8939	0.0193	0.1057	0.0018	647.8	± 11.7	648.5	± 19.4	317	258
Standards												
91500epo 4-4	0.0745	0.0013	1.8405	0.0502	0.1790	0.00480	1061	± 31	1060	± 50	75	30
91500epo 4-5	0.0749	0.0013	1.8677	0.0509	0.1807	0.00485	1071	± 31	1070	± 50	75	31
91500epo 4-6	0.0746	0.0012	1.8807	0.0564	0.1827	0.00462	1082	± 30	1074	± 56	73	27
91500epo 4-7	0.0754	0.0011	1.8872	0.0559	0.1814	0.00453	1074	± 29	1077	± 55	76	26
OD3 4-4	0.0454	0.0016	0.0320	0.0012	0.0051	0.00010	32.8	± 0.6	32.0	± 1.2	722	984
OD3 4-5	0.0481	0.0017	0.0338	0.0012	0.0051	0.00010	32.8	± 0.6	33.8	± 1.2	705	963
OD3 4-6	0.0471	0.0016	0.0332	0.0013	0.0051	0.00009	32.9	± 0.6	33.2	± 1.3	709	945

Table A7 Zircon U–Pb isotopic data for sample Mtg-09.5 obtained by quadrupole inductively coupled plasma mass spectrometry.

No.	Isotopic ratios						U-Pb age (Ma)				U (ppm)	Th (ppm)
	$^{207}Pb/^{206}Pb$	Error 2σ	$^{207}Pb/^{235}U$	Error 2σ	$^{206}Pb/^{238}U$	Error 2σ	$^{206}Pb/^{238}U$	Error 2σ	$^{207}Pb/^{235}U$	Error 2σ		
1	0.0507	0.0019	0.1875	0.0075	0.0268	0.0006	170.6 ±	4.1	174.5 ±	7.6	276	199
2	0.0519	0.0011	0.2965	0.0073	0.0414	0.0008	261.6 ±	5.3	263.7 ±	7.4	618	349
3	0.0530	0.0026	0.2905	0.0157	0.0397	0.0013	251.0 ±	8.1	258.9 ±	15.8	99	92
4	0.1150	0.0016	5.4020	0.1368	0.3403	0.0088	1888.2 ±	56.5	1885.2 ±	130.2	151	128
5	0.0497	0.0018	0.1843	0.0071	0.0268	0.0006	170.8 ±	4.0	171.7 ±	7.2	300	243
6	0.0491	0.0028	0.1817	0.0109	0.0268	0.0008	170.7 ±	5.3	169.5 ±	11.0	118	87
7	0.0491	0.0019	0.2389	0.0099	0.0352	0.0009	223.3 ±	5.7	217.5 ±	10.0	208	115
8	0.0500	0.0016	0.1855	0.0063	0.0269	0.0006	170.9 ±	3.8	172.8 ±	6.4	402	375
9	0.0525	0.0030	0.3011	0.0189	0.0416	0.0015	262.7 ±	9.7	267.3 ±	19.1	70	48
10	0.0496	0.0018	0.2087	0.0083	0.0305	0.0007	193.8 ±	4.7	192.5 ±	8.4	252	222
11	0.0500	0.0016	0.1949	0.0066	0.0283	0.0006	179.7 ±	4.0	180.8 ±	6.7	388	162
12	0.0521	0.0012	0.3045	0.0083	0.0424	0.0009	267.6 ±	5.6	269.9 ±	8.3	472	244
13	0.0506	0.0021	0.1868	0.0085	0.0268	0.0007	170.3 ±	4.4	173.9 ±	8.6	208	103
14	0.0515	0.0015	0.2153	0.0070	0.0303	0.0007	192.3 ±	4.2	198.0 ±	7.1	396	165
15	0.0513	0.0027	0.2750	0.0160	0.0389	0.0013	245.9 ±	8.3	246.7 ±	16.1	88	40
16	0.0559	0.0017	0.5699	0.0209	0.0738	0.0020	459.3 ±	12.9	457.9 ±	21.0	143	63
17	0.0522	0.0024	0.2101	0.0104	0.0292	0.0008	185.3 ±	5.2	193.6 ±	10.5	157	219
18	0.0513	0.0012	0.2955	0.0079	0.0417	0.0009	263.5 ±	5.5	262.9 ±	8.0	494	369
19	0.0526	0.0023	0.2494	0.0120	0.0344	0.0010	217.9 ±	6.2	226.1 ±	12.1	143	93
20	0.0495	0.0014	0.1817	0.0057	0.0266	0.0006	169.2 ±	3.6	169.6 ±	5.8	499	421
21	0.0521	0.0012	0.2922	0.0070	0.0407	0.0009	257.0 ±	5.8	260.3 ±	7.1	924	283
22	0.0511	0.0015	0.1870	0.0057	0.0265	0.0006	168.8 ±	4.0	174.0 ±	5.8	588	411
23	0.0512	0.0021	0.2051	0.0088	0.0290	0.0008	184.5 ±	5.1	189.4 ±	8.9	230	122
24	0.0513	0.0026	0.2058	0.0108	0.0291	0.0009	184.7 ±	5.7	190.0 ±	10.9	145	50
25	0.0488	0.0019	0.1775	0.0072	0.0263	0.0007	167.6 ±	4.4	165.9 ±	7.3	294	167
26	0.0522	0.0027	0.2124	0.0114	0.0295	0.0009	187.4 ±	6.0	195.6 ±	11.5	134	57
27	0.0489	0.0022	0.1823	0.0083	0.0270	0.0007	171.9 ±	4.8	170.0 ±	8.4	218	110
28	0.1149	0.0020	5.3386	0.1033	0.3368	0.0074	1871.2 ±	47.6	1875.1 ±	99.8	769	53
29	0.0518	0.0019	0.2908	0.0114	0.0407	0.0011	257.0 ±	7.1	259.2 ±	11.5	217	104
30	0.0508	0.0014	0.1851	0.0053	0.0264	0.0006	168.0 ±	3.9	172.4 ±	5.4	721	135
31	0.0494	0.0017	0.1822	0.0065	0.0267	0.0007	170.2 ±	4.2	170.0 ±	6.6	403	190
32	0.0518	0.0011	0.2473	0.0053	0.0346	0.0007	219.1 ±	4.7	224.4 ±	5.3	1811	618
33	0.0508	0.0030	0.1838	0.0114	0.0262	0.0009	167.0 ±	5.7	171.3 ±	11.5	110	63
34	0.0486	0.0023	0.1795	0.0088	0.0268	0.0008	170.4 ±	5.0	167.6 ±	8.9	190	104
35	0.1500	0.0027	8.7685	0.1973	0.4238	0.0105	2277.5 ±	67.1	2314.2 ±	182.8	292	35
36	0.0505	0.0023	0.1871	0.0090	0.0268	0.0008	170.8 ±	5.0	174.2 ±	9.1	190	194
37	0.0492	0.0018	0.1824	0.0070	0.0269	0.0007	170.9 ±	4.4	170.1 ±	7.1	327	224
38	0.0509	0.0024	0.1895	0.0094	0.0270	0.0008	171.6 ±	5.1	176.2 ±	9.5	177	83
39	0.1574	0.0029	9.1239	0.2134	0.4202	0.0107	2261.3 ±	68.6	2350.5 ±	196.4	246	66
40	0.0496	0.0017	0.1836	0.0066	0.0268	0.0007	170.6 ±	4.3	171.2 ±	6.7	393	294
41	0.0497	0.0020	0.1842	0.0050	0.0268	0.0006	170.8 ±	4.1	171.7 ±	5.1	746	222
42	0.0483	0.0024	0.1771	0.0072	0.0266	0.0007	169.0 ±	4.6	165.6 ±	7.3	290	178
43	0.0519	0.0021	0.2837	0.0084	0.0396	0.0010	250.3 ±	6.4	253.6 ±	8.5	428	134
44	0.0491	0.0030	0.2408	0.0138	0.0356	0.0012	225.3 ±	7.9	219.1 ±	14.0	105	83
45	0.0498	0.0026	0.2865	0.0136	0.0417	0.0013	263.3 ±	8.4	255.8 ±	13.7	138	114
46	0.0510	0.0019	0.1911	0.0044	0.0272	0.0006	172.8 ±	4.0	177.5 ±	4.4	1241	407
47	0.0479	0.0025	0.1789	0.0079	0.0270	0.0008	172.0 ±	4.9	167.1 ±	8.0	239	170

Table A7 Continued.

No.	Isotopic ratios						U-Pb age (Ma)				U (ppm)	Th (ppm)
	$^{207}Pb/^{206}Pb$	Error 2σ	$^{207}Pb/^{235}U$	Error 2σ	$^{206}Pb/^{238}U$	Error 2σ	$^{206}Pb/^{238}U$	Error 2σ	$^{207}Pb/^{235}U$	Error 2σ		
48	0.0515	0.0023	0.1869	0.0066	0.0263	0.0007	167.3	± 4.3	174.0	± 6.6	391	379
49	0.0499	0.0022	0.1876	0.0066	0.0273	0.0007	173.4	± 4.5	174.6	± 6.7	387	149
50	0.0513	0.0022	0.1887	0.0063	0.0267	0.0007	169.7	± 4.3	175.5	± 6.4	440	322
51	0.0512	0.0020	0.2498	0.0063	0.0354	0.0008	224.0	± 5.3	226.4	± 6.3	745	371
52	0.0487	0.0027	0.1786	0.0087	0.0266	0.0008	169.1	± 5.1	166.8	± 8.8	193	204
53	0.0501	0.0024	0.1811	0.0091	0.0262	0.0007	166.6	± 4.6	169.0	± 9.2	181	112
54	0.0500	0.0016	0.1822	0.0063	0.0264	0.0006	168.0	± 3.7	170.0	± 6.4	460	413
55	0.1145	0.0022	5.1158	0.1505	0.3238	0.0089	1808.3	± 56.9	1838.7	± 142.3	135	201
56	0.0497	0.0022	0.1812	0.0086	0.0264	0.0007	168.0	± 4.4	169.1	± 8.7	211	124
57	0.0500	0.0015	0.1932	0.0064	0.0280	0.0006	178.1	± 3.9	179.4	± 6.4	506	201
58	0.0490	0.0017	0.1793	0.0065	0.0265	0.0006	168.8	± 3.8	167.4	± 6.6	411	143
59	0.0511	0.0018	0.1835	0.0070	0.0260	0.0006	165.6	± 3.8	171.1	± 7.0	360	298
60	0.0505	0.0023	0.1866	0.0090	0.0268	0.0007	170.3	± 4.6	173.7	± 9.1	197	184
61	0.0510	0.0016	0.1873	0.0062	0.0266	0.0006	169.2	± 3.7	174.3	± 6.3	515	311
62	0.0485	0.0016	0.1766	0.0061	0.0264	0.0006	168.0	± 3.7	165.2	± 6.1	484	442
Standards												
91500epo 1-6	0.0746	0.0031	1.8124	0.0736	0.1760	0.0066	1044.8	± 42.5	1049.9	± 72.1	66	23
91500epo 1-7	0.0749	0.0030	1.8774	0.0741	0.1816	0.0067	1075.5	± 43.0	1073.1	± 72.6	70	27
91500epo 2-1	0.0762	0.0022	1.8779	0.0792	0.1787	0.0064	1059.8	± 41.0	1073.3	± 77.3	64	24
91500epo 2-2	0.0751	0.0022	1.8137	0.0752	0.1751	0.0061	1040.3	± 39.3	1050.4	± 73.6	67	24
OD3 1-6	0.0485	0.0023	0.0342	0.0012	0.0051	0.0001	32.8	± 0.8	34.1	± 1.3	1732	2059
OD3 1-7	0.0473	0.0022	0.0331	0.0011	0.0051	0.0001	32.5	± 0.8	33.0	± 1.1	2057	2502
OD3 1-8	0.0460	0.0034	0.0332	0.0022	0.0052	0.0001	33.6	± 1.0	33.1	± 2.2	472	500
OD3 2-1	0.0480	0.0018	0.0331	0.0013	0.0050	0.0001	32.1	± 0.6	33.0	± 1.3	1638	1936

Table A8 Zircon U–Pb isotopic data for sample Mtg-12 obtained by quadrupole inductively coupled plasma mass spectrometry.

No.	Isotopic ratios						U-Pb age (Ma)				U (ppm)	Th (ppm)
	$^{207}Pb/^{206}Pb$	Error 2σ	$^{207}Pb/^{235}U$	Error 2σ	$^{206}Pb/^{238}U$	Error 2σ	$^{206}Pb/^{238}U$	Error 2σ	$^{207}Pb/^{235}U$	Error 2σ		
1	0.0513	0.0022	0.2174	0.0109	0.0307	0.0008	195.2 ±	5.2	199.8 ±	11.0	283	125
2	0.0546	0.0024	0.3292	0.0176	0.0437	0.0013	275.5 ±	8.4	289.0 ±	17.7	164	76
3	0.0519	0.0020	0.2881	0.0138	0.0403	0.0011	254.4 ±	6.8	257.0 ±	13.9	263	91
4	0.0509	0.0017	0.2110	0.0087	0.0300	0.0007	190.8 ±	4.4	194.4 ±	8.8	616	297
5	0.0503	0.0022	0.2111	0.0110	0.0304	0.0008	193.3 ±	5.3	194.5 ±	11.1	257	207
6	0.1155	0.0029	5.3023	0.2300	0.3327	0.0111	1851.5 ±	71.0	1869.2 ±	210.2	98	100
7	0.0531	0.0017	0.3110	0.0129	0.0425	0.0010	268.1 ±	6.4	275.0 ±	13.0	445	293
8	0.0539	0.0031	0.2326	0.0151	0.0313	0.0010	198.6 ±	6.7	212.3 ±	15.2	127	84
9	0.0498	0.0016	0.2046	0.0084	0.0298	0.0007	189.2 ±	4.3	189.0 ±	8.5	659	329
10	0.0509	0.0024	0.2085	0.0114	0.0297	0.0008	188.8 ±	5.4	192.3 ±	11.6	220	147
11	0.0516	0.0013	0.2970	0.0105	0.0417	0.0009	263.6 ±	5.5	264.0 ±	10.6	1379	26
12	0.0505	0.0024	0.2130	0.0117	0.0306	0.0009	194.1 ±	5.5	196.0 ±	11.8	215	60
13	0.0497	0.0032	0.2814	0.0208	0.0410	0.0016	259.2 ±	10.2	251.8 ±	20.9	78	51
14	0.0530	0.0029	0.2972	0.0188	0.0407	0.0014	256.9 ±	8.9	264.2 ±	18.9	110	65
15	0.0520	0.0017	0.2017	0.0084	0.0281	0.0006	178.8 ±	4.1	186.6 ±	8.5	636	233
16	0.1145	0.0027	5.2554	0.1492	0.3328	0.0056	1851.8 ±	36.3	1861.6 ±	141.2	385	201
17	0.0538	0.0017	0.4210	0.0149	0.0567	0.0010	355.5 ±	6.5	356.8 ±	15.0	380	151
18	0.0518	0.0031	0.2146	0.0136	0.0300	0.0009	190.8 ±	5.6	197.4 ±	13.7	125	75
19	0.1157	0.0027	5.4523	0.1553	0.3417	0.0058	1894.8 ±	37.6	1893.1 ±	146.6	374	78
20	0.1152	0.0029	5.5085	0.1836	0.3465	0.0081	1917.8 ±	52.2	1901.9 ±	171.2	160	50
21	0.0509	0.0022	0.2139	0.0100	0.0305	0.0006	193.4 ±	4.2	196.8 ±	10.1	267	178
22	0.0508	0.0020	0.2097	0.0087	0.0299	0.0006	189.9 ±	3.6	193.3 ±	8.8	381	246
23	0.0521	0.0021	0.2389	0.0101	0.0332	0.0006	210.7 ±	4.2	217.5 ±	10.2	324	136
24	0.0559	0.0017	0.5494	0.0189	0.0713	0.0013	443.9 ±	8.3	444.6 ±	19.0	349	406
25	0.0511	0.0017	0.2132	0.0076	0.0302	0.0005	192.0 ±	3.1	196.2 ±	7.7	626	307
26	0.0509	0.0022	0.2844	0.0131	0.0405	0.0009	255.7 ±	5.8	254.1 ±	13.2	222	220
27	0.0517	0.0017	0.2520	0.0088	0.0353	0.0006	223.7 ±	3.6	228.2 ±	8.9	600	466
28	0.0515	0.0022	0.2116	0.0096	0.0297	0.0006	188.9 ±	3.9	194.9 ±	9.7	294	251
29	0.0499	0.0016	0.2085	0.0071	0.0303	0.0005	192.4 ±	2.9	192.3 ±	7.2	760	438
30	0.0485	0.0026	0.1933	0.0109	0.0289	0.0007	183.6 ±	4.6	179.5 ±	11.0	181	112
31	0.0508	0.0016	0.2063	0.0070	0.0295	0.0004	187.1 ±	2.8	190.5 ±	7.1	760	411
32	0.0561	0.0019	0.5729	0.0220	0.0740	0.0016	460.3 ±	10.1	459.9 ±	22.1	230	158
33	0.0551	0.0037	0.3000	0.0218	0.0395	0.0015	249.6 ±	9.4	266.4 ±	21.9	69	43
34	0.0514	0.0026	0.2889	0.0166	0.0408	0.0014	257.5 ±	8.7	257.7 ±	16.8	136	102
35	0.0527	0.0030	0.3038	0.0195	0.0418	0.0015	263.8 ±	9.9	269.4 ±	19.6	98	83
36	0.0509	0.0027	0.2172	0.0130	0.0309	0.0010	196.5 ±	6.5	199.6 ±	13.1	154	83
37	0.0503	0.0018	0.1895	0.0080	0.0273	0.0007	173.6 ±	4.5	176.2 ±	8.0	548	217
38	0.0509	0.0017	0.2431	0.0096	0.0346	0.0009	219.3 ±	5.6	220.9 ±	9.7	580	671
39	0.0499	0.0019	0.2369	0.0103	0.0344	0.0009	218.1 ±	5.8	215.9 ±	10.4	398	262
40	0.0524	0.0018	0.2973	0.0122	0.0411	0.0011	259.7 ±	6.9	264.3 ±	12.4	411	215
41	0.0520	0.0023	0.1909	0.0095	0.0266	0.0007	169.3 ±	4.8	177.4 ±	9.6	299	137
42	0.0513	0.0014	0.2883	0.0098	0.0408	0.0009	257.6 ±	6.1	257.2 ±	10.0	1330	614
43	0.0570	0.0043	0.3644	0.0309	0.0463	0.0023	292.0 ±	14.6	315.5 ±	30.9	44	31
44	0.0516	0.0019	0.2813	0.0124	0.0395	0.0011	249.9 ±	6.9	251.7 ±	12.5	330	243
45	0.0504	0.0018	0.2118	0.0087	0.0305	0.0008	193.5 ±	5.0	195.1 ±	8.8	543	184
46	0.0518	0.0021	0.2887	0.0134	0.0404	0.0011	255.4 ±	7.3	257.5 ±	13.5	265	117
47	0.0529	0.0026	0.2908	0.0162	0.0399	0.0013	252.0 ±	8.3	259.2 ±	16.3	148	110

Table A8 Continued.

No.	Isotopic ratios						U-Pb age (Ma)				U (ppm)	Th (ppm)
	$^{207}Pb/^{206}Pb$	Error 2σ	$^{207}Pb/^{235}U$	Error 2σ	$^{206}Pb/^{238}U$	Error 2σ	$^{206}Pb/^{238}U$	Error 2σ	$^{207}Pb/^{235}U$	Error 2σ		
48	0.1141	0.0028	5.2773	0.1847	0.3352	0.0091	1863.3	± 58.2	1865.2	± 172.1	274	236
49	0.0518	0.0020	0.2903	0.0133	0.0406	0.0011	256.8	± 7.3	258.8	± 13.5	273	88
50	0.1123	0.0033	5.1578	0.2538	0.3328	0.0139	1851.8	± 89.1	1845.7	± 229.6	56	92
51	0.0501	0.0016	0.2087	0.0081	0.0302	0.0007	191.6	± 4.8	192.5	± 8.2	728	289
52	0.1148	0.0031	5.2148	0.2194	0.3292	0.0114	1834.4	± 73.0	1855.0	± 201.4	98	179
53	0.0496	0.0016	0.1935	0.0073	0.0283	0.0007	179.9	± 4.4	179.6	± 7.4	910	374
54	0.0509	0.0021	0.2177	0.0103	0.0310	0.0009	196.9	± 5.5	200.0	± 10.4	309	163
55	0.0481	0.0024	0.2013	0.0113	0.0303	0.0009	192.7	± 6.0	186.2	± 11.4	198	55
56	0.0519	0.0018	0.2923	0.0118	0.0408	0.0010	257.9	± 6.7	260.4	± 11.9	461	331
57	0.0524	0.0021	0.2893	0.0136	0.0400	0.0011	253.1	± 7.4	258.0	± 13.8	250	140
58	0.0513	0.0016	0.2846	0.0106	0.0403	0.0010	254.4	± 6.3	254.3	± 10.7	712	452
59	0.0502	0.0024	0.2429	0.0134	0.0350	0.0011	222.1	± 7.0	220.8	± 13.5	178	143
60	0.0499	0.0013	0.2229	0.0075	0.0324	0.0007	205.4	± 4.7	204.3	± 7.6	1977	553
Standards												
91500epo 2-1	0.0728	0.0026	1.7618	0.0953	0.1754	0.0070	1042	± 45	1031	± 92	60	23
91500epo 2-2	0.0775	0.0027	1.9074	0.1026	0.1785	0.0072	1059	± 46	1084	± 99	59	20
91500epo 2-3	0.0757	0.0027	1.8690	0.0934	0.1789	0.0066	1061	± 43	1070	± 91	58	20
91500epo 2-4	0.0772	0.0028	1.9245	0.1017	0.1807	0.0075	1071	± 48	1090	± 98	58	22
OD-3 2-1	0.0496	0.0059	0.0350	0.0042	0.0051	0.0002	32.9	± 1.31	35.0	± 4.25	171	181
OD-3 2-2	0.0475	0.0054	0.0339	0.0039	0.0052	0.0002	33.3	± 1.26	33.8	± 3.94	194	162
OD-3 2-3	0.0462	0.0052	0.0314	0.0035	0.0049	0.0002	31.7	± 1.06	31.4	± 3.57	210	219
OD-3 2-4	0.0447	0.0042	0.0303	0.0029	0.0049	0.0002	31.6	± 1.07	30.3	± 2.90	315	350

Table A9 Zircon U–Pb isotopic data for sample Hrp-05 obtained by quadrupole inductively coupled plasma mass spectrometry.

No.	Isotopic ratios						U-Pb age (Ma)				U (ppm)	Th (ppm)
	$^{207}Pb/^{206}Pb$	Error 2σ	$^{207}Pb/^{235}U$	Error 2σ	$^{206}Pb/^{238}U$	Error 2σ	$^{206}Pb/^{238}U$	Error 2σ	$^{207}Pb/^{235}U$	Error 2σ		
1	0.0492	0.0022	0.1754	0.0087	0.0258	0.0005	164.3 ±	3.3	164.1 ±	8.7	885	391
2	0.0497	0.0019	0.1492	0.0061	0.0218	0.0003	138.9 ±	2.2	141.2 ±	6.2	2325	1493
3	0.0496	0.0021	0.1767	0.0080	0.0258	0.0005	164.3 ±	3.0	165.2 ±	8.1	1226	1001
4	0.0496	0.0026	0.1799	0.0101	0.0263	0.0006	167.4 ±	4.0	168.0 ±	10.2	568	288
5	0.0497	0.0026	0.1840	0.0102	0.0269	0.0006	170.8 ±	4.0	171.5 ±	10.3	565	183
6	0.0508	0.0028	0.1808	0.0105	0.0258	0.0006	164.3 ±	4.1	168.8 ±	10.6	498	176
7	0.0500	0.0020	0.1622	0.0071	0.0235	0.0004	149.9 ±	2.6	152.6 ±	7.2	1557	1329
8	0.0481	0.0023	0.1732	0.0088	0.0261	0.0005	166.0 ±	3.5	162.2 ±	8.9	790	322
9	0.0514	0.0020	0.1672	0.0071	0.0236	0.0004	150.4 ±	2.5	157.0 ±	7.1	1800	1380
10	0.0503	0.0021	0.1847	0.0083	0.0266	0.0005	169.5 ±	3.1	172.1 ±	8.4	1199	871
11	0.0518	0.0024	0.1938	0.0099	0.0271	0.0006	172.4 ±	3.7	179.9 ±	10.0	729	358
12	0.0493	0.0020	0.1763	0.0079	0.0259	0.0005	165.0 ±	3.0	164.9 ±	8.0	1283	993
13	0.0499	0.0023	0.1791	0.0091	0.0260	0.0005	165.6 ±	3.5	167.3 ±	9.2	782	570
14	0.0495	0.0026	0.1813	0.0104	0.0265	0.0006	168.8 ±	4.1	169.2 ±	10.5	529	329
15	0.0507	0.0026	0.1902	0.0105	0.0272	0.0006	172.8 ±	4.1	176.8 ±	10.7	556	401
16	0.0509	0.0022	0.1617	0.0085	0.0230	0.0005	146.8 ±	3.4	152.2 ±	8.6	1675	2668
17	0.0468	0.0026	0.1717	0.0112	0.0266	0.0008	169.3 ±	4.9	160.9 ±	11.3	546	514
18	0.0507	0.0024	0.1536	0.0089	0.0220	0.0006	140.0 ±	3.6	145.1 ±	9.0	1022	1320
19	0.0486	0.0027	0.1819	0.0119	0.0271	0.0008	172.6 ±	5.1	169.7 ±	12.0	505	253
20	0.0480	0.0022	0.1727	0.0096	0.0261	0.0006	165.9 ±	4.1	161.8 ±	9.7	1167	781
21	0.0484	0.0024	0.1659	0.0097	0.0248	0.0006	158.1 ±	4.1	155.9 ±	9.8	889	455
22	0.0503	0.0025	0.1808	0.0109	0.0261	0.0007	165.9 ±	4.5	168.7 ±	11.0	731	345
23	0.0488	0.0023	0.1800	0.0103	0.0268	0.0007	170.2 ±	4.4	168.1 ±	10.4	913	562
24	0.0496	0.0021	0.1784	0.0095	0.0261	0.0006	165.8 ±	3.9	166.7 ±	9.6	1454	856
25	0.0502	0.0025	0.1793	0.0106	0.0259	0.0007	164.8 ±	4.4	167.5 ±	10.7	791	507
26	0.0489	0.0029	0.1790	0.0121	0.0265	0.0008	168.8 ±	5.1	167.2 ±	12.3	453	475
27	0.0482	0.0022	0.1743	0.0099	0.0262	0.0007	166.9 ±	4.2	163.2 ±	10.0	999	658
28	0.0484	0.0021	0.1754	0.0096	0.0263	0.0006	167.1 ±	4.1	164.1 ±	9.7	1266	726
29	0.0475	0.0022	0.1748	0.0099	0.0267	0.0007	169.6 ±	4.3	163.6 ±	10.0	1039	665
30	0.0486	0.0020	0.1754	0.0092	0.0261	0.0006	166.3 ±	3.9	164.1 ±	9.3	1714	838

Standards are the same as in Table A1

Table A10 Zircon U–Pb isotopic data for sample Odr-Kass-01 obtained by quadrupole inductively coupled plasma mass spectrometry. Shadowed data indicate discordant age data.

No.	Isotopic ratios						U-Pb age (Ma)				U (ppm)	Th (ppm)
	$^{207}Pb/^{206}Pb$	Error 2σ	$^{207}Pb/^{235}U$	Error 2σ	$^{206}Pb/^{238}U$	Error 2σ	$^{206}Pb/^{238}U$	Error 2σ	$^{207}Pb/^{235}U$	Error 2σ		
1	0.0506	0.0017	0.2495	0.0087	0.0357	0.0006	226.4 ±	4.2	226.2 ±	8.7	374	182
2	0.1143	0.0018	5.2501	0.1058	0.3328	0.0055	1852.1 ±	35.7	1860.8 ±	102.1	385	207
3	0.0524	0.0015	0.2946	0.0087	0.0408	0.0007	257.7 ±	4.3	262.2 ±	8.8	490	172
4	0.0502	0.0011	0.2335	0.0051	0.0337	0.0004	213.8 ±	2.7	213.1 ±	5.1	1404	490
5	0.0513	0.0022	0.2084	0.0093	0.0294	0.0006	187.0 ±	4.1	192.2 ±	9.4	246	110
6	0.1145	0.0018	5.2831	0.0970	0.3345	0.0050	1860.0 ±	31.9	1866.1 ±	94.0	560	171
7	0.0530	0.0018	0.2524	0.0090	0.0345	0.0006	218.7 ±	4.2	228.6 ±	9.1	344	166
8	0.0455	0.0044	0.2544	0.0263	0.0405	0.0020	255.8 ±	13.1	230.1 ±	26.3	36	35
9	0.0540	0.0024	0.2140	0.0098	0.0287	0.0006	182.7 ±	4.2	196.9 ±	9.9	228	156
10	0.1136	0.0018	5.1435	0.0942	0.3282	0.0048	1829.5 ±	31.2	1843.3 ±	91.4	568	108
11	0.0492	0.0013	0.1878	0.0052	0.0277	0.0004	176.1 ±	2.6	174.8 ±	5.3	819	441
12	0.0502	0.0013	0.1907	0.0052	0.0276	0.0004	175.3 ±	2.5	177.3 ±	5.2	876	442
13	0.1146	0.0021	5.2972	0.1435	0.3349	0.0079	1862.0 ±	50.8	1868.4 ±	136.2	154	43
14	0.0515	0.0014	0.2670	0.0074	0.0376	0.0006	238.0 ±	3.7	240.3 ±	7.5	623	229
15	0.0492	0.0014	0.2019	0.0057	0.0297	0.0004	188.9 ±	2.8	186.7 ±	5.7	751	385
16	0.1135	0.0018	5.0057	0.1009	0.3197	0.0053	1788.4 ±	34.2	1820.3 ±	97.6	387	120
17	0.0508	0.0018	0.2083	0.0079	0.0297	0.0006	188.8 ±	3.9	192.2 ±	8.0	369	137
18	0.0479	0.0023	0.2285	0.0120	0.0346	0.0009	219.0 ±	5.9	209.0 ±	12.1	166	107
19	0.0531	0.0020	0.4286	0.0187	0.0586	0.0015	366.8 ±	10.0	362.2 ±	18.8	153	79
20	0.0490	0.0013	0.2008	0.0060	0.0297	0.0005	188.6 ±	3.2	185.8 ±	6.1	691	500
21	0.0497	0.0014	0.1898	0.0061	0.0277	0.0005	176.0 ±	3.1	176.4 ±	6.2	600	334
22	0.0478	0.0021	0.1969	0.0093	0.0298	0.0007	189.5 ±	4.5	182.5 ±	9.4	236	183
23	0.0508	0.0014	0.2494	0.0077	0.0356	0.0006	225.2 ±	4.1	226.1 ±	7.8	537	740
24	0.0490	0.0016	0.2372	0.0084	0.0351	0.0007	222.2 ±	4.4	216.1 ±	8.5	389	323
25	0.0495	0.0023	0.2044	0.0102	0.0299	0.0007	189.9 ±	4.8	188.8 ±	10.3	203	138
26	0.0500	0.0012	0.2382	0.0063	0.0345	0.0006	218.6 ±	3.6	216.9 ±	6.4	821	643
27	0.0498	0.0015	0.1966	0.0065	0.0286	0.0005	181.9 ±	3.3	182.2 ±	6.6	541	325
28	0.0611	0.0036	0.2889	0.0188	0.0342	0.0012	217.1 ±	7.7	257.7 ±	18.9	87	105
29	0.0491	0.0019	0.1865	0.0078	0.0275	0.0006	175.1 ±	3.7	173.6 ±	7.9	327	189
30	0.0501	0.0015	0.2408	0.0082	0.0349	0.0007	220.9 ±	4.2	219.1 ±	8.3	433	280
31	0.0485	0.0010	0.1992	0.0046	0.0298	0.0004	189.1 ±	2.8	184.5 ±	4.7	1437	631
32	0.1214	0.0014	5.7653	0.1084	0.3441	0.0056	1906.2 ±	35.9	1941.2 ±	104.5	614	44
33	0.1144	0.0013	4.9316	0.0936	0.3123	0.0051	1752.2 ±	32.8	1807.7 ±	90.9	601	223
34	0.0479	0.0018	0.1675	0.0069	0.0254	0.0005	161.5 ±	3.3	157.3 ±	6.9	376	98
35	0.0496	0.0013	0.2415	0.0072	0.0353	0.0006	223.4 ±	3.9	219.7 ±	7.3	588	422
36	0.0509	0.0019	0.2432	0.0099	0.0346	0.0008	219.4 ±	4.9	221.0 ±	10.0	280	202
37	0.0510	0.0023	0.2093	0.0103	0.0298	0.0008	189.0 ±	5.2	193.0 ±	10.4	211	109
38	0.0485	0.0032	0.2964	0.0219	0.0443	0.0018	279.6 ±	11.5	263.6 ±	22.0	66	36
39	0.0504	0.0013	0.1918	0.0060	0.0276	0.0006	175.5 ±	3.6	178.2 ±	6.1	717	320
40	0.0525	0.0018	0.2500	0.0101	0.0345	0.0008	218.5 ±	5.4	226.5 ±	10.2	291	154
41	0.0521	0.0018	0.2548	0.0103	0.0355	0.0009	224.7 ±	5.6	230.5 ±	10.4	290	36
42	0.0517	0.0015	0.2509	0.0089	0.0351	0.0008	222.7 ±	5.1	227.3 ±	9.0	405	301
43	0.0479	0.0029	0.1988	0.0129	0.0301	0.0010	190.9 ±	6.4	184.1 ±	13.0	120	53
44	0.0505	0.0024	0.1856	0.0095	0.0266	0.0007	169.5 ±	4.7	172.9 ±	9.6	215	195
45	0.0506	0.0011	0.2433	0.0069	0.0348	0.0007	220.8 ±	4.5	221.1 ±	7.0	789	558
46	0.0498	0.0012	0.1896	0.0056	0.0276	0.0005	175.6 ±	3.5	176.3 ±	5.7	856	438
47	0.0489	0.0016	0.1857	0.0069	0.0275	0.0006	175.0 ±	3.9	173.0 ±	7.0	452	276

Table A10 Continued.

No.	Isotopic ratios						U-Pb age (Ma)				U (ppm)	Th (ppm)
	$^{207}Pb/^{206}Pb$	Error 2σ	$^{207}Pb/^{235}U$	Error 2σ	$^{206}Pb/^{238}U$	Error 2σ	$^{206}Pb/^{238}U$	Error 2σ	$^{207}Pb/^{235}U$	Error 2σ		
48	0.0515	0.0020	0.2489	0.0109	0.0350	0.0009	222.1 ±	5.8	225.6 ±	11.0	243	162
49	0.0501	0.0014	0.1861	0.0062	0.0269	0.0006	171.3 ±	3.6	173.3 ±	6.2	620	362
50	0.1117	0.0014	4.0239	0.1045	0.2611	0.0063	1495.6 ±	40.7	1639.0 ±	100.9	241	67
51	0.0502	0.0016	0.1959	0.0070	0.0283	0.0006	179.9 ±	4.0	181.6 ±	7.1	482	315
52	0.1248	0.0012	6.1996	0.1335	0.3600	0.0074	1982.1 ±	47.7	2004.4 ±	127.2	501	64
53	0.1138	0.0025	5.2361	0.1249	0.3336	0.0079	1855.7 ±	50.5	1858.5 ±	119.5	299	71
54	0.0507	0.0015	0.2419	0.0066	0.0346	0.0007	219.1 ±	4.6	220.0 ±	6.7	847	383
55	0.0501	0.0020	0.1906	0.0076	0.0276	0.0007	175.4 ±	4.3	177.2 ±	7.7	367	209
56	0.0503	0.0013	0.2379	0.0058	0.0343	0.0007	217.2 ±	4.3	216.7 ±	5.8	1305	747
57	0.0510	0.0021	0.1974	0.0080	0.0280	0.0007	178.2 ±	4.4	182.9 ±	8.1	343	228
58	0.0496	0.0023	0.2408	0.0115	0.0352	0.0010	223.0 ±	6.3	219.1 ±	11.6	198	178
59	0.1301	0.0029	6.5462	0.1568	0.3648	0.0087	2004.7 ±	55.8	2052.1 ±	147.9	284	73
60	0.0504	0.0017	0.2459	0.0081	0.0354	0.0008	224.1 ±	5.1	223.3 ±	8.2	477	118
61	0.0519	0.0023	0.2479	0.0111	0.0346	0.0009	219.5 ±	6.0	224.9 ±	11.2	224	123
62	0.0491	0.0016	0.1840	0.0058	0.0272	0.0006	172.7 ±	3.7	171.5 ±	5.9	684	330
63	0.0493	0.0017	0.2018	0.0069	0.0297	0.0007	188.6 ±	4.3	186.7 ±	7.0	514	195
64	0.0484	0.0026	0.2359	0.0132	0.0353	0.0011	223.9 ±	7.1	215.1 ±	13.4	140	98
Standards												
91500epo 3-1	0.0754	0.0020	1.8638	0.0708	0.1792	0.0054	1063 ±	35	1068 ±	69	89	36
91500epo 3-2	0.0733	0.0020	1.7753	0.0671	0.1755	0.0053	1042 ±	34	1036 ±	66	91	38
91500epo 3-3	0.0748	0.0018	1.8439	0.0742	0.1788	0.0061	1060 ±	39	1061 ±	73	87	33
91500epo 3-4	0.0737	0.0018	1.8351	0.0734	0.1804	0.0061	1069 ±	39	1058 ±	72	88	34
91500epo 3-5	0.0732	0.0023	1.8379	0.0743	0.1820	0.0063	1078 ±	41	1059 ±	73	84	31
OD-3 3-1	0.0502	0.0030	0.0362	0.0022	0.0052	0.0001	33.6 ±	0.67	36.1 ±	2.18	659	927
OD-3 3-2	0.0490	0.0043	0.0343	0.0030	0.0051	0.0001	32.6 ±	0.89	34.2 ±	3.02	315	341
OD-3 3-3	0.0451	0.0029	0.0328	0.0021	0.0053	0.0001	33.9 ±	0.84	32.8 ±	2.16	639	709
OD-3 3-4	0.0429	0.0040	0.0313	0.0029	0.0053	0.0002	34.0 ±	1.05	31.3 ±	2.95	314	314
OD-3 3-5	0.0463	0.0039	0.0329	0.0027	0.0052	0.0002	33.1 ±	0.98	32.9 ±	2.76	374	367

Table A11 Zircon U–Pb isotopic data for sample Tcs-E-03 obtained by quadrupole inductively coupled plasma mass spectrometry.

No.	Isotopic ratios						U-Pb age (Ma)				U (ppm)	Th (ppm)
	$^{207}Pb/^{206}Pb$	Error 2σ	$^{207}Pb/^{235}U$	Error 2σ	$^{206}Pb/^{238}U$	Error 2σ	$^{206}Pb/^{238}U$	Error 2σ	$^{207}Pb/^{235}U$	Error 2σ		
1	0.1251	0.0042	6.1566	0.3293	0.3567	0.0114	1966.4 ±	72.8	1998.3 ±	289.1	286	183
2	0.0491	0.0024	0.1694	0.0104	0.0250	0.0007	159.4 ±	4.7	158.9 ±	10.5	323	127
3	0.0485	0.0035	0.1706	0.0143	0.0255	0.0010	162.1 ±	6.3	159.9 ±	14.4	582	247
4	0.0476	0.0031	0.1621	0.0123	0.0247	0.0009	157.0 ±	5.5	152.5 ±	12.5	397	291
5	0.0488	0.0044	0.1635	0.0164	0.0243	0.0011	154.5 ±	7.0	153.8 ±	16.5	1250	800
6	0.0488	0.0036	0.1700	0.0145	0.0253	0.0010	160.9 ±	6.3	159.5 ±	14.6	171	129
7	0.0502	0.0035	0.1721	0.0140	0.0248	0.0009	158.1 ±	6.0	161.2 ±	14.1	137	106
8	0.0471	0.0035	0.1624	0.0138	0.0250	0.0010	159.0 ±	6.1	152.8 ±	13.9	343	295
9	0.0503	0.0043	0.1728	0.0166	0.0249	0.0011	158.6 ±	7.0	161.8 ±	16.7	281	195
10	0.0479	0.0028	0.1637	0.0114	0.0248	0.0008	157.9 ±	5.2	153.9 ±	11.5	418	302
11	0.0511	0.0034	0.1712	0.0133	0.0243	0.0009	154.6 ±	5.6	160.5 ±	13.4	814	420
12	0.0497	0.0023	0.1702	0.0101	0.0248	0.0007	158.0 ±	4.5	159.6 ±	10.2	173	251
13	0.0493	0.0036	0.1664	0.0139	0.0245	0.0009	155.9 ±	6.0	156.3 ±	14.0	265	189
14	0.0511	0.0028	0.1692	0.0114	0.0240	0.0008	153.0 ±	4.9	158.7 ±	11.5	788	371
15	0.0501	0.0032	0.1715	0.0130	0.0248	0.0009	158.1 ±	5.6	160.7 ±	13.2	386	95
16	0.0498	0.0031	0.1693	0.0118	0.0247	0.0007	157.1 ±	4.8	158.8 ±	12.0	363	268
17	0.0527	0.0038	0.1905	0.0152	0.0262	0.0009	166.6 ±	6.0	177.0 ±	15.4	319	197
18	0.0471	0.0034	0.1601	0.0128	0.0246	0.0008	156.8 ±	5.4	150.8 ±	12.9	393	224
19	0.0486	0.0032	0.1657	0.0122	0.0247	0.0008	157.4 ±	5.0	155.7 ±	12.4	644	202
20	0.0475	0.0042	0.1608	0.0153	0.0246	0.0010	156.4 ±	6.4	151.4 ±	15.4	526	296
21	0.0507	0.0030	0.1712	0.0114	0.0245	0.0007	155.9 ±	4.5	160.5 ±	11.5	1079	1063
22	0.0505	0.0020	0.1679	0.0083	0.0241	0.0005	153.6 ±	3.3	157.6 ±	8.4	370	263
23	0.0503	0.0023	0.1701	0.0093	0.0245	0.0006	156.0 ±	3.7	159.5 ±	9.4	295	217
24	0.0489	0.0030	0.1627	0.0112	0.0241	0.0007	153.5 ±	4.5	153.1 ±	11.3	183	138
25	0.0483	0.0029	0.1650	0.0113	0.0248	0.0007	157.7 ±	4.7	155.1 ±	11.4	274	212
26	0.0511	0.0023	0.1738	0.0095	0.0247	0.0006	157.0 ±	3.7	162.7 ±	9.6	904	368
27	0.0498	0.0048	0.1668	0.0173	0.0243	0.0011	154.6 ±	7.0	156.6 ±	17.4	261	189
28	0.0511	0.0035	0.1684	0.0129	0.0239	0.0008	152.3 ±	5.1	158.0 ±	13.0	272	82
29	0.0484	0.0032	0.1602	0.0119	0.0240	0.0008	152.9 ±	4.9	150.9 ±	12.0	229	170
30	0.0492	0.0025	0.1682	0.0098	0.0248	0.0006	157.8 ±	4.0	157.9 ±	9.9	410	111

Standards are the same as in Table A1

Table A12 Zircon U–Pb isotopic data for sample 200824-07 obtained by quadrupole inductively coupled plasma mass spectrometry. Shadowed data indicate discordant age data.

No.	Isotopic ratios						U-Pb age (Ma)				U (ppm)	Th (ppm)
	$^{207}Pb/^{206}Pb$	Error 2σ	$^{207}Pb/^{235}U$	Error 2σ	$^{206}Pb/^{238}U$	Error 2σ	$^{206}Pb/^{238}U$	Error 2σ	$^{207}Pb/^{235}U$	Error 2σ		
1	0.0466	0.0031	0.1735	0.0120	0.0270	0.0008	171.7	± 5.4	162.5	± 12.1	120	108
2	0.0486	0.0032	0.1849	0.0128	0.0276	0.0009	175.3	± 5.6	172.2	± 12.9	113	148
3	0.1141	0.0026	5.2235	0.1702	0.3317	0.0091	1846.8	± 58.5	1856.5	± 159.6	119	79
4	0.0484	0.0021	0.1731	0.0077	0.0259	0.0005	165.0	± 3.3	162.1	± 7.8	317	122
5	0.0489	0.0041	0.1747	0.0151	0.0259	0.0010	164.7	± 6.5	163.5	± 15.2	75	139
6	0.0522	0.0030	0.2668	0.0164	0.0370	0.0012	234.5	± 7.5	240.1	± 16.5	108	100
7	0.1124	0.0023	4.2247	0.0855	0.2725	0.0037	1553.4	± 24.1	1678.8	± 83.3	641	84
8	0.0497	0.0018	0.1833	0.0064	0.0267	0.0004	170.0	± 2.8	170.9	± 6.5	529	483
9	0.1116	0.0023	4.0948	0.0875	0.2658	0.0040	1519.6	± 25.8	1653.3	± 85.2	495	68
10	0.0500	0.0019	0.1841	0.0068	0.0267	0.0005	169.6	± 2.9	171.5	± 6.9	467	362
11	0.0488	0.0024	0.1796	0.0091	0.0267	0.0006	169.6	± 4.0	167.7	± 9.2	225	190
12	0.0481	0.0025	0.1763	0.0093	0.0266	0.0006	169.0	± 4.1	164.9	± 9.4	210	207
13	0.0458	0.0034	0.1504	0.0115	0.0238	0.0008	151.7	± 5.0	142.2	± 11.6	110	147
14	0.0485	0.0021	0.1830	0.0080	0.0274	0.0005	174.0	± 3.5	170.6	± 8.1	316	272
15	0.0496	0.0023	0.1871	0.0088	0.0274	0.0006	174.0	± 3.8	174.1	± 8.9	261	146
16	0.0471	0.0025	0.1728	0.0096	0.0266	0.0006	169.4	± 3.9	161.9	± 9.7	229	87
17	0.1132	0.0031	5.0970	0.1617	0.3263	0.0060	1820.5	± 38.7	1835.6	± 152.2	278	40
18	0.0521	0.0022	0.1938	0.0083	0.0270	0.0005	171.7	± 3.0	179.9	± 8.4	429	161
19	0.1134	0.0034	5.2470	0.2177	0.3354	0.0104	1864.4	± 66.6	1860.3	± 200.0	91	127
20	0.0496	0.0029	0.1815	0.0112	0.0265	0.0007	168.7	± 4.5	169.4	± 11.3	168	173
21	0.0471	0.0024	0.1736	0.0093	0.0267	0.0006	170.0	± 3.8	162.6	± 9.4	246	94
22	0.0511	0.0018	0.2785	0.0103	0.0395	0.0006	249.5	± 3.8	249.4	± 10.4	530	12
23	0.0474	0.0027	0.1705	0.0102	0.0261	0.0006	166.1	± 4.1	159.8	± 10.3	192	117
24	0.0507	0.0025	0.2000	0.0102	0.0286	0.0006	181.9	± 4.0	185.1	± 10.3	252	116
25	0.1296	0.0037	7.0014	0.2805	0.3915	0.0117	2129.8	± 74.8	2111.6	± 251.0	98	113
26	0.0496	0.0026	0.1847	0.0098	0.0270	0.0006	171.7	± 3.9	172.1	± 9.9	239	82
27	0.0511	0.0019	0.2724	0.0107	0.0386	0.0006	244.2	± 4.1	244.6	± 10.8	422	47
28	0.1144	0.0033	5.2160	0.1916	0.3305	0.0083	1840.9	± 53.5	1855.2	± 178.0	140	68
29	0.0507	0.0020	0.1889	0.0077	0.0270	0.0004	171.7	± 2.8	175.7	± 7.8	499	312
30	0.0518	0.0020	0.2906	0.0117	0.0406	0.0007	256.8	± 4.6	259.0	± 11.8	375	214
31	0.0510	0.0013	0.2406	0.0069	0.0342	0.0007	216.8	± 4.3	218.9	± 7.0	219	222
32	0.0504	0.0008	0.2313	0.0045	0.0333	0.0005	211.0	± 3.3	211.3	± 4.6	762	944
33	0.0494	0.0009	0.1760	0.0036	0.0258	0.0004	164.4	± 2.6	164.6	± 3.7	803	351
34	0.0496	0.0009	0.1902	0.0042	0.0278	0.0005	176.8	± 2.9	176.8	± 4.3	578	262
35	0.0499	0.0015	0.1841	0.0060	0.0267	0.0005	170.0	± 3.5	171.6	± 6.0	205	119
36	0.1133	0.0013	4.9411	0.0962	0.3161	0.0059	1770.9	± 38.0	1809.3	± 93.3	170	136
37	0.0501	0.0012	0.1819	0.0050	0.0263	0.0005	167.4	± 3.1	169.7	± 5.0	319	192
38	0.0484	0.0018	0.1781	0.0068	0.0267	0.0006	169.9	± 3.9	166.4	± 6.9	141	76
39	0.0497	0.0009	0.1769	0.0037	0.0258	0.0004	164.3	± 2.6	165.4	± 3.7	773	461
40	0.0497	0.0009	0.1904	0.0039	0.0278	0.0004	176.6	± 2.8	176.9	± 3.9	755	881
41	0.1196	0.0013	4.5639	0.0858	0.2766	0.0050	1574.1	± 32.1	1742.7	± 83.6	200	96
42	0.0510	0.0009	0.2433	0.0052	0.0346	0.0006	219.1	± 3.6	221.1	± 5.2	537	154
43	0.1127	0.0012	4.5349	0.0823	0.2917	0.0051	1649.8	± 32.7	1737.4	± 80.3	236	124
44	0.0522	0.0010	0.3587	0.0082	0.0498	0.0009	313.3	± 5.6	311.2	± 8.3	313	80
45	0.0499	0.0017	0.1953	0.0073	0.0283	0.0006	180.2	± 4.1	181.1	± 7.4	139	76
46	0.0499	0.0011	0.1950	0.0048	0.0283	0.0005	179.9	± 3.1	180.9	± 4.9	396	319
47	0.0510	0.0017	0.1992	0.0072	0.0283	0.0006	179.9	± 4.0	184.4	± 7.3	147	55
48	0.0490	0.0012	0.1841	0.0049	0.0272	0.0005	173.3	± 3.1	171.6	± 4.9	344	123

Table A12 Continued.

No.	Isotopic ratios						U-Pb age (Ma)				U (ppm)	Th (ppm)
	$^{207}Pb/^{206}Pb$	Error 2σ	$^{207}Pb/^{235}U$	Error 2σ	$^{206}Pb/^{238}U$	Error 2σ	$^{206}Pb/^{238}U$	Error 2σ	$^{207}Pb/^{235}U$	Error 2σ		
49	0.1102	0.0011	3.7128	0.0570	0.2441	0.0036	1408.0	± 23.4	1574.1	± 56.3	778	14
50	0.0498	0.0009	0.1673	0.0034	0.0243	0.0004	155.1	± 2.4	157.1	± 3.4	877	674
51	0.0503	0.0012	0.1840	0.0049	0.0265	0.0004	168.6	± 2.8	171.5	± 5.0	365	240
52	0.0491	0.0012	0.1786	0.0047	0.0264	0.0004	167.8	± 2.7	166.8	± 4.7	392	196
53	0.0492	0.0015	0.1889	0.0060	0.0278	0.0005	176.9	± 3.3	175.7	± 6.1	222	180
54	0.0483	0.0027	0.1867	0.0107	0.0280	0.0008	178.0	± 5.5	173.8	± 10.8	58	51
55	0.0495	0.0010	0.1819	0.0039	0.0266	0.0004	169.3	± 2.4	169.7	± 4.0	727	554
56	0.0568	0.0011	0.4114	0.0088	0.0525	0.0008	329.7	± 5.1	349.9	± 8.9	388	154
57	0.0496	0.0012	0.1936	0.0051	0.0283	0.0005	179.7	± 2.9	179.7	± 5.1	366	495
58	0.0490	0.0008	0.1755	0.0033	0.0260	0.0003	165.4	± 2.2	164.2	± 3.3	1385	597
59	0.0480	0.0014	0.1863	0.0057	0.0281	0.0005	178.8	± 3.2	173.5	± 5.8	246	224
60	0.0496	0.0012	0.1799	0.0047	0.0263	0.0004	167.3	± 2.7	168.0	± 4.8	387	420
61	0.0481	0.0013	0.1650	0.0047	0.0249	0.0004	158.4	± 2.7	155.0	± 4.7	335	216
62	0.0475	0.0023	0.1887	0.0094	0.0288	0.0008	182.9	± 4.9	175.5	± 9.5	78	58
63	0.0492	0.0013	0.1959	0.0056	0.0288	0.0005	183.3	± 3.2	181.7	± 5.7	285	239
64	0.0502	0.0014	0.2430	0.0071	0.0351	0.0006	222.1	± 4.1	220.9	± 7.2	224	268
Standards												
91500epo 5-1	0.0817	0.0026	2.0551	0.0938	0.1823	0.00671	1079.8	± 43.1	1134.0	± 91.0	66	25
91500epo 5-2	0.0797	0.0026	2.0292	0.0943	0.1846	0.00691	1092.1	± 44.4	1125.4	± 91.5	63	42
91500epo 5-3	0.0816	0.0026	2.0735	0.0952	0.1842	0.00683	1090.0	± 43.9	1140.1	± 92.3	65	35
91500epo 5-4	0.0818	0.0030	2.0800	0.1042	0.1844	0.00678	1090.9	± 43.6	1142.2	± 100.7	65	25
91500epo 5-5	0.0837	0.0030	2.1430	0.1065	0.1855	0.00678	1097.1	± 43.6	1162.8	± 102.7	66	27
91500epo 5-6	0.0841	0.0030	2.0622	0.0964	0.1777	0.00596	1054.6	± 38.3	1136.3	± 93.5	79	25
OD3 5-1	0.0445	0.0036	0.0318	0.0025	0.0052	0.00012	33.3	± 0.8	31.8	± 2.5	442	865
OD3 5-2	0.0458	0.0034	0.0326	0.0024	0.0052	0.00011	33.2	± 0.7	32.6	± 2.4	557	804
91500epo 2-4	0.0745	0.0015	1.8132	0.0544	0.1764	0.00461	1047.2	± 29.6	1050.2	± 53.7	59	23
91500epo 2-5	0.0741	0.0015	1.8181	0.0540	0.1779	0.00461	1055.5	± 29.6	1052.0	± 53.4	60	33
91500epo 2-6	0.0738	0.0014	1.8520	0.0552	0.1819	0.00473	1077.6	± 30.4	1064.1	± 54.5	59	33
91500epo 2-7	0.0746	0.0016	1.8194	0.0546	0.1767	0.00440	1048.7	± 28.3	1052.5	± 54.0	61	26
91500epo 2-8	0.0750	0.0016	1.8391	0.0558	0.1777	0.00448	1054.6	± 28.8	1059.5	± 55.2	59	36
OD3 2-4	0.0479	0.0025	0.0334	0.0017	0.0051	0.00012	32.6	± 0.8	33.4	± 1.8	342	663
OD3 2-5	0.0475	0.0024	0.0339	0.0017	0.0052	0.00011	33.3	± 0.7	33.9	± 1.7	375	813

Table A13 Zircon U–Pb isotopic data for sample Oka-03 obtained by quadrupole inductively coupled plasma mass spectrometry.

No.	Isotopic ratios						U-Pb age (Ma)				U (ppm)	Th (ppm)
	$^{207}Pb/^{206}Pb$	Error 2σ	$^{207}Pb/^{235}U$	Error 2σ	$^{206}Pb/^{238}U$	Error 2σ	$^{206}Pb/^{238}U$	Error 2σ	$^{207}Pb/^{235}U$	Error 2σ		
1	0.0548	0.0043	0.1750	0.0146	0.0232	0.0009	147.5	± 5.7	163.7	± 14.7	333	443
2	0.0505	0.0026	0.1643	0.0090	0.0236	0.0006	150.1	± 3.8	154.4	± 9.1	36	48
3	0.0548	0.0049	0.1783	0.0168	0.0236	0.0010	150.3	± 6.5	166.6	± 16.9	76	176
4	0.0478	0.0025	0.1561	0.0088	0.0237	0.0006	150.8	± 3.9	147.3	± 8.9	259	363
5	0.0517	0.0043	0.1692	0.0146	0.0237	0.0009	151.1	± 5.9	158.7	± 14.7	101	75
6	0.0489	0.0042	0.1603	0.0143	0.0238	0.0009	151.5	± 5.9	151.0	± 14.4	307	91
7	0.0506	0.0020	0.1660	0.0073	0.0238	0.0005	151.5	± 3.2	155.9	± 7.4	114	177
8	0.0495	0.0024	0.1626	0.0080	0.0238	0.0005	151.6	± 3.5	153.0	± 8.1	272	453
9	0.0490	0.0026	0.1610	0.0092	0.0238	0.0006	151.7	± 4.0	151.6	± 9.3	281	329
10	0.0502	0.0020	0.1655	0.0072	0.0239	0.0005	152.1	± 3.2	155.5	± 7.3	91	63
11	0.0466	0.0035	0.1536	0.0120	0.0239	0.0008	152.3	± 5.2	145.1	± 12.2	74	135
12	0.0519	0.0025	0.1712	0.0084	0.0239	0.0005	152.5	± 3.5	160.5	± 8.5	260	381
13	0.0495	0.0021	0.1635	0.0076	0.0239	0.0005	152.5	± 3.4	153.8	± 7.7	128	76
14	0.0475	0.0024	0.1577	0.0080	0.0240	0.0006	153.2	± 3.5	148.7	± 8.1	390	639
15	0.0488	0.0025	0.1621	0.0087	0.0241	0.0006	153.3	± 3.8	152.6	± 8.8	106	252
16	0.0516	0.0024	0.1713	0.0086	0.0241	0.0006	153.3	± 3.7	160.6	± 8.7	339	425
17	0.0503	0.0028	0.1671	0.0101	0.0241	0.0007	153.4	± 4.3	156.9	± 10.2	196	561
18	0.0496	0.0035	0.1648	0.0119	0.0241	0.0008	153.4	± 5.0	154.9	± 12.0	116	246
19	0.0484	0.0020	0.1611	0.0069	0.0241	0.0005	153.8	± 3.1	151.7	± 7.0	187	154
20	0.0523	0.0040	0.1745	0.0137	0.0242	0.0009	154.1	± 5.5	163.3	± 13.8	237	259
21	0.0516	0.0061	0.1724	0.0211	0.0242	0.0013	154.2	± 8.4	161.5	± 21.2	330	520
22	0.0500	0.0022	0.1676	0.0081	0.0243	0.0006	154.8	± 3.6	157.3	± 8.2	59	89
23	0.0490	0.0018	0.1643	0.0066	0.0243	0.0005	154.8	± 3.1	154.4	± 6.7	407	690
24	0.0504	0.0033	0.1689	0.0114	0.0243	0.0007	154.9	± 4.7	158.5	± 11.5	290	438
25	0.0486	0.0022	0.1632	0.0074	0.0243	0.0005	154.9	± 3.3	153.5	± 7.5	211	630
26	0.0509	0.0024	0.1711	0.0082	0.0243	0.0005	155.1	± 3.5	160.4	± 8.3	161	96
27	0.0523	0.0036	0.1780	0.0128	0.0247	0.0008	157.2	± 5.2	166.4	± 13.0	256	197
28	0.0491	0.0022	0.1678	0.0082	0.0248	0.0006	157.8	± 3.7	157.5	± 8.3	204	129
29	0.0447	0.0031	0.1529	0.0111	0.0248	0.0008	158.0	± 5.0	144.5	± 11.2	77	135
30	0.1125	0.0025	4.9805	0.1299	0.3207	0.0062	1793.4	± 39.8	1816.0	± 124.0	265	263
Standards												
91500epo 4-1	0.0753	0.0026	1.8673	0.0905	0.1796	0.0068	1065	± 44	1070	± 88	58	15
91500epo 4-2	0.0731	0.0026	1.8479	0.0913	0.1832	0.0071	1084	± 45	1063	± 89	55	20
OD-3 4-1	0.0419	0.0048	0.0297	0.0033	0.0051	0.0002	33.1	± 1.09	29.7	± 3.38	222	231
OD-3 4-2	0.0440	0.0049	0.0306	0.0034	0.0050	0.0002	32.4	± 1.07	30.6	± 3.43	223	230

地質調査研究報告, 第 76 巻, 第 1/2 号, p. 101–132, 2025

概報 - Report

5 万分の 1 地質図幅「大河原」地域に産する領家深成岩類及び変成岩類の全岩化学組成

山崎　徹 [1, *]

YAMASAKI Toru (2025) Whole-rock geochemical compositions of the Ryoke plutonic rocks and metamorphic rocks from the 1:50,000, OGAWARA Quadrangle. *Bulletin of the Geological Survey of Japan*, vol. 76 (1/2), p. 101–132, 12 figs and 1 table.

Abstract: In order to provide a geochemical basis for the lithological classifications of the plutonic rocks identified during the preparation of the 1:50,000 scale geological map of the Ogawara Quadrangle, an analysis of the major and trace elements of the rocks from the Ryoke Plutono–Metamorphic Complex within this map area was conducted. Previous studies have suggested that the plutonic rocks in the Ogawara area are similar in lithology and that in some cases it is difficult to distinguish between rock types or the existence of intermediate lithologies. The results of this study show that lithological classification based on field occurrences and petrography can also be distinguished by a combination of different indices of whole-rock chemical composition. While the whole-rock chemical compositions of these lithological types correspond to the modal compositions of the constituent minerals, they cannot be explained by a simple parent-child relationship, suggesting the existence of individual parent magmas. Furthermore, based on preliminary examinations, the compositions of these rocks are similar to those of plutonic rocks in the Akechi area of the Mikawa–Tono district, about 60 km away. This suggests that an inter-regional comparison of the lithological types can be made by combining whole-rock chemical compositions with field occurrences and petrography.

Keywords: 1:50,000, OGAWARA Quadrangle, Ryoke Plutono-Metamorphic Complex, granite, gabbro, whole-rock major element composition, whole-rock trace element composition

要　旨

5 万分の 1 地質図幅「大河原」の作成にあたって識別した領家深成変成コンプレックスの岩体区分の地球化学的根拠を得るため，それらの全岩主成分・微量成分分析を実施した．先行研究によると，深成岩類の岩相的類似性から岩型ごとの識別が困難な場合や中間的な岩相の存在が指摘されていたが，本研究における産状や岩石記載に基づく岩型区分は，全岩化学組成の各種指標の組み合わせに基づく特徴によっても識別できることが明らかとなった．これらの全岩化学組成の特徴は，主として構成鉱物の量比に対応したものであるが，それらの違いは相互の単純な親子関係では説明できず，岩型ごとの個別の親マグマの存在を示唆する．さらに，予察的検討により約 60 km離れた三河–東濃地方の明智地域に産する深成岩類とも類似した組成を示すことが確認され，野外での産状や岩石記載に全岩化学組成を組み合わせることによって，岩型の広域的な対比が可能であることが示唆される．

1．はじめに

産業技術総合研究所地質調査総合センターでは，陸域地質図の体系的整備を進めており，縮尺 5 万分の 1 と 20 万分の 1 の地質図幅がシリーズとして出版されている．このうち，20 万分の 1 地質図幅は主として既存資料からの編纂によって作られるのに対し，5 万分の 1 地質図幅は自らの調査に基づいて作成する最も高精度の地質図で，基本地質図あるいは全ての地質図の基礎となる地質図と位置づけられている（山田ほか，2012；宮崎，2016）．

本論では，5 万分の 1 地質図幅「大河原（おおがわら）」（中村ほか，2025）において示した岩体区分の地球化学的根拠として，同図幅内の領家深成変成コンプレックス構成岩の全岩主成分・微量成分分析結果を示す．5 万分の 1 地質図幅「大河原」地域（以降，単に大河原地域と記述する）は，長野県下伊那郡大鹿村，豊丘村，松川町，中川村，駒ヶ根市，及び伊那市の一部を含む地域で，このうち西側約 1/3 の領域が西南日本内帯に属する（第 1 図）．本論では，西南日本内帯に分布する後期白亜紀の高温低圧型変成作用を

[1] 産業技術総合研究所 地質調査総合センター地質情報研究部門（AIST, Geological Survey of Japan, Research Institute of Geology and Geoinformation）

* Corresponding author: YAMASAKI, T., AIST Tsukuba Central 7, 1-1-1 Higashi, Tsukuba, Ibaraki 305-8567, Japan. Email: t.yamasaki@aist.go.jp

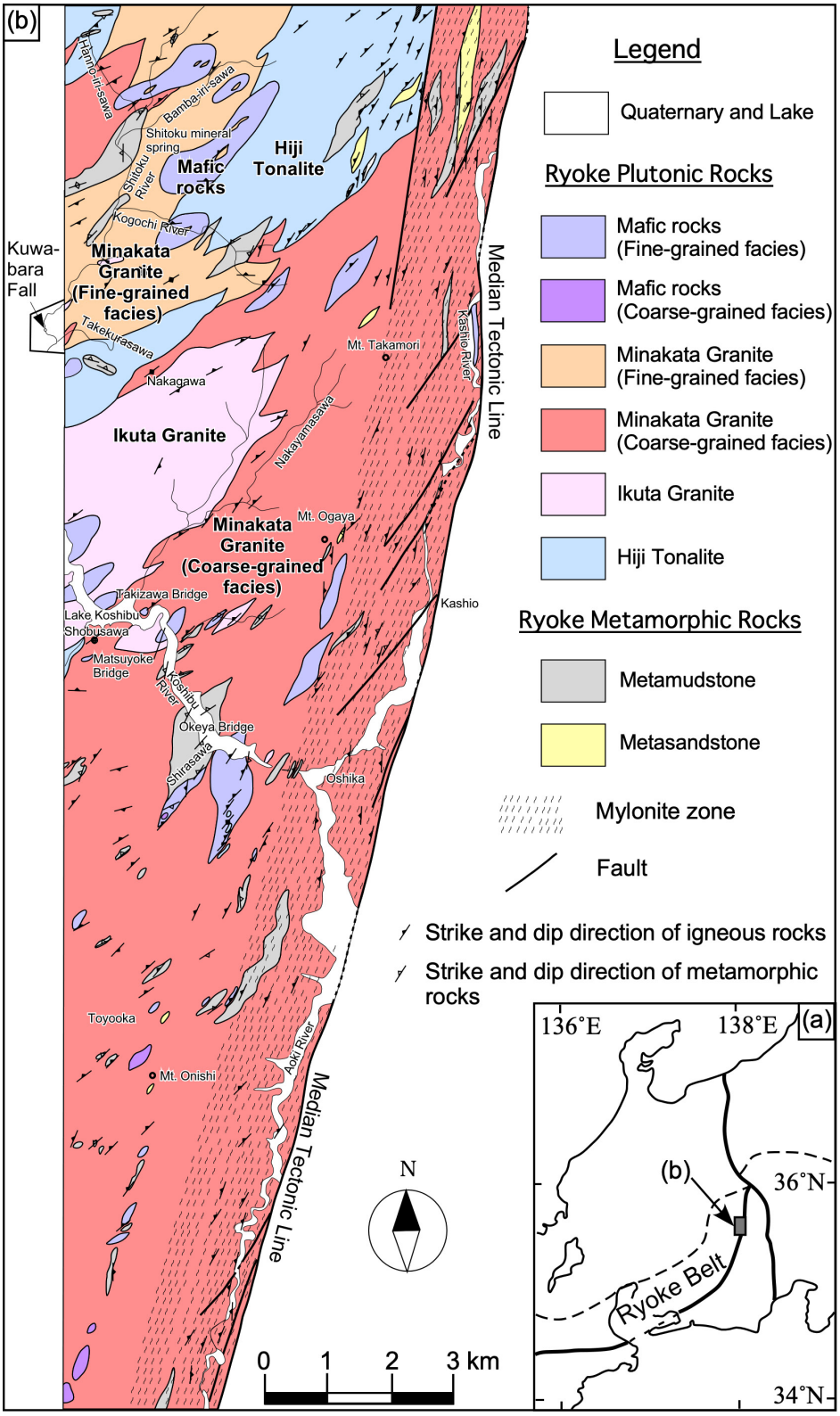

第 1 図　大河原地域の位置 (a) と領家深成変成コンプレックスの地質図 (b)．中央構造線の位置及びマイロナイト帯の分布とその中の構造ならびに第四系の分布は，中村ほか (2025) に基づく．地質単元・地名の日本語表記は付録に示した．

Fig. 1　Location of the mapped area (a) and geological map of the Ryoke Plutono-Metamorphic Complex at 1:50,000, OGAWARA Quadrangle. Locations of the Median Tectonic Line, distribution of the mylonite zone, and Quaternary strata are from Nakamura *et al.* (2025).

被った変成岩類とこれに貫入する火成岩類を，領家深成変成コンプレックスとして一括し，これを構成する変成岩類のことを領家変成岩類，深成岩類のことを領家深成岩類と呼ぶ．また，領家深成変成コンプレックスの分布域を領家帯と呼ぶ．これらに基づくと，大河原地域の西南日本内帯には，第四系を除くと領家深成変成コンプレックスが分布する（第1図）．

後に詳しく述べるように，大河原地域を構成する領家深成岩類は一般に様々な程度に変形しており，面構造が発達する上に，岩相上も類似し帰属の判定が困難な場合がある．モード組成の上でもトーナル岩や花崗閃緑岩が複数の岩型（一般に「○○花崗岩」等と呼ばれる地質単元名．必ずしも“岩体名”ではないため，以降も岩型名と表記する）に共通して産するほか，変形の程度が大きい場合，仮に鏡下でモード組成を測定しても，細粒な無色鉱物の同定は困難を伴う．こうした事情を反映し，既存の研究においては岩型の判別が困難な岩相や，異なる岩型間の中間的な岩相の存在が報告されている（領家団研グループ，1955；Yamada, 1957；Hayama, 1959）．その結果，帰属認定の客観的な基準が不明確となっており，先行研究間で各岩型の分布範囲も異なる．このことは，大河原地域に産する深成岩類の中部地方領家帯における広域的な対比や，年代値の解釈に不確実さをもたらしている．

その一方で，先行研究において大河原地域を構成する領家深成岩類の代表的な岩相や産状については，概ね共通の認識が示されているのも事実である（例えば，Yamada, 1957, 1967；Hayama, 1959；山田ほか，1974；Hayama and Yamada, 1977；下伊那誌編纂会，2006）．このことはつまり，各岩型の代表的あるいは典型的な部分については，先行研究間で共通の認識が示されているものの，各岩型の分布域の境界付近では帰属認定に相違があったり，中間的岩相の存在が報告されているということを意味する．先行研究で報告されている異なる岩型間の中間的な岩相が実際に存在するとしても，仮に，一般的な地質学的プロセスとして想定し得る，マグマ混合や，後に貫入した岩型（岩体）による既存岩体の部分的同化によって形成されたものであるならば，それらの産物は，比較的限られた範囲の反応帯として識別されるものと期待される．そして，そのような場合，反応帯以外の部分の岩相は，代表的な岩相と共通の特徴もつ一連の岩相として識別され，岩型を定義する基準が存在するはずである．そうした岩型の定義をなす岩相上の特徴は，一般にはモード組成のほか，粒度や色，組織・鉱物粒子の形態などの見た目上の違いである．このうち，標本サイズの試料における特徴として識別される色は，モード組成，すなわち鉱物の量比のほか，構成鉱物自体の色の違いに反映される．そうした鉱物の色の違いは，化学組成の違いに対応する場合が多いため，鉱物量比の違いとあわせて，見た目の色の違いは全岩化学組成の違いとして定量的に把握できることが期待される．

山崎（2019）でも述べたように，中部地方の領家深成岩類は長い研究史をもつものの，全岩微量成分組成の報告は依然少なく，従来力が注がれてきた岩相上の特徴と貫入関係に基づく岩型区分に加えて，微量元素を含む全岩化学組成の情報を追加することは，岩型間の広域的対比や成因の検討に重要な貢献をなすものと期待される．そこで，本論では5万分の1地質図幅「大河原」の作成にあたって採取した領家深成岩類の試料のうち，分析に堪え得るもの全てと，それらとの比較のためのいくつかの領家変成岩類の試料について，全岩主成分・微量成分組成を報告し，地質単元（岩型）ごとの岩相上の特徴と，全岩化学組成上の特徴を整理する．なお，本論における研究史を含む地質・岩石等の記載は，5万分の1地質図幅「大河原」の記述（山崎，2025）と内容的に重複するが，以下では，本論の完結性を保つためにあらためて必要最低限の記載を行う．

本論で引用している年代値のうち，ジルコンU–Pb年代値，CHIME（chemical Th-U-total Pb isochron）年代値，そしてU–Pb SHRIMP（Sensitive High Resolution Ion Microprobe）年代値の誤差は全て2σで示されている．なお，本論においては，5万分の1地質図幅「大河原」西端よりわずかに西の図郭外（5万分の1地質図幅「飯田」地域）に位置する，上伊那郡中川村の四徳川の“桑原の滝”露頭についても取り扱う．この桑原の滝は，複数の先行研究によって度々言及されており，位置を特定し得て先行研究で認定された岩相を追認できる重要な露頭である．

2．大河原地域に分布する領家深成変成コンプレックスの地質概説

2.1　各岩型（地質単元）の相互関係と特徴

大河原地域に分布する領家深成変成コンプレックスを対象とした地質学的・岩石学的研究は少なく，1950年代までは広域的な地質図の一部として，大部分が単一岩相の片麻岩とされたり（鈴木，1888），片状普通花崗岩・斑状花崗岩・雲母片岩（杉山，1939）や，シャールスタイン（塩基性火成岩源変成岩）・混成岩（石井ほか，1955）といった2種類～3種類程度の岩相に区分され，岩体名や岩型名は与えられていなかった．領家団研グループ（1955）が示した中部地方領家帯地質図以降，中部地方全域で岩相及び貫入関係をもとに岩型の対比がはじまり，例えば“天竜峡（てんりゅうきょう）花崗岩”といった，現在まで使用されている岩型名が使用されるようになった．ただし，領家団研グループ（1955）によって現在の全ての岩型名が整理されたわけではなく，また，様々な先行研究においては，同一の岩型に対しても文献によって様々な名称が与えられている．例えば非持（ひじ）型に対しては，非持花崗閃緑岩，非持石英閃緑岩，あるいは非持トーナル岩等といった岩型名が使用されている．このため，先行研究の記述にあたっては，

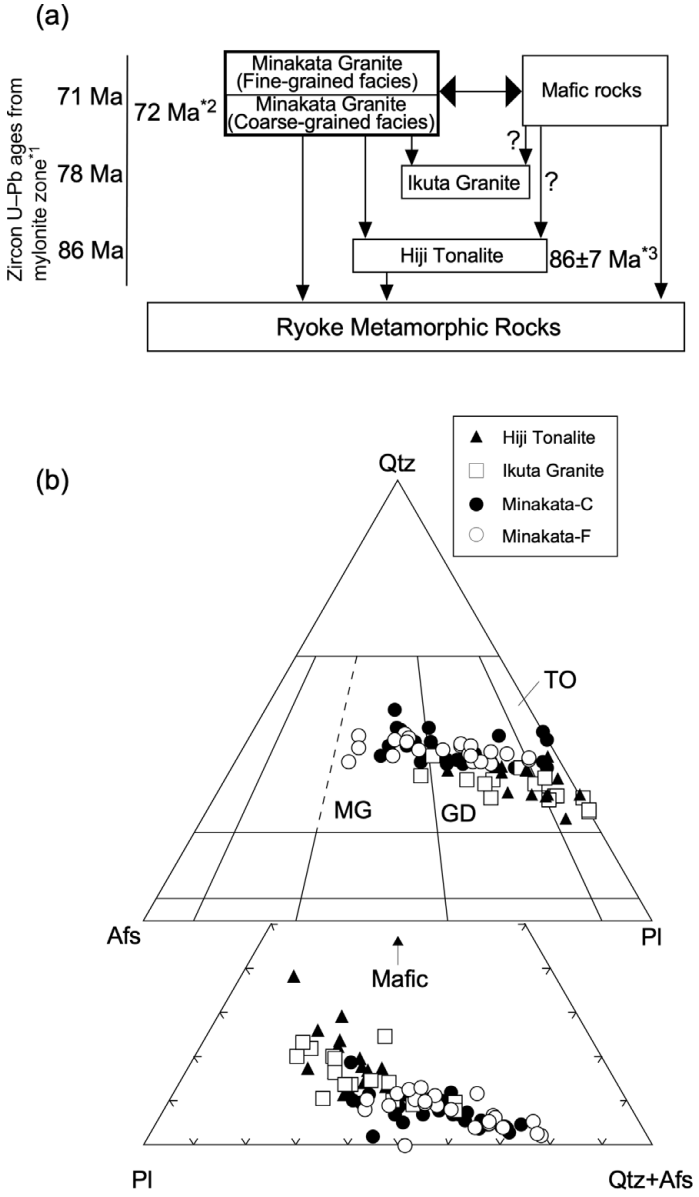

第2図　大河原地域に産する領家深成岩類の貫入関係及び年代とモード組成．(a) 大河原地域に産する領家深成岩類の貫入関係及び年代．年代値は，*1: Nakamura *et al.* (2022)，*2: Yokoyama *et al.* (2016)，*3: 坂島ほか(2000)に基づく．詳しい説明は本文参照．(b) 大河原地域に産する領家深成岩類のモード組成図．Qtz: 石英，Afs: アルカリ長石，Pl: 斜長石，Mafic: 苦鉄質鉱物，TO: トーナル岩，GD: 花崗閃緑岩，MG: モンゾ花崗岩．Qtz–Afs–Pl図の境界はLe Maitre (2002) に基づく．

Fig. 2　Solidification ages, mutual relationship, and modal composition of Ryoke Plutonic Rocks in the Ogawara area. (a) Solidification ages and mutual relationship of Ryoke Plutonic Rocks in the Ogawara area. *1: Nakamura *et al.* (2022), *2: Yokoyama *et al.* (2016), *3: Sakashima *et al.* (2000). (b) Modal composition of Ryoke Plutonic Rocks in the Ogawara area. Qtz: quartz, Afs: alkali feldspar, Pl: plagioclase, Mafic: mafic minerals, TO: tonalite, GD: granodioraite, MG: monzogranite, Minakata-C: Minakata Granite coarse-grained facies, Minakata-F: Minakata Granite fine-grained facies.　Qtz–Afs–Pl discrimination diagram after Le Maitre (2002).

報告の順に記載すると同一の岩型に対して様々な名称が混在し煩雑になるとともに，本研究における区分との対応関係が分かりにくくなるため，以下では，本研究における岩型及び分布に基づいて記述し，必要に応じて領家団研グループ(1955)以降の先行研究の解釈をそれと比較する．

大河原地域の位置及び地質図をそれぞれ，第1図a, bに示す．これらの岩相グループの認定は野外での岩相認定および鏡下での岩石記載を基本としている．本研究では，大河原地域の領家深成岩類を，活動時期の順に，非持トーナル岩，生田花崗岩，南向(みなかた)花崗岩及び苦鉄質岩類の4つの岩型に区分し，南向花崗岩及び苦鉄質岩類については，それぞれ粗粒相と細粒相とに細分した．これらの貫入関係及び活動時期を第2図aに示す．なお，南向花崗岩は，大河原地域図郭外の南西方向に広く分布し，天竜峡花崗岩の模式地まで岩相的に連続していると解釈されており，天竜峡・南向花崗岩と表現されたり(山田ほか，1974)，天竜峡花崗岩に含められたり(Yamada and Hayama，1977)している．しかしながら，Yamada and Hayama (1977)では，その著作 (巡検案内書)の目的のための便宜的扱いであるとされているし，詳しくは述べないが既存の年代値の報告に基づくと，天竜峡花崗岩とされる岩型には異なる活動時期の岩相が混在している可能性もあるため，本研究では大河原地域周辺の研究によって命名された南向型 (Hayama，1959)を用い，模式地付近の天竜峡花崗岩と区別して表記する．

領家変成岩類は，変成泥岩・変成砂岩・変成珪質岩から構成される(第1図b)．これらの変成岩のうち，北西端付近の四徳鉱泉周辺に分布するものは，西部～北西部にかけて大河原地域の図郭外に連続して広く分布する岩体

の一部と思われる．これ以外は全て，大きさは様々であるが領家深成岩類中に包有される捕獲岩体である．ただし，これらの捕獲岩体中の変成岩類の構造は，ほとんどの場合，周囲の領家深成岩類の片麻状構造と概ね調和的である．変成泥岩の鉱物組み合わせには，明確ではないものの系統性があり，伊那山脈の稜線北部及び稜線より西の小渋川桶谷（おけや）橋付近の苦鉄質岩体周辺を除く部分では，ざくろ石を含む鉱物組合せが，小渋湖から高森山を結ぶ地域より南東の伊那山脈の稜線付近及び小渋川桶谷橋付近の苦鉄質岩体周辺ではカリ長石+菫青石±珪線石の組合せが卓越する．いずれも領家深成岩類に包有されているか貫入境界のごく近傍であるため，広域変成作用と領家深成岩類による接触変成作用とを重複して被っており，全体としては，最終的にカリ長石+菫青石の組合せを記録しているものと考えられる．

本図幅地域の領家深成岩類は，南向花崗岩が最も広く分布し，伊那山脈主稜線北部の高森山付近から，大河原地域南端部まで分布する（第1図b）．大局的には分布域北西部には南向花崗岩細粒相が，南東部には広く粗粒相が分布する．北西部の南向花崗岩細粒相の周囲には，非持トーナル岩が分布する．小渋湖畔から北東に向けて延びる尾根及びその両翼には，生田花崗岩のまとまった分布が認められる．さらに，これらの全ての岩相中には，大小の苦鉄質岩類の貫入岩体や捕獲岩体が存在する．大河原地域に分布する領家深成岩類のモード組成を第2図bに示す．領家深成変成コンプレックスの苦鉄質深成岩類の記載には，かんらん石を含み角閃石の巨晶を多く含むものにはコートランダイトという岩石名が伝統的に使われており，これらは，IUGS Subcomission（Le Maite，2002）の名称では，かんらん石単斜輝石斜方輝石含有角閃石岩，かんらん石単斜輝石斜方輝石斜長石含有角閃石岩，斜長石含有かんらん石角閃石岩，そして，かんらん石斜長石含有角閃石岩といった様々な岩石名となる．このように，IUGSの定義に準拠した場合，構成鉱物の量比の違いにより，意味合いとしては同一グループの岩相であっても異なった名称となり，冗長で分かりにくい上，先行研究で言及されている岩相との対応関係が不明確となるため，以下の記述では，かんらん石もしくはその仮像を含み角閃石の巨晶（オイコクリスト）を多く含む粗粒苦鉄質深成岩について，特定のグループの岩相を指す名称としてコートランダイトを用いる．

それぞれの岩型の特徴と相互関係についての概略は以下の通りである．先行研究の地質図及び解釈と本研究の岩型区分や分布表現の違いとを分かりやすく説明するために，貫入順序や分布上の配列とは異なる順に説明する．

苦鉄質岩類は，非持トーナル岩，生田花崗岩，南向花崗岩いずれの分布域にも存在し，小渋湖の桶谷橋周辺より北西では細粒斑れい岩ないし石英閃緑岩から構成されるが，桶谷橋周辺の岩体以南には，極粗粒の角閃石斑れい岩や，いわゆるコートランダイトが単体または細粒苦鉄質岩内に産する．南向花崗岩細粒相中の苦鉄質岩類は，数10 cm–数 cmの細粒斑れい岩～閃緑岩の暗色包有岩として産することが多いが，地質図ではそれらが集中して産し，露頭において苦鉄質岩類が優勢な岩相を示す部分を苦鉄質岩類の分布域として表現している．

南向花崗岩中の暗色包有岩は，露頭～地質図スケールでは周囲の南向花崗岩に包有される産状を示し，ほとんどの場合，細粒苦鉄質岩から構成される．暗色包有物（苦鉄質岩類細粒相）とホストの南向花崗岩との露頭内の岩相境界部ではマグマ混合（mixing）様にシャープな境界で接して様々な程度に混交（mingling）する（第3図a，b）か，ミクロにはディフューズな境界を示し数mmないし数cmで漸移的に変化する産状を示し，しばしば境界部～周縁部が閃緑岩質の岩相を呈する．従来，こうした細粒苦鉄質岩類は，非持トーナル岩の構成岩相とみなされ，本研究で南向花崗岩細粒相中の苦鉄質岩類と表現した部分及びその周辺の南向花崗岩細粒相は，既存の地質図では非持トーナル岩分布域として地質図に表現されてきた（領家団研研究グループ，1955；Yamada，1957，1967；Hayama，1959；下伊那誌編纂会，2006）．こうした理解を前提として，先行研究においては，非持トーナル岩は，一般に顕著な片麻状構造を示すものの，四徳川付近では片麻状構造のない花崗閃緑岩に地質図スケールにおいて漸移（領家団研グループ，1955），あるいは，より片状構造が弱く珪長質な岩相に漸移し，南向花崗岩との区別が困難である（Yamada，1957）などと記載されてきた．しかしながら，本研究の観察結果に基づくと，大河原地域の苦鉄質岩類は，少なくともそのほとんどが非持トーナル岩の構成岩相ではなく，南向花崗岩細粒相と同時期の活動として識別される．そして，先行研究によって非持トーナル岩が漸移したほぼ塊状の花崗閃緑岩とされた四徳川流域に分布する岩相は，南向花崗岩と解釈される．苦鉄質岩類は，南向花崗岩細粒相のみならず，粗粒相とも一部で相互貫入の関係を示す（第3図a，b）．南向花崗岩細粒相は，粗粒相に比べて明らかに細粒である点と，小規模な苦鉄質包有岩をしばしば含む点で区別される．本研究において同時期の活動であると認定した南向花崗岩中の苦鉄質岩類を，Yamada（1957）では，明瞭な境界（界線）を持たずに角閃石黒雲母片麻岩が混在する表現で描いている．従って，岩型名や岩相名（片麻岩）の認定は異なるものの，産状の観察結果自体は本研究と概ね整合的であると考えられる．

南向花崗岩粗粒相は，一般に片麻状構造を有する黒雲母花崗岩を主体とする．代表的な岩相は，黒雲母がリボン状に連なって強い片麻状構造を有するとともに斑状の長石結晶をしばしば含み，先行研究で指摘されているように，模式地付近の天竜峡型に類似する（第3図c）．片麻状構造はところによって程度が異なり，概して中央構造

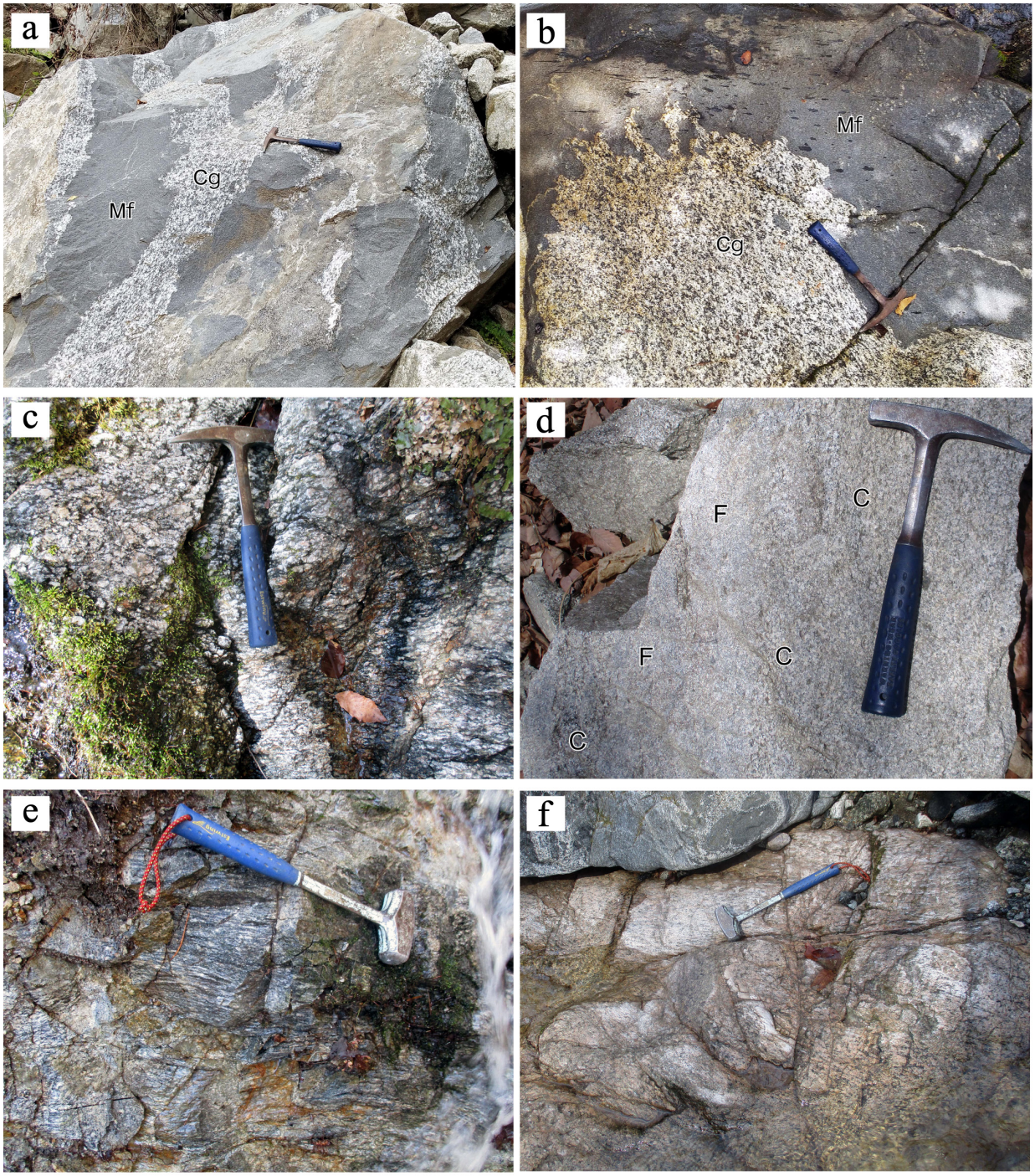

第3図　大河原地域に産する領家深成岩類の野外での産状．(a) 生田花崗岩粗粒相 (Cg) 中の不規則な形態の苦鉄質岩類細粒相 (Mf) の包有物．Mfの文字のある包有物の境界は，写真 (b) のような入道雲様を示す．(b) 生田花崗岩粗粒相 (Cg) と苦鉄質岩類細粒相 (Mf) の境界．境界部では，両岩相が相互に貫入し，入道雲様を示す．(c) 片麻状構造の発達する南向花崗岩粗粒相．(d) 南向花崗岩細粒相の産状．数cmの範囲で急激に粒度が変化し，粗粒部 (C) と細粒部 (F) とが不規則に分布する．(e) 縞状構造の発達する非持トーナル岩．(f) 片麻状構造を示す生田花崗岩．

Fig. 3　Field occurrences of Ryoke Plutonic Rocks in the Ogawara area. (a) Irregurarly shaped enclaves (Mf) of fine-grained facies of mafic rocks in the coarse-grained facies of Ikuta Granite (Cg). The contact between the enclaves and the host granite shows crenulate or caspate structure as in the panel (b). (b) Contact between fine-grained facies of mafic rocks (Mf) and coarse-grained facies of Ikuta Granite (Cg). (c) Coarse-grained facies of Ikuta Granite showing gneissose structure. (d) Mode of occurrence of fine-grained facies of Ikuta Granite. Grain size changes rapidly within a few centimeters and the relatively coarse-grained portion (C) and fine-grained portion (F) were irregularly distributed. (e) Hiji Tonalite with banded structure. (f) Ikuta Granite showing gneissose structure.

線に近づくにつれてその程度が強くなる傾向があり，眼球片麻岩状の岩相を呈する場合もある．野外で識別できる岩相上の特徴は，本研究地域の領家深成岩類の中で最も有色鉱物に乏しい点である．苦鉄質岩類の暗色包有岩は，南向花崗岩粗粒相では普遍的に含まれるわけではなく，ところにより集中して存在する．そのような場合，暗色包有岩を包有するホストである南向花崗岩粗粒相は有色鉱物に富む傾向があり，角閃石含有黒雲母花崗閃緑岩から構成される．ただし，角閃石含有黒雲母花崗閃緑岩が必ず暗色包有岩を多く含むわけではない．このため，有色鉱物に富み片麻状構造が顕著な場合，野外において非持トーナル岩や生田花崗岩との識別が困難である．

南向花崗岩細粒相の代表的な岩相は，塊状黒雲母花崗岩で，見かけ上，粗粒相よりもさらに優白質である場合が多い（第3図d）．粗粒相と同じく，苦鉄質包有岩を多く含む露頭では有色鉱物が多く角閃石を含むことがあり，しばしば花崗閃緑岩質である．また，粒度も単一の露頭内で変化し，相対的に粗粒なものは粗粒相分布域に産する相対的に細粒な岩相とほぼ区別できない．細粒相は塊状に近い場合が多いが，片麻状構造を示す場合もある．細粒相は稀にざくろ石や白雲母を含む場合がある．南向花崗岩は，領家団研グループ（1955）では“片麻岩源ミグマタイト”あるいは片麻状花崗岩と呼ばれ，非持トーナル岩（“塩基性岩源ミグマタイト”）に極めて密接に伴われ，しばしば両者が狭い範囲で漸移すると記述されている．

非持トーナル岩は，大河原地域北東部の，駒ヶ根市の伊那山脈稜線部から南西に向け分布する岩体と，その延長部の岩体，そして本図幅地域北西端に分布する．一般に粗粒～中粒で顕著な片麻状構造を示すトーナル岩質岩から構成される．しばしば，角閃石や黒雲母の濃集した優黒質部と斜長石や石英に富む優白質部とが数mm間隔で縞状に産する（第3図e）．それ以外に，厚さ数10 cm～数 cmの層状の苦鉄質部を含む場合もある．南向花崗岩粗粒相とは，南向花崗岩粗粒相のほうが粗粒である点と，全体として有色鉱物に乏しい点，そして，南向花崗岩粗粒相では有色鉱物がリボン状に連続するものの，非持トーナル岩のように優黒質部と優白質部が縞状構造を示さない点で区別される．南向花崗岩粗粒相と非持トーナル岩との境界は，伊那山脈の高森山林道沿いのカッティングや四徳川支流の小河内川流域において，ほぼ連続した露頭が観察されるが，肉眼的な特徴が類似している上に，両岩相の片麻状構造が調和的であるため，風化によって両岩相の正確な境界を識別することが困難である．ただし，このことは，両者が漸移することを意味するものではない．

生田花崗岩は，先行研究においては，塊状に近い花崗岩質岩であると識別されてきた（Yamada, 1957, 1967）．しかしながら，本図幅で区分した生田花崗岩は全体的に片麻状構造を有し，非持トーナル岩や南向花崗岩粗粒相の片麻状部と酷似する（第3図f）．先行研究の記載において生田花崗岩の典型的な岩相とされてきた塊状の花崗岩は，小渋湖南西の「飯田」図幅地域に卓越する（河田・山田，1957）．その他の先行研究では，本研究地域の南向花崗岩細粒相の分布域の一部が生田花崗岩に含めて表現されている（例えば，Hayama and Yamada, 1977）．さらに，Yamada（1957, 1967）の記載では，生田花崗岩の特徴として多量の苦鉄質岩や変成岩の捕獲岩を含むとしている．また，Yamada（1957）では，一部において生田花崗岩は片状ないし斑状の場合もあり，生田花崗岩が片麻状花崗岩に漸移する産状も認められると述べている．すなわち，先行研究間で生田花崗岩の特徴の認定や分布に相違があり，それらの記述を参考に本研究の区分に照らすと，塊状で多量の苦鉄質岩の包有物を含むと記述されている部分は，本研究の南向花崗岩細粒相に相当し，片状ないし斑状の岩相と，生田花崗岩が漸移するとされている片麻状花崗岩は，主として南向花崗岩粗粒相に相当し，一部，非持トーナル岩を含むと解釈される．なお，Yamada（1957, 1967）では，本研究の生田花崗岩南東域の滝沢左岸に滝沢花崗閃緑岩（Yamada, 1957では滝沢花崗岩）の独立した岩体を描いており，この岩体は生田花崗岩から漸移する局所的な岩相とされている．本研究では，この滝沢花崗岩は生田花崗岩周囲の南向花崗岩に含めた．

生田花崗岩は，多くの場合，非持トーナル岩や南向花崗岩とよく似た片麻状構造を示すが，南向花崗岩と比べると，角閃石に富み有色鉱物全体としても富む特徴をもつ．また，南向花崗岩には，露頭においてしばしば苦鉄質岩類の包有岩が含まれるのに対し，生田花崗岩にはこれが認められない．一方，非持トーナル岩とは有色鉱物の量比も岩相も酷似するが，非持トーナル岩にしばしば見られる縞状構造を持たず，多くの場合，生田花崗岩には特徴的に自形の角閃石が含まれる点で区別される．さらに，生田花崗岩には副成分鉱物として褐れん石が普遍的かつ比較的多量に含まれるのに対し，非持トーナル岩や南向花崗岩はこれを欠くか，ごくわずかしか含まれない．褐れん石の有無を野外で識別するのは一般には困難であるが，生田花崗岩ではしばしばルーペで識別可能な粒度の褐れん石が含まれる．

大河原地域を構成する領家深成岩類について，既存の研究で名称の異なる岩石名部分を除いて中部地方領家帯全体で使用されている岩型名で表現すると，非持型，天竜峡型（南向花崗岩に相当），生田型（もしくは三都橋（みつはし）・生田型）及び苦鉄質岩類となる．先行研究に基づいて各岩型の特徴をあらためて整理すると，以下の通りとなる．(1)いずれの岩型も多様な岩相から構成される．例えば非持型は花崗閃緑岩，トーナル岩，石英閃緑岩から構成されるとともに苦鉄質岩類（変輝緑岩や角閃岩と記載）を伴い，天竜峡型は花崗岩，花崗閃緑岩，トーナル岩及び少量の斑れい岩（苦鉄質岩）から構成される．生田型は花崗

閃緑岩，トーナル岩及び花崗岩から構成され，多量の苦鉄質岩や変成岩の捕獲岩を含む．これらの捕獲岩は，変輝緑岩と記述されている場合もある．(2) 非持型及び天竜峡型は，一般に片麻状構造で特徴づけられるが，片麻状構造が弱く塊状に近い部分もある．一方，生田型は一般に塊状に近いが，片麻状構造を示す部分もある．(3) いずれの岩型も，相互の接触部付近で漸移する産状が観察され，場合によっては岩型の判定が不可能な中間的岩相を示す．

以上の整理に基づくと，大河原地域の領家深成岩類は，片麻状構造の有無や苦鉄質捕獲岩の有無といった野外での産状や，モード組成（岩石名の違い）による記載的特徴からは，ほとんど区別できないことになる．そして，実際に，(3) のように帰属の判定が不可能な中間的岩相の存在が報告されている．こうした問題のいくつかは，上述の通り，本研究の観察結果をもとに岩型ごとに分布域を再整理することによって解消されるが，いずれにせよ，野外における産状及び鏡下での記載による識別の困難さが，岩型（地質単元）の定義に不確かさをもたらしている．

2. 2　大河原地域の領家深成岩類の固結年代

大河原地域から報告されている年代値は必ずしも多くないため，以下の記述では，同じ岩型の周辺地域から得られた年代も含めて整理する．ここで問題となるのは，これまで述べてきたように各岩型の定義が先行研究ごとに不明確であるため，年代測定試料が，真にその岩型に属するものであるのか，逆に，周辺地域で報告された年代が，真に大河原地域の岩型と対比されうるものであるのかについて，必ずしも確証がない点である．加えて，各岩型間の漸移する産状や中間的な産状の存在は，それぞれの岩型間でのマグマ混合や同化作用の可能性を排除できず，そうであるとすると，同位体年代の場合，系の同位体平衡が成立していたか否かの問題も孕んでいる（詳細な議論は山崎，2025 を参照されたい）．そこで，本論では，それぞれの岩体の固結年代として，CHIME年代とジルコンU–Pb年代とを現時点では最も信頼性が高いものとする．ただし，モナザイトCHIME年代は，同一の岩体・岩型から得られたジルコンU–Pb年代よりも系統的に古い傾向をもつ可能性が指摘されており，それらの一部は母岩の領家変成岩類からのモナザイトの混入に起因する可能性も示唆されている（例えば，Takatsuka *et al.*, 2018）．本論ではこうした議論については立ち入らず，ジルコンU–Pb年代とCHIME年代の両方が報告されており，かつ，ジルコンU–Pb年代のほうが若い場合はジルコンU–Pb年代を固結年代として採用する．

Nakamura *et al.*（2022）は，本図幅地域のマイロナイト帯北部地域の試料からジルコンU–Pb年代を求め，85.6 ± 1.5 Ma，77.7 ± 0.4 Ma，及び70.9 ± 0.3 Maの3つの年代パルスを報告した．Yokoyama *et al.*（2016）は，日本全国から約400試料のウラニナイト及びトーライトCHIME年代を報告した．このうち3試料が本図幅地域の南向花崗岩からのもので，72.6 ± 0.9 Ma，72.2 ± 1.2 Ma，及び71.6 ± 1.0 MaのウラニナイトCHIME年代を示す．なお，3試料のうち1試料が採取された位置（桑原の滝）の南向花崗岩は，Yamada（1957）によって，典型的な天竜峡花崗岩と岩相的に同一であると述べられている．よって，Nakamura *et al.*（2022）による70.9 ± 0.3 Maの年代パルスは，南向花崗岩及びそれと同時期に活動した苦鉄質岩類の固結年代に相当すると判断される（第2図a）．坂島ほか（2000）は，本図幅地域内と判断される高森山林道沿いの“塊状”の非持トーナル岩から86 ± 7 MaのジルコンU–Pb SHRIMP年代を報告した．ここで“塊状”と表現されるものは，非持トーナル岩を特徴づける縞状構造を欠く岩相という意味で，片状構造を欠くわけではない． Nakamura *et al.*（2022）による85.6 ± 1.5 Maの年代パルスは，この坂島ほか（2000）による年代と一致し，非持トーナル岩の固結年代に相当すると解釈される（第2図a）．坂島ほか（2000）は，より北部の溝口地域の非持トーナル岩の縞状部から71 ± 3 MaのジルコンU–Pb SHRIMP年代も報告しているが，この年代値は，上述の南向花崗岩及びそれと同時期に活動した苦鉄質岩類の固結年代と一致するため，恐らく縞状の苦鉄質部分の年代であり，少なくとも年代測定を行った試料においては，非持トーナル岩の苦鉄質部は後の貫入体であることを意味していると推察される．生田花崗岩からは，ジルコンU–Pb年代やCHIME年代の報告はなく，84.1 MaのRb–Sr全岩アイソクロン年代（Kagami, 1973）及び142 MaのRb–Sr全岩アイソクロン年代（Hayama and Yamada, 1977）が報告されているのみである．先行研究においては，生田花崗岩は，大河原地域のその他全ての岩型に貫入する最も若い岩型であると解釈されており，もしもこれが正しいとすると，Rb–Sr全岩アイソクロン年代は，上に述べた最近のジルコンU–Pb年代に基づく他岩型の固結年代とも大きく矛盾する．先に述べたように，生田花崗岩には先行研究による非持トーナル岩や南向花崗岩（及び同時期の苦鉄質岩類）との識別上の混乱が見られた．従って，全岩アイソクロン年代測定に用いた試料に他岩型の試料が混入している可能性も排除できず，大きく異なるRb–Sr全岩アイソクロン年代のどちらかを採用する根拠を得ることは困難である．ただし，84.1 Maの年代（Kagami, 1973）に意味がある場合は，生田花崗岩が非持トーナル岩の一部であるか，あるいは本研究の非持トーナル岩の部分を生田花崗岩として分析した可能性が示唆される．一方，本研究においては，地質分布や他岩型との関係から，生田花崗岩の貫入時期を非持トーナル岩と南向花崗岩（及び苦鉄質岩）との間と想定していることから，消去法的に，Nakamura *et al.*（2022）の77.7 ± 0.4 Maのパルスが生田花崗岩の固結年代に相当するものと推定し，これを採用する（第2図a）．

3．分析手法

全岩化学組成分析のための岩石試料は，厚さ数mmのスラブもしくはチップ状に切断し，切断面に付着した岩石カッターの金属をダイヤモンドディスクで削り取った後，イオン交換水で30分以上超音波洗浄した．洗浄した試料は110°Cのオーブンで一昼夜乾燥させ，タングステンカーバイド乳鉢で粗粉砕した後，四区分法にて縮分し，地質調査総合センター共同利用実験室（GSJ-Lab.）設置の全自動粉砕装置（タングステンカーバイド・ミル）にて粉末岩石試料を作成した．なお，全自動粉砕装置による粉砕にあたっては，WとNi以外には装置による深刻なコンタミネーションはないことが確認されている（Yamasaki, 2018）．

全岩主成分化学組成は，GSJ-Lab. 設置の蛍光X線分析装置（XRF：PANalytical Axios）を用いて分析し，分析用ガラスビードの作成法を含む分析手法はYamasaki（2014）に従った．全岩微量元素組成は，XRF分析に用いたガラスビードを用いて，GSJ-Lab. 設置のレーザーアブレーション誘導結合プラズマ質量分析装置（LA-ICP-MS）を用いて分析した．分析装置及び分析手法の詳細はそれぞれYamasaki *et al.*（2015）及びYamasaki and Yamashita（2016）に示されている．XRF及びLA-ICP-MS分析の精度はそれぞれ，米国地質調査所（USGS）地球化学標準物質BCR-2（Wilson, 2000）及び産業技術総合研究所地質調査総合センター地球化学標準物質JA-1（Imai *et al.*, 1995）を用いてモニターした．第1表にそれらの地球化学標準物質の分析結果を示す．

4．検討試料と分析結果

検討試料の代表的な分析結果を第1表に示す．分析試料は162試料と多数であるため，全ての分析値は付録として産総研リポジトリに公開している（URLは第1表脚注に示した）．

4.1　検討試料の岩石記載

これまで述べてきたように，大河原地域を構成する領家深成岩類の各岩型は，岩相変化が大きく，紙面の都合上，検討試料全ての特徴を記載することは困難である．そこで，各岩型を代表する典型的な岩相について以下に記述する．

非持トーナル岩

顕著な片麻状構造を示す角閃石黒雲母トーナル岩及び花崗閃緑岩から構成される．構成鉱物は斜長石，石英，黒雲母，ホルンブレンドを主体とし，少量のアルカリ長石を含む場合がある．構成鉱物の量比はところによって異なり，稀に融食形を示す単斜輝石を含むこともある．完晶質で，長柱状のホルンブレンドと板状の黒雲母とが配列し，それらが連結した部分や連結して濃集した優黒質部と，石英長石質の優白質部とが数 mm程度の間隔で繰り返し現れることにより，片麻状構造を示す（第4図a）．主成分鉱物の粒度は1.5 mmから0.2 mm程度まで連続的に変化する．斜長石は半自形で弱い累帯構造が発達する場合がある．アルカリ長石は他形で粒状に産し，単純双晶を示すことがある．石英は他形で他の鉱物の粒間を充填し，弱い波動消光が認められる．黒雲母は自形–半自形で，黒褐色–淡褐色の多色性を示す．ホルンブレンドは半自形–他形で，しばしば虫食い状の組織を示す．暗帯緑褐色もしくは暗褐色–淡褐色の多色性を示し，単純双晶を示す場合がある．単斜輝石が含まれる場合，他形・粒状もしくは短柱状融食形結晶として産し，周囲をホルンブレンドに取り囲まれるとともに，結晶内にもブレッブ状にホルンブレンドが生じている（第4図b）．

生田花崗岩

主として粗粒–中粒角閃石含有黒雲母トーナル岩，角閃石含有花崗閃緑岩及び黒雲母花崗閃緑岩から構成され，ところにより黒雲母モンゾ花崗岩を伴う．ほぼ普遍的に弱い片麻状構造を示し，塊状に近い岩相は稀である．ただし，非持トーナル岩に認められるような縞状の片麻状構造は示さず，また，概して南向花崗岩よりも片麻状構造が弱い傾向にある．生田花崗岩の岩石記載上の特徴は自形性の強いホルンブレンドを含むこと（第4図c）と，自形で粒径の大きな褐れん石（最大長径3.0 mm程度）を多量に含むこと（第4図d）である．典型的な岩相の鏡下での産状は，完晶質で，板状の黒雲母が弱く配列する．ただし，長柱状のホルンブレンドの長軸は必ずしも定向配列を示さず，また，黒雲母も部分的に濃集して弱い定向配列を示すものの，連続性は良くない．主成分鉱物の粒度は5.0 mmから0.2 mm程度まで連続的に変化する．斜長石は自形–半自形で累帯構造を示すことがある．また，石英との粒界でミルメカイト組織を示すことがある．石英は他形で他の鉱物の粒間を充填し，弱い波動消光が認められる．アルカリ長石は他形で他の鉱物の粒間に不定形に産する．ホルンブレンドは自形–半自形で，暗緑褐色もしくは暗褐色–淡褐色の多色性を示し，単純双晶を示す場合がある．黒雲母は自形–半自形で，暗赤褐色–淡褐色の多色性を示し，クロット状に濃集する場合もある．長径2.1 mmに達する自形の褐れん石を特徴的に多量に含む．褐れん石は単純双晶や累帯構造を示すことがある．

南向花崗岩粗粒相

一般に片麻状構造を有する黒雲母花崗岩を主体とする．片麻状構造の程度や鉱物の量比はところによって変化し，岩相的には角閃石含有黒雲母花崗岩も認められる．暗色包有岩を包有する場合，周辺の南向花崗岩粗粒相は有色鉱物に富む傾向があり，角閃石含有黒雲母花崗閃緑岩か

第1表 大河原地域に産する領家深成変成コンプレックス構成岩類及び地球化学標準試料の全岩主成分 (wt.%)・微量成分 (μg g^{-1}) 組成分析値.

Table 1 Whole-rock major element (wt.%) and trace element (μg g^{-1}) geochemistry of rocks for Ryoke Plutono-Metamorphic Complex in the Ogawara area and reference materials.

	Hiji Tonalite					Ikuta Granite					Minakata Granite									
											fine-grained facies					coarse-grained facies				
	OG117	OG303	OG010	OG026B	OG004	OG031	OG033	OG314	OG020	OG029	OG316	OG052	OG212	OG402C	OG110	OG114	OG035	OG016	OG019A	OG013
SiO_2	65.41	66.56	61.31	67.55	63.02	64.22	61.90	66.17	71.88	69.12	73.19	70.94	69.91	70.62	71.84	71.13	69.71	72.33	72.99	75.98
TiO_2	0.58	0.54	0.83	0.46	0.69	0.55	0.66	0.43	0.30	0.30	0.24	0.33	0.31	0.28	0.33	0.30	0.37	0.25	0.25	0.13
Al_2O_3	16.59	15.66	17.80	15.99	16.79	17.34	17.26	16.71	14.59	15.93	13.91	15.23	15.03	15.85	15.11	15.38	15.17	14.46	13.78	12.88
Fe_2O_3*	5.08	4.59	6.66	4.09	5.97	5.42	6.90	4.60	2.63	3.12	1.79	2.86	2.95	2.68	2.61	2.42	3.64	2.43	2.47	1.56
MnO	0.08	0.09	0.11	0.07	0.11	0.08	0.12	0.08	0.04	0.06	0.03	0.05	0.05	0.05	0.06	0.04	0.07	0.04	0.06	0.03
MgO	1.10	1.92	1.81	1.19	1.70	0.65	0.84	0.53	0.32	0.30	0.43	0.61	0.88	0.59	0.62	0.41	0.69	0.34	0.44	0.19
CaO	4.18	4.11	6.08	4.13	5.06	4.24	4.75	3.96	2.02	3.13	1.27	3.13	3.56	3.82	2.99	2.69	3.08	1.67	1.59	1.05
Na_2O	4.34	3.73	3.79	3.83	3.81	4.28	4.51	4.14	3.44	3.69	2.02	4.00	3.36	4.01	3.60	3.56	3.44	3.87	3.70	3.42
K_2O	2.02	2.63	1.69	2.16	2.00	2.68	2.17	2.57	4.34	3.96	6.58	2.30	3.21	1.77	2.57	3.54	3.50	4.41	4.15	4.57
P_2O_5	0.14	0.11	0.17	0.13	0.16	0.14	0.17	0.10	0.05	0.07	0.03	0.11	0.05	0.08	0.09	0.06	0.08	0.06	0.06	0.03
Total	99.50	99.92	100.26	99.59	99.30	99.59	99.27	99.30	99.61	99.66	99.46	99.56	99.31	99.73	99.81	99.51	99.76	99.85	99.49	99.83
LOI	0.71	0.77	0.69	0.59	0.90	1.84	0.47	0.60	0.57	0.36	0.86	0.48	0.51	0.50	0.73	0.62	0.69	0.85	0.45	0.49
Sc	11.4	13.0	20.5	9.1	16.6	15.2	17.8	12.5	8.9	7.7	4.0	7.5	13.8	5.6	7.5	6.6	11.6	3.8	7.8	4.9
Ti	3493	3223	5258	2630	4213	3489	3964	2402	1707	1735	1313	2156	1856	1751	1984	1842	2191	1402	1435	780
V	52.3	80.3	99.3	47.8	79.8	43.1	52.1	32.6	18.8	18.2	19.2	17.3	37.0	17.9	21.0	25.2	38.7	16.9	16.2	10.7
Cr	8.7	24.5	14.3	12.3	34.6	10.5	14.8	2.1	12.2	3.1	8.5	24.4	22.4	35.7	11.9	15.2	20.8	4.7	12.9	12.9
Mn	639	727	955	542	892	716	923	616	348	501	227	458	434	410	473	341	606	335	486	251
Ni	3.4	8.4	6.9	2.6	16.2	4.7	13.6	0.9	4.7	1.5	0.6	8.9	6.5	12.0	3.9	6.1	19.3	2.4	6.9	6.1
Zn	87.6	70.9	107.0	68.1	109.4	84.5	114.1	91.6	68.0	76.4	36.6	106.2	50.9	59.0	95.2	53.6	100.7	85.0	65.9	54.2
Rb	102.3	110.8	60.3	79.0	81.7	50.8	60.9	39.0	96.7	88.2	157.6	68.0	76.3	37.0	87.7	89.8	106.0	115.1	114.1	108.3
Sr	301	270	423	283	378	485	429	367	253	324	173	457	264	384	369	220	287	150	154	98
Y	43.1	24.5	27.3	25.4	36.8	21.0	23.9	16.4	20.0	20.8	9.8	14.4	14.7	9.3	11.2	17.1	24.7	17.1	21.3	21.3
Zr	251.9	137.2	229.2	176.8	241.7	587.7	736.9	474.7	312.4	381.2	210.8	189.1	137.2	147.3	186.6	189.1	204.9	135.9	137.9	105.7
Nb	10.75	7.01	14.31	13.67	9.74	15.44	13.81	10.04	8.42	7.92	6.87	7.39	6.16	10.08	9.85	10.67	9.73	8.55	10.56	7.03
Cs	4.69	5.05	1.70	2.32	2.28	1.92	2.44	2.24	1.14	1.62	2.09	1.80	3.26	0.98	5.61	4.01	2.46	2.27	1.00	1.64
Ba	482	477	639	366	632	2508	1738	2698	2614	2723	838	954	870	524	974	636	680	800	684	371
La	33.65	15.52	25.83	16.87	25.91	80.49	99.27	57.71	85.40	68.27	31.47	19.68	18.94	21.17	28.92	26.63	24.85	31.11	18.79	14.78
Ce	94.78	43.20	69.42	53.44	75.56	192.57	237.78	157.24	207.74	180.47	93.84	52.43	46.05	50.93	82.48	71.58	65.85	82.28	56.89	45.92
Pr	10.94	5.53	7.72	6.78	9.33	20.52	21.95	15.51	19.46	18.67	8.99	5.42	5.49	5.69	7.07	7.96	7.50	8.49	5.59	5.14
Nd	37.73	19.34	28.92	24.27	38.28	63.57	73.63	48.92	65.87	56.78	33.36	19.58	18.71	19.42	28.00	28.03	30.57	30.13	22.71	19.22
Sm	9.64	4.35	5.75	4.05	8.91	11.21	11.66	8.56	8.18	9.68	5.45	3.88	3.55	3.90	4.99	6.40	4.96	7.17	5.03	4.52
Eu	1.35	1.24	1.25	0.93	1.42	2.54	2.90	2.59	1.84	2.46	0.80	1.45	0.97	1.02	1.16	1.17	1.12	0.79	0.60	0.61
Gd	8.39	4.58	7.21	5.02	7.07	4.86	8.34	5.23	5.47	5.90	3.62	3.23	3.07	2.51	3.60	3.42	4.85	4.56	3.93	3.69
Tb	1.33	0.66	0.90	0.74	1.18	0.69	0.97	0.61	0.80	0.83	0.45	0.58	0.57	0.32	0.48	0.71	0.74	0.53	0.59	0.65
Dy	8.01	4.41	4.49	4.49	6.41	4.04	5.34	3.75	3.71	4.16	2.27	2.88	3.15	1.72	2.81	3.86	5.39	3.10	4.25	4.13
Ho	1.52	0.85	0.74	0.78	1.24	0.87	1.12	0.70	0.74	0.82	0.46	0.58	0.48	0.34	0.55	0.89	0.98	0.53	0.84	0.74
Er	4.78	2.91	2.48	2.38	3.57	2.65	3.06	1.88	1.86	2.40	1.19	1.68	1.74	0.92	1.06	2.45	2.75	1.59	2.55	2.40
Tm	0.61	0.44	0.25	0.40	0.53	0.40	0.43	0.30	0.28	0.31	0.15	0.30	0.28	0.20	0.14	0.43	0.36	0.25	0.40	0.33
Yb	4.04	2.64	1.94	2.20	3.05	2.51	2.97	2.29	1.82	2.13	0.97	1.77	1.64	1.22	1.30	2.35	2.79	1.84	2.31	2.19
Lu	0.42	0.33	0.33	0.56	0.35	0.37	0.41	0.34	0.26	0.30	0.15	0.37	0.30	0.16	0.20	0.42	0.44	0.24	0.30	0.27
Hf	6.83	3.90	7.10	4.50	5.39	11.74	14.71	8.89	6.43	9.62	5.68	4.41	3.53	3.76	4.05	4.56	4.53	3.46	3.88	3.17
Ta	0.72	0.65	1.13	0.76	0.53	0.74	0.76	0.44	0.50	0.79	0.51	0.56	0.61	0.66	0.49	0.71	0.59	0.96	0.95	0.46
Pb	13.02	17.15	11.28	17.70	13.04	12.65	11.70	14.64	21.50	26.87	22.47	30.88	21.06	14.81	27.84	28.22	25.79	26.17	27.01	24.32
Th	11.05	13.85	8.39	9.90	7.68	10.76	12.55	8.38	17.97	15.19	28.45	6.45	10.24	5.13	8.65	9.23	9.05	12.48	62.01	29.31
U	5.33	1.83	1.01	1.87	0.85	1.51	2.20	1.44	0.78	2.27	1.87	0.49	1.33	0.65	1.10	1.56	1.60	1.42	1.86	2.11

Fe_2O_3* denotes total Fe as Fe_2O_3. LOI: loss on ignition, R.V.: reccommended or reference values, M.V.: measured values. Major element values for reference material is BCR-2 (*N=1*), and trace element values for reference material is JA-1 (*N=28*), and reccommended or reference values are from Wilson (2000) and Imai *et al.* (1995), respectively. The complete table of analytical results is available in the AIST repository (https://doi.org/10.50886/0002003294).

Table 1 続き.

Table 1 Continued.

	Mafic rocks									Ryoke Metamorphic Rocks					Reference materials	
	fine-grained facies			amphibolite			coarse-grained facies									
	OG410B	OG064	OG205	OG102	OG019B	OG042B	OG126A	OG116	OG126B	OG410D	OG003C	OG112	OG057	OGX05	OG311	M.V.	R.V.
SiO_2	48.45	46.60	50.35	51.62	53.30	54.03	44.21	48.10	46.65	45.47	74.63	66.31	62.37	68.02	66.75	66.75	66.75
TiO_2	1.92	1.20	1.63	1.30	0.90	1.22	0.29	0.47	0.09	3.21	0.53	0.61	0.79	0.70	0.76	0.76	0.76
Al_2O_3	17.11	18.44	20.19	18.00	18.19	18.23	17.62	8.19	21.26	16.22	11.75	16.10	16.86	16.97	16.68	16.68	16.68
Fe_2O_3*	13.30	13.59	10.28	9.85	8.77	8.56	11.65	11.27	8.37	14.33	4.29	5.14	6.83	5.30	5.82	5.82	5.82
MnO	0.21	0.17	0.19	0.18	0.23	0.14	0.18	0.17	0.11	0.17	0.14	0.17	0.17	0.08	0.07	0.07	0.07
MgO	4.85	5.76	5.03	4.65	4.39	4.22	15.60	20.42	10.67	7.18	1.66	1.92	3.11	1.86	2.04	2.04	2.04
CaO	9.83	10.36	8.78	8.82	7.57	7.47	8.84	9.97	10.81	10.65	1.76	2.42	3.33	1.04	1.54	1.54	1.54
Na_2O	2.47	2.56	2.28	3.46	5.09	3.93	0.90	0.98	1.48	2.13	2.29	3.83	3.11	1.75	2.10	2.10	2.10
K_2O	1.18	1.06	1.19	1.45	1.64	1.72	0.20	0.16	0.41	0.61	2.78	3.25	3.14	4.04	3.76	3.76	3.76
P_2O_5	0.65	0.09	0.24	0.23	0.18	0.37	0.04	0.03	0.06	0.05	0.12	0.11	0.19	0.12	0.16	0.16	0.16
Total	99.96	99.81	100.16	99.55	100.28	99.89	99.53	99.77	99.90	100.01	99.94	99.86	99.90	99.86	99.67	99.67	99.67
LOI	1.75	3.00	2.43	0.61	0.78	1.24	3.54	1.30	2.95	1.11	1.05	0.88	0.89	2.10	2.17	2.17	2.17
Sc	43.8	35.2	30.2	26.0	24.2	24.1	11.1	40.5	1.9	46.7	9.6	12.4	17.6	11.9	12.9	28.6	28.5
Ti	10863	6865	9746	7309	5315	7611	1897	2779	557	18653	2993	3379	4595	3701	3815	5133	5132
V	323.4	360.5	198.3	181.5	172.9	179.4	60.9	215.9	15.1	904.4	73.8	90.8	121.6	82.8	90.2	105.8	105.0
Cr	11.2	16.4	39.7	50.3	41.2	63.2	19.7	2092.9	13.0	19.9	62.0	38.4	143.0	59.1	44.4	9.3	7.8
Mn	1566	1285	1442	1375	1865	1258	1465	1397	896	1267	1143	1280	1294	537	480	1236	1224
Ni	3.9	5.8	9.6	19.0	12.0	16.4	138.9	367.8	41.2	11.1	39.4	29.5	49.7	16.0	8.5	3.9	3.5
Zn	102.9	95.7	97.4	101.8	182.0	85.7	91.6	84.0	55.1	89.0	155.7	86.3	383.9	98.0	100.1	94.3	90.9
Rb	56.1	29.2	57.2	77.2	106.4	150.4	6.6	6.0	20.2	23.2	134.3	119.7	165.0	147.9	147.4	11.9	12.3
Sr	426	557	426	437	397	427	282	127	616	357	158	197	212	136	159	264	263
Y	28.7	23.0	32.8	25.5	20.0	35.3	5.8	9.4	3.6	11.2	19.7	23.2	26.6	22.0	21.8	27.9	30.6
Zr	132.9	69.7	104.8	120.8	93.8	195.7	30.8	26.3	36.3	44.3	132.2	169.4	152.9	170.9	175.5	85.3	88.3
Nb	8.93	4.76	9.15	9.24	5.19	15.44	1.52	1.41	1.66	3.23	11.15	8.97	10.62	11.67	10.42	1.59	1.85
Cs	2.00	1.89	2.10	2.29	2.94	6.80	0.94	0.40	1.16	4.21	4.52	12.22	10.51	12.12	8.57	0.64	0.62
Ba	207	263	267	210	268	458	59	73	88	182	591	412	323	512	469	311	311
La	11.98	8.10	10.33	12.47	12.85	17.78	3.28	2.10	3.03	3.13	20.68	19.25	19.90	26.34	18.80	5.48	5.24
Ce	37.31	28.77	30.98	36.85	27.73	58.25	9.28	5.69	7.79	9.89	58.89	60.77	54.31	70.31	56.18	13.34	13.30
Pr	5.22	4.05	4.89	4.16	4.36	7.31	1.26	0.70	1.06	1.41	6.68	6.69	5.96	7.64	6.20	1.89	1.71
Nd	21.70	18.03	21.17	18.64	17.74	31.49	5.84	3.87	3.94	6.16	27.10	23.54	24.98	29.24	26.72	10.80	10.90
Sm	6.82	6.67	5.01	4.06	5.31	7.45	1.42	1.10	1.01	1.91	4.21	5.30	5.76	5.67	4.81	3.49	3.52
Eu	1.63	1.89	1.68	1.34	1.05	1.96	0.54	0.45	0.59	0.66	1.12	1.06	0.99	1.08	0.83	1.22	1.20
Gd	6.76	5.04	4.71	4.26	4.28	7.25	1.49	1.31	0.78	2.06	4.15	4.35	4.99	5.23	4.01	4.44	4.36
Tb	0.80	0.60	0.86	0.84	0.71	1.07	0.20	0.22	0.16	0.25	0.56	0.70	0.81	0.72	0.66	0.74	0.75
Dy	5.07	4.15	5.25	5.14	3.95	6.16	1.26	1.50	0.76	2.46	3.69	4.80	4.69	4.09	4.45	4.66	4.55
Ho	0.91	0.80	1.28	1.02	0.81	1.40	0.24	0.34	0.16	0.49	0.70	0.91	1.05	0.74	0.91	1.02	0.95
Er	2.71	2.76	3.13	2.91	2.29	3.70	0.82	0.93	0.43	1.44	2.35	2.68	3.02	2.63	2.45	3.04	3.04
Tm	0.38	0.37	0.38	0.36	0.34	0.54	0.13	0.12	0.06	0.17	0.30	0.37	0.42	0.40	0.31	0.47	0.47
Yb	2.53	2.09	2.55	3.06	1.96	3.07	0.83	0.82	0.41	1.35	1.78	3.02	2.34	2.05	2.50	3.06	3.03
Lu	0.30	0.34	0.36	0.47	0.24	0.46	0.11	0.13	0.06	0.23	0.24	0.45	0.29	0.39	0.36	0.46	0.47
Hf	3.37	2.21	4.03	2.93	1.98	3.78	0.88	1.01	0.99	1.62	4.57	4.62	3.96	4.70	4.82	2.46	2.42
Ta	0.45	0.48	0.47	0.54	0.60	0.95	0.04	0.08	0.22	0.17	1.24	0.96	0.88	0.90	0.90	0.13	0.13
Pb	7.87	5.62	10.59	10.45	14.77	7.30	2.26	2.48	4.66	5.20	52.90	21.22	135.93	23.66	84.69	6.42	6.55
Th	1.83	2.94	3.25	3.09	1.00	3.52	0.64	0.39	1.06	1.15	11.72	11.26	10.54	14.65	12.25	0.82	0.82
U	0.39	0.61	0.53	2.03	0.38	2.59	0.29	0.04	0.32	0.28	1.65	2.64	2.82	2.97	3.62	0.36	0.34

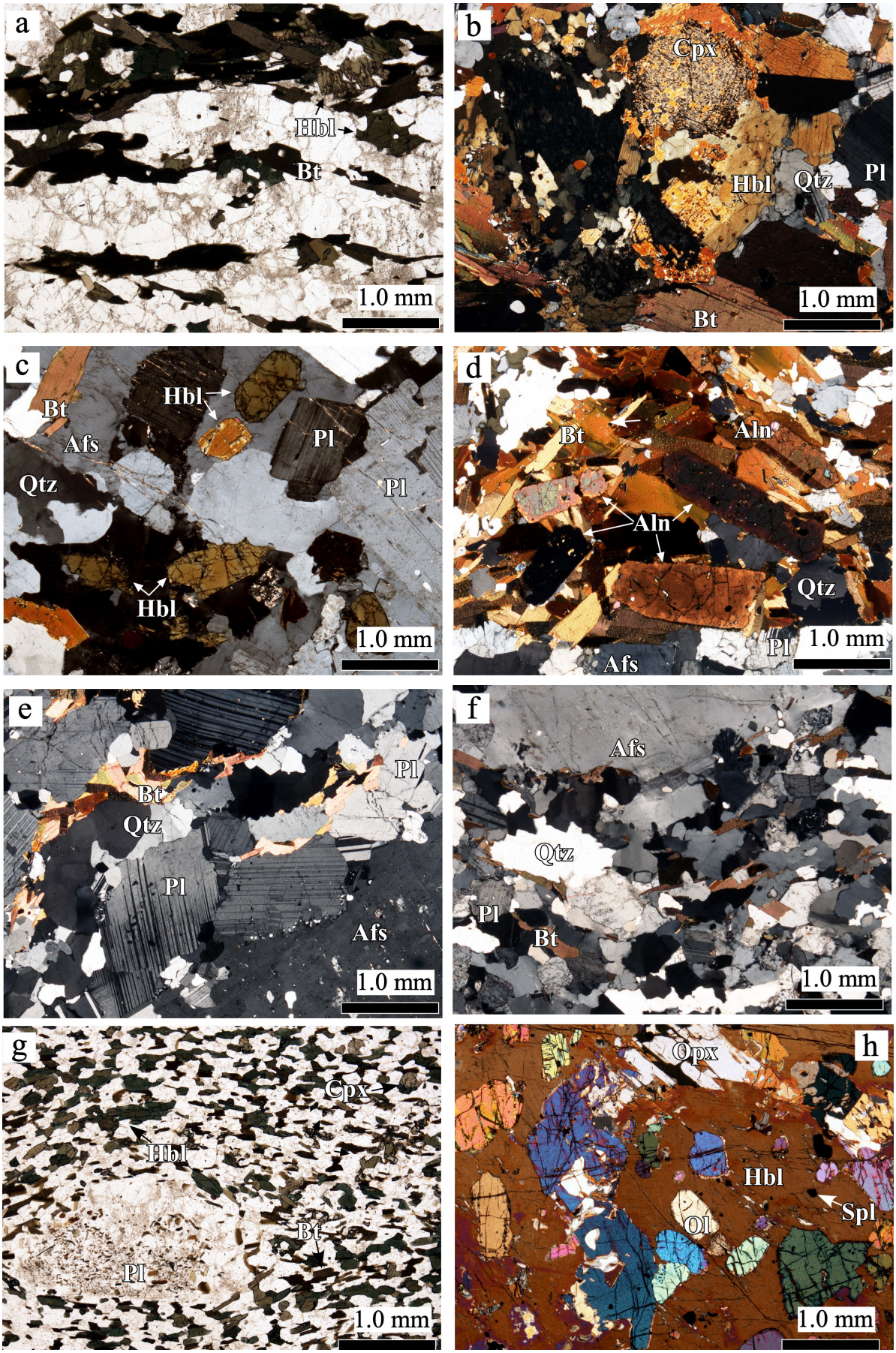
a
Hbl
Bt
1.0 mm
b
Cpx
Hbl
Qtz
Pl
Bt
1.0 mm
c
Bt
Hbl
Afs
Pl
Qtz
Pl
Hbl
1.0 mm
d
Bt
Aln
Aln
Qtz
Pl
1.0 mm
Afs
e
Pl
Bt
Qtz
Pl
Afs
1.0 mm
f
Afs
Qtz
Pl
Bt
1.0 mm
g
Cpx
Hbl
Bt
Pl
1.0 mm
h
Opx
Hbl
Spl
Ol
1.0 mm

ら構成される．代表的な岩相の鏡下での産状は，完晶質で，板状の黒雲母が長石の縁に集合して配列し，弱い片麻状構造を示す（第4図e）．ただし，黒雲母の連続性は良くない．主成分鉱物の粒度は10 mmから0.2 mm程度まで連続的に変化する．斜長石は半自形–自形で累帯構造を示す．石英は他形で他の鉱物の粒間を充填し，弱い波動消光が認められる．アルカリ長石は，ほとんどの場合他形で他の鉱物の粒間に不定形に産する．斜長石との粒界でミルメカイト組織を示すことがある．粒間の結晶が全体として長柱状ないし短柱状の半自形を示す場合もあり，半自形の結晶は稀に単純双晶を示す．アルカリ長石は，しばしば0.1 mm以下の斜長石，石英，融食形黒雲母を多量に包有し汚濁した産状を示す．ホルンブレンドは他形で，融食形を示す．暗緑色–淡緑褐色の多色性を示す．黒雲母は自形–半自形で，暗褐色–淡褐色の多色性を示し，しばしば斜長石の縁に濃集する．

南向花崗岩細粒相

南向花崗岩細粒相の代表的な岩相は，塊状優白質黒雲母花崗岩で，粗粒相と同じく，苦鉄質包有岩を多く含む露頭では有色鉱物に富み，花崗閃緑岩質である．粒度は単一の露頭内で変化する場合があり（第3図d），相対的に粗粒なものは粗粒相の相対的細粒部とほぼ区別できない．細粒相は塊状に近い場合が多いが，片麻状構造を示す場合もある．代表的な岩相の鏡下での産状は，完晶質で，平板状の黒雲母が定向配列する片麻状組織を示す（第4図f）．主要鉱物は1.5 mmから0.2 mm程度まで連続的粒径が変化する．斜長石は半自形，短柱状で弱い累帯構造を示すことがある．石英は他形で他の鉱物の粒間を充填し，弱い波動消光が認められる．アルカリ長石は，一般に粒間にも他形結晶として産し，最大粒径3.5 mm程度の短柱状の斑晶状結晶として産し，径0.1 mm未満の融食形の斜長石や黒雲母を含み汚濁している場合がある（第4図f）．黒雲母は自形–半自形で，暗褐色–淡褐色の多色性を示す．定向配列した黒雲母は比較的よく連結するが，薄片全体に連続するほどではない．

苦鉄質岩類

主として小渋川沿い及び小渋川以北の伊那山脈稜線沿いに産する小岩体及び南向花崗岩中の暗色包有岩として細粒相が産し，これらの地域以南の桶谷橋付近の岩体及び伊那山脈稜線沿いに粗粒相が産する．細粒相は黒雲母含有角閃石斑れい岩ないし石英閃緑岩から構成され，単斜輝石を含むことがある．粗粒相は角閃石斑れい岩，コートランダイトから構成される．桶谷橋付近の岩体においては，数10 cmの範囲内で鉱物組合せの同じ塊状の粗粒相と細粒相とが不規則に分布し，両者は数cmの間に漸移的かつ急激に変化する場合や，数10 cmの範囲内で鉱物組合せの同じ塊状の粗粒相中に葉片状構造をもつ細粒相が発達する場合，葉片状構造を示しつつ，有色鉱物の量

（← p. 112）

第4図　大河原地域に産する領家深成岩類の鏡下写真．(a) 非持トーナル岩．角閃石及び黒雲母と無色鉱物とが縞状構造を呈する．(b) 非持トーナル岩中の単斜輝石と角閃石の産状．単斜輝石は虫食い状あるいはブレッブ状に角閃石を含む．右上の角閃石結晶は単純双晶を示す．(c) 生田花崗岩．自形性の強いホルンブレンドを含む．(d) 生田花崗岩．粗粒の褐れん石の濃集部．写真のスケールは (c) と同じであり，角閃石と同程度の粒度であることが分かる．(e) 南向花崗岩粗粒相．長石や石英の粒間に黒雲母がリボン状に産するが，(a) の非持トーナル岩に比べ，連続性はよくない．アルカリ長石の巨晶を含む．(f) 南向花崗岩細粒相．写真のスケールは (e) の粗粒相と同じで，相対的に細粒であることが分かる．アルカリ長石の巨晶を含む．(g) 苦鉄質岩類細粒相．包有物に富み汚濁した斑晶状の斜長石を含む．(h) コートランダイト（スピネルかんらん石斜方輝石単斜輝石含有角閃石岩）．ホルンブレンドのオイコクリスト中にスピネル・かんらん石・斜方輝石を含む．Hbl: ホルンブレンド，Bt: 黒雲母，Cpx: 単斜輝石，Qtz: 石英，Pl：斜長石，Afs: アルカリ長石，Aln: 褐れん石，Opx: 斜方輝石，Ol: かんらん石．(a) 及び (g) :オープン・ニコル，(b)–(f): クロス・ニコル．

Fig. 4　Photomicrographs of Ryoke Plutonic Rocks in the Ogawara area. (a) Hiji Tonalite. Aligned hornblende and biotite and transparent minerals show banded structure. (b) Mode of occurrence of clinopyroxene and hornblende in the Hiji Tonalite. Clinopyroxene crystals include bleb-like hornblende. Hornblende crystal at the upper right of the field show simple twin. (c) Ikuta Granite. Euhedral hornblende is a distinctive feature of Ikuta Granite. (d) Ikuta Granite. Concentrated portion of the coarse-graind euhedral allanite. The scale of the photograph is the same as (c), showing that the grain size is comparable to that of hornblende. (e) Minakata Granite, coarse-grained facies. While biotite occurs in ribbon-like shapes between the grains of feldspar and quartz, the continuity is not well-developed compared to the Hiji Tonalite in (a). Large alkali feldspar crystals are characteristic. (f) Minakata Granite, fine-grained facies. The scale of the photo is the same as the coarse-grained phase in (e), indicating the relatively fine-grained characteristics. Large alkali feldspar crystals are characteristic. (g) Mafic rocks, fine-grained facies. Phenocrystic dusty plagioclase due to numerous fine-grained inclusions is characteristic. (h) Cortlandite (spinel-olivine-orthopyroxene-clinopyroxene-bearing hornblendite). Spinel, olivine, and orthopyroxene are included as chadacrysts in the hornblend oikocryst. Hbl: hornblende, Bt: biotite, Cpx: clinopyroxene, Qtz: quartz, Pl: plagioclase, Afs: alkali feldspar, Aln: allanite, Opx: orthopyroxene, Ol: olivine. (a) and (g): open nicol, and (b)–(f): crossed nicols.

比の違いにより，モーダル・レイヤリング状の構造を示す場合など，複雑で多様な産状を示す．

細粒相の代表的岩相の鏡下での産状は，完晶質で，板状の黒雲母及び長柱状のホルンブレンド・斜長石が定向配列し，顕著な葉片状構造を示す(第4図g)．長径最大2 mm程度の斑晶状の斜長石を含み，それ以外の主成分鉱物の粒度は長径0.4 mmから0.2 mm程度まで連続的に変化する．斑晶状の斜長石は半自形で，融食形の微細な黒雲母・角閃石・斜長石を多量に含み汚濁した産状を示すとともに，顕著な累帯構造を示す．基質の斜長石は半自形–自形で，しばしば顕著な累帯構造を示す．ホルンブレンドは自形–半自形で，暗緑褐色–淡褐色の多色性を示す．黒雲母は自形–半自形で，暗褐色–淡褐色の多色性を示す．

細粒粗は，南向花崗岩中の暗色包有物以外の産状として，非持トーナル岩，生田花崗岩，南向花崗岩粗粒相の片麻状構造に調和的に板状に産する場合がある．こうした産状を構成する岩相は，葉理状の細粒黒雲母含有角閃石斑れい岩–閃緑岩である．多くの場合，斜長石の累帯構造の存在等をもとに面構造の発達した火成岩であることが確認できるが，場合によっては，変成岩としての角閃岩と区別できないこともある．

粗粒相の代表的岩相である角閃石斑れい岩の鏡下での産状は，オルソキュムレイト組織を示し，主としてホルンブレンド・斜長石から構成される．鉱物の粒度は，長径8 mmから0.2 mm程度まで連続的に変化する．ホルンブレンドは半自形–自形で，帯緑褐色–淡褐色の多色性を示す．しばしば，中心部がより褐色を帯びる累帯構造が認められる．また，単純双晶を示す場合がある．斜長石は半自形で，顕著な累帯構造を示すほか，単結晶中の消光位がパッチ状に異なる，まだらな消光を示すことが多い．また，融食形を示す細粒のホルンブレンドをしばしば包有する．不透明鉱物は他形・不定形で，斜長石とホルンブレンドの粒間にプール状に産するほか，粒状の結晶として両鉱物に包有される．少量の黒雲母 (自形–半自形，暗褐色–淡褐色の多色性)が含まれる場合や，カミングトン閃石 (自形–半自形，しばしば集片双晶を示し，淡緑褐色–無色の弱い多色性を示す)を含みアドキュムレイト組織を示す場合もある．粗粒相のうち，コートランダイトは，完晶質で，最大粒径15 mm程度のホルンブレンドオイコクリスト中に，かんらん石，斜方輝石，スピネルがチャダクリストとして包有されるオルソキュムレイト組織を示す(第4図ｈ)．ホルンブレンドのオイコクリストは，半自形–他形，粒径15–8 mmで，褐色–淡褐色の多色性を示す．かんらん石は，粒状–不定形の他形–半自形で，粒径1.5–<0.1mmを示す．斜方輝石は他形でチャダクリストとして産するほか，ホルンブレンドオイコクリストの粒間にも産する．単斜輝石はチャダクリスト中の残晶として産し，虫食い状ないしスポンジ状の他形結晶として産する．この単斜輝石結晶の周囲は，ホルンブレンドが淡色である．スピネルは半自形–他形，粒径<0.1 mmで，全ての鉱物中に産する．

4. 2　全岩主成分化学組成

4. 2. 1　花崗岩類及び変成岩類

第5図に花崗岩類及び変成岩類のハーカー図を示す．苦鉄質岩類については，花崗岩類とSiO_2含有量が大きく異なることから，花崗岩類とともにプロットするとそれぞれの岩型のトレンドの識別が難しくなるため，ここでは花崗岩類及び変成岩類の主成分化学組成についてまず記述し，その後，苦鉄質岩類を含めて記述する．大河原地域を構成する花崗岩類は，数試料の例外はあるものの，ほぼSiO_2含有量69 wt.%を境に大きく2分される．非持トーナル岩及び生田花崗岩は，生田花崗岩の1試料を除いてSiO_2<69 wt.%の組成範囲内にプロットされ，南向花崗岩は粗粒相及び細粒相のそれぞれ1試料を除き，SiO_2>69 wt.%の組成範囲内にプロットされる(第5図)．ただし, SiO_2 = 69 wt.%付近に組成の不連続(空白域)は認められない．SiO_2含有量に対するTiO_2, Al_2O_3, 及びMnO含有量は，全ての岩型が一体となって見かけ上単一のトレンドを示す．CaO及びP_2O_5については，やはり大局的に単一のトレンドを示すように見えるが，詳細に見ると非持トーナル岩及び生田花崗岩のトレンドと，南向花崗岩のトレンドの傾きが僅かに異なる．MgO, Na_2O及びK_2Oについては，非持トーナル岩と生田花崗岩の組成の分散が大きい．MgOにおいて両者はやや異なるトレンドを示すようにも見えるが，不明瞭である．Na_2O及びK_2Oにおいては，分散はするものの，組成範囲としては非持トーナル岩，生田花崗岩ともに概ね同じ領域にプロットされる．南向花崗岩はMgOとK_2Oにおいて非持トーナル岩や生田花崗岩よりも組成の分散が小さく，組成変化トレンドを識別することができる．また，Na_2Oについても，細粒相の一部において組成の分散が大きいが，大局的には粗粒相と細粒相の組成とが集中する領域が認められる．このNa_2Oにおける組成集中域及び他の全ての元素について，南向花崗岩粗粒相と細粒相とは，ほぼ組成の違いは識別できず，ともに共通の組成変化トレンドを示す．

変成岩類は，全ての主成分元素で花崗岩類の組成幅を超える幅広い組成範囲を示す．CaO，Na_2O及びK_2Oにおいて大きな分散を示すほかは，SiO_2含有量と概ね協調的な組成変化を示す．

4. 2. 2　苦鉄質岩類及び花崗岩類との関係

ハーカー図に苦鉄質類を追加してプロットしたものを第6図に示す．細粒相のうち，記載的に角閃岩と区別できないものについては，便宜上，角閃岩の名称を用い区別して示した．SiO_2含有量と各主成分元素との関係は，

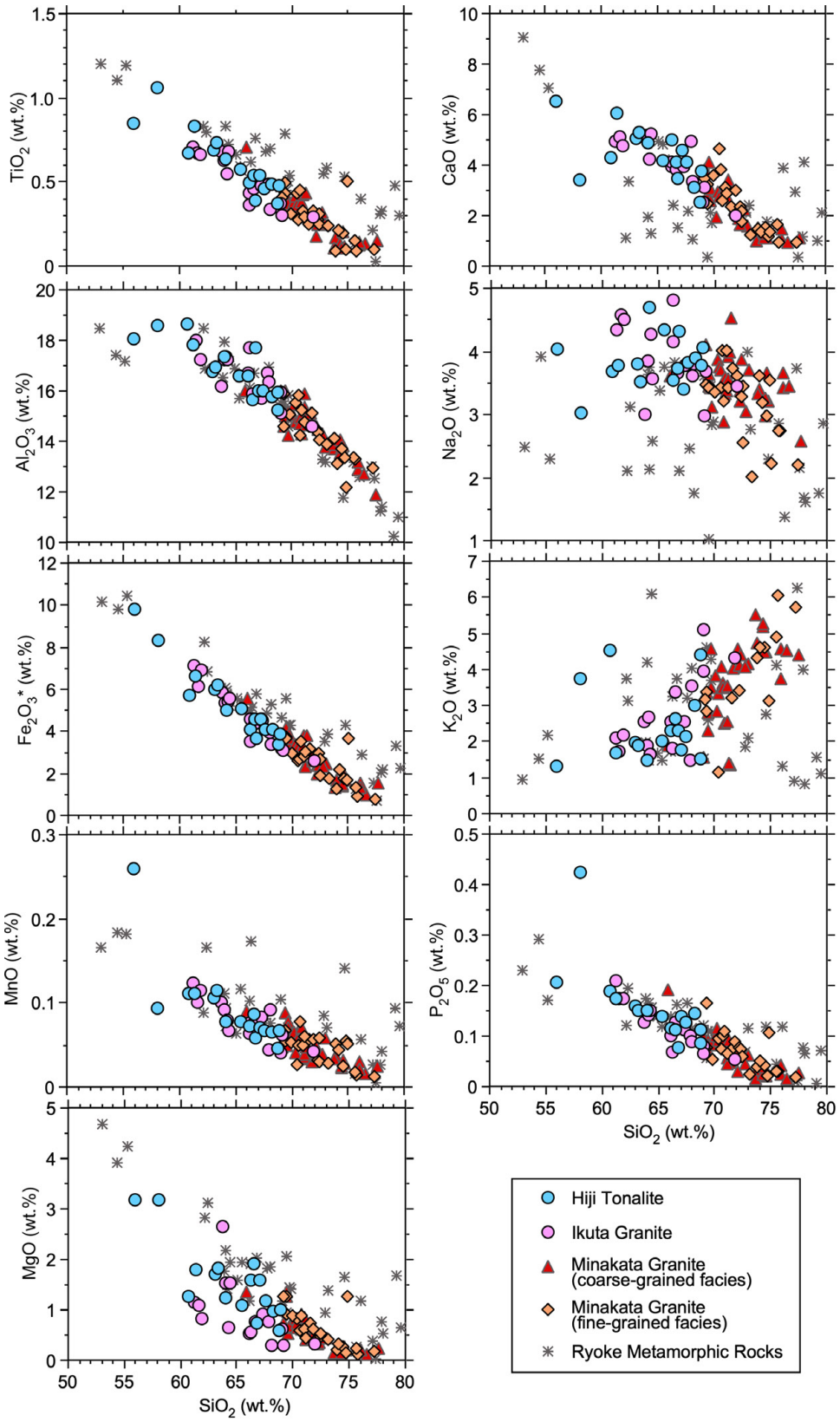

第5図　大河原地域に産する花崗岩類と変成岩類の全岩主成分化学組成のハーカー図．Fe_2O_3*は全鉄をFe_2O_3として示したもの．

Fig. 5　Whole-rock major oxide Harker diagrams of granitic and metamorphic rocks in the Ogawara area. Fe_2O_3* denotes total Fe as Fe_2O_3.

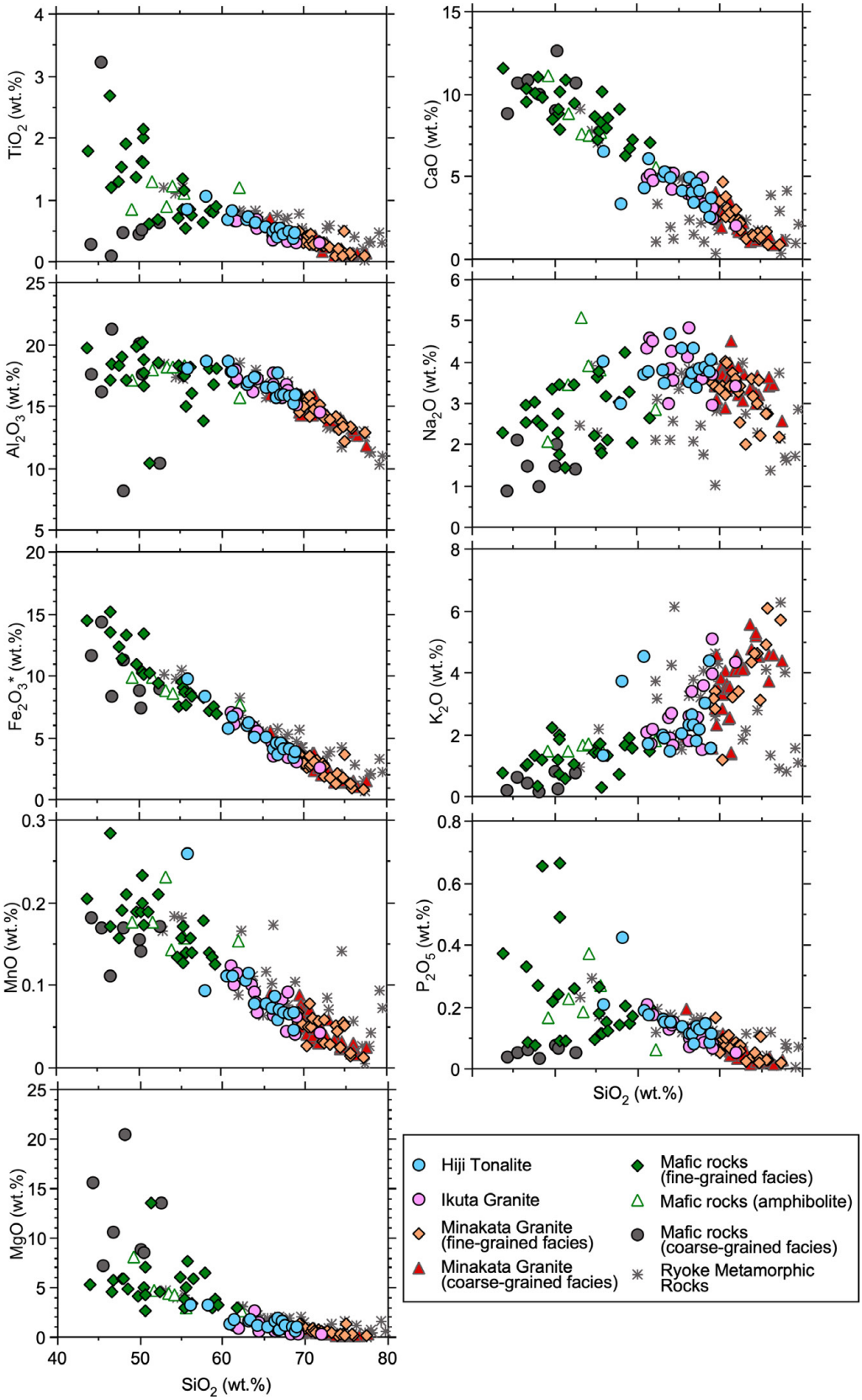

第6図　大河原地域に産する深成岩類及び変成岩類の全岩主成分化学組成のハーカー図．Fe_2O_3*は全鉄をFe_2O_3として示したもの．

Fig. 6　Whole-rock major oxide Harker diagrams of plutonic and metamorphic rocks in the Ogawara area. Fe_2O_3* denotes total Fe as Fe_2O_3.

組成が集中してトレンドを形成する花崗岩類のうち，非持トーナル岩及び生田花崗岩の最もSiO_2に乏しい試料群と苦鉄質岩類細粒相とは，見かけ上ほぼ連続する．具体的には，Fe_2O_3*（全鉄をFe_2O_3として示したもの），MnO，CaO，Na_2O及びK_2Oにおいて，花崗岩類から概ね連続する単一のトレンドとして識別される．TiO_2，Al_2O_3，MgO及びP_2O_5については，花崗岩類の組成トレンドが苦鉄質岩類に連続するとともに，苦鉄質岩類内で2つのトレンドに枝分かれするように見える．そして，枝分かれした2本のトレンドのうちのひとつは，苦鉄質岩類細粒相のみから構成されるが，もうひとつは苦鉄質岩類粗粒相と細粒相とで構成される．苦鉄質岩類のうち，角閃岩様の組織を示すものは，それ以外の苦鉄質岩類の示すトレンドからやや外れた組成を示す傾向にあるものの，大きく異なる組成を示すわけではない．

苦鉄質岩類については，FeO*/MgOに対する各主成分元素の挙動についても第7図に示す（FeO*は，全鉄をFeOとして示したもの）．この図には花崗岩類についても参考のためプロットしている．苦鉄質岩類について，FeO*/MgOに対する各主成分元素は，やや分散があるものの，概ね単一の単調増加ないしは単調減少のトレンドを示す．これらのトレンドは，FeO*/MgOの範囲が花崗岩類と重複するが，TiO_2，Al_2O_3，Fe_2O_3*，MnO，CaO及びP_2O_5において花崗岩類のトレンドと斜交する．苦鉄質岩類粗粒相及び細粒相のうち角閃岩様の組織を示すものは，概ね苦鉄質岩類全体のトレンドもしくは組成範囲と区別できない．

アルミナ飽和度[= Al_2O_3/(CaO + Na_2O + K_2O)，モル比]（第8図）は，非持トーナル岩，生田花崗岩，南向花崗岩の順に，SiO_2の増加につれてメタアルミナスからパーアルミナスに見かけ上連続するトレンドを示す．非持トーナル岩と南向花崗岩には，一部このトレンドから外れる試料がある．苦鉄質岩類は粗粒相の1試料を除き全てメタアルミナスな組成を示し，組成が集中する部分は花崗岩類のトレンドから連続するようにも見えるが，分散が大きく不明瞭である．変成岩類は，花崗岩類及び苦鉄質岩類のトレンドないし組成範囲に重なるものも多いが，著しくアルミナ飽和度の高いものも存在する．また，苦鉄質岩類と区別できないメタアルミナスなものも存在する．

苦鉄質岩類細粒相は十分に細粒で花崗岩類（南向花崗岩）と液状態で混交した産状を示すため，苦鉄質岩類について火山岩類の判別図にプロットした（第9図）．トータルアルカリ（Na_2O+K_2O）–シリカ図では，細粒苦鉄質岩の多くが玄武岩–安山岩領域にプロットされる（第9図a）．苦鉄質岩類粗粒相は，少なくとも一部は明らかにキュムレイトであるため判別図は意味をなさないが，組成的にはピクロ質玄武岩–玄武岩質安山岩にプロットされる．苦鉄質岩類細粒相のうち，角閃岩様の組織を示すものは玄武岩質安山岩–安山岩組成を示し，一部が玄武岩質粗面安山岩領域にプロットされる．FeO*/MgO–SiO_2図においては，苦鉄質岩類細粒相は図中T_1–T_3の3つのトレンドを示すように見える（第9図b）．このうちT_1はMiyashiro（1974）によるカルクアルカリ系列とソレアイト系列の境界線よりもカルクアルカリ領域にプロットされるが，トレンドの大局的な傾きは境界線よりも低角でソレアイト質である．T_2とT_3は相対的にFeO*/MgOの大きな試料の組成に強く影響を受けているものの，FeO*/MgOの増加に伴いSiO_2の減少する明瞭なソレイアイト質のトレンドを示す．FeO*/MgO–FeO*図においては3つのトレンドは明確には識別できないが，仮に全体が単一のトレンドであるとしても，カルクアルカリ領域の試料の下限を結んだ線は，Miyashiro（1974）によるカルクアルカリ系列とソレアイト系列の境界線よりも低角の曲線，つまりソレアイト質のトレンドとなる（第9図c）．

4. 3　全岩微量成分組成

大河原地域構成岩類のC1コンドライト規格化全岩希土類元素（rare-earth elements；REEs）パターンを第10図に示す．花崗岩類は，いずれもGd–Luにかけての中–重希土類元素の含有量がコンドライトの10倍程度で，全体としてゆるやかな左上がりのパターンを示す．詳しく見ると，非持トーナル岩は，コンドライトの5倍–40倍程度のLu含有量から，コンドライトの50倍–200倍程度のLa及びCe含有量にかけて，比較的緩やかな左上がりのパターンを示す（La/Yb_N = 1.8–9.0）．Euの負の異常が存在する試料と存在しない試料とがあり，Eu/Eu*[Eu* = (Sm+Gd)/2，いずれも規格値] の平均値は0.8である．これに対し生田花崗岩は，Lu含有量がコンドライトの8倍から15倍程度で，La含有量が100–400倍程度と，全体として非持トーナル岩よりも急角度の左上がりのパターンを示す（La/Yb_N = 6.5–35.9）．また，La–Smにかけての軽希土類元素は非持トーナル岩の組成範囲を超える含有量をもつ（一般に軽希土類元素はLaからEuまでとされるが，Euは異常の有無や程度の違いにより他の軽希土類元素と挙動が異なる場合があることから，以下の記述では単に軽希土類元素とした場合はLa–Smのことを指す）．Euの負異常は存在する試料と存在しない試料とがあり，Eu/Eu*の平均値は0.9で非持トーナル岩とほぼ同じである．南向花崗岩粗粒相は軽希土類元素の含有量やパターンの角度は概ね非持トーナル岩と同程度であるが，中–重希土類元素含有量は平均的に非持トーナル岩よりもやや少なく，パターンの角度は急である（La/Yb_N = 3.4–32.4）．また，Euの負異常が弱い試料もあるが，全体としては非持トーナル岩よりも顕著であり，Eu/Eu*の平均値は0.6で，明らかに非持トーナル岩や生田花崗岩よりも小さい．南向花崗岩細粒相はその組成範囲が南向花崗岩粗粒相と完全に一致する．

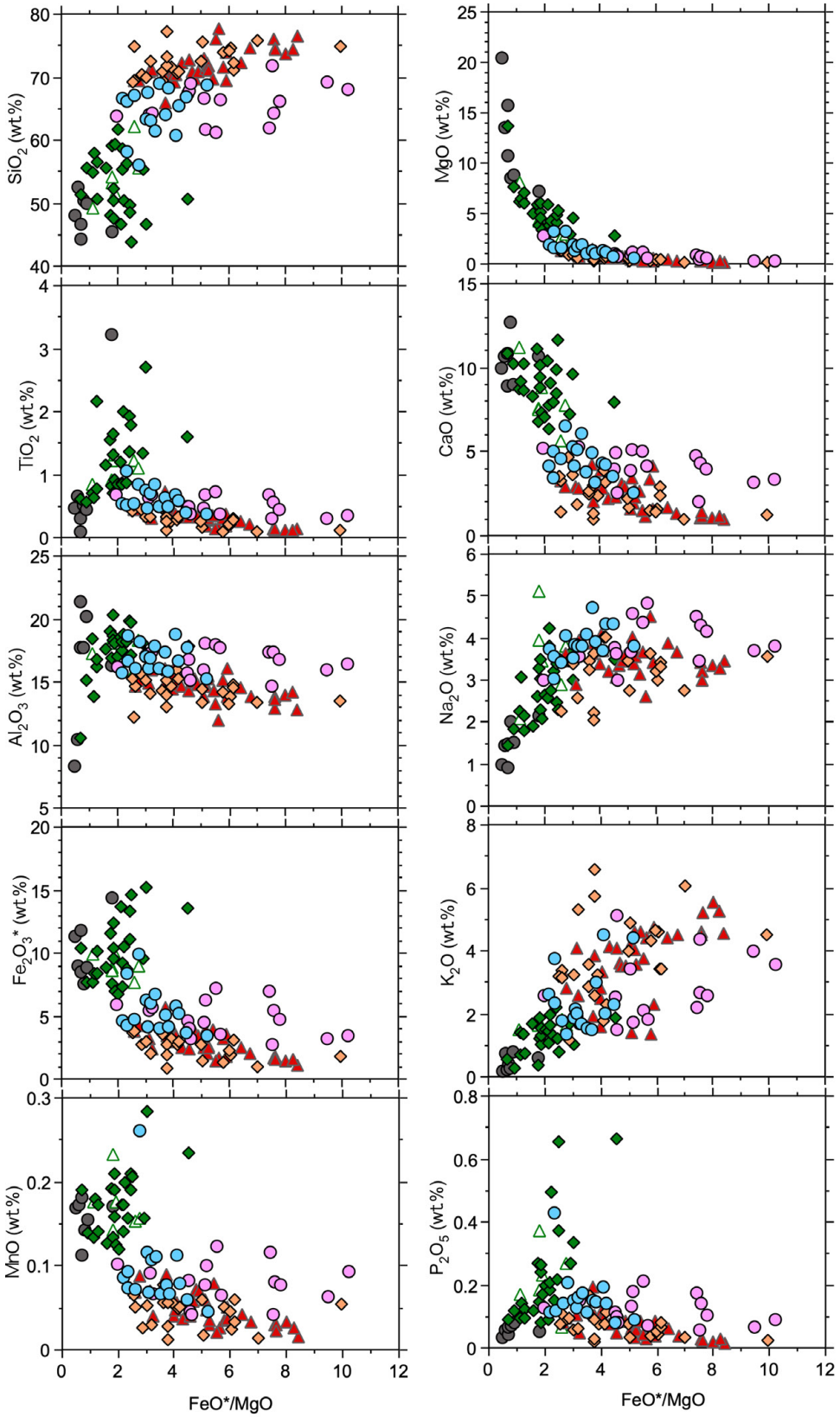

第7図　大河原地域に産する深成岩類のFeO*/MgOに対する全岩主成分組成図．Fe_2O_3*は全鉄をFe_2O_3として，FeO*はFeOとして示したもの．凡例は第5図と同じ．

Fig. 7　Whole-rock major oxide–FeO*/MgO diagrams for Ryoke Plutonic Rocks in the Ogawara area. Fe_2O_3* denotes total Fe as Fe_2O_3 and FeO* denotes total Fe as FeO, respectively. Symbols are the same as for Fig. 5.

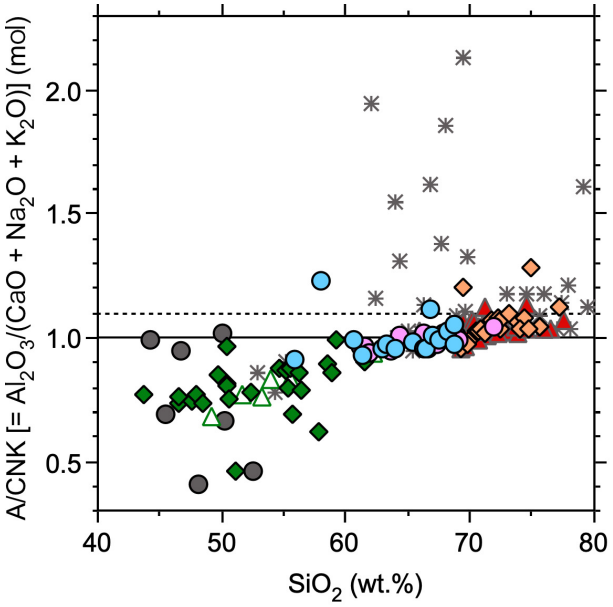

第8図　大河原地域に産する深成岩類及び変成岩類の全岩主成分化学組成のアルミナ飽和度（A/CNK）．A/CNK = 1.0の実線は，パーアルミナス（A/CNK>1.0）とメタアルミナス（A/CNK<1.0）の境界．点線は，Chappell and White（1974）による，Sタイプ花崗岩（A/CNK>1.1）とIタイプ花崗岩（A/CNK<1.1）の境界．凡例は第5図と同じ．

Fig. 8　Alumina saturation index (A/CNK) of Ryoke Plutonic Rocks and Ryoke Metamorphic Rocks in the Ogawara area. Solid line in A/CNK = 1.0 indicates the boundary between per-aluminous (A/CNK>1.0) and meta-aluminous (A/CNK<1.0). Dashed line is the boundary between S-type granite (A/CNK>1.1) and I-type granite (A/CNK<1.1) according to Chappell and White (1974). Symbols are the same as in Fig. 5.

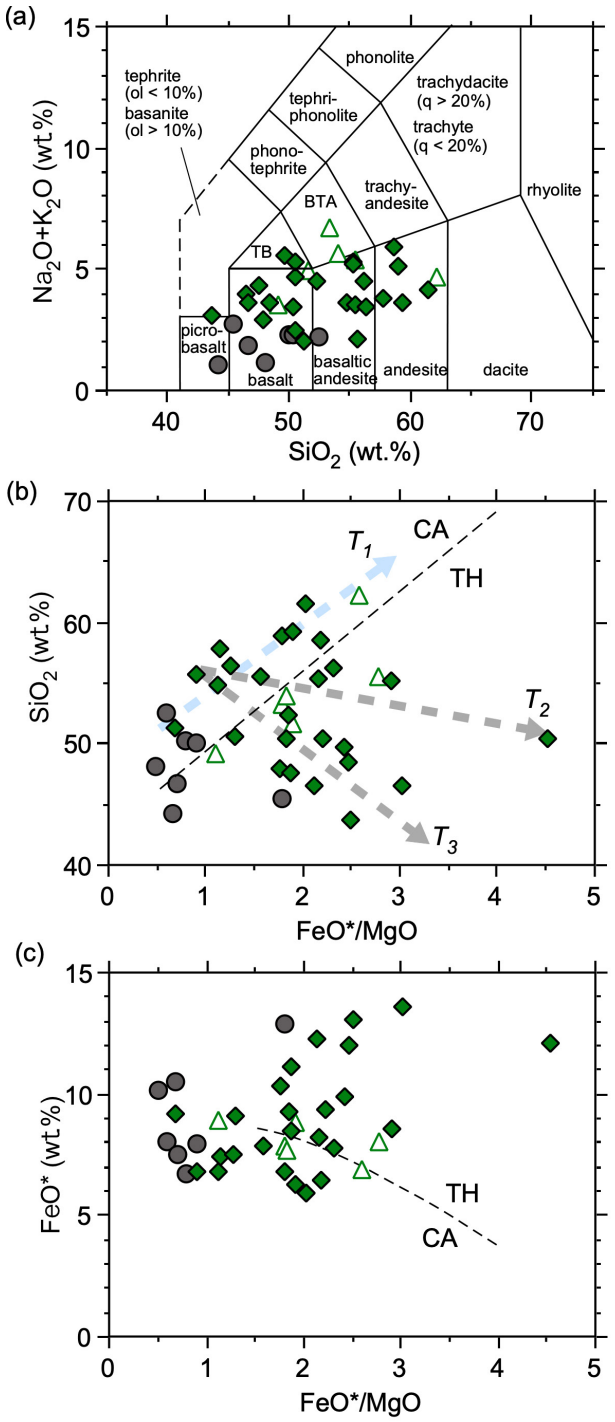

（↗右上）

第9図　大河原地域に産する苦鉄質岩類の全岩主成分化学組成．(a) トータルアルカリ（$Na_2O + K_2O$）–SiO_2図．境界はLe Maitre（2002）に基づく．BTA: basaltic trachyandesite，TB: trcachybasalt．(b) FeO*/MgO–SiO_2図．TH: ソレアイト，CA: カルク・アルカリ．THとCAの境界はMiyashiro（1974）に基づく．FeO*は全鉄をFeOとして算出したもの．以上，(c) も同じ．T_1, T_2及びT_3は見かけ上のマグマティック・トレンド．詳細は本文参照．(c) FeO*/MgO–FeO*図．凡例は第5図と同じ．

Fig. 9　Selected whole-rock major element geochemistry of mafic rocks in the Ogawara area. (a) total alkali–SiO_2 diagram, after Le Maitre (2002). BTA: basaltic trachyandesite, TB: trcachybasalt. (b) FeO*/MgO–SiO_2 diagram. TH: tholeiite and CA: calc-alkali. CA–TH boundary is from Miyashiro (1974). FeO* denotes total Fe as FeO. The same also applies to (c). T_1, T_2 and T_3 are apparent magmatic trend. (c) FeO*/MgO–FeO* diagram. Symbols are the same as in Fig. 5.

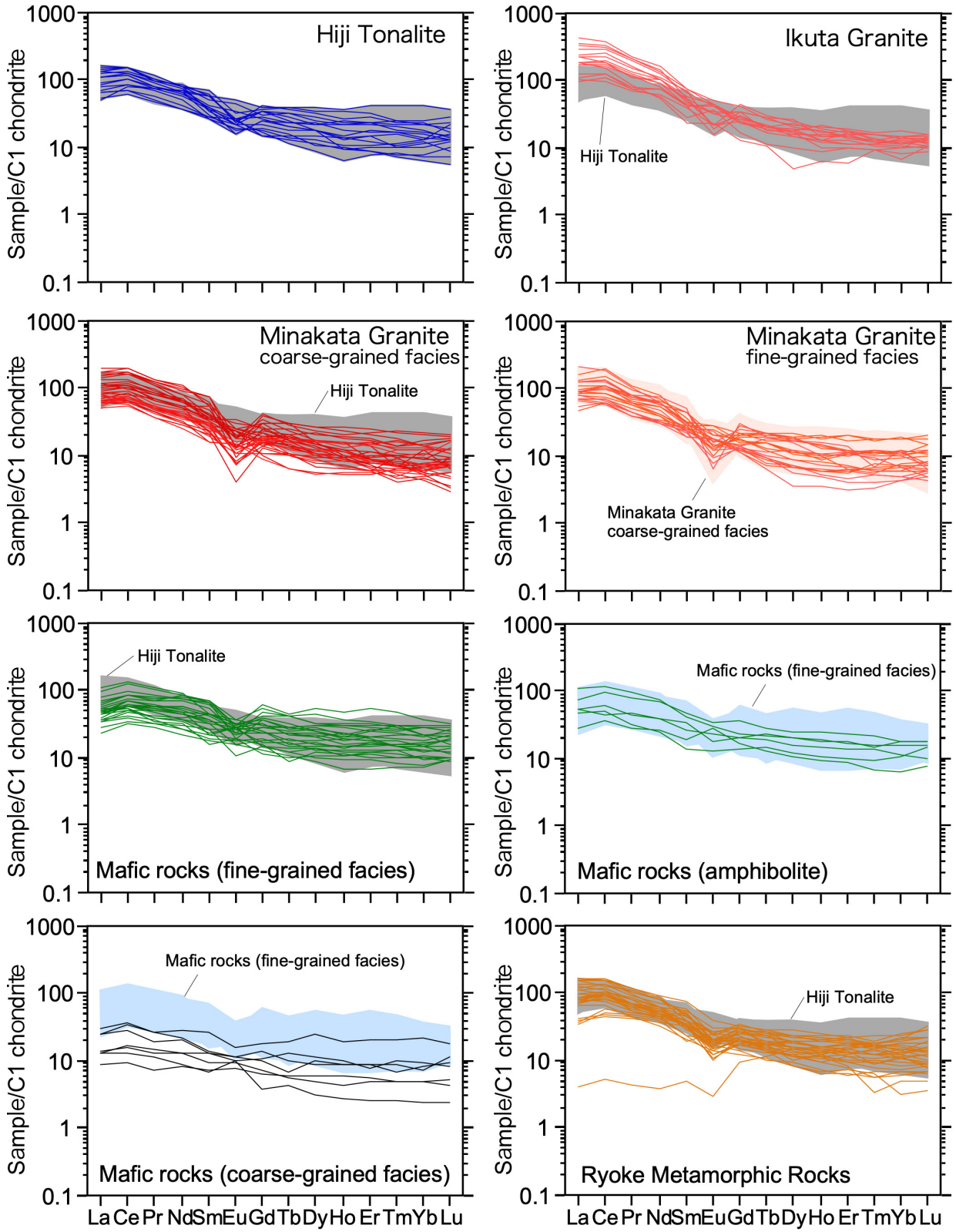

第10図　大河原地域に産する深成岩類及び変成岩類の全岩希土類元素組成のコンドライト規格化パターン．規格化に用いたC1コンドライトの値はSun and McDonough (1989) による．

Fig. 10　Whole-rock rare-earth element patterns of Ryoke Plutonic Rocks and Ryoke Metamorphic Rocks in the Ogawara area. Chondrite values are from Sun and McDonough (1989).

苦鉄質岩類細粒相のうち，明らかな火成組織を示す細粒斑れい岩–閃緑岩（図中においては単に苦鉄質岩類細粒相と表記）は，非持トーナル岩と含有量及びパターンがほぼ重なるが，軽希土類元素において，非持トーナル岩の領域よりもやや低い含有量を示すものがある（La/Yb_N = 1.5–5.8）．このことは，全体として苦鉄質岩類細粒相のパターン（La/Yb_N = 1.5–5.8）が非持トーナル岩よりもフラットに近いことを意味し，Eu/Eu*の平均値も0.9と，わずかな負異常を意味する．苦鉄質岩細粒相のうち，明瞭な火成組織が確認できず，見かけ上，角閃岩様を呈する試料は，少なくとも希土類元素のパターンや含有量の観点からは，火成組織を示す細粒斑れい岩–閃緑岩と全く区別できない（La/Yb_N = 2.9–5.6）．一方，苦鉄質岩類粗粒相は，試料数は少ないものの，細粒相に比べて全体として含有量が少なく，パターンもフラットである（La/Yb_N = 1.4–5.3）．また，1試料明瞭なEuの正異常が認められるほかは，明らかなEu異常は認められない（Eu/Eu*の平均値 = 1.1）．

変成岩類は含有量・パターンともに非持トーナル岩の範囲内で，一般にEuの負異常が顕著である．

Sun and McDonough（1989）による中央海嶺玄武岩（N-MORB）の値で規格化した，大河原地域構成岩類の微量元素マルチエレメントパターンを第11図に示す．希土類元素と同じく，花崗岩類は全ての岩型において大局的に類似したパターンを示し，Nb及びTiの負異常とPbの正異常を共通して示す，左上がりのパターンが認められる．これらの共通した特徴のほか，Ba，Th，La–Ce，Sr，Nd及びZr–Hfにおいて，岩型ごとに固有の特徴的傾向が認められる．これらの傾向はそれぞれの岩型間における相対的なものであるため，以下に非持トーナル岩を基準に比較して述べる．生田花崗岩は，非持トーナル岩に比べて，ばらつきはあるものの，大局的にRbやBaに富む傾向をもつ．また，すでに見たように軽希土類元素に富むため，La–Ceが高く，これら隣接元素が左上がりのパターンを示すことで特徴づけられる．さらに，非持トーナル岩では隣接元素に対してNdの正異常は認められないが，生田花崗岩では比較的明瞭な正異常を示す．Zr–Hfに富む傾向は，非持トーナル岩にも認められるが，生田花崗岩ではより顕著である．南向花崗岩粗粒相は，非持トーナル岩に比してBaが乏しくThに富む傾向があり，その結果，Thの正異常が認められる．La–Ceの含有量は非持トーナル岩と同程度であるが，これにより，それらに富む生田花崗岩とパターン形状として区別される．また，Srの含有量が非持トーナル岩や生田花崗岩よりも少なく，Nd含有量は生田花崗岩と概ね同程度であるため，Sr負異常として認識される．Zr–Hfの含有量は概ね非持トーナル岩と同程度で，やはりそれらに富む生田花崗岩とパターン形状として区別される．Tiの負異常は非持トーナル岩や生田花崗岩よりも顕著である．南向花崗岩細粒相は，Thに著しく富む試料が少ないものの，組成範囲や大局的なパターンとしては南向花崗岩粗粒相と基本的に区別できない．

苦鉄質岩類細粒相のうち，火成組織を示す細粒斑れい岩–閃緑岩（図中において単に苦鉄質岩類細粒相と表記）は，非持トーナル岩に比べてRb–U，La–Ce，Pb及びZr–Hfに乏しく，Tiに富む傾向を示す．その結果，Pbの正異常及びTiの負異常の程度が小さく，SrからLuにかけて異常の目立たない緩やかな右下がりのパターンを示す．苦鉄質岩類細粒相のうち，角閃岩様の組織を示す試料は，マルチエレメントで見ても火成組織を示す苦鉄質岩類細粒相と区別できない．苦鉄質岩類粗粒相は，大局的には細粒相と似たパターンを示し，含有量は全体に低い．パターン上の細粒相との目立った違いは，Srの正異常が認められる点と，一部の試料でTiの正異常が認められる点である．

変成岩類はThとPbの正異常が顕著な以外は，概ね含有量・パターンともに非持トーナル岩と似る．

5．議論

5. 1　岩型ごとの地球化学的特徴の意味

これまで述べた通り，大河原地域構成岩類には，野外ならびに標本サイズで識別可能な岩型区分と全岩化学組成との間に，ある程度系統的な対応が認められる．しかしながら，そもそもこうした岩型ごとの全岩化学組成の違いは，本来は一連の分化に伴って形成された岩相を，晶出相（鉱物組合せ）の違いに基づいて任意に区分しただけの可能性もある．また，微量元素組成においては，全体として，あるいは大局的には岩型ごとの共通の特徴が識別できるものの，いずれの岩型においても組成のばらつきがあり，異なる岩型において相互にほぼ区別できないパターンの試料も存在する．従って，岩型を区別する基準として本質的に重要なのは，見かけ上の組成範囲やパターンの類似性ではなく，それらの地球化学的特徴の違いをもたらすマグマプロセスの必然性，すなわち岩石学的な意味である．そこで，以下ではまず，野外ならびに標本サイズで識別可能な岩型区分との対応関係において，岩型ごとの地球化学的特徴の意味について検討を行った上で，肉眼観察と全岩化学組成の情報に基づく岩型区分の妥当性について議論する．

花崗岩類

花崗岩類のうち，非持トーナル岩及び生田花崗岩のSiO_2含有量の上限と，南向花崗岩のSiO_2含有量の下限は，約69 wt.%で一致している．このSiO_2 = 69 wt.%は，比較的アルカリに富む火山岩類（Na_2O+K_2O>8 wt.%）の場合，IUGSによる粗面岩・粗面デイサイトと流紋岩との境界に一致する（LeMaitre，2002）．火山岩類において岩石名の区分の定義として採用されているということは，そこ

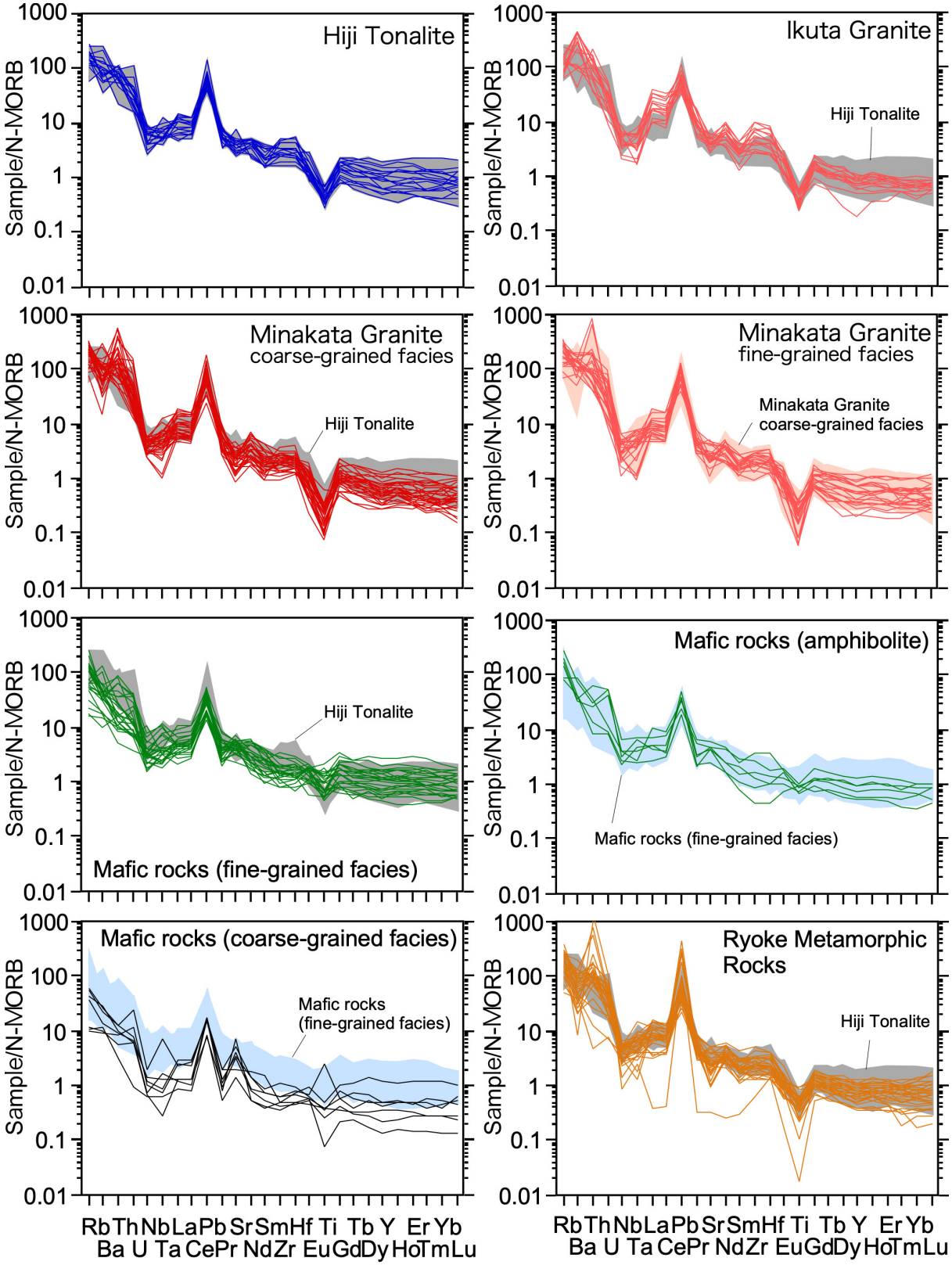

第 11 図　大河原地域に産する深成岩類及び変成岩類の全岩微量成分組成の中央海嶺玄武岩（N-MORB）規格化パターン．規格化に用いたN-MORBの値はSun and McDonough（1989）による．

Fig. 11　Whole-rock multi-trace element patterns of Ryoke Plutonic Rocks and Ryoke Metamorphic Rocks in the Ogawara area. N-MORB values are from Sun and McDonough (1989).

には岩石学的あるいは地球化学的に何らかの意味のある境界が存在し，花崗岩類の岩型がこれを境に区分されることにも何らかのマグマティックな意味がある可能性がある．そこで，以下では，この点について検討する．

粗面岩類とは，語源的には，記載的に斜方輝石や角閃石もしくは黒雲母を含む岩石に対して用いられていた名称であり，流紋岩は斑晶として石英とアルカリ長石を含み，しばしば斜長石や黒雲母を含む珪長質岩に対して用いられる（LeMaitre, 2002）．大河原地域の花崗岩類の場合，角閃石の有無で完全に区分することは不可能であるが，記載でも述べたように南向花崗岩は角閃石に乏しく，有色鉱物全体の量比も小さく相対的に優白質であることから，こうしたモード組成の違いがSiO_2 = 69 wt.%を境に明瞭に現れていると解釈するのが合理的である．第2図bの苦鉄質鉱物（角閃石＋黒雲母）–斜長石–石英+アルカリ長石図においても非持トーナル岩と生田花崗岩とは南向花崗岩と概ね異なった領域にプロットされ，その境界は苦鉄質鉱物10–11 vol.%に相当する．従って，このSiO_2 = 69 wt.%は，野外ならびに標本サイズで識別可能な岩型区分のモード組成に対応したものといえる．なお，全岩化学組成において，組成の密集するトレンドから大きく外れる試料がいくつか存在し，例えば生田花崗岩の1試料はSiO_2 = 72 wt.%程度を示し，SiO_2 = 69 wt.%の境界よりも明らかにSiO_2に富む組成をもつ．こうしたトレンドから大きく外れる試料については，例えば変成岩類の同化，マグマティックな苦鉄質鉱物の濃集等のそれぞれ試料固有の原因が想定されるが，各種組成図において例外的な組成であることは明らかであるため，本論ではそれぞれの詳しい原因については追求せず，組成の密集する大局的なトレンドについて議論する．

非持トーナル岩と生田花崗岩とは，モード組成（第2図）では明確には区別できず，全岩主成分組成においても，ハーカー図（第5図）及びアルミナ飽和度（第8図）では区別できない．しかしながら，FeO*/MgOと各種成分元素の挙動（第7図）においては，ほぼ同程度の主成分元素酸化物含有量であるにも関わらず，生田花崗岩のFeO*/MgOが，約4.5を境に非持トーナル岩のそれよりも明らかに大きい特徴を示す．一般に全岩のFeO*/MgOは，岩石を構成する有色鉱物のFeO*/MgOと，鉄チタン酸化物（磁鉄鉱やチタン鉄鉱）の有無や量比を反映している．非持トーナル岩と生田花崗岩はともに少量の鉄チタン酸化物を含むことはあるが，ハーカー図（第5図）においてFe_2O_3*含有量に違いが認められないことからも明らかなように，鉄チタン酸化物の量自体に両岩型で系統的かつ顕著な違いは認められない．従って，FeO*/MgOの違いは，岩石を構成する有色鉱物のFeO*/MgOの違いを主に反映しているものと判断される．そのような観点からMgO–SiO_2図（第5図）を見ると，ばらつきはあるものの，非持トーナル岩に対し生田花崗岩は平均的にMgO含有量が低い傾向にある．

その他に，非持トーナル岩と生田花崗岩とは，すでに述べたように微量元素組成において異なる特徴を示し，生田花崗岩は，非持トーナル岩に比べて軽希土類元素に富む傾向がある（第10図，第11図）．ここで，褐れん石は極めて急な左上がりの希土類元素パターンを示すことが知られており，具体的な程度としては，同一結晶においてLuが10 ppm，Ybが87 ppmのとき，Laは4.92 wt.%，Ceは10.45 wt.%に達する（例えば，Brooks *et al.*, 1981）．生田花崗岩は肉眼で識別可能なほどの粒径の褐れん石を多量に含むことで特徴づけられるため，同岩型を特徴づける軽希土類元素に富む全岩化学組成は，褐れん石の量比の違いを反映しているものと考えられる．一方，やはり生田花崗岩において系統的に非持トーナル岩よりも富むZr及びHfは，ジルコンに強く分配される元素であり，この量比の違いはジルコンのモード量に対応しているものと解釈される．褐れん石やジルコンは，マグマの分化段階の相対的に後期のある時点で晶出を開始することから，全岩FeO*/MgO比と，褐れん石及びジルコンの飽和の観点からは，非持トーナル岩に対し生田花崗岩のほうがより分化していると考えることができる．

一方，生田花崗岩は非持トーナル岩に比べてTa含有量も系統的に低い（第11図）．Taは褐れん石，ジルコン及び黒雲母にも一定程度分配されるが，これらの鉱物は非持トーナル岩に比べて生田花崗岩の方が富むため，これらの鉱物の量比が影響しているのであれば，むしろ生田花崗岩がTaに富むはずである．また，それらの鉱物にはNbも同様に一定程度分配されるため，それらの鉱物の量比に起因しているのであればNbも協調的な変化を示すはずであり，Taのみの挙動の違いは説明できない．珪長質マグマにおいて，Taの分配係数が著しく大きく，Nbのそれが小さい鉱物は，鉄チタン酸化物もしくはチタナイト（スフェーン）である（例えば，Rollinson and Pease, 2021及びその中の文献）．すでに述べたように，全岩主成分化学組成の鉄やチタン含有量には大きな違いはないが，生田花崗岩では非持トーナル岩よりも全岩FeO*/MgO比が大きいにも関わらず，例えば同程度の南向花崗岩の組成トレンドに比べてTiO_2に富む傾向がある（第7図）．さらに，それらのTiO_2に富む試料は，共通してFe_2O_3*やMnOにも富んでいる（第7図）．鉄チタン酸化物ではTaの分配係数が100を超える報告もあるため（Rollinson and Pease, 2021及びその中の文献），全岩主成分化学組成では明確には識別できないものの，一部の非持トーナル岩の試料において相対的に鉄チタン酸化物にわずかに富むことが微量元素組成に敏感に現れている可能性が考えられる．その他に，生田花崗岩では非持トーナル岩に比べてBaに富む傾向が認められる．Baは花崗岩類構成鉱物の中では黒雲母やアルカリ長石に比較的分配される（例えば，Rollinson and Pease, 2021及びその中の文献）．より

アルカリ長石に富む南向花崗岩では，Baの含有量はさほど多くないため，アルカリ長石よりも黒雲母のモード比に対応しているものと考えられる．

南向花崗岩はSiO_2含有量において非持トーナル岩及び生田花崗岩と明瞭に区別される．ハーカー図（第5図）においては，非持トーナル岩及び生田花崗岩と南向花崗岩とはほとんどの元素においてトレンドが連続するように見えるが，FeO*/MgOを横軸にとった図（第7図）では，非持トーナル岩及び生田花崗岩と南向花崗岩とはFeO*/MgOが重複しつつ，特にSiO_2，Al_2O_3，CaOにおいて顕著なトレンドの傾きの差異もしくは組成領域の違いを示す．これらは，基本的に非持トーナル岩及び生田花崗岩に対し，南向花崗岩の有色鉱物がより少なく，石英及びアルカリ長石がより多いモード組成の特徴を反映したものであると解釈される．微量元素組成のうち，希土類元素パターンは，軽希土類元素の濃度が非持トーナル岩と同程度であるのに対し，中希土類元素から重希土類元素においては，非持トーナル岩よりも乏しい傾向を示す（第10図）．一方，南向花崗岩と生田花崗岩とは，希土類元素パターンの中希土類元素から重希土類元素においては区別できないものの，軽希土類元素に関しては生田花崗岩が大局的に富む傾向がある（第10図）．また，すでに述べたようにEuの負異常は非持トーナル岩や生田花崗岩に対して顕著である（第10図）．マルチエレメントパターンにおいては，非持トーナル岩や生田花崗岩に対して南向花崗岩の多くはThに富み，Pbの正異常とTiの負異常が顕著である（第11図）．Thは一般に褐れん石やジルコンに強く分配され，その他にチタン鉄鉱や黒雲母にある程度分配され得る（例えば，Rollinson and Pease，2021及びその中の文献）．しかし，南向花崗岩がThに富む傾向を，褐れん石やジルコンの存在量に求めた場合，肉眼・顕微鏡下におけるモード組成の特徴やその他の元素から示唆される全岩化学組成の特徴と一致しない．従って，南向花崗岩がThに富む原因は，現時点では明確ではないものの，他の岩型に比べて突出して富む傾向から考えると，褐れん石やジルコンが，他の岩型と比べてThに著しく富んでいる可能性が示唆される．いずれにしても，これら大局的な南向花崗岩の微量成分元素の特徴は，南向花崗岩が非持トーナル岩や生田花崗岩に対してSiO_2に富み，K_2Oを除く主成分元素に大局的に乏しい傾向や，有色鉱物に乏しくアルカリ長石に富むモード組成と併せて考えると，南向花崗岩が非持トーナル岩や生田花崗岩よりも分化した組成であることを示していると解釈できる．

ハーカー図においては，非持トーナル岩と生田花崗岩に対して南向花崗岩がSiO_2含有量に富み，各種元素において一連のトレンドを形成しているように見える（第5図）．しかし，全てがほぼ同一の組成のマグマから晶出したか，あるいは非持トーナル岩と生田花崗岩のいずれかのマグマの分化によって南向花崗岩が導かれたと仮定した場合，南向花崗岩の希土類元素組成は非持トーナル岩や生田花崗岩に対し，より軽希土類元素に富み，中希土類元素から重希土類元素に枯渇した特徴を示すはずであり，得られた微量元素パターンとは矛盾する．また，上述のように南向花崗岩を特徴づけるThに富む傾向は，連続的な組成・モード変化では説明が難しい．従って，南向花崗岩は非持トーナル岩や生田花崗岩と単純な親子関係にあるわけではないものと考えられる．

以上のことから，非持トーナル岩，生田花崗岩，そして南向花崗岩は，標本サイズの試料の肉眼的特徴に基づいて区分した岩型ごとに固有の地球化学的特徴を有しており，それらは，共通の親マグマからの一連の分化によって形成された岩相の任意の部分を区分したものではないと判断される．

苦鉄質岩類

苦鉄質岩類のうち，粗粒相である粗粒斑れい岩の少なくとも一部は，明瞭なオルソキュムレイト組織を示すことから，全岩化学組成は液組成を示していないものと考えられる．FeO*/MgOがほとんど変化せずにAl_2O_3含有量が15 wt.%程度の変化幅をもつ（第7図）のは，スピネルや斜長石と他の鉱物とのモード比の違いに起因しており，特にAl_2O_3含有量が少ない試料については，斜長石以外の苦鉄質鉱物が集積した結果を示している．キュムラス鉱物の粒間にトラップされたメルトがほとんど存在しないアドキュムレイトの場合は，特定の相，具体的にはマグマの分化の相対的後期に晶出する鉄チタン酸化物やアパタイトに強く分配されるTiO_2やP_2O_5が極めて低い濃度を示すことが知られている（例えば，TiO_2 < 1 wt.%, P_2O_5 < 0.1 wt.%；Godard *et al.*, 2009）が，本地域の粗粒相にはこうした傾向は認められない．このことは，オルソキュムレイト組織に示されるように，粗粒斑れい岩がキュムラス鉱物の粒間に様々な程度にメルトをトラップしていることを意味する．一方，粗粒斑れい岩の一部は，全体としてメルト組成を保持している可能性が高い細粒相の細粒斑れい岩–閃緑岩と，各種組成図において区別できない（第6図，第7図）．しかしながら，粗粒相は細粒相に対し，全体として微量元素含有量が低いにも関わらず，顕著なSr正異常を示し（第10図，第11図），斜長石の集積の効果を明瞭に示していることから，全岩化学組成としては，いずれの試料も厳密な意味では液組成を保持していないものと判断される．

苦鉄質岩類細粒相の，少なくとも南向花崗岩と液状態で混交した産状（第3図a，b）を示すものについては，何らかの液組成を保持していると判断される．その一方で，苦鉄質岩類細粒相には，TiO_2，MnO及びP_2O_5に著しく富み，Al_2O_3に乏しい試料も認められ，一部においては，やはり特定の相が集積していることを示唆する．苦鉄質岩類細粒相のうち，最もFeO*/MgOの大きな試料は，

SiO_2，TiO_2，Fe_2O_3*，MnO，MgOそしてP_2O_5において他の多くの試料の組成が集中する領域ないしはトレンドから大きく離れた組成を示している（第7図）．従って，この試料については液組成を保持していないか，単純な閉鎖系でのマグマの分化によって形成された組成を示していないものと判断される．この試料は，第9図bにおいて，見かけ上のトレンドT_2の根拠となるものであることから，T_2トレンド自体がマグマの分化トレンドとしての意味を持たないものと解釈され，第9図bにおいて，マグマティックなトレンドである可能性のあるものは，T_1及びT_3に限られる．

第9図bは第7図のSiO_2–FeO*/MgO図と同一であり，また，第9図cも縦軸が全鉄を意味するという意味で第7図のFe_2O_3*–FeO*/MgO図と本質的に同じである．そこで，第7図において南向花崗岩との関係を含めて検討すると，第9図bT_1に相当する，カルク・アルカリ質のトレンドは，第7図において花崗岩類のトレンドに向かって延びている．また，第6図では，Na_2OやK_2Oの含有量は苦鉄質岩類細粒相と南向花崗岩とでほぼ同程度であるが，苦鉄質岩類細粒相は南向花崗岩に比べて明らかに苦鉄質であり，また，微量元素組成はアルカリ岩的ではないため不自然である．露頭において観察される細粒苦鉄質岩のマグマ混交様の産状は，ホストの花崗岩質岩と完全には混合していないことを意味するものの，全岩化学組成上はホストとの間で何らかの相互作用が生じているのが一般的である（例えば，Yamasaki, 2022）．このとき，苦鉄質マグマと珪長質マグマとは，温度や物性が大きく異なるため，直ちに均質化せず，拡散によって両者の界面を越えて元素が移動し，その程度は元素によって異なることが知られている（例えば，Sparks and Marshall, 1986；Debon, 1991；Grasset and Albaréde, 1994；Bateman, 1995；Perugini *et al.*, 2008；Morgavi *et al.*, 2013）．主成分元素の中で最も移動性の高い元素がNaであり，Kがそれに続く（例えば，Morgavi *et al.*, 2013）．これらのことから，FeO*/MgOの増加に伴い，花崗岩類に向かってSiO_2, Na_2O及びK_2Oが増加するトレンド，すなわち第9図bT_1は，苦鉄質マグマの分化トレンドではなく，珪長質マグマ（花崗岩質マグマ）との化学的相互作用を示すコントロールライン（混合線，ただし元素によって挙動が異なる）であるものと解釈される．従って，苦鉄質マグマは，第9図bT_3に示される，FeO*/MgOの増加に伴ってSiO_2が減少しFeO*が増加するソレアイト質の分化トレンドを示しているものと考えられる．さらに，第9図b においてT_1を構成するSiO_2>55 wt.%の試料が様々な程度に珪長質マグマとの化学的相互作用を行っているとすると，第9図aに示される玄武岩質安山岩の高シリカ側から安山岩にかけての試料は，マグマの分化によって形成されたものではない可能性が高く，領家深成岩類あるいは類似した産状をもつ花崗岩中の苦鉄質岩類の全岩化学組成の解釈においては注意が必要である．

以上の検討をもとにすると，ハーカー図（第6図）においては，広範なSiO_2の範囲で苦鉄質岩類細粒相と花崗岩類とが見かけ上単一の組成トレンドを示すものの，マグマの分化という観点からは苦鉄質岩類と花崗岩類とは成因的に無関係であると言える．一方，苦鉄質岩類細粒相のうち角閃岩様の組織を示すものについては，明らかな火成組織を示すものと同様の定常的な造構場によって，極めて類似した組成の苦鉄質マグマが継続的に長期間にわたって（600万年間；第2図a）発生した結果，変成作用を受けたものと受けていないものとが存在する可能性も否定はできないが，全岩主成分・微量成分組成において区別できないことや，大河原地域の領家変成岩類中に明らかに角閃岩の層と認められるほどの分布がないことから，明らかな火成組織を示す苦鉄質岩類細粒相と同一のマグマの一部が，貫入時の流理や貫入後の変形作用により板状または長柱状の鉱物が配列したものである可能性が高い．

5. 2　領家深成岩類の広域的対比・理解への示唆

苦鉄質岩類

大河原地域と同様に，小規模な苦鉄質岩体において細粒苦鉄質岩が周囲の花崗岩類と混交する産状は，中部地方の領家深成岩類のうち，武節花崗岩（Ishihara and Chappell, 2007），三都橋花崗閃緑岩（山崎，2012），そして伊奈川花崗岩（山崎，2020；Yamasaki, 2022）において報告されているほか，苦鉄質岩体中にも認められる（Nakajima *et al.*, 2004）．中部地方の領家帯において，こうした細粒苦鉄質岩は，伝統的に変輝緑岩（あるいは変塩基性岩）と呼ばれてきた（例えば，Hayama, 1959；Yamada, 1959；山田ほか，1974；Kutsukake, 1975, 1997, 2000；沓掛, 1980）．このような，細粒苦鉄質岩類がある種の変成作用を被った岩相であるという考え方は，1980年代以降のRb–Sr系・Sm–Nd系全岩アイソクロン年代の検討により，中部地方以外も含む領家帯中の苦鉄質小岩体の少なくとも一部から，領家深成岩類の花崗岩類よりも明らかに古い年代が報告された（例えば，Kagami *et al.*, 1995；Okano *et al.*, 2000；柚原・加々美，2007）ことなどを踏まえ，苦鉄質岩類が花崗岩類に先行する火成活動の産物とみなされた研究史的な背景を反映している（例えば，山崎，2012；山崎ほか，2012；中島ほか，2021）．しかしながら，産状に示されるような領家深成岩類の花崗岩類と同時期の苦鉄質岩類が，領家帯全域にわたって分布するとすれば，山崎ほか（2012）でも述べているように，マントル由来苦鉄質マグマ活動の証拠としてその造構場の考察に強い制約を与える．そこで，以下では，中部地方の領家深成変成コンプレックスにおけるマントル由来苦鉄質マグマ活動を考えるための情報整理の一環として，三河–東濃地域に位置する明智地域の伊奈川花崗岩中の

細粒苦鉄質岩（Yamasaki，2022）との全岩化学組成の比較を行う．

大河原地域と明智地域の細粒苦鉄質岩のN-MORB規格化及びコンドライト規格化全岩微量元素パターンをそれぞれ第12図aとbに示す．一見して明らかなように，明智地域の細粒苦鉄質岩の一部において，ややTaの負異常が顕著であることを除けば，含有量・パターンの上で大河原地域と明智地域の細粒苦鉄質岩の組成は，ほぼ一致する．Yamasaki（2022）では，明智地域の細粒苦鉄質岩が，周囲の伊奈川花崗岩と同時期的に活動することによって様々な程度に化学的混合を行っていることが示されているため，これらの微量元素組成は，マントル由来苦鉄質マグマそのものの特徴を示しているとは限らない．それにも関わらず，結果として両地域の細粒苦鉄質岩の組成が一致することは，初生マグマの組成や，地殻内での組成改変プロセスが，両地域でほぼ同じであることを反映していると解釈される．

Nakajima *et al.*（2004）は，細粒苦鉄質岩が初生メルトの組成的特徴を保持しているとみなし，高Mg安山岩組成であったと考えた．しかしながら，Yamasaki（2022）や先の議論でも述べている通り，一般に花崗岩中でマグマ混交様の産状を示す細粒苦鉄質岩包有物は，ホストの花崗岩質マグマと様々な程度に化学的相互作用を行っていることが普通で，実際に明智地域においてもそのような現象が確認されている．従って，マントル由来メルトの地球化学的性質については，マントルと共存可能な程度にMgに富む有色鉱物を含み，地殻内での化学的相互作用の影響を無視できると期待されるキュムレイト中の構成鉱物の組成の検討が鍵となると考えられる．そうしたキュムレイトは，いわゆるコートランダイトや斑れい岩の小岩体として領家帯の各所から報告されている（例えば，手塚，1979；山崎ほか，2012）．それらのコートランダイトや斑れい岩の小岩体は，しばしば“変輝緑岩”と密接に伴って産するものの，直接的な関係は不明であった．これに対し，大河原地域では，相対的に北方域の細粒相から南方域の粗粒相へ岩相が系統的に変化するとともに，桶谷橋付近の岩体では両岩相が密接に伴って産し，成因的に同源であることが強く示唆される．コートランダイトはかんらん石を含む密度の大きなキュムレイトであることから，こうした岩体が花崗岩と密接に産するメカニズムも十分に解明されていない．大河原地域の産状からは，キュムレイトが細粒苦鉄質岩類（苦鉄質岩細粒相）と関連した早期晶出相であり，中部–下部地殻で小規模なマグマ溜まりとして晶出したか，細粒苦鉄質岩類の貫入に伴って相対的に地殻深部で捕獲されて現在の位置にもたらされたことが示唆される．ところで，大河原地域以南には，コートランダイトを含む粗粒な斑れい岩の小岩体が主として伊奈山脈の稜線付近に点々と存在することが知られている（例えば，手塚，1979，1980；手塚・福沢，1980，山崎ほか，2012）．こうした事実は，大河原地域の桶谷橋付近の岩体を境とし，それ以南に粗粒苦鉄質岩類（キュムレイト）の小岩体が卓越するという系統的な傾向を示している可能性が高く，そうであるとすると，こうした産状・岩相の違いには，削剥レベルの違い等の何らかの地質学的意味があるものと推察される．

一方，中島ほか（2021）は，Nakajima *et al.*（2004）で報告した花崗岩中の同時性岩脈（syn-plutonic dike）の優白質部（花崗閃緑岩）が，94 Maと70 MaのジルコンU–Pb年代の2つの年代クラスターを示すとともに，約90 Maのコアと約70 Maのリムをもつジルコンを含むことから，94–90 Maに貫入・定置した花崗岩に苦鉄質マグマが貫入することによって，周囲の花崗岩が部分的に融解して再度マッシュ状となり，その部分が苦鉄質マグマと物理的に混合して同時性岩脈様の産状が生じたと考えた．この年代測定結果及び解釈は，大変興味深いものであるが，地質学的・岩石学的な情報や検討が未だ十分ではなく，現状では評価が難しい．山田ほか（1974）やKutsukake（1975）による既存の地質学的関係に基づくと，この苦鉄質岩類の周囲に分布する岩型は，三都橋花崗閃緑岩（ジルコンU–Pb年代81–75 Ma；Takatsuka *et al.*, 2018，以下同じ）もしくは伊奈川花崗岩（75–69 Ma）と天竜峡花崗岩（81–75 Ma），武節花崗岩（75–69 Ma）そして神原トーナル岩（99–95 Ma）であり，同時性岩脈の優白質部が，これらのうちどの岩型に由来するのかが正確には不明である．中島ほか（2021）によれば，優白質部は中粒角閃石黒雲母花崗閃緑岩から細粒の優白質花崗岩まで様々であり，このうちジルコンU–Pb年代測定を行ったのは，中粒角閃石黒雲母花崗閃緑岩であるとされる．その古い年代値のクラスターに基づけば，この花崗閃緑岩は神原トーナル岩（99–95 Ma）に相当するものと推定される．中島ほか（2021）の解釈のように，花崗閃緑岩中のジルコンは苦鉄質マグマの貫入によって一部オーバーグロースしたものと思われるが，岩体周囲には70 Ma頃の固結年代を示す伊奈川花崗岩や武節花崗岩が存在することから，同時性岩脈周辺部の“細粒の優白質花崗岩”が，花崗閃緑岩（神原トーナル岩）と同一であるかは必ずしも明らかではない．すなわち，“細粒苦鉄質岩と細粒優白質花崗岩の同時性岩脈”，例えば，苦鉄質岩と同時共存した伊奈川花崗岩由来の優白質マグマとが同時性岩脈として，花崗閃緑岩（神原トーナル岩）に貫入している可能性も排除できない（この場合，90 Ma頃のコアをもつジルコンは外来結晶となる）．また，仮に94 Maに固結した花崗閃緑岩（神原トーナル岩）が苦鉄質マグマの貫入によって部分的に再溶融したのであれば，この現象は花崗閃緑岩を源岩とした部分溶融を伴う高温変成作用と捉えられ，中島ほか（2021）が報告しているジルコンのコアに認められる融食構造と同様の現象，あるいはこうした現象に伴って期

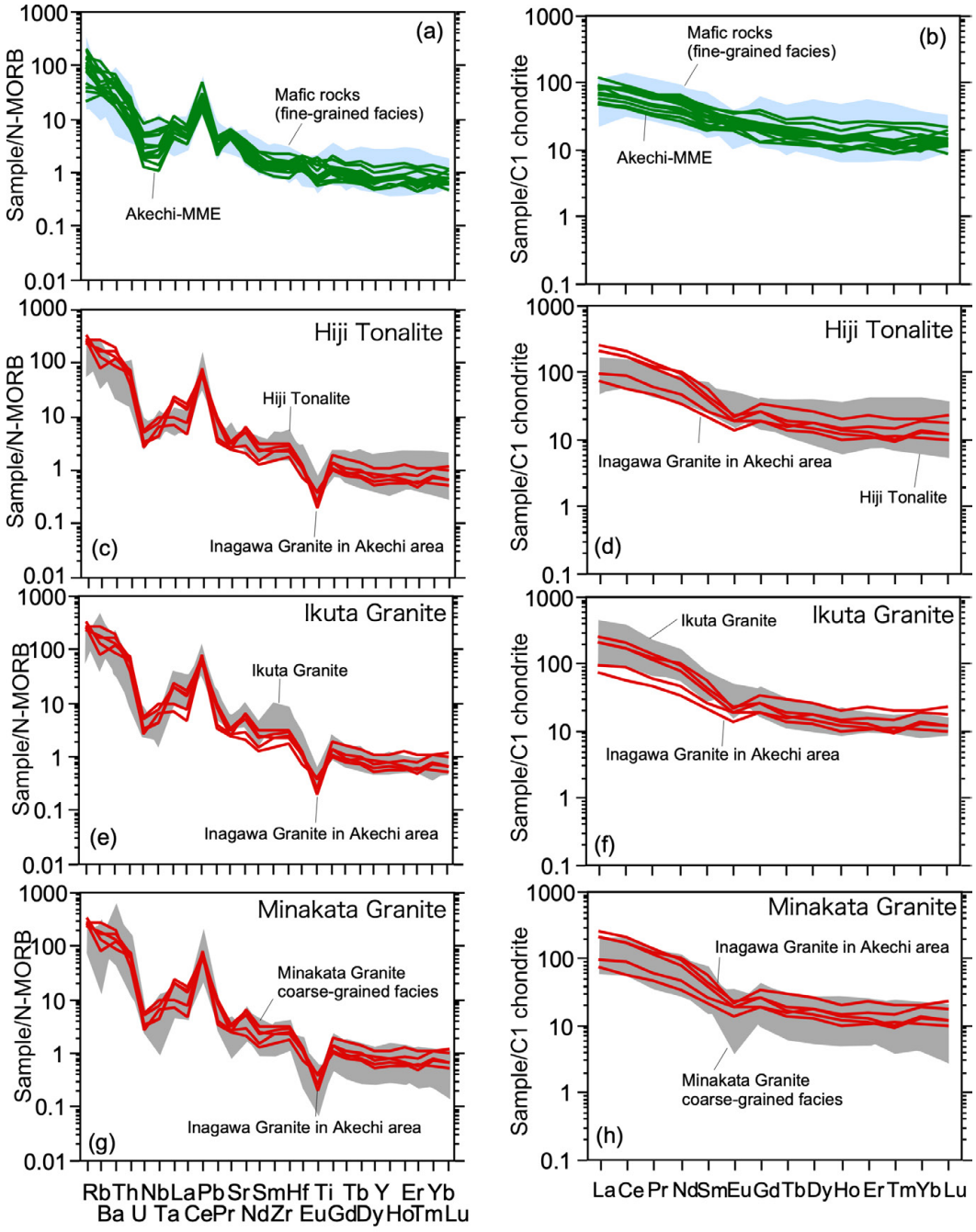

第12図　大河原地域に産する深成岩類と，三河–東濃地方明智地域に産する深成岩類との全岩微量成分組成の比較．(a) 大河原地域に産する苦鉄質岩類細粒相と明智地域に産する細粒苦鉄質岩（Akechi-MME）の全岩微量成分組成の中央海嶺玄武岩（N-MORB）規格化パターンによる比較．(b) 大河原地域に産する苦鉄質岩類細粒相と明智地域に産する細粒苦鉄質岩（Akechi-MME）の全岩希土類元素組成のコンドライト規格化パターンによる比較．(c), (e), (g) 大河原地域に産する花崗岩類と明智地域に産する伊奈川花崗岩の全岩微量成分組成の中央海嶺玄武岩（N-MORB）規格化パターンによる比較．(d), (f), (h) 大河原地域に産する花崗岩類と明智地域に産する伊奈川花崗岩の全岩希土類元素組成のコンドライト規格化パターンによる比較．規格化に用いたN-MORB及びコンドライトの値はSun and McDonough (1989) による．

Fig. 12　Comparison of whole-rock trace element patterns of Ryoke Plutonic Rocks from the Ogawara area and the Akechi area in the Mikawa–Tono region. (a) Comparison of N-MORB–normalized trace element patterns between mafic rocks in the Ogawara area and fine-grained mafic rocks (Akechi-MME) in the Akechi area. (b) Comparison of chondrite–normalized trace element patterns between mafic rocks in the Ogawara area and fine-grained mafic rocks (Akechi-MME) in the Akechi area. (c), (e), (g) Comparison of N-MORB–normalized trace element patterns of granitic rocks from the Ogawara area and the Akechi area. (d), (f), (h) Comparison of chondrite–normalized trace element patterns of granitic rocks from the Ogawara area and the Akechi area. N-MORB and chondrite values are from Sun and McDonough (1989).

待される組織が花崗閃緑岩中に認められる可能性が高い．例えば黒雲母の分解反応や，斜長石の異常な累帯構造が顕著に認められることが期待され，そのような特筆すべき組織に言及されていないことから，全体として中島ほか(2021)が提案するような現象が生じていたのかには疑問が残る．ところで，中島ほか(2021)は，94 Ma頃に定置・固結していた花崗岩マグマ溜まりが，70 Ma前後の苦鉄質マグマの活動によって部分的に再生したという表現も使用している．この点に関しては，Cooper and Kent (2014)やCooper *et al.* (2017)の米国オレゴン州やニュージーランドにおける検討から，確かに，“マグマ溜まり”への高温のマグマの注入あるいは再流入により，レオロジカルに固化 (rheological lock-up)した珪長質マグマが急速に再流動する現象が生じ得ることが提案されている．しかしながら，当時の領家深成変成コンプレックスの地殻内でこのような現象が起こり得る温度や物質的状態が維持されていたのかや，そうした現象が生じた際の深成岩類における具体的な岩石学的メカニズムについてはより多角的な検討が必要で，ジルコンの形態とU–Pb年代値のみから判断することは難しい．以上のことは，中島ほか(2021)の解釈が誤りである旨を主張するものではないが，同時性岩脈に伴われる年代的な矛盾・不一致については，より詳細な地質学的・岩石学的検討が今後の課題であるといえる．

花崗岩類

大河原地域を構成する花崗岩類は，微量元素組成のパターンにおいて，大局的には相互に非常に類似した地球化学的特徴を示す．このことは，それぞれの岩型あるいは少なくともその一部が，広い意味で親子関係にあるか，共通の起源物質に由来する可能性を示唆する．すでに述べたように，大河原地域を含め，各岩型には固結年代に数千万年の年代差が存在することから，ほぼ同時期の岩型以外は親子関係を想定することはできず，前節の検討からも単純な親子関係は考えにくい．それにも関わらず，大局的に微量元素組成がそれぞれの岩型で非常に類似することは，ほぼ同質の起源物質から，起源物質–メルト–晶出相間の元素の分配関係が変わらない程度に，すなわち，圧力や晶出相が大きく異ならない，類似した環境でマグマが発生・固化したことを示唆する．

1970年代頃までに一旦ほぼ確立された中部地方の領家深成岩類の広域対比 (例えば，山田ほか，1974)によると，中部地方領家深成変成コンプレックスにおいて最も広範に分布する伊奈川花崗岩は北東–南西方向に約95 km，次いで広範な分布を示す天竜峡花崗岩は約75 kmにわたって分布する．これらの膨大な量の花崗岩類が，同時期に単一の火成活動で形成されたか否かは自明のことではなく，仮に同時期的な火成作用の産物であるとしても，最大100 km程度にわたって均質な起源物質が存在したかどうかも不明である．その一方で，1970年代頃までに岩相(記載的特徴)をもとに対比された各岩型は，前節までに確認されたように，見た目の類似性が全岩化学組成の類似性に対応しており，化学組成的にも広域的に対比 (グループ化)できる可能性も十分に考えられる．全岩化学組成の，特に微量元素パターンの単なる絵合わせは，それらの成因が同一であることを必ずしも意味するものではないが，先行研究によって識別された岩型の広域的な対比を，全岩化学組成の観点から追認できれば，野外における岩相上 (見た目)の類似性をもとに区分された岩型に地球化学的根拠を加えることが可能となる．そこで，細粒苦鉄質岩と同じく，中部地方の領家深成岩類の全体像把握のための情報整備の一環として，同じ元素セットの得られている明智地域の花崗岩類と微量元素組成を比較する．明智地域からは, 伊奈川花崗岩 (Yamasaki, 2022)，武節花崗岩及び苗木花崗岩 (山崎，2019)の全岩微量元素組成が報告されているが，武節花崗岩及び苗木花崗岩については，大河原地域の花崗岩類と明らかに異なる組成を示すため，以下の検討からはあらかじめ除外し，伊奈川花崗岩 (Yamasaki, 2022)との比較を行った．なお，武節花崗岩は，全岩主成分化学組成のアルミナ飽和度が1.1を超えるパーアルミナスな組成で特徴づけられる(例えば，山崎，2019)．大河原地域の南向花崗岩は，ざくろ石や白雲母を含むことがあるが，アルミナ飽和度はほぼ1.1未満で，これを超えるものは例外的である(第8図)．従って，武節花崗岩に匹敵するほどパーアルミナスな組成を示す花崗岩類は，岩体規模では大河原地域には存在せず，アルミナ飽和度が1.1を超える南向花崗岩構成岩は，あくまでも局所的に砂泥質変成岩の同化作用等により形成されたものと推察される．

Yamasaki (2022)による明智地域の伊奈川花崗岩の全岩微量元素組成と，大河原地域の花崗岩類のN-MORB規格化全岩微量元素パターンを第12図b, d, f，そしてコンドライト規格化全岩微量元素パターンを第12図c, e, gに示す．大河原地域の非持トーナル岩，生田花崗岩及び南向花崗岩の微量元素組成が相互に類似するため，明智地域の伊奈川花崗岩も大局的にはそれら全てとよく似たパターンを示す．しかし，詳細に見ると，明智地域の伊奈川花崗岩はEuの負異常が顕著ではなく，南向花崗岩の特徴とは区別される．非持トーナル岩及び生田花崗岩と明智地域の伊奈川花崗岩とは，N-MORB規格化とコンドライト規格化全岩微量元素パターンいずれにおいてもほぼ組成範囲が重なるが，生田花崗岩を特徴づける，REEパターンのLa–Ceに富む傾向，そしてN-MORB規格化パターンにおけるNdの正異常が，明智地域の伊奈川花崗岩に共通して認められる．一方，生田花崗岩を特徴づける，N-MORB規格化パターンのZr–Hfに富む傾向は，明智地域の伊奈川花崗岩では認められない．生田花崗岩は記載的にも三河–東濃地域の伊奈川花崗岩と類似して

おり，特に粗粒な褐れん石を含む共通した特徴をもつため，結果的に化学組成の上でも大河原地域の各岩型の中では生田花崗岩と最もよく似た特徴を示している．三河地域の伊奈川花崗岩のジルコンU–Pb年代は75–69 Ma（Takatsuka *et al.*, 2018）であることから，この年代は大河原地域においては南向花崗岩と重なるが，本論において生田花崗岩の固結年代と想定しているNakamura *et al.*（2022）の77.7 ± 0.4 Maと伊奈川花崗岩の最も古い75 ± 1 Ma（Takatsuka *et al.*, 2018）とは，誤差を考慮すると1.3 Ma程度の差であり，生田花崗岩の固結年代がそもそも約78 Maではない可能性も考慮すると，矛盾しているとまでは言えない．大河原地域の西隣の5万分の1地質図幅「飯田」地域では，天竜川を挟んで西側に伊奈川花崗岩が広く分布するため（河田・山田，1957），生田花崗岩はこれの延長である可能性があり，先に述べたように，本地域周辺は年代値が得られている三河地域からは90 km以上離れているため，この付近の伊奈川花崗岩の固結年代が78 Ma頃である可能性も現時点では否定できない．

以上の生田花崗岩と明智地域の伊奈川花崗岩との微量元素組成上の類似性は，記載的特徴に対応した全岩化学組成上の特徴と年代値によって，中部地方の領家深成岩類が広域的に再定義できる可能性を示唆している．本報告では，地理的に60 km以上離れた地点間の，必ずしも成因的関係の明らかではない広域的な絵合わせを試みたが，近接する範囲での検討を順次拡大することによって，より信頼性の高い広域的な岩型毎の再評価が可能であると考えられる．さらに，領家帯全体に関わる課題としては，中部地方や中国地方の柳内〜瀬戸内海島嶼地域に分布する領家変成岩類と，四国地域に分布する領家変成岩類とは源岩構成が異なることが指摘されている（宮崎ほか，2016；宮崎・長田，2021）ことから，変成岩類の直接的な全岩化学組成の比較と合わせ，領家深成岩類についても，地殻構成物質の組成的差異から，岩石区（都城・久城，1975）が識別される可能性がある．

6．まとめ

5万分の1地質図幅「大河原」地域に産する領家深成岩類及び領家変成岩類の全岩主成分・微量成分組成が，岩型ごとの記載的特徴と一致し，野外及び鏡下での観察結果の裏付けとなり得ることを示した．大河原地域を構成する領家深成岩類である，非持トーナル岩，生田花崗岩及び南向花崗岩は，異なる分化指標であるSiO_2とFeO*/MgOに対する主成分元素の変化傾向と，微量元素組成のコンドライト規格化希土類元素パターンとN-MORB規格化マルチエレメントパターンの組み合わせにとって，相互に異なる地球化学的特徴の識別が可能である．大河原地域の非持トーナル岩，生田花崗岩及び南向花崗岩は，微量元素組成において大局的に互いに類似し，特定の元素に濃集する構成鉱物の有無や量比に起因する，わずかではあるが系統的な差異が認められるほかは，顕著な違いは認められない．このことは，これらの深成岩類のマグマが，ほぼ同質の起源物質から，部分溶融及び結晶化の際の分配係数が変わらない程度に類似した環境で発生・固化したことを示唆する．

苦鉄質岩類は，粗粒相と細粒相とで明らかな地球化学的特徴の差異を示し，前者がキュムレイトであり，後者が液組成を保持していることに対応している．細粒苦鉄質岩（細粒相）は，全岩主成分化学組成において見かけ上花崗岩類と連続するトレンドを示すが，この主たる原因は，野外において混交状の産状を示す生田花崗岩との組成的混合であり，マグマの分化における成因関係（親子関係）ではないと解釈される．混合による組成改変の効果を差し引くと，苦鉄質岩類はソレアイト質の分化トレンドを示す．

中部地方の領家深成岩類のうち，同じ元素セットのデータが利用可能な三河–東濃地域の明智地域に産する細粒苦鉄質岩との比較では，大河原地域の細粒苦鉄質岩とほぼ同一の組成を示すことが明らかとなった．このことは，初生マグマの組成や地殻内での組成改変プロセスを総合したマグマ・プロセスが，結果的に両地域でほぼ同じであることを反映していると解釈される．一方，明智地域に産する伊奈川花崗岩は，大局的に大河原地域の花崗岩類とよく似た全岩微量元素組成を示し，大河原地域の各岩型を特徴づける組成傾向と比較すると，生田花崗岩と概ね共通の特徴をもつ．明智地域と大河原地域とは，60 km以上離れているため，本報告における組成的類似性が成因的関係の直接的根拠とはなり得ないが，記載的特徴に対応した全岩化学組成上の特徴と年代値をもとにした近接する範囲での検討を拡大し，領家深成岩類の広域的対比・岩型定義の追認もしくは再定義が可能であることが示唆される．

謝辞：本研究は，陸域地質図プロジェクト5万分の1地質図幅「大河原」地域の調査研究の一環として実施されたものである．国有林地域の地質調査に際しては，中部森林管理局南信森林管理署に便宜を図って頂いた．苦鉄質岩類について，下伊那郡高森町の手塚恒人氏に情報提供を頂いた．査読においては活断層・火山研究部門の石塚治氏に，原稿のハンドリングにおいては担当編集委員の藤井孝志氏にお世話になった．岩石試料の処理及び化学分析に際しては，地質調査総合センター共同利用実験室を使用した．以上の関係諸機関ならびに関係者に記してお礼申し上げる．

文　献

Bateman, R.（1995）The interplay between crystallization, replenishment and hybridisation in large felsic magma chambers. *Earth-Science Reviews*, **39**, 91–106.

Brooks, C. K., Henderson, P. and Ronsbo, J. G. (1981) Rare earth element partitioning between allanite and glass in the obsidian of Sandy Braes, northern Ireland. *Mineralogical Magazine*, **44**, 157–160.

Chappell, B. W. and White, A. J. R. (1974) Two constrasting granite types. *Pacific Geology*, **8**, 173–174.

Cooper, K. M. and Kent, A. J. R. (2014). Rapid remobilization of magmatic crystals kept in cold storage. *Nature*, **506**, 480–483.

Cooper, G. F., Morgan, D. J. and Wilson, C. J. N. (2017). Rapid assembly and rejuvenation of a large silicic magmatic system: Insights from mineral diffusive profiles in the Kidnappers and Rocky Hill deposits, New Zealand. *Earth and Planetary Science Letters*, **473**, 1–13.

Debon, F. (1991) Comparative major element chemistry in various “microgranular enclave–plutonic host” pairs. *In* Didier, J. and Barbarin, B., eds., *Enclaves and Granite Petrology*, Developments in Petrology, **13**, Elsevier, Amsterdam, 293–312.

Godard, M., Awaji, S., Hansen, H., Hellebrand, E., Brunelli, D., Johnson, K., Yamasaki, T., Maeda, J., Abratis, M., Christie, D., Kato, Y., Mariet, C. and Rosner, M. (2009) Geochemistry of a long in-situ section of intrusive slow-spread oceanic lithosphere: Results from IODP Site U1309 (Atlantis Massif, 30°N Mid-Atlantic-Ridge). *Earth and Planetary Science Letters*, **279**, 110–122.

Grasset, O. and Albaréde, F. (1994) Hybridization of mingling magmas with different densities. *Earth and Planetary Science Letters*, **121**, 327–332.

Hayama, Y. (1959) The Ryoke granitic rocks in Kimagane District, Nagano Pref., Japan. *Journal of agricultural science, Tokyo Nogyo Daigaku*, **5**, 1–35.

Hayama, Y. and Yamada, T. (1977) Ryoke Metamorphic Belt in the Komagane–Kashio district. *In* Yamada, N., Npzawa, T., Hayama, Y. and Yamada, T., eds., *Mesozoic Felsic Igneous Activity and Related Metamorphism in Central Japan –From Nagoya to Toyama–*. Guide Book for Field Excursion 4, Geological Survey of Japan, 7–32.

Imai, N., Terashima, S., Itoh, S. and Ando, A. (1995) 1994 compilation values for GSJ reference samples, "Igneous rock series". *Geochemical Journal*, **29**, 91–95.

Ishihara, S. and Chappell, B. W. (2007) Chemical compositions of the late Cretaceous Ryoke granitoids of the Chubu District, central Japan – Revised. *Bulletin of the Geological Survey of Japan*, **58**, 323–350.

石井清彦・植田良夫・島津光夫 (1955) 長野県伊那地方の領家花崗岩および領家変成岩．岩石鉱物鉱床学会誌，**39**，1–10.

Kagami, H. (1973) A Rb–Sr geochronological study of the Ryoke granites in Chubu District, central Japan. *Journal of the geological Society of Japan*, **79**, 1–10.

Kagami, H., Yuhara, M., Tainosho, Y., Iizumi, S., Owada, M. and Hayama, Y. (1995) Sm–Nd isochron ages of mafic igneous rocks from the Ryoke Belt, Southwest Japan: Remains of Jurassic igneous activity in a late Cretaceous granitic terrane. *Geochemical Journal*, **29**, 123–135.

河田清雄・山田直利 (1957) 5万分の1地質図幅「飯田」及び報告書．地質調査所，62p.

Kutsukake, T. (1975) Metabasites in the Ryoke zone of the Toyone-mura area, Aichi Prefecture, Japan. *Journal of the Japanese Association of Mineralogists, Petrologists and Economic Geologists*, **70**, 177–193.

沓掛俊夫 (1980) 三河地方領家帯の塩基性岩類．愛知大学綜合郷土研究所紀要，**25**，50–56.

Kutsukake, T. (1997) Petrology and geochemisatry of a calcic and ferrous granitoid pluton: the Mitsuhashi Granite in the Ryoke Belt, southwest Japan. *Journal of Mineralogy, Petrology and Economic Geology*, **92**, 231–244.

Kutsukake, T. (2000) Petrographic features of the gabbroic rocks in the Ryoke Belt of the Mikawa district, southwest Japan. *Science Report of the Toyohashi Museum of Natural History*, **10**, 1–12.

Le Maitre, W. D., ed. (2002) *Igneous Rocks: A Classification and Glossary of Terms*. Cambridge University Press, 236p.

Miyashiro, A. (1974) Volcanic rocks series in island arcs and active continental margins. *American Journal of Science*, **274**, 321–355.

都城秋穂・久城育夫 (1975) 岩石学II–岩石の性質と分類. 共立出版，東京，171p.

宮崎一博 (2016) 20万分の1地質図幅「松山」（第2版）とその編纂に至るまでの話．GSJ地質ニュース，**5**, 209–217.

宮崎一博・長田充弘 (2021) 第3章　領家コンプレックス. 池田地域の地質，地域地質研究報告 (5万分の1地質図幅)．産総研地質調査総合センター，13–41.

宮崎一博・脇田浩二・宮下由香里・水野清秀・高橋雅紀・野田　篤・利光誠一・角井朝昭・大野哲二・名和一成・宮川歩夢 (2016) 20万分の1地質図幅「松山」（第2版），産総研地質調査総合センター.

Morgavi, D., Perugini, D., De Campos, C. P., Ertl-Ingrisch, W., Lavallée, Y., Morgan, L. and Dingwell, D. B. (2013) Interactions between rhyolitic and basaltic melts unraveled by chaotic mixing experiments. *Chemical Geology*, **346**, 199–212.

Nakajima, T., Kamiyama, H., Williams, I.S. and Tani, K. (2004) Mafic rocks from the Ryoke Belt, southwest Japan: implications for Cretaceous Ryoke/San-yo granitic

magma genesis. *Transactions of the Royal Society of Edinburgh: Earth Sciences*, **95**, 249－263.

中島　隆・神山裕幸・Williams, I. S.（2021）領家花崗岩類に伴う同時性岩脈の形成過程：マグマだまりプロセスに関する問題への年代学からのアプローチ．地質学雑誌，**127**，69–78.

Nakamura, Y., Miyazaki, K., Takahashi, Y., Iwano, H., Danhara, T. and Hirata, T.（2022）Amalgamation of the Ryoke and Sanbagawa metamorphic belts at the subduction interface: New insights from the Kashio mylonite along the Median Tectonic Line, Nagano, Japan. *Journal of Metamorphic Geology*, **40**, 389–422.

中村佳博・山崎　徹・宮崎一博・高橋　浩（2025）大河原地域の地質．地域地質研究報告（5万分の1地質図幅）．産総研地質調査総合センター，186p.

Okano, O., Sato, T. and Kagami, H.（2000）Rb–Sr and Sm–Nd isotopic studies of mafic igneous rocks from the Ryoke plutono-metamorphic belt in the Setouchi area, Southwest Japan: implications for the genesis and thermal history. *Island Arc*, **9**, 21–36.

Perugini, D., De Campos, C. P., Dingwell, D. B., Petrelli, M. and Poli, G.（2008）Trace element mobility during magma mixing: Preliminary experimental results. *Chemical Geology*, **256**, 146–157

Rollinson, H. and Pease, V.（2021）*Using Geochemical Data. 2nd Edition*, Cambridge Universty Press, Cambridge, 346p.

領家団研グループ（1955）領家帯の団体研究と中部地方領家帯地質図．地球科学，**25**，1–3.

下伊那誌編纂会（2006）下伊那誌 地質編，下伊那誌編纂会，263p.

坂島俊彦・高木秀雄・寺田健太郎・竹下　徹・早坂康隆・佐野有司（2000）領家帯非持トーナル岩および浅川沢花崗岩のSHRIMP年代．日本地質学会第107年学術大会講演要旨，155p.

杉山隆二（1939）所謂中央線に沿へる地帯に分布せる諸岩類の研究（第1報）(I) 所謂鹿塩片麻岩を主題とする野外調査に依って得たる諸考察，並に之と連携して所謂中央線に就いての再検討．地質学雑誌，**46**，169–187.

Sparks, R. S. J and Marshall, L. A.（1986）Thermal and mechanical constraints on mixing between mafic and silicic magmas. *Jornal of Volcanology and Geothermal Research*, **29**, 99–124.

Sun, S.-S. and McDonough, W.F.（1989）Chemical and isotopic systematics of oceanic basalts: implications for mantle composition and processes. *In* Saunders, A.D. and Norry, M.J., eds., *Magmatism in the Ocean Basins*, Geological Society Special Publication, no. 42, 313–345.

鈴木　敏（1888）20万分の地質図幅「甲府図幅」及び説明書．農商務省地質局，128p.

Takatsuka, K., Kawakami, T., Skrzypek, E., Sakata, S., Obayashi, H. and Hirata, T.（2018）Spatiotemporal evolution of magmatic pulses and regional metamorphism during a Cretaceous flare-up event: Constraints from the Ryoke belt (Mikawa area, central Japan). *Lithos*, **308–309**, 428–445.

手塚恒人（1979）長野県飯田市卯月山苦鉄質複合岩体について．下伊那教育会自然研究紀要，**2**，85–129.

手塚恒人（1980）中川村南向，銭不動苦鉄質岩体について．下伊那教育会自然研究紀要，**3**，137–145.

手塚恒人・福沢　宏（1980）安康南沢苦鉄質岩体について．下伊那教育会自然研究紀要，**3**，81–111.

Wilson, S. A.（2000）Data compilation for USGS reference material BCR-2, Columbia River Basalt, *U.S.G.S. Open file report* (in progress).

Yamada, T.（1957）On the gneissose granites of Minakata—Kashio District Nagano Prefecture, central Japan. *Journal of Faculty of Liberal Arts and Science, Shinshu University*, **7**, 43–73.

Yamada, T.（1967）Petrochemical studies of the Ryoke granitic rocks from the River Koshibu District, central Japan. *Journal of the Faculty of Science, Shinshu University*, **2**, 149–193.

山田直利・片田正人・端山好和・山田哲雄・仲井　豊・沓掛俊夫・諏訪兼位・宮川邦彦（1974）中部地方領家帯地質図．地質調査所.

山田直利・宮崎一博・栗本史雄・加藤碵一（2012）20万分の1地質図幅全国完備までの道．地学雑，**121**，N29-N41.

山崎　徹（2012）第4章　領家深成岩類．足助地域の地質，地域地質研究報告（5万分の1地質図幅）．産総研地質調査総合センター，27–50.

Yamasaki, T.（2014）XRF major element analyses of silicate rocks using 1:10 dilution ratio glass bead and a synthetically extended calibration curve method. *Bulletin of the Geological Survey of Japan*, **65**, 97–103.

Yamasaki, T.（2018）Contamination from mortars and mills during laboratory crushing and pulverizing. *Bulletin of the Geological Survey of Japan*, **69**, 201–210.

山崎　徹（2019）岐阜県恵那市明智町東方及びその周辺地域に産する花崗岩類の全岩主成分・微量成分組成とその帰属．地質調査研究報告，**70**，335–355.

山崎　徹（2020）第4章　領家深成岩類．明智地域の地質，地域地質研究報告（5万分の1地質図幅）．産総研地質調査総合センター，28–54.

Yamasaki, T.（2022）Magma hybridization and crystallization in coexisting gabbroic and granitic bodies in the mid-

crust, Akechi district, central Japan. *Mineralogy and Petrology*, **116**, 189–228

山崎　徹 (2025) 第 7 章　領家深成変成コンプレックス. 大河原地域の地質,地域地質研究報告 (5 万分の 1 地質図幅). 産総研地質調査総合センター, 91–128.

Yamasaki, T. and Yamashita, K. (2016) Whole rock multiple trace element analyses using fused glass bead by laser ablation-ICP-MS. *Bulletin of the Geological Survey of Japan*, **67**, 27–40.

山崎　徹・青矢睦月・木村希生・宮崎一博 (2012) 長野県飯田市, 卯月山苦鉄質複合岩体の岩石学的性質–領家帯における苦鉄質火成作用の成因解明への予察的検討–. 地質調査研究報告, **63**, 1–19.

Yamasaki, T., Yamashita, K., Ogasawara, M. and Saito, G. (2015) Multiple trace element analyses for silicate minerals and glasses by laser ablation-inductively coupled plasma-mass spectrometry (LA-ICP-MS). *Bulletin of the Geological Survey of Japan*, **66**, 179–197.

Yokoyama, K., Shigeoka, M., Otomo, Y., Tokuno, K. and Tsutsumi, Y. (2016) Uraninite and Thorite ages of around 400 granitoids in the Japanese Island. *Memoirs of the National Science Museum (Tokyo)*, **51**, 1–24.

柚原雅樹・加々美寛雄 (2007) 伊那領家変成帯に分布する苦鉄質岩の同位体年代. 福岡大学理学集報, **37**, 57–78.

(受 付：2024 年 2 月 22 日； 受 理：2024 年 12 月 9 日)
(早期公開：2025 年 4 月 4 日)

付表

第 1 表の全データを産総研リポジトリ (doi:10.50886/0002003294) に収録している.

付録

英語表記の地質単元・地名一覧

- Minakata Granite：南向花崗岩
- Ikuta Granite：生田花崗岩
- Hiji Tonalite：非持トーナル岩
- Nakagawa：中川村
- Oshika：大鹿村
- Toyooka：豊丘村
- Kashio：鹿塩
- Mt. Onishi：大西山
- Mt. Ogayasan：大萱山
- Mt. Takamori：高森山
- Lake Koshibu：小渋湖
- Koshibu River：小渋川
- Kashio River：鹿塩川
- Aoki River：青木川
- Shitoku River：四徳川
- Kogochi River：小河内川
- Shirasawa：白沢
- Shobusawa：菖蒲沢
- Nakayamasawa：中山沢
- Bamba-iri-sawa：番場入沢
- Hanno-iri-sawa：ハンノ入沢
- Takekurasawa：竹倉沢
- Kuwabara Fall：桑原の滝
- Okeya Bridge：桶谷橋
- Takizawa Bridge：滝沢橋
- Matsuyoke Bridge：松除橋
- Shitoku mineral spring：四徳鉱泉

地質調査総合センター研究資料集

758	第 41 回地質調査総合センターシンポジウム講演要旨集「デジタル技術で繋ぐ地質情報と防災対策　活断層 - 火山 - 斜面災害 - 海洋地質」	地質調査総合センター（編）
759	点群法線ベクトルを用いた震源クラスタリングによる地震断層面抽出法（FaultNVC）	佐脇 泰典・佐藤 圭浩・内出 崇彦
760	桜島の大規模噴火による降下テフラ分布の GIS データ	河野 裕希・西原　歩・宝田 晋治
761	大規模火砕噴火推移時系列データ集 その 3	池上 郁彦・長田 美里・河野 裕希・米谷 珠萌・宝田 晋治
762	産総研綾川千疋観測点の地質概要とコア資料	木口　努・板場 智史・松本 則夫・山本 和広・長谷 和則・須永 崇之
763	産総研佐伯蒲江観測点の地質概要とコア資料	木口　努・北川 有一・落　唯史・松本 則夫・長谷 和則・猪狩 一晟
764	焼岳火山の火口位置データおよび完新世噴火イベント集	及川 輝樹・宝田 晋治
765	日本の火山ガスの化学・同位体組成（1991-2024）	篠原 宏志・齋藤 元治・関　香織・風早 康平・風早 竜之介・森田 雅明・萬年 一剛
766	樽前火山及び磐梯火山の火口位置データ及び完新世噴火イベント集	古川 竜太・山元 孝広・宝田 晋治・及川 輝樹
767	機械学習に基づく地震信号分類器と観測点アソシエーション手法	寒河江 皓大・矢部　優・内出 崇彦

地質調査総合センターの最新出版物

5 万分の 1 地質図幅	高見山 門 大河原 米子（第 2 版）
20 万分の 1 地質図幅	広尾（第 2 版修正版）
海洋地質図	No. 95　熊野灘海底地質図
火山地質図	No. 24　御嶽火山地質図 No. 23　秋田焼山火山地質図
海陸シームレス地質図	S-8　海陸シームレス地質情報集「伊勢湾・三河湾沿岸域」
大規模火砕流分布図	No. 5　洞爺カルデラ洞爺火砕流堆積物分布図
水文環境図	No. 15　「大井川下流域」
重力図（ブーゲー異常）	No. 36　甲府－静岡地域重力図
土壌評価図	E-10　表層土壌評価基本図 ～中国地方～
特殊地質図	Sr. 41　栃木県シームレス地質図（第 2 版）
その他	東・東南アジア磁気異常図 改訂版（第 3 版） 中部地方の地球化学図

事務局
国立研究開発法人 産業技術総合研究所
地質調査総合センター
地質情報基盤センター　出版室
https://www.gsj.jp/inquiries.html

Secretariat Office
National Institute of Advanced Industrial Science and Technology
Geological Survey of Japan
Geoinformation Service Center　Publication Office
https://www.gsj.jp/en/

地質調査研究報告 第76巻 第1/2号
令和7年6月11日　発行

国立研究開発法人 産業技術総合研究所
地質調査総合センター

〒305-8567
茨城県つくば市東1-1-1 中央事業所7群

Bulletin of the Geological Survey of Japan
Vol. 76 No. 1/2 Issue June 11, 2025

Geological Survey of Japan, AIST

AIST Tsukuba Central 7, 1-1-1, Higashi,
Tsukuba, Ibaraki 305-8567 Japan

AIST16-G68699-76-1

Online ISSN : 2186-490X
Print ISSN : 1346-4272

BULLETIN OF THE GEOLOGICAL SURVEY OF JAPAN

Vol. 76 No. 1/2 2025

CONTENTS

Geological Survey of Japan, AIST

地 調 研 報
Bull. Geol. Surv. Japan
Vol. 76, No. 1/2, 2025